THE LOW FREQUENCY CORROSION FATIGUE PERFORMANCE OF SOME SURGICAL IMPLANT ALLOYS: WITH REFERENCE TO STRESS CONCENTRATION, ENVIRONMENTAL FACTORS, AND THE BEHAVIOUR OF MILD STEEL

THESIS

presented for the degree of

DOCTOR OF PHILOSOPHY

to the

COUNCIL FOR NATIONAL ACADEMIC AWARDS

by

R.A. WHITAKER BSc MSc CEng MIMechE MRAeS

City of London Polytechnic
Whitechapel High Street
London E1 7PF

JUNE 1978

ABSTRACT

A review of the literature on corrosion fatigue and fatigue testing is followed in this work by an analysis of the variables involved and of the various mechanisms which have been advanced. Particular reference is made to the corrosion fatigue of surgical implant alloys. An experimental programme was devised to be particularly relevant to the environmental variations possible in implant/body systems.

A multi-specimen, reverse-bend, strain facility was designed and produced for this research. Small smooth specimens were tested at a 'walking pace' of 1.7 Hz. A multi-channel, mini-potentiostat was also designed and produced for electrochemical studies during corrosion fatigue. Scanning and transmission electron microscopy was used to examine fracture surfaces.

The corrosion fatigue performance of some alloys (stainless steel type 316, titanium 130 and 318) currently used for surgical implants has been evaluated. A comparative study of the performance of mild steel, a material which has in the past been used for implants, was also made. A series of experiments was conducted to simulate normal conditions with a 0.17M saline solution buffered at pH 6.5. Some extreme conditions were also investigated at pH 1.5 and pH 11.5. In order to evaluate the comparative influence of saline, additional experiments were conducted in air and in distilled water for each material.

A considerable number of metal/environment combinations was thereby investigated, involving corrosion fatigue in both the passive-state and the active state. Since it is common place for some implants to be drilled for fitting, a further series of experiments was conducted using specimens containing a drilled hole. The influence of such stress concentrating features was thus established for each material.

The behaviour of mild steel in all the environments tested, and that of S316 in pH 1.5 saline was described using a single model for interaction between stress concentration and corrosion during fatigue. A different model was found to represent the behaviour of all the other metal/environment combinations tested. The two models were seen to represent, respectively, active-state corrosion fatigue and fatigue under passive state conditions. The drilling of holes in mild steel and T130 showed a small stress concentration effect. No such effect was produced with holes in stainless steel. By contrast, however, the drilling of a hole in T318 resulted in a dramatic reduction in the fatigue limit: a reduction of the order of 50% was obtained in both distilled water and saline solutions. Unlike other materials S316 produced a wide scatter band of results in saline pH 6.5. This was attributed to a naturally fluctuating corrosion potential indicative of an irregular film breakdown and repair.

The results are generally discussed and the evidence produced shows that the use of S316 for surgical implants cannot

be recommended because of poor resistance to corrosion fatigue at low pH. T130 was superior in this respect. However, T318 showed the best resistance to corrosion fatigue even allowing for the drastic reduction in performance with a drilled hole.

ACKNOWLEDGEMENTS

During the course of this work I have received considerable support and assistance. I am deeply indebted to my supervisors Dr. C.J.L. Booker, at the City of London Polytechnic, and Mr. A.N. Hughes, at the Aldermaston Atomic Weapons Research Establishment. The help and cooperation received from research staff at AWRE, during many implant research progress meetings, was particularly valuable. In this respect I wish to record my gratitude to Dr. S Orman, Dr. J. White and Dr. C.J.E. Smith.

CONTENTS

cont..

CONTENTS Page No.

cont.

CONTENTS Page No.

cont.

CONTENTS Page No.

1. INTRODUCTION

The corrosion fatigue failure of both large structures and of relatively small engineering components in service is a common occurrence. Every pure metal and metal alloy is susceptible to corrosion fatigue, regardless of its structural constitution and whether it is in an active or a passive state with its immediate environment. Total life data, based on stress S/N cycle plots, has been accumulated over the years for many materials in various environments. Such data include the time to initiate and then subsequently to propagate a crack, to a length which causes catastrophic failure. Crack propagation rate studies have similarly amassed results which have enabled certain design criteria to be generally applied to large structures. In spite of this data, there are many uncharted areas on the 'map' of knowledge and the understanding of corrosion fatigue mechanisms is far from clear.

Corrosion fatigue is a complex subject primarily because of the very large number of inter-related variables involved. The separate effects of these variables are generally difficult to measure or control. It is for this reason that the results obtained from one programme of research have sometimes, in the past, appeared to be at variance with the results of another investigation. Different variables may be controlled in a variety of different ways depending on the objectives of the study. It is then problematical whether the results for a

particular system may be more generally applied.

This programme of research was primarily concerned with the corrosion fatigue of surgical implants. Unlike large structures, where cracks are assumed to be present and must not be allowed to propagate in an undetermined way, surgical implants must not be allowed to initiate a crack. Crack growth cannot be monitored in surgical implants. Crack initiation is therefore the most important aspect of the corrosion fatigue process. Since observation of this even when it occurs is experimentally difficult, S/N data for small smooth specimens is useful. When it can be demonstrated that the time for crack initiation is more than 90% of the total time to failure, S/N plots may be considered appropriate for small precision made components. Well designed medical implants are just such components. They are subjected to fluctuating stresses, particularly in bending, and are exposed to corrosive body fluids.

Surgical implants are more frequently being fitted to young patients with fractures. Implants must therefore be designed not to initiate a crack within a human lifespan. Incorrect alignment during orthopaedic surgery, bone resorption or cement degradation, will all contribute to increased bending stress as well as the promotion of crevice conditions. Holes are also commonly drilled through some implants during fitting. The actual effect of such holes on corrosion fatigue performance has not previously been determined. The application of vee-notch data to well designed smooth implants with a drilled hole seems most inappropriate. Mathematically determined stress concentrations

cannot be viewed with any confidence as a method of predicting performance for the corrosion fatigue of such implants. The conjoint action of corrosion and fatigue for implant plates with holes was planned to be investigated here.

The metal alloys currently used for implants are specified by British Standards, largely as the result of research on similar materials in the aero-space industry. The environment and loading used for such research is obviously in general quite different from that required for medical implants. It is thus highly desirable that research, with relevant criteria for implants, should be urgently undertaken. On behalf of the Department of Health and Social Security, considerable progress has been made at AWRE Aldermaston in recent years to establish the performance of implants generally. Much of this work, however, was at frequencies of 100 Hz or above with single-specimen, push-pull or rotating bending fatigue machines. A test programme using such machines at human walking pace frequencies of 1 to 2 Hz was previously considered to be too protracted for test results. In this present work, however, a multi-specimen reverse-bend test facility was designed and built by the author to operate at 1.7 Hz for surgical implant research. It was thus planned to obtain results under conditions more typical of those actually occurring in service.

With the object of furthering the understanding of corrosion fatigue behaviour for surgical implants, a wide range of environments was planned to be investigated during this research. Air, distilled

water, and simulated body fluid saline at high, neutral and low pH was considered so that behavioural differences could be highlighted during fatigue. The behaviour of mild steel, which has been used for implants in the past, was considered also in this research so that a wide range of metal/environment couples could be compared. Active-state corrosion fatigue conditions were thus planned to be studied together with the conditions under which the more desirable passive-state behaviour is observed. The results of this research are applicable therefore to a wider range of environments than that usual in service for surgical implants. High pH cleaning solutions, applied during preparation, and low pH conditions locally for a period after the fitting of implants, are two examples of more extreme conditions of service investigated here. Such results are of course also applicable to a wider range of engineering components generally. They should be particularly useful in the design of small precision made components for chemical plant, where the frequency of loading is relatively low and where stress concentrations are known to exist.

Section 2 of this thesis generally presents a review of corrosion fatigue and the mechanisms advanced to account for the observed behaviour in past research. Relevant variables and their interaction are discussed with respect to past results. Section 3 of this work then presents the experimental research undertaken by the author. The results and a preliminary discussion appear in Section 4. Finally, in Section 5 there follows a general discussion of the investigation and conclusions are drawn on the information derived.

2.1 Early Major Historical Developments

2.1.1 Fatigue

The fatigue failure of metals has been recognized for many years. Fatigue tests were carried out on chains and wrought iron beams around the middle of the last century. Repeated bending test results were published by Sir William Fairbairn[1] in 1864. Fatigue failure was then defined simply as a failure at loads less than those required for static fracture. Wohler[2] conducted a series of fatigue tests, using small specimens of wrought iron, and accurately controlled repeated loads. Load or stress amplitude S was plotted against specimen life measured as the number of cycles N to fracture, as shown in Figure R . 1.

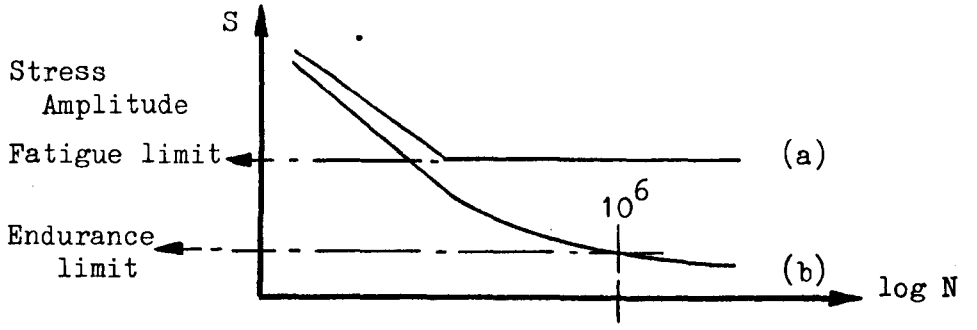

Figure R.1 The form of the classical S/N fatigue curve

The fatigue limit was considered to be the critical upper limit of stress amplitude for the material, below which fatigue failure would not occur no matter how many cycles of loading were applied (see curve (a) in Figure R.1).Endurance limit, the stress amplitude for a given fatigue life (e.g. 10^6 cycles in Figure I for the curve (b)), was a concept introduced later when it was found that a fatigue limit for some materials did not exist. Around 1870

sufficient S/N data had been collected for wrought iron to establish a fatigue limit for this material and to determine the effect of mean stress. Figure R.2 shows the general relationships between the cycled stress of amplitude S (range 2.S), the mean stress σ_m, and the maximum and minimum stresses occuring in a cycle.

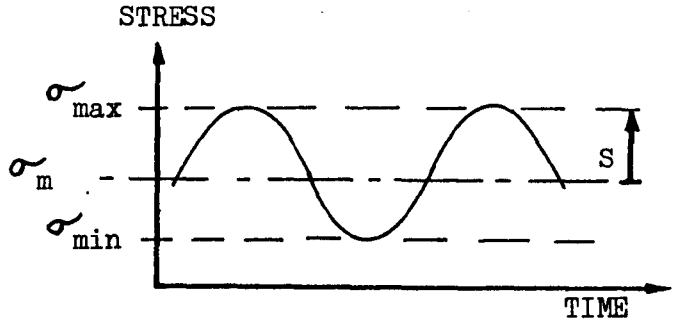

Figure R.2 cyclic stress and mean stress relationship

The mean stress can of course be compressive or tensile, and for the special case where the mean stress is zero the fatigue was usually referred to as reversed stress cycling. The work of Wohler was extended to other materials by Bauschinger[3] in 1886 and, using these results, Gerber[4] and Goodman[5] deduced respectively parabolic and straight line mean stress relationships. These 'laws' deduced in the latter part of the nineteenth century are still used today in design procedures to predict the effect of tensile mean stress.

Metallographic studies on single crystals and on polycrystalline materials were extensively made during the early part of this century. Ewing and Humphrey[6] in 1903 recorded the formation of slip lines during the fatigue of iron. They observed that these slip lines broadened into bands before developing into surface cracks. Moore and Ver[7] in 1930 and Gough[8] in 1933 reported similar findings in other materials and investigated differences

of slip line formation with structure. In all their tests, slip occurred on the same crystallographic planes and directions as for tensile static loadings. There was however a marked difference in the appearance of the slip lines produced by fatigue and those produced by uniaxial tension. Little change occurred in the appearance of the original slip lines in a tensile test, and new fine slip lines appeared between the original ones. In the case of fatigue, however, after an initial period during which fine slip lines were produced, the subsequent changes consisted of the broadening of certain of the original slip lines to quite broad bands. These broadened lines were called slip bands "SB". Fatigue cracks were seen to initiate from the SB of most pronounced slip by further cyclic loading.

Two classic books, both entitled "The Fatigue of Metals" were written in 1924 by Gough[9] and in 1927 by Moore and Kommers[10]. These books described testing machines and test methods for fatigue. Also included are photographs of slip lines and the idea of fatigue as a progressive failure involving the initiation of a crack, often at a stress raiser, and its subsequent slow progression. Considering the date of these publication, this idea of fatigue was very advanced.

The Institution of Mechanical Engineers were very concerned in 1913[11] at the very frequent breakage of wrought iron railway axles. The crystalline appearance of the fracture surfaces convinced many members that cyclic stressing made tough fibrous iron, crystalline and brittle. It was however recognised that, since axle failure always occurred at the wheel location shoulder, it was important to redesign the axle with less sudden changes in

cross-section. A notch effect was suspected and, also in 1913, Inglis[12] published his work on the elastic stress analysis of plates due to the presence of cracks and sharp corners. A more general theory of elastic notch stresses was not published until 1946 by Neuber[13]. A classical contribution on crack instability under a static load was made as early as 1920 by Griffiths[14], but the ideas expressed were not developed for application to fatigue studies for some twenty years. Taylor[15] introduced the concept of a dislocation in 1934, by which metal crystals and crystalline grains shear through the movement of dislocations when stress is applied. X-ray examinations of the changes of lattice state in cyclic stressed steel by Gough and Wood[16] in 1936, Barrett[17] in 1937, and Wener[18] in 1938, showed that fatigue limit represented a deformation limit. During cyclic loading, plastic deformation was found to occur which lead to lattice distortions. It could be determined from X-ray pictures whether or not the fatigue limit had been exceeded for a given steel specimen.

Studies, using the optical microscope, of the fracture faces created by macrocracks revealed the presence of line-markings, called striations. These were generally accepted as marks indicating the position of the crack tip on successive stress cycles. The presence of striations on fatigue fracture surfaces was considered evidence which could be interpreted to analyse the cause of failure in practical situations. Unfortunately many fatigue fracture surfaces did not clearly show striations, owing to metallurgical or environmental factors not yet appreciated.

Slip band extrusions, first recognised in 1953 by Forsyth[19] in Al-4% Cu alloy, were found in the form of thin metal ribbons

extended from fine slip bands. Interferometry and electron microscopy was used to measure these extrusions which were typically 10μ high, above the previously electrolytically polished surface, and about 0.1μ thick. Extrusions were subsequently found to occur in almost every material examined. Extrusions were thicker and more irregular at higher temperatures[20]. Cold rolling was found to stimulate the production of extrusions for pure metals[21]. Thompson and Wadsworth[22] showed in 1958 that extrusion occurred, in annealed single crystals of copper, along the slip plane in the most highly stressed slip direction. They also found that extrusions did not occur when the most highly stressed slip direction was parallel to the surface. For single crystals of copper it was established that extrusion took place during "a few cycles" after some initial period of cyclic load.[22] This result was however not observed for some other materials. Extrusions were found generally to be developed gradually over many thousands of cycles for annealed metals. Hardened materials produced the most rapid extrusions. Thompson et al[23], using specimens of high purity copper in push-pull fatigue with electropolishing of surfaces at various stages of fatigue life, found that they could remove practically all the slip bands from the specimen surface from about 4% up to about 7.5% total life. However a few slip bands did remain, and at higher percentages of total life the number of slip bands remaining after electropolishing the surface increased and became very black in appearance. These remaining bands were referred to by Thompson et al[23] in 1956 as persistent slip bands "PSB". The origin of the final fatigue crack was thus established as the PSB, formed at about 4% of total fatigue life, for high purity copper. Slip bands which are going to form extrusions (PSB) and cracks

could then be distinquished quite early in life from other more normal slip bands. Slip bands produced by tensile deformation were largely removed by electropolishing and any ones remaining were faint and indistinct, and quite unlike the dark broad PSB remaining on fatigue specimens. Hempel[24] examined slip band formation in steels, and Harries & Smith working with pure aluminium (reviewed by Smith[25]), found similar PSB behaviour for these materials. Slip band intrusions were often found associated with extrusions.

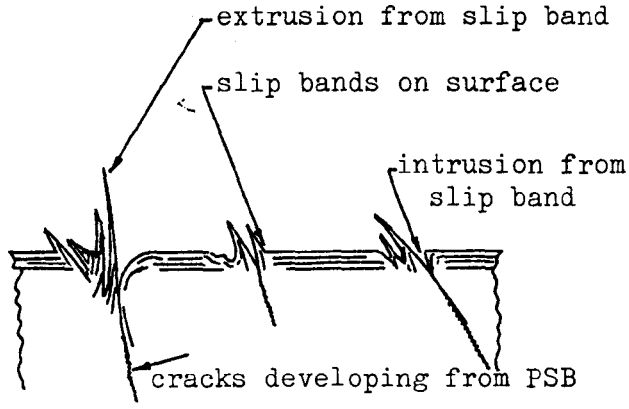

Figure R.3 Extrusion/Intrustion phenomenon

Cottrell and Hull[26], Wood and Segall[27], and Hull[28], found extrusions and intrusions in a variety of f.c.c. metals. The intrusions were generally equivalent to cracks of a few microns in depth and were directly adjacent to extrusions. Intrusions were typically paired with extrusions, as show diagramatically in Figure R.3. Plastic strain was thus identified by such work as a prerequisite for fatigue, and the nucleation of cracks required localization of strain.

2.1.2 Environment

The effect of environment on fatigue failure was first seriously examined by Haigh[29] in 1917. The failure of medium

carbon steel towing ropes attached to the paravane equipment used for mine sweeping during the first world war was investigated. Higher tensile steel wires were found to behave no better than the normal medium carbon steel wires in service. This result was contrary to all expectations at that time: fatigue performance was known to be proportional to tensile strength. Clearly fatigue, resulting from vibrating tensile load on the wire at sea, in an aggresive environment was a somewhat different phenomenon. Haigh found the solution to the problem in galvanized steel wires. These wires showed considerable improvement in service and demonstrated the importance of materials selection for a specific environment rather than for high tensile strength. McAdam[30] in 1926 described the conjoint action of corrosion with fatigue. He was the first to use the term "Corrosion Fatigue" to describe this action. In an attempt to increase the rate of heat removal from fatigue specimens of Monel he surrounded them with water. The result he noted was that although only slight corrosion occurred, life was very much shorter and a new lower corrosion fatigue limit was produced. A vast quantity of data was amassed by systematic testing. He showed that shorter lives were always obtained with corrosion fatigue than that produced by the sum of the damage by corrosion and by fatigue acting separately, in whatever order. Gough and Sopwith[31] in 1932 found that, by comparison with tests in vacuo, the fatigue lives of most structural metals are significantly reduced by the presence of air. In 1933 these authors[31] compiled a wide variety of data for materials in conditions of corrosion fatigue. In general it was found that compositions which are resistant to corrosion also have superior corrosion fatigue properties. In particular it was found that specimens of iron of increasing purity

showed less difference between the S/N curves in "corrosive" and "non-corrosive" conditions the purer the iron.

Electrochemical corrosion studies by Evans[32] established the behaviour of local anodes and cathodes during the corrosion of metals. In 1929 he produced a graphical method of showing how the corrosion rate depends on the polarization of the anode and cathode. Evans' diagrams, showing current-potential relationships, can be regarded as the fundamental basis of the theory of corrosion of metals. Figure R4 illustrates the ideas of polarization using an Evans type diagram. The points A and C represent the potentials of the anode and cathode respectively when no current is flowing, i.e. the unpolarized potentials. At the start of a corrosion process, the current which would flow between the anodic and cathodic areas is given by the potential difference AC divided by the external resistance of the circuit. However, as soon as a current starts to flow, chemical changes at the electrodes alter their character and therefore their potential. The change in potential, known as polarization, is represented in FigureR.4 by the two lines CP and AP. The resistance may be considered low, if anodic and cathodic areas are adjacent, so that the corrosion current may be assumed to be the abscissa of P. The corrosion rate in gram-equivalents per second is given by dividing the current by Faraday's constant. Evans and Simnad[33] found in 1946 that when steel is strained below the elastic limit there is little effect on an Evans diagram. When strained beyond the elastic limit, however, the unpolarized anode potential of mild steel in acid solutions is shifted some 25 mV in a more base direction: the anodic polarization is also reduced. Simnad[34] suggested in 1950 that the latent energy in a deformed metal should be manifest as a change in the electrode potential of the metal and in its resistance to corrosion. Film free aluminium was tested by Simnad[34] in neutral solutions and an appreciable lowering

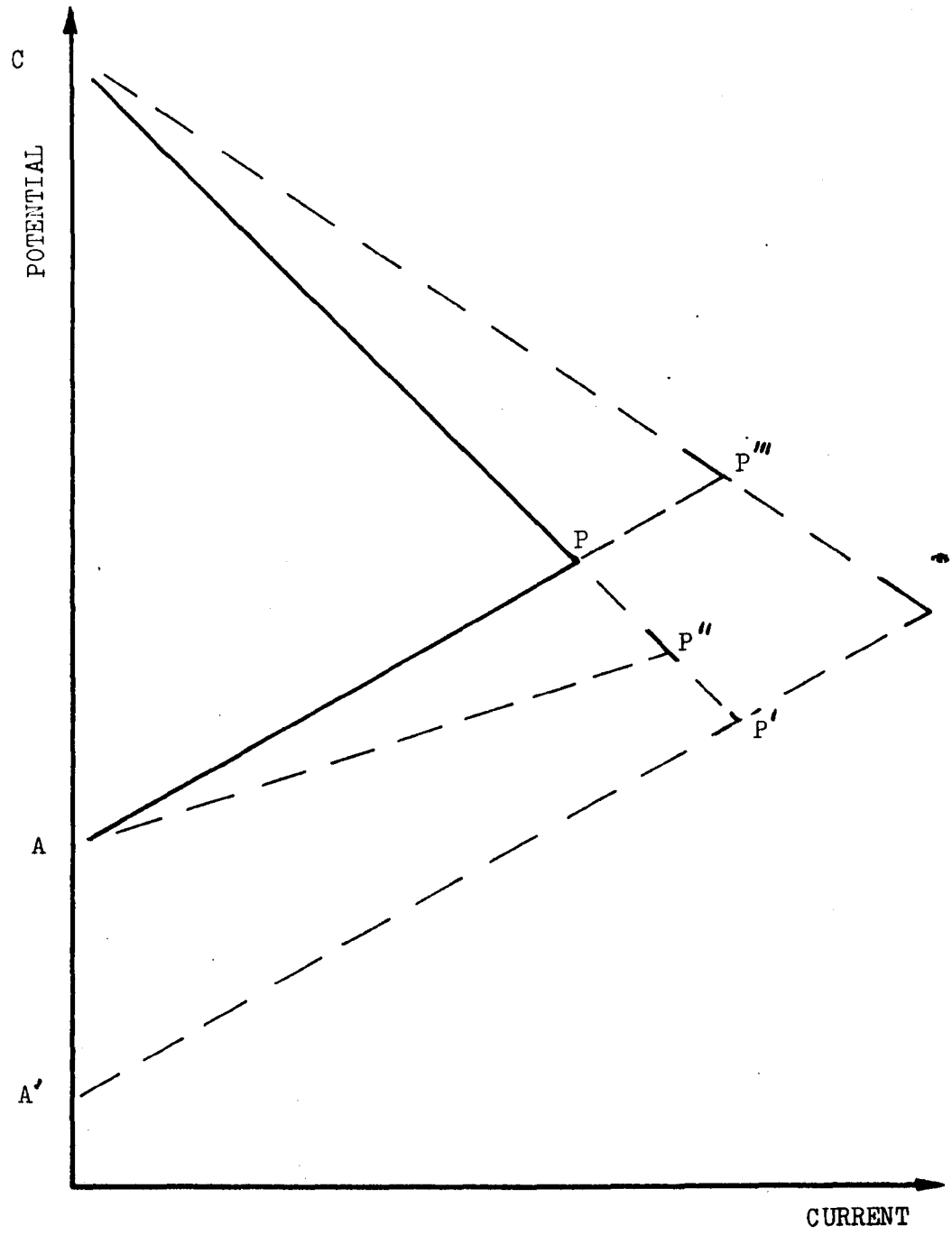

Figure R.4 Rudimentary Polarization Diagram According to Evans[32]

of potential was found for cold worked metal.

During the process of corrosion fatigue a number of possibilities are shown as dotted lines in Figure R.4. If the applied stress shifts the anode potentional to a more base potential A', the corrosion current will be increased to P'. If the stress decreases the anode polarization so that the anode curve rises less steeply, the point of intersection is P''. If on the other hand the anode curve is unaffected but the cathodic polarization is reduced, the point of intersection is shifted to P'''. All of these possibilities increase the corrosion rate. For some metal/environment combinations possibilities may exist for decreasing the corrosion rate. Results from considerable research work have been often contradictory, supposedly due to not being able to measure the actual reversible potential, and the fact that the corrosion potential of a metal does not usually bear a simple relationship to its unpolarized potential. The effect of the oxide film was studied by Gould and Evans[35] in 1939. They found an immediate tendency towards the repair of imperfections in an oxide film when a solution was introduced to the metal surface. It was also found that, after rising, the potential started to fall as soon as breakdown of the film exceeded the rate of repair. They termed the time to commencement of the fall in potential the "film life" and found longer life in less corrosive solutions and at lower stress conditions. In distilled water a film life of just over 30 minutes was observed on steel at a stress range of $\pm$ 20 ton_f/in^2 ($\pm$ 309 MN/m^2). Evans and Simnad[33] also found that the initial rate of corrosion was proportional to stress range in fatigue. In the first half hour the rate for $\pm$ 309 MN/m^2

was double that for zero stress. Inglis and Lake[36] in 1931 and later Gould[37] in 1949 saw film repair after cracking as the main criterion for corrosion fatigue. They showed that the stress range S was the only important factor in their tests influencing film repair, and that providing the mean stress of the cycle was not excessive it did not have any great affect on life. This is in contrast to pure fatigue where mean stress determines the safe range of stress which may be applied.

2.1.3 Conjoint Action and Crack Growth

Some of the early major historical developments have been outlined here to illustrate the conjoint nature of corrosion fatigue and the fact of its early study separately as fatigue or corrosion phenomena. Corrosion fatigue has been developed and advanced intermittently in three traditionally separate work disciplines. Engineering stress analysts and designers, metallurgists and electrochemists (in historical order) have each had periods of intense interest in corrosion fatigue sandwiched between periods of research stagnation. Interest has been shown when a new idea has been put forward and is capable of being substantiated by practical experimental measurement: diminishing returns or difficulties with measurement tends to slow further research. Lack of knowledge by one discipline about the difficulties and attempts at solution to problems by workers in another field of study has been largely responsible for the past slow progress of work in corrosion fatigue. Further, more recent work shows that not only is corrosion fatigue a conjoint process requiring multi-disciplinary study, but also that the mechanisms occuring during the early stages of the process are often quite different to those responsible for final fracture.

Forsyth[38] and Ryder[39] showed, in the mid-fifties that a two-stage process for crack development in fatigue was operative. Metallographic studies showed slip band cracks developing under the action of resolved shear stresses: these cracks were termed "Stage I". A "Stage II" crack was formed when one or more of the cracks reached such a length that it changed its direction, growing normal to the maximum cyclic principal tensile stress. Stage II cracks were observed to grow much faster than Stage I cracks. These two stages of crack growth are now generally accepted and replace more descriptive terms such as microcrack and macrocrack. The distinction between Stage I and Stage II, determined by crack direction with reference to applied cyclic stress, is usually clear and avoids debates such as "When is a microcrack not a microcrack?" Unfortunately this debate is still unresolved for microcracks which are very small. The boundary for crack initiation, followed by Stage I cracks provides a dilemma. A generally accepted limit for microcracks is - 1μm for the start of Stage I in ductile materials. However, for some brittle materials the inherent flaw theory has been postulated and accepted. This theory assumes defects are always present and no initiation of crack is necessary, fatigue failure being merely a consequence of Stage I and Stage II propagation.

Fatigue in vacua is considered to be a purely mechanical process whereby cracks of a certain critical length are propagated as the result of local stress concentration - relieving processes. Corrosion under immersed conditions is essentially an electrochemical phenomenon. Corrosion fatigue has been suggested by various workers to result from a combination of mechanisms, ranging from almost purely mechanical to almost purely electrochemical or chemical. For any particular metal alloy/environment many factors may vary and cause a mechanism change during any of the separate stages of

fatigue. These factors have largely been identified during the last two decades and are listed in the following section of this review.

2.2 Identification of the Relevant Variables

The corrosion fatigue of any metal alloy/environment combination to be studied requires the identification of the relevant factors active in the process. The factors to be considered must be selected from the following list of variables:-

2.2.1 Mechanical Variables

(i) Cyclic stress amplitude or intensity related factor

(ii) Cyclic strain range (elastic/plastic)

(iii) Maximum stress/strain or intensity related factor

(iv) Geometric: component size, notch size and shape

(v) Type of stress/strain state (method of testing)

(vi) Residual stress

(vii) Interactions of load for applied variable amplitude loading

(viii) Cyclic stress/strain wave-form and strain rate for constant amplitude conditions

(ix) Cyclic loading frequency

2.2.2. Metallurgical Variables

(i) Microstructure; grain size, preferred orientation of grains and boundaries.

(ii) Mechanical properties

(iii) Metal alloy composition and lattic structure

(iv) Element and impurity distribution in the alloy

(v) Heat treatment

(vi) Cold working, surface treatment and coating properties relative to bulk properties

(vii) Surface finish and surface films

2.2.3 Environmental Variables

(i) Environment type - gaseous, atmospheric, liquid, etc.

(ii) Concentration of damaging species

(iii) Temperature of metal alloy and environment

(iv) Mass or volume of environment relative to surface area of metal exposed.

(v) Viscosity of the environment

(vi) Velocity of the environment relative to exposed metal

(vii) Current density and electrical potential

(viii) pH

(IX) Interface reactions and reaction rates, inhibition, passivation, embrittlement, etc.

2.3 Which Variables?

Corrosion fatigue properties of any metal alloy/environment combination are in general a function of all the above variables. Of the 25 listed above, some parameters may be inter-related for any particular system and in general they are by no means independent variables. For reasons of time and expense, a complete analysis for a given system is seldom justified even if it were practical to attempt one. Only those variables which are considered relevant for a particular need are studied. The other factors are discarded by attempts to control them at constant states, or are ignored by reason of their small contribution compared with the larger effects being studied. The effect of these variables in general may be indicated by studying the results of research work to date. Caution must be exercised however when attempting to apply such results to any new work. It is not uncommon to find apparent contradictions for the influence of any parameter studied, until it is realised that the parameter is highly specific in its effect to some combination of the other variables. A general literature review of the variables will now be made to show the relative importance of each for the process of crack initiation, Stage I, and Stage II corrosion fatigue.

2.4 Which Mechanical Variables?

2.4.1 Stress or Strain Amplitude

Mechanical variables have been investigated traditionally using S - N curves for smooth or notched specimens. Total fatigue life prediction for particular metal alloys in service have been based on experimentally determined stress amplitude versus life curves. More recently, for particular applications of high stress, plastic ranges or thermal fatigue, strain amplitude versus life curves have been found more useful. Figure R.5 shows such a plot: total strain amplitude (log scale) is the ordinate instead of the traditional stress amplitude (normally linear scale).

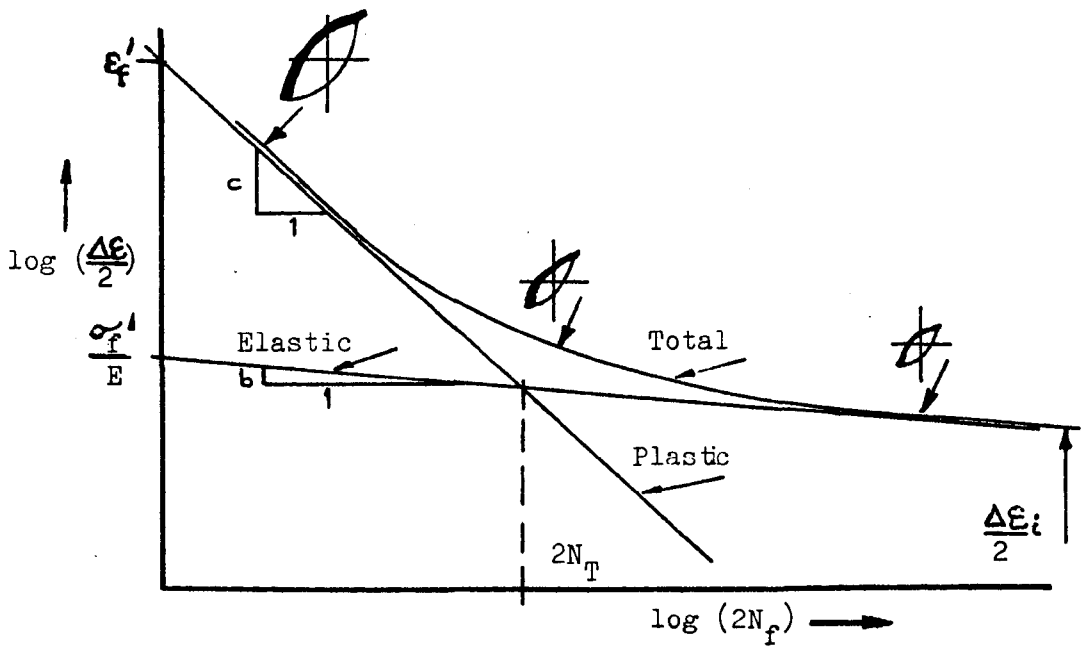

Figure R.5 A strain/cycle diagram due to Landgraf[40]

Microyield stress $\sigma_i = \frac{\Delta\varepsilon_i}{2} E$ = intrinsic fatigue strength limit

Landgraf[40] shows that this plot represents elastic, plastic and total strain amplitude-fatigue relations. The curve breaks into two linear plots; the plastic strain Manson-Coffin Law and the elastic strain Basquin relationship. A transition fatigue life $2N_T$, defined as the point at which the elastic and plastic strains are equal, conveniently serves as a useful definition of the quantitative boundary between low cycle (high stress) fatigue and high cycle (low stress) fatigue. An empirical equation can be written which describes the whole curve of Figure R.5.

$$(\Delta\varepsilon/2) = (\Delta\varepsilon_e/2) + (\Delta\varepsilon_p/2) = (\sigma_f'/E)(2N_f)^b + \varepsilon_f'(2N_f)^c \quad \text{---(i)}$$

where the parameters in the equation, and Figure R.5 are:

σ_f' = fatigue strength coefficient (σ = stress)

ε_f' = fatigue ductility coefficient (ε = strain)

E = Young's modulus

N_f = number of cycles to failure ($2N_f$ = number of reversals)

$\Delta\varepsilon$ = total strain range ($\Delta\varepsilon/2$ = amplitude)

suffix e = elastic value

suffix p = plastic value

suffix i = intrinsic value

suffix f = fatigue

b and c = constants for a specific system

At short lives it is clear that the plastic strain component predominates, emphasizing the importance of ductility. At long lives the elastic component becomes predominant, emphasizing the role of strength. Experimentally it is often most convenient to control the total strain amplitude, since stress or local cycling control can lead to instabilities or require sophisticated equipment. Frequently, strain cycling is also more applicable to service applications of structural members. S - N (or ε - N) curves are often

produced, for traditional reasons, but have led to difficulties in some cases. Owing to a lack of information on the relative contribution of the crack initiation and the crack growth stages to total fatigue life, other methods of presenting data have been established. Corrosion fatigue tests can now usually be classified into two distinct test types. Those traditionally based on S - N or ε - N curves for the determination of total fatigue life, and those based on 'Crack Growth Laws' developed to predict the behaviour of stage I and stage II fatigue failure only. Smooth specimens of ductile material tested at low stress have generally been found to be cracked in air-fatigue after $<10\%$ of their total life[41]. This is not the case however for many situations with corrosion fatigue. Surface films can be responsible for prolonged initiation periods so that cracks will not be found in smooth specimens until after $>90\%$ of their total life. Grosskreutz[42] has found that the crack initiation phase becomes a larger fraction of total life at lower stress amplitudes and that surface film effects can be very significant. Most large structures either contain crack-like defects introduced during manufacture or develop them early, so that virtually the whole fatigue life is occupied by fatigue crack growth. Testing to determine fatigue crack growth data is now virtually universal for corrosion fatigue. For plain or mildly notched components which have been carefully made, and which are highly stressed (e.g. turbine blades) or which have low stress amplitudes in corrosive environments, (e.g. surgical implants), traditional total life test data is more appropriate. Attempts to establish the proportion of life occupied by initiation are then usually made as a supplement to S - N data.

2.4.2 Specimen Geometry and Crack Growth

The difficulties often experienced in the past when interpreting fatigue data were due mainly to a lack of appreciation of the starting position for fracture, i.e. was the data obtained from an uncracked body requiring initiation of a crack, or was the data obtained from tests on pre-cracked bodies? Stage I and Stage II corrosion fatigue crack growth tests and results are based on a fracture mechanics approach. Notched specimens pre-cracked by fatigue, of sufficient size and proportion[43, 44], have been used for some years to establish the fracture toughness of metallic materials. Paris[45], in 1961, showed that fatigue crack growth rate was a unique power function of the range of the elastic stress intensity factor "K". Figure R6 shows the shape of a typical crack growth plot: the cyclic crack growth rate $(\frac{da}{dn})$ (mm/cycle) is plotted versus range of stress intensity ΔK $(N.mm^{-3/2})$, both variables having a log scale. A linear region of slope m (where $m \simeq 3$) is usually found for such a graph.

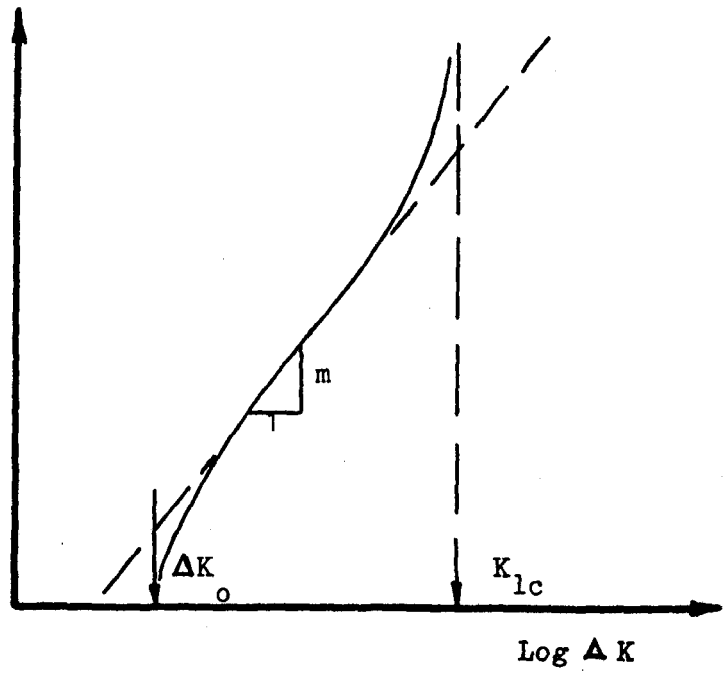

Figure R.6

A typical crack growth rate plot

There has been a wide variety of 'laws' of fatigue - crack growth developed for special cases in order to predict rates and further the understanding of growth phenomena. The Paris-Erdogan law[46] is the most generally applicable, and simplest to use:

$$\frac{da}{dN} = C\,(\Delta K)^m \qquad \text{(ii)}$$

The parameters of this equation are:

a = crack size (mm)

N = number of cycles of stress

ΔK_1 = range of stress intensity in fatigue cycles = $K_{max} - K_{min}$

K_1 = $\sigma . a^{\frac{1}{2}} . Y$ $(N.mm^{-3/2})$

σ = applied stress (MN/m^2)

Y = stress intensity factor coefficient which corrects for geometric effects

C & m = scaling constants

suffix I = mode I opening of the crack which is usually relevant to fatigue crack growth perpendicular to the maximum principal applied tensile stress.

The life of a component, or structural member, in which cracks are present initially can be predicted from equation (ii). A knowledge of C, which is a particular function of Young's Modulus, and the initial flaw size is required. The value of K for the initial flaw shape is also needed and, although precise values of K are not available for many complex crack shapes, engineering approximations for K are often used.

A review of fatigue crack growth data and analysis has been made by Pook[47], Irving & McCartney[48], and McEvily & Wei[49]. It is generally agreed that crack growth driving forces are a function of applied stress, and that they are also a function of crack dimension and of component geometry. Stage II crack growth is

adequately described by equation (ii) and growth rates are typically 10^{-5} to 10^{-3} mm/cycle. At higher growth rates when K_{max} approaches K_{1C} (Figure R.6), this equation often underestimates the propagation rate which increases rapidly towards final brittle fracture. However, of greatest interest generally is the region of the lower growth rates (see Figure R6.) where it is found that equation (ii) is too conservative. ΔK approaches a threshold stress intensity ΔK_o below which crack propagation cannot be detected. Few laws have been advanced which contain provision for a threshold for fatigue crack growth. Threshold values are usually determined experimentally and are then used, together with a theoretical law, as the value of ΔK below which growth will not occur. A modification of the Paris equation, equation (iii), to take account of the threshold stress intensity was suggested by Liu[50], but was found not to be generally applicable.

$$\frac{da}{dN} = C\,(\Delta K - \Delta K_o)^m \qquad \text{(iii)}$$

Many other attempts have been made more recently to account for threshold but with very limited general success. Priddle[51] reviews some of these attempts and suggests the following modification for mild steel.

$$\frac{da}{dN} = 2.2 \times 10^{-7} \left\{ \frac{\Delta K - \Delta K_o}{K_c - K_{max}} \right\}^2 + 2 \times 10^{-10} \qquad \text{(iv)}$$

Priddle[51] also concludes that the Paris equation cannot account for non-propagation, fast fracture, or mean stress intensity effects. Hence the introduction of K_c (the fast fracture strength) as well as K_o in equation (iv).

The effect of mean stress on the fatigue limit of a material, in the absence of corrosion, is historically well known (Gerber[4] & Goodman[5]). Frost, Pook & Denton[52] have recently also shown marked dependence on tensile mean stress in some structures due to brittle

intermetallics. In general however, rates of crack growth were found to be largely independent of mean stress. It is also known that mean stress has little effect on surface film life (Inglis & Lake[36], and Gould[37]). The effect of mean stress on initiation of corrosion fatigue requires investigation for each and every particular case. It usually has very little overall effect on the high endurance corrosion fatigue performance of materials: stress amplitude having by far the major effect. However, high tensile mean stresses can result in material failure other than that by corrosion fatigue in certain environments. For example, stress corrosion cracking and hydrogen embrittlement processes may result. Such possibilities must be remembered when considering stress levels generally and the effect of mean stress in particular. Mean stress is taken into account for crack growth studies by noting the effect of stress ratio. The ratio $R = K_{min} / K_{max}$ has been found to have little influence on Stage II crack growth but to have a large effect on the results at threshold ΔK_o and near K_{1C} (Ritchie[53] and Schmidt & Paris[54]). Increased near-threshold crack-growth rates and a decrease in the threshold for crack propagation (ΔK_o) were found as the load ratio R was increased. The value of ΔK_o was found to be inversely related to R.

2.4.3 Stress/Strain State and Notches

The type of test and the state of stress or strain applied to specimens has taken many forms during the last 100 years. Fatigue tests for total life S/N data have used smooth or mildly notched specimens utilizing rotating bending, flat plate bending, torsional, or axial load type configurations. Results from these tests have caused concern. Because of complex stress states and a shifting neutral axis in some cases, the different fatigue limit

obtained in each case has been difficult to explain. For example, the ratio of the torsional to uniaxial fatigue limit for ductile metals is between 0.5 to 0.6: the main reason for this is generally accepted to be the presence of a normal stress on the maximum shear stress planes in uniaxial loading and its absence in torsional loading. For corrosion fatigue the state of applied stress/strain could cause changes in mechanism for initiation and/or propagation. State of applied stress/strain is clearly an important variable. Crack growth tests are now usually conducted using recommended specimen proportions and load methods (ref. 43 and 44 previously mentioned) to enable either plane-strain or plane-stress conditions to be established. Total life or initiation studies have been recommended to utilize axial loading, for simplicity of stress state, where appropriate (Recent ASTM Committee E9). However, other types of test are sometimes more appropriate for corrosion fatigue initiation studies and will no doubt continue to be used. Environmental and frequency simulation of "real life structures", for example, may overide the importance of a simple stress state condition. Geometric variables are then inter-related with stress/strain state and stress intensities. Standardization [43,44] of the geometric variables now largely removes uncertainties in this area for crack growth type tests. The effect of notches on low-cycle fatigue is well documented in a review by Wundt[55] based on Neubers [13] early work, applicable to S - N tests, and updated to include the work of many other researchers. Calculations of stress concentration factor, fatigue strength reduction factor or similar related term, may now be estimated from such theoretical analyses for fatigue tests. However, notch profiles encountered in practice are likely to be difficult to predict. Fatigue limits of notched specimens have long been known to be different, in many cases, from that

predicted by the plain specimen fatigue limit of the material divided by the elastic stress concentration factor for the notch. Attempts to correct this difference were made by introducing a notch-sensitivity index q where,

$$q = \frac{k_f - 1}{k_t - 1} \quad , \qquad \text{(v)}$$

k_t = theoretical geometric concentration of stress factor

$= \sigma_{max}$ calculated for notch/σ_{max} calculated nominal value

k_f = fatigue strength reduction factor at a given endurance life

$= \sigma$ unnotched specimen/σ notched specimen

This index, with q typically 0.6 ~ 0.9, although much used by some designers today, can give unsafe predictions for fatigue life. At conception it was hoped that q would be a material constant, indicating notch sensitivity, for a given material. Unfortunately neither k_f nor q is constant for a material and both depend upon the size of the specimen tested. Fatigue limits decrease generally as the specimen size increases. The volume of material subjected to maximum stress affects the fatigue properties and this will differ considerably in plain and notched specimens. The effect of stress gradient and the apparent ineffectiveness of small notches suggests that, in cases of non-uniform stress, the fatigue behaviour is governed not by the peak stress but by a value averaged in some way over a volume of material including the point of maximum stress. These problems have been extensively studied by the fracture mechanics approach and to some extent resolved for crack growth data. Stress intensity factors K change radically as soon as crack growth starts and, as discussed earlier, stage II growth data for a given material can be made to fall on a single line (Figure R6). The effect of notches and size effects on corrosion fatigue is however uncertain. Nominally considered a

mechanical variable, notches have been found to have considerable influence on the environment. Such a concomitant effect is difficult to assess and must be considered for any particular application.

On a purely mechanical basis the local stress-strain response at notches has been studied more recently, and an anlysis developed by Topper et al[56], from the work originally by Neuber[13], can be stated as follows: in a notched member the peak-to-peak changes in nominal stress, $\Delta\sigma$, and nominal strain, $\Delta\varepsilon$, are related to the peak-to-peak changes in local stress, $\Delta\sigma_L$, and local strain, $\Delta\varepsilon_L$, through the fatigue concentration factor K_f

$$K_f\ (\Delta\sigma\Delta\varepsilon E)^{\frac{1}{2}} = (\Delta\sigma_L\Delta\varepsilon_L\ E)^{\frac{1}{2}} \qquad \text{(vi)}$$

K_f is a fatigue concentration factor considered a constant throughout the life range and E = elastic modulus. This analysis should apply equally well at short and long lives since non-linear stress-strain behaviour is accounted for.

2.4.4 Residual Stress

Residual stress in a material under fatigue is another mechanical variable with environmental as well as metallurgical implications. Considered, for the moment, as a purely mechanical variable it can be mathematically taken into consideration for its effect on mean stress. In practice residual stresses are difficult to measure with any degree of accuracy. It has been long established, from early work-hardening and coaxing studies, that induced residual compressive stresses will retard the development of a microcrack to the macrocrack stage. The reason for this retarded development, from stage I to stage II growth, is now realized to be due to the reduction of the effective value of ΔK_1. Residual tensile stresses accelerate the process for the similar reason that the effective

ΔK_1 is increased. Most structures in service are subjected to varying-amplitude loads and this generally results in residual stress complications. The order in which loads of varying amplitudes are applied can have a profound influence on the rates of fatigue-crack growth, and also on the threshold[57]. Crack growth is found to be retarded for a time following load reduction, and the threshold is often increased. These effects occur because of the compressive residual stress which arises at the crack tip, or in the vicinity of crack initiation. For stage II growth and a loading spectrum in which the current tensile peak is never less than its predecessor, a crack growth law of the form eqn (ii) is valid. As yet, there is no simple means of assessing the case of load reduction and resultant crack retardation. Mechanically, it is thought that the residual compressive stresses are not an important variable for initiation in fatigue, but coaxing effects on strain-ageing materials could be important. Metallurgically and environmentally residual stresses require consideration for interaction effects in corrosion-fatigue studies.

2.4.5 Wave-form

Wave-form for constant amplitude stress cycling is a variable which, until recently, has not been studied to any great extent. Figure R.7 shows several possible wave-forms to depict the loading cycle. The sine-wave is the most common form assumed in practice even if the actual form is somewhat different. Laboratory tests recently, using square waves with various hold times and saw tooth waves, has thrown new light on the effect of strain rate. Computer linked simulated real life load amplitude and wave-form tests are now possible.

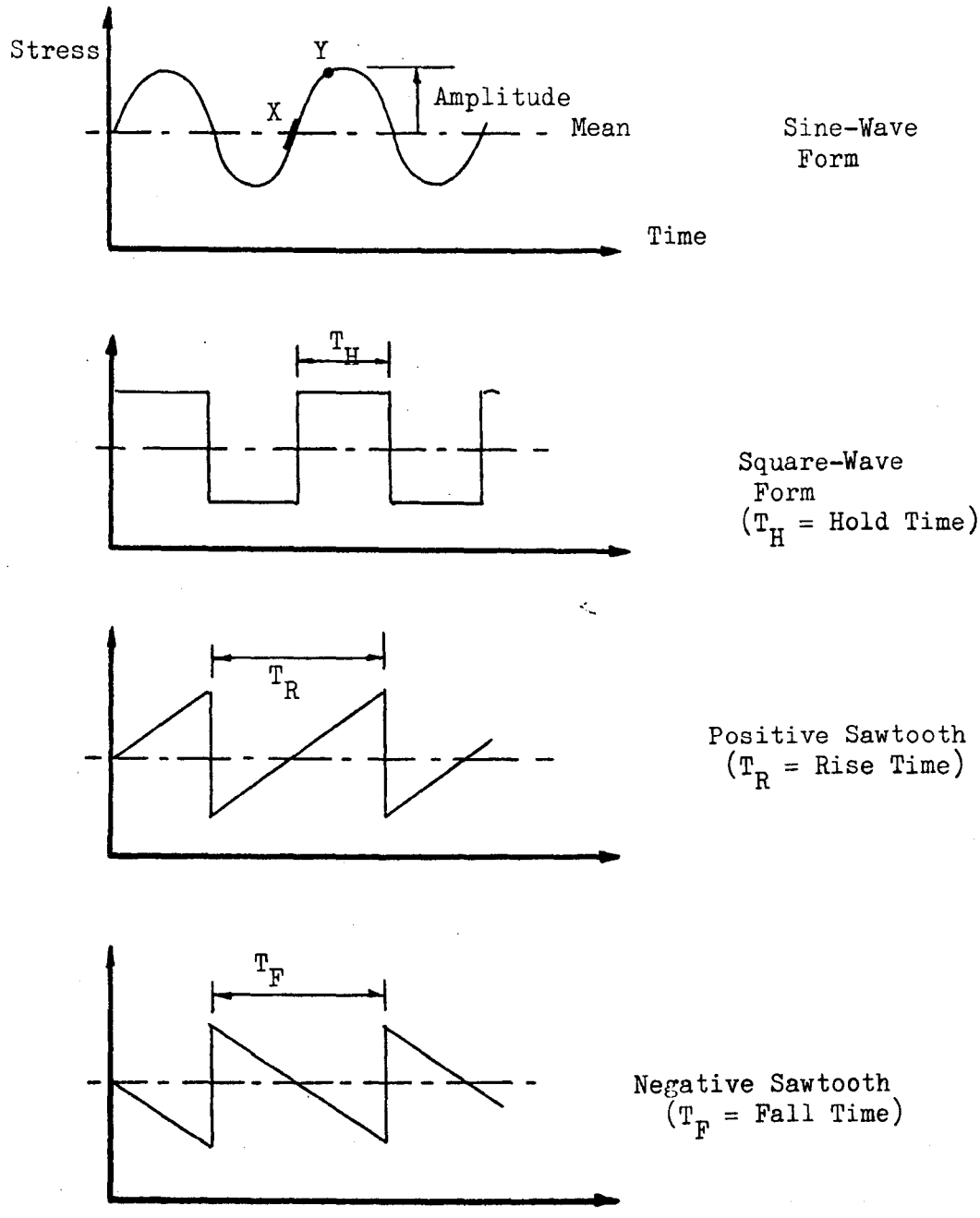

Figure R.7 some idealized approximations to possible wave-form shapes

X is the position of maximum strain rate for the cyclic load. During crack growth cleavage is terminated at position Y by plastic

deformation. Strain rate is an important variable for initiation and crack growth phenomena, and because wave-form controls strain rate it too must be considered important. Atkinson & Lindley[58], using distilled water at 90°C in the corrosion fatigue of steels, investigated the effect of triangular, square, sinusoidal, trapezoidal, positive and negative sawtooth waveforms, on the crack growth rates at a ΔK of 50 MN $m^{-3/2}$. The square wave or negative sawtooth loading at 0.1 Hz reduced the fatigue crack growth rate almost to the level observed in air. Triangular and positive sawtooth waveforms with the same rise times (over a range of frequency 0.001 - 10 Hz) lead to the same environmental enhancement of fatigue crack growth rate, although the cycle time of course differs by a factor of 2. These results suggest that, in this instance, hold time effect if any is similar to that of fall (square wave versus negative sawtooth). Most significant, however, is the result showing that rise time (or strain rate) is a prime variable for crack growth instead of frequency. The environmental component of crack growth was found to be primarily controlled by mechanical rise time and not the total cycle time, provided hold times at K_{max} were short. Longer hold times at K_{max} caused a reduction in fatigue crack growth. All waveforms produced results within a general scatterband for $(\frac{da}{dN})$, when plotted against rise time, showing a small environmental enhancement of growth rate at very slow rise times and at very fast rise times. A peak result, at approximately 40 seconds rise time (corresponding to a rate of increase of stress intensity $(\dot{K})$ of 1.3 MN $m^{-3/2}$ per second), was found in this research. It seems therefore that a critical rate of increase of stress intensity $\dot{K}$ might be a generally important variable controlled by waveform and frequency.

2.4.6 Frequency

Corrosion is a time-dependent process so that frequency is obviously a prime variable for corrosion fatigue. Stress cycles of low frequency are individually more damaging than similar ones of high frequency, because the former present a longer time per cycle during which conjoint action can take place. The early work of McAdam (reviewed by Gough[59]) expressed the complex correlation of frequency, stress, time and damage by a series of curves for specific metal/environment combinations. Frequency has been found to be important to initiation processes as well as to propagation of cracks in more recent research. James[60], for example, finds that the decreasing of frequency for stainless (type 304) steels results in a significant increase in the fatigue-crack growth rate ($^{da}/_{dN}$). Smith & Hughes[61] find that, from stainless steel (type 316) in 0.17m saline, the total life fatigue strength is almost independent of frequency up to 60 Hz. It is anticipated that the fatigue strength in saline would approach the air value at higher frequencies. Jordan[62] conducted rotating bending corrosion fatigue tests at frequencies of 1 - 80 Hz and compared these results, for titanium and stainless steel alloys, with those obtained for an Amsler Vibrophore 100 Hz test. Even allowing for the difference usually found between rotating beam and push-pull fatigue tests, Jordan was surprised at the high 10^7 cycle endurance limit obtained for stainless steel bar compared with the results obtained from the Amsler tests. For the range tested endurance limits in air were constant with frequency for each alloy. Tests in 0.17 m saline solution however showed some variation of endurance limit with frequency: stainless steel showed a slight increase in endurance limit with frequency,

titanium (T318) showed a slight decrease and titanium (T160) remained constant. Luther & Williams[63], investigating the shape of the S/N curve of a ferritic steel, obtained results which showed fatigue limits in air for both R = o and R = -1 tests are raised by approximately 24% when the frequency is increased from 50 to 100 H in axial loading. They also discovered no such improvement in fatigue resistance under rotating cantilever testing for a comparable increase in frequency of testing. The onset of strain ageing at the higher frequency for the axial loadings was established as an explanation of these results. Forsyth[64] reports that at very low frequencies (in the region of 0.3 H) for aluminium, normal stage II cracks become intergranular instead of the normal transgranular mode. He asks the question whether corrosion fatigue ceases at such low frequencies and is replaced by another failure mechanism such as stress corrosion cracking. Ryder and Lynch[65], reviewing the effect of environment and frequency on the fatigue of some aluminium alloys, report that stage II crack growth rates for corrosion fatigue are markedly increased at low frequencies for the low stress intensity ranges. They also examined the effect of frequency on stage I growth and found the direct opposite effect to those observed for stage II. In particular, it was found that salt solutions were less damaging to stage I growth at low freqancies than at 10 H . Strain rate sensitivity, over the frequency range tested, was ruled out as an explanation of this result. The increase in stage II crack growth rates with decrease in frequency was thought to be only partly an environmental effect: an "inherent frequency effect" was concluded to operate. Generally, it seems that the effect of frequency alone is difficult to assess since frequency is indirectly the cause of changes in the effect of many other variables. Mechanical pumping of a fluid environment within

a crack, for example, is an environmental variable possibly controlled by frequency in phase with stress intensity.

2.5 Which Metallurgical Variables?

2.5.1. Microstructure

Microstructure has been found to have very little influence on the fatigue crack growth rates in steels during stage II [53]. Failure generally occurs by a transgranular ductile striation mechanism in steels [66, 67], and striation advancement of cracks in stage II generally is not dependent upon the microstructure[68]. At the higher growth rates, where K_{max} approaches K_{1c}, microstructure does however become important since the striation type crack growth no longer operates. In this region, static type fracture modes such as cleavage, intergranular, and fibrous fracture, have been observed [53, 68]. Crack initiation, near threshold and stage I type crack growth rates are strongly influenced by microstructure[69-73]. The threshold region has been termed "microstructurally sensitive" [70, 74], and work so far has not provided a clear understanding of which microstructures provide the best near threshold growth resistance. For steels [72] and titanium alloys [70], near threshold crack growth rates have been reduced by increasing the grain size. Yet increasing grain size decreases the fatigue limit of steels and the life at a given stress amplitude[75]. Aluminium and copper large grained specimens have been found to have a relatively shorter life to initiation than finer grained specimens[76]: cracks nucleated earlier at the grain boundaries for the large grained specimens. Generally total life decreases with increasing grain size, although the opposite result is occasionally found[77]. Also some small grain size steels

are known to be more notch-sensitive[78]. High local stress concentrations occur with mechanical notches of small root radii, and it seems that small grains can cause similar high local stress concentrations in certain cases. The effect of grain size is difficult to assess from much of the past research owing to heat treatment variations required to produce the different grain sizes. The structure of the grain boundary and its immediate vicinity is simultaneously changed with size of grain, which could also affect resistance to both crack initiation and propagation. For example[77], Nimonic 80A solutionized at 1975 F and aged at 1290 F to produce small grains has been found to contain $Cr_7 C_3$ in the grain boundaries: this is not found in the grain boundaries after a 2190 F solutionizing and the same aging treatment to produce large grains. Additional research is required to separate the effect of grain size from the concomitant changes in grain boundary structure. It is also not yet clear what effect grain size has on each stage of the fatigue process, other than on stage II where it is considered unimportant.

2.5.2 Mechanical Properties

Higher threshold values for crack growth were obtained in low strength steels by decreasing the yield strength[69, 72]. Strength as well as scale of microstructure are likely to be important variables in the vicinity of threshold. Stage II crack growth, apart from showing little influence of microstructure, also appears to be independent of mechanical properties such as tensile strength and toughness[79]. Large structures, containing crack-like flaws, have virtually the whole of their fatigue life occupied by stage II crack growth. Fatigue strength of the material from which such structures

are made is therefore determined by the crack growth characteristics. Since these characteristics are largely mechanical in nature, stage II crack growth is independent of material strength. The use of higher strength steels with higher design working stresses would result in increased probability of fatigue failure for this reason, even excluding environmental effects for the time being. Toughness is simply strength in the presence of a crack, so that metallurgical techniques for producing stronger materials by inhibiting plastic flow cannot result in a tougher material. Inhibiting plastic flow at a crack tip will not improve resistance to fatigue. Optimum resistance is obtained for the higher crack growth rates, which again become sensitive to microstructure, with high-toughness materials. Near-threshold crack growth rates were observed by Ritchie[79] as the strength of steel was reduced. He found the value of K_o to be inversely related to the 'cyclic yield strength'. When annealed metals are cycled, in the plastic region, either between fixed stress limits or strain limits, they usually harden[80, 81]. Cold worked metals, however, usually soften when subjected to such cycling conditions. Low carbon steel in the annealed condition has also been found to soften [75] during the first stages of fatigue, by the formation of free dislocations in expanding zones in which plastic strain occurs. Figure R.8 schematically illustrates the process of cyclic hardening (a) and the process of cyclic softening (b), both under conditions of strain control. In the case of pure metals, hardening (i.e. decrease of strain amplitude or, as illustrated in Figure R.8, increase of stress amplitude at constant strain controlled amplitude) is usual. Under strain

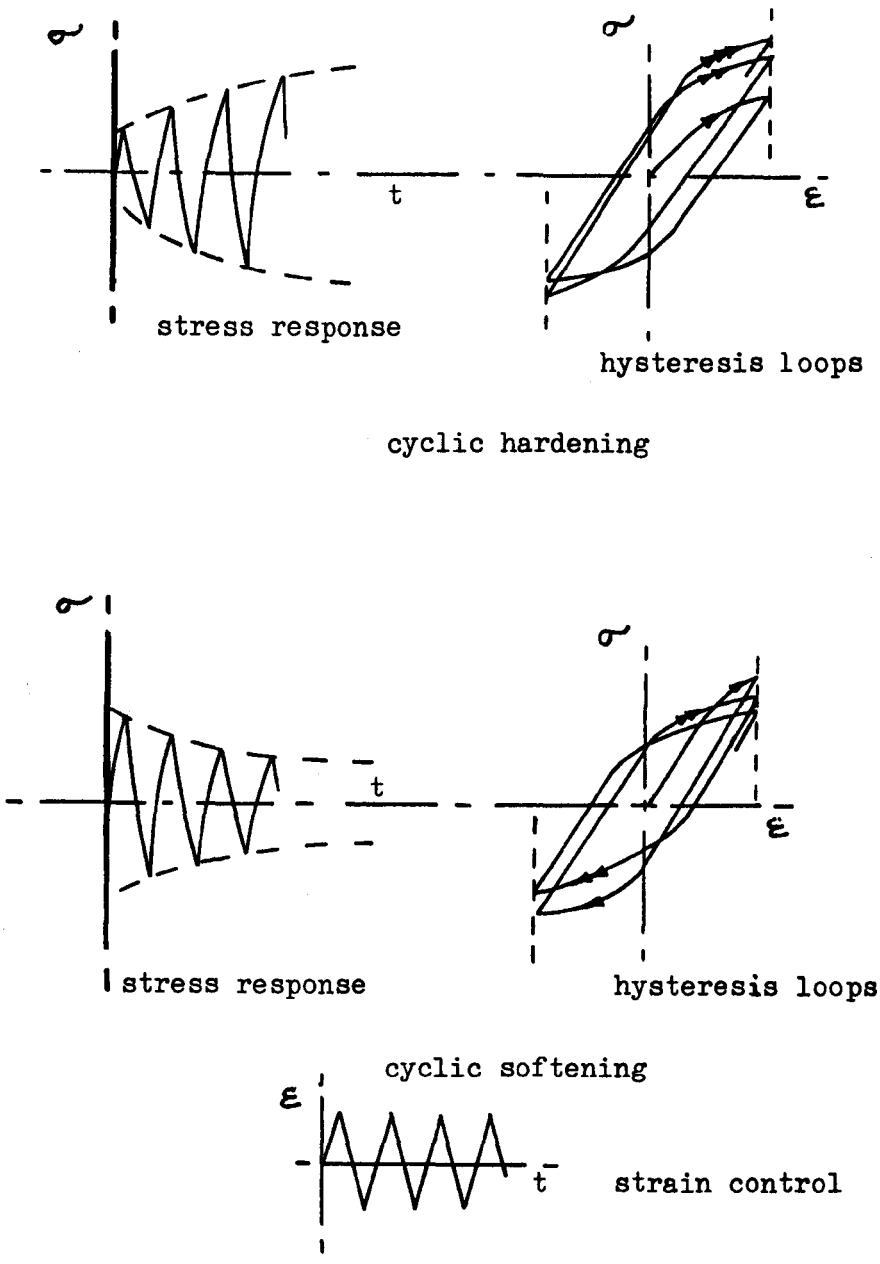

Figure R.8 Schematic representation of the response of metals to reversed strains.

control, stress concentrations within a structure would thus be increased if the material cyclicly hardens or would decrease if the material cyclicly softens. It is important to note also that stress adjustments take place early in life

(first few cycles shown in Figure R.8) so that the stress amplitude becomes constant over most of the fatigue life under strain control. During high-stress fatigue copper hardens at a rate dependent on the orientation of single crystals[82]; at low stress fatigue the influence of crystal orientation disappears and the hardening rate is the same for both single crystals and polycrystals. Mono-and polycrystalline specimens of aluminium[83] at low stress amplitudes also have the same hardening rate. Copper crystals nucleate cracks, in regions of strain concentration, when the matrix structure becomes unstable after initial cyclic strain hardening. Cyclic strain softening has been found to occur locally in P.S.B.'s, after initial hardening, so that these bands are softer than the matrix[84].

2.5.3 Lattice Structure

Mild steels with distinct yield points[85-87] and pure body centred cubic structure (bcc) metals like molybdenum[88] and iron[89] exhibit a net softening at low strain amplitudes, and a net hardening at high strain amplitudes. At low strain amplitudes first softening and then hardening occurs[87]. The intrinsic fatigue strength limit in bcc metals should be higher than in other structures such as face centred cubic (fcc) or hexagonal Peierls stress (or lattice friction stress).[90] Owing to difficulties of separating out the effects of interstitial impurities this is hard to demonstrate in practice. Slip bands exhibit differences in appearance between structure and hexagonal metals introduce complications in that twinning and also grain boundary cracking could occur. There is less

fatigue data available for metals having hcp structures but it is known that slip is confined almost entirely to basal planes for many and that cross slip is difficult. Slip band extrusion has been found to occur in cadmium and magnesium but not in zinc[91]. Lattice structure is a basic variable which defines dislocation mobility. For example, cleavage (a fast mechanical fracture along well-defined crystallographic planes) occurs in materials with low dislocation mobility such as bcc and hcp structures. In these structures, a fast propagating crack can outrun dislocation movement to the crack tip and thereby remain sharp. This effect results in the common cleavage type failure observed for bcc and hcp structures, especially at high strain rates. Lattice spacing and crack growth rates have been studied. It is common practice to relate propagation rates to lattice spacing. Ritchie[79], for example, concludes that if propagation rates become less than a lattice spacing per cycle then growth is not occuring uniformly over the entire crack front.

2.5.4 Impurities

Working on "impurity-induced embrittlement during heat treatment" specimens, which were then subjected to fatigue, Ritchie[79] also found increased near-threshold crack-growth rates and significantly lower thresholds. When inclusions were present, Boettner et al[76] found these to be the primary sites for crack initiation for aluminium and copper. It has also been found, at short endurances, that stronger materials initiated cracks from inclusions rather than from slip bands. Two general properties of ductile metals which are responsible for fatigue behaviour are clearly their structural inhomogeneities

and their capacity for slip and strain hardening. Gell et al[77], reviewing the role of defects, concludes that crack initiation and propagation resistance, to a lesser extent, can be improved by removal of the defect or a reduction in its size. They also conclude that this may be accomplished in a given material by alloying, casting, or heat treatment modifications depending on the type of defect. Where crack initiation along annealing twin boundaries is the limiting factor, the density and length of the twins can be controlled by the amount of deformation prior to recrystallization and by the grain size, respectively. Twins can be avoided by using cast materials, and brittle phase cracking may be eliminated by better fabrication or surface-finish practices. High cycle fatigue is most likely to benefit from reduced defects of structure, since in both wrought and cast materials growth of a crack is usually from a single dominant defect.

2.5.5 Coldwork and Surface Treatment

Kramer[92] has shown that during cyclic hardening, the surface plastic resistance of materials is increased.

The material properties of the surface layer are therefore important metallurgical variables to be considered apart from the obvious environmental factors. Commercial alloys, frequently strengthened by cold work and/or surface treatments producing residual compressive stresses (see mechanical variables), are common. The dislocation substructures introduced by cold working are however generally unstable so that appreciable softening occurs.

The cyclic stress-strain behaviour and changes in dislocation structures for cold-worked materials has received considerable attention[93-96]. In low-strength single-phase

metals and alloys, good fatigue properties have been associated with a planar slip character and a high degree of slip dispersal[97-99]. Slip dispersal has been achieved by increasing the number of active slip nucleating sites and the cyclic strain hardening rate[100]. This was made possible by the introduction of a finely spaced, hard, incoherent dispersoid at the surface or throughout the volume of the material. Dispersal of slip in surface grains is helped by surface working treatments. Surface treatments such as short-peening, glass bead blasting, and nitriding have been found effective over many years in low stress, long life fatigue where crack initiation is a significant fraction of total life. Residual compressive stresses (as discussed in section 2.4.4) as well as beneficial changes in surface structure being responsible for the improved performance resulting from these hardening processes. Coating the surface with a soft layer, as in aluminium cladding, has been shown to be detrimental to fatigue resistance[64].

Alloying, heat treatment, and cyclic work hardening can also effect a change in slip dispersal by changing the density, size, and location of hard second-phase particles. Some materials, for example copper, exhibit a 'wavy' mode slip. A 70/30 brass is an alloy found to exhibit planar slip and if this can possibly be changed to that of the wavy mode, an improvement in fatigue properties would result[77]. Materials which have a wavy slip mode show a unique cyclic stress-strain curve and a unique saturation dislocation structure has been found irrespective of prior history. This explains why cold work has virtually no effect on fatigue life behaviour at high amplitudes[101, 95]. Materials having a planar slip-mode have such a marked softening, during high amplitude load

cycling, that little effect of cold work on fatigue life is observed for these materials either[101]. At long lives, the effect of macroscopic softening is however small and cold working should have a considerable effect: in practice a small improvement in fatigue strength relative to tensile strength is usually found, but not so great an effect as might be expected[88]. Steels, for example, cold-worked by drawing or rolling have long been known to show improved fatigue strength, but not to the same extent as the improvement in the tensile strength[102, 103]. During aqueous corrosion fatigue of steel the rate of solution is usually increased by cold work[34] which is an environmental factor, changed by this metallurgical variable, often responsible for shortened life. However, in aerated salt solutions the rate of solution is not increased by cold work, since attack is largely controlled by the supply of oxygen[34]. For steels the pH of a solution generally has to be below four before the effect of cold work becomes appreciable[34]. More recent studies[88], on low amplitude fatigue dislocation structures in cold worked pure metals, revealed large dislocation-free regions about 10μm in extent after fatigue at various percentages of life. Yet prior to fatigue, after cold working, a uniformly dense dislocation cell structure of about 0.5μm diameter was present. The dislocation-free or softened areas, present only after load cycling, had little or no effect on bulk softening measurements. Because these areas also developed early in life, the long-life fatigue resistance was not increased by cold working to the extent expected. It seems therefore, from this work and the other limited data available, that cold work does generally increase long-life

fatigue resistance but that this effect is related to the initiation stages only. Cold work has very little effect on crack growth rates[104], owing to appreciable softening of material at the high-strain crack-tip region.

Surface coatings, deposited during component manufacture, for corrosion protection and/or improved fatigue performance have proved useful. For example, the fatigue limit of steel can be changed by chromium or nickel plating[105]. Such coatings are an obvious complication to the problem of isolating the variables of corrosion fatigue and will not be reviewed in any detail here. Suffice it to say that the possibility of either crack initiation in the base metal at the metal/coating interface, or alternatively, crack initiation in the coating at the coating/environment interface exist in such cases. Additional variables such as adhesion strength of coating, residual stresses in coatings, and the relative strength of coating and the base metal, determine initiation behaviour[105].

2.5.6 Surface Finish and Surface Films

The condition of a metal alloy surface has been understood for many years to be of prime importance for fatigue resistance. Corrosion fatigue studies have as the focus of attention a metal/environment interface. The single most important metallurgical variable is therefore likely to be that of surface finish. In addition, whenever surface films are present, environmental variables are probably impossible to separate in effect from metallurgical ones. Owing to the varying nature of the mechanical, chemical and electrochemical properties of films, they can have an influence on the behaviour of the entire metal alloy structure that is out of proportion

to their volume fraction. The nucleation of fatigue cracks during corrosion fatigue is strongly influenced by surface films and surface films in turn are influenced by the surface finish. Surface finish embraces not only the topography of a surface but also its mechanical, metallurgical, and environmental factors, relative to the properties of the bulk material and relative to the local environment. Surface finish properties, because of such factors, are time-dependent. Steel abraded with emery, annealed in vacuo and again abraded, is attacked in acid solutions 30% more quickly than steel on which the final abrasion is omitted[34]. The increased reactivity of a freshly deformed surface is now well established. Mechanical polishing also often alters the chemical composition of the oxide film formed on a metal[106]. Chemical analysis of films stripped from 18/8 stainless steel have shown, for example, a marked enrichment of chromium in the film compared with that in the underlying metal[106]. Chromium enrichment of the film has been shown to increase with mechanical polishing up to a maximum of 80% chromium, the balance being mainly ferric oxide. No enrichment of nickel was observed but the film thickness increased with mechanical polishing. Electrode potential measurements of 18/8 stainless steel specimens immersed in sodium chloride solutions confirmed also that polishing with alumina yielded a less passive surface than polishing with chromic acid[106]. When alumina was used for the final polishing it appeared in the film and the enrichment of chromium was less. The use of chromic acid as a polishing agent did not affect the content of chromic oxide in the film. Too much attention can be given to the topography of surface finish and insufficient thought given to the other resultant

factors. The metallurgical condition of the surface layers resulting from the method of specimen preparation is too easily forgotten. A roughly finished surface might be associated with a deeply disturbed surface layer, and a fine finish with less disturbance, but this is not necessarily the case. For example, a subsequent fine finish operation following a rough one might smooth the surface without appreciably reducing the thickness of the disturbed layer. Surface scratches, particularly those running perpendicular to the direction of applied tensile stress, can be responsible for experimental scatter of results owing the the notch effect. Small surface imperfections may also cause scatter of results if the surface is otherwise too smooth: the notch effect of the imperfection in this case is far less on a rougher surface! For experimental accuracy it would be far better to have a uniformly disturbed surface and a uniformly produced surface finish. Electrolytic polishing often produces a disappointing accuracy of results because although it removes surface scratches it may also introduce pits. The net effect of electropolishing is to lower the fatigue strength of the material below that obtained with mechanical finished surfaces[107]. Fatigue strength is enhanced by the disturbed layer but if this layer is not uniformly thick scatter of results can be greater than that obtained with electropolishing[107]. Cold-rolled bright mild steel has been fatigued in air and in distilled water while the following surface finish preparations were compared[108]: degreasing only (carbon tetrachloride and acetone); mechanical abrasion and degreasing (to 1 micron); electropolish (20V, 4A, in 133 cc acetic acid with 20 cc water and 25 g chromic acid); oxide film growth and degrease (400°C for three hours or 250°C for one hour). The results of this work showed that the

corrosion fatigue life was longest for the 'degreased-only' treatment. Electropolishing markedly reduced life, and the life of the 'oxide-film-treatment' specimens was somewhere between the electropolishing result and the 'degrease-only' result: 400°C for three hours being a better treatment than 250°C for one hour[108]. The removal of beneficial compressive stresses from the original cold-rolling process was thought to account for these results, especially since 'mechanical-abrasion prepared' specimens also had a slightly shorter life than those specimens which were 'degreased-only'. The 'degreased-only' treatment of specimens also produced the more precise results. It seems, from this work[108], that the best surface preparation sometimes can be the least preparation! From a practical point of view, therefore, the surface of the test specimen should be identical with the surface of the actual service component. This is usually, though not always, impossible because the surfaces of large commercial metal alloy components vary as produced and as fabricated. Film formation on components depends on the practical environment which is not always easily reproduced in the laboratory. A "standard" clean metal surface condition is usually created on specimens for laboratory tests and the results sometimes call for 'experience in the field' when interpretation to real-life situations is required. For example, is the test specimen result from an electropolished surface, producing on a microscale a structure which is not representative of the state of affairs on the surface of the component, conservative or otherwise? For small components of simple geometry it can be much easier to simulate practical conditions for laboratory testing than for larger structures. Test specimen surface

finish preparation should logically therefore be either such as to truly represent that of the component, or alternatively, it should be of a standard conducive to precise results.

2.6 Which Environmental Variables?

2.6.1 Type and General Effect of Environment

A considerable amount of evidence exists, as discussed in section 2.1.2 and reviewed in the literature[109], to show that fatigue life is shortened by chemically aggresive environments. Materials which normally show a fatigue limit in mild or neutral environments, e.g. Fig R.1 curve (a), often show no such limit in more aggressive environments, e.g. Fig R.1 curve (b). Fatigue results from tests in a vacuum generally indicate best resistance to fatigue. The effect of environment is usually most marked at low stress intensities and at low test frequencies: an observation consistent with a time-dependent process. Stage II crack growth rates in steels and aluminium alloys are increased by chemically aggressive environments[49, 110-112]. Stage I cracks in aluminium-zinc-magnesium alloys have also been found to have enhanced growth rates in aggressive environments[65]. All stages of initiation and crack growth are in general likely to be affected by the environment[109] and the question remains: what is an aggressive environment for a particular metal or alloy? Environments have been classified at NEL [113-115], for the purpose of studying crack growth behaviour, according to their effect.

(i) "Neutral" - those which have little or no effect on the basic deformation process of fatigue crack growth; crack growth rates at the threshold are approximately one lattice spacing per cycle.

(ii) "Inert" - those which retard crack growth by allowing some rebonding of freshly created surfaces; crack growth rates at the threshold tend to be greater than one lattice spacing per cycle.

(iii) "Corrosive" - those which accelerate crack growth by chemical action at the crack tip; the threshold can be drastically reduced, possibly corresponding to crack growth rates very much less than one lattice spacing per cycle, and time-dependent effects appear, so that test frequency becomes significant.

During initiation, surface variables can produce the same effects in corrosion fatigue as they would for stressless corrosion. Of the many possible forms of corrosive attack on unstressed materials which have in general to be considered, the following discussion in this work will be limited to corrosion in aqueous NaCl solutions. Reference will also be made to the atmospheric corrosion resistant properties of materials in judging the relative effect of other environments. Aqueous corrosion fatigue involves the same variables as aqueous corrosion but the effect of each will in general be modified by the application of a load cycle. These variables will affect the interaction, chemically and electrochemically, between the metal alloy surface and the bulk environment via interface films.

Reactions occur in aqueous systems which can, for instance, result in the dissolution of the metal, the adsorption on the metal surface of atoms or molecules from the electrolyte, adsorption into the metal of species initially adsorbed on the surface, and the formation of solid films at the metal electrolyte interface. Aqueous corrosion is an electrochemical process and certain areas of the metal alloy surface are anodic to adjacent areas. For example, iron corroding in water will have metal ions passing into solution

at the anodes according to the reaction

$$Fe \rightarrow Fe^{++} + 2e$$

The principal corresponding reaction

$$H_2O + \tfrac{1}{2}O_2 + 2e \rightarrow 2OH^-$$

will be occuring at the cathodic areas on the surface. Since the cathodic reaction requires oxygen, those parts of the surface which are more accessible to oxygen will become cathodes. The availability of oxygen is an important variable in this case: if uniformly supplied to the metal surface, anodic and cathodic areas will be equally uniformly distributed so that uniform dissolution of metal is encouraged. In general, metallurgical inhomogeneities such as inclusions or plastically worked material, as discussed in Section 2.5.4-6, can also cause anode and cathode formation. Differences of chemical reactivity between different areas on the surface can produce localized attack. A uniform metal surface structure and a uniform environment encourage uniform dissolution in unstressed metal. Localized attack can result also from localized stress concentrations and geometric variables in fatigue.

The initial metal/environment interface becomes modified, often very rapidly, by the oxidation of metal. The corrosion products may in some cases form a barrier at the interface so that, as the oxide film thickens, ions and electrons have increasing difficulty in passing through the barrier: corrosion in such cases is stifled. On the other hand, as exemplified above for iron, a barrier may not be produced at the interface. The reaction of anodically produced ferrous ions with cathodically produced hydroxyl ions takes place in the bulk of the solution initially to form ferrous hydroxide $Fe(OH)_2$, before oxidation to a

higher valency state, $Fe_2O_3.H_2O$: since this occurs away from the metal alloy surface there is no possibility of corrosion being stifled in this case.

2.6.2 Damaging Species

Mild steel has been fatigued in various solutions at various concentrations[116-118]. Below 0.025M concentration, KCl solutions have been found to have the same effect as distilled water during fatigue. Also, concentrations within the range 0.025M to 2M produced the same corrosion fatigue life. The damaging species has here a critical concentration, below which it has no effect and above which its effect is unchanged by further increases in concentration. The most commonly occuring damaging species in practice for steels is the chloride ion. Immersion in 3% NaCl can dramatically reduce ΔK_c[119]. The damage ratio, as measured by 10^7 cycle endurance life stress divided by the fatigue limit in air, has been established for mild steel[120] at 24Hz as 0.57 in well water. In river water, having about one-sixth the salinity of sea water, the damage ratio was reduced to only 0.2 . Salt solutions are also damaging to aluminium alloys[65]. An increased rate of stage I crack growth results from the presence of chloride ions, yet surprisingly salt solutions are much less damaging in this case at very low frequencies than at 10 Hz and above. This effect, is directly opposite to that found for stage II crack growth. Geometric effects as cracks extend could, by concomitant changes in local environment, be responsible for this change in environmental effect between stage I and stage II crack growth.

In general since corrosion fatigue is caused by any

species which causes corrosion in stress-free material, no ion type specific to fatigue is necessary for the conjoint process. It is this observation, apart from the cyclic nature of the stress, which distinguishes corrosion fatigue from either intergranular or transgranular stress corrosion where a specific ion type is certainly required. Solutions which are generally chemically aggressive are also more effective in reducing fatigue life than water. The intensity of attack can increase with the concentration of the solution. However, a limit may be set to this attack because the solubility of air decreases with increasing concentration of the solution, and oxygen is required for most corrosion fatigue processes. The importance of oxygen has been well established. Hydrogen gas bubbled through NaCl solutions[121] to purge out most of the dissolved oxygen produced far less damaging liquid environments for fatigue. Solutions heated to 96°C to limit the solubility of oxygen[122] also produced longer life fatigue results. The supply of oxygen to the cathodic areas of a material during fatigue is the single most important variable to consider with its effect on possible damaging species. Restriction of oxygen can stifle action[117] or, in other circumstances where chemical solutions of certain concentrations are intended to inhibit corrosion, localized attack at otherwise filmed surfaces may occur as the result of fatigued bare anodic areas.[31] Such inhibitors are more dangerous in use for corrosion fatigue than for simple corrosion protection and the supply of oxygen is a critical variable. During stress-free corrosion, inhibiting ions can retard or even prevent localized pitting attack. The concentration of such

inhibiting ions as OH^-, NO_3^-, and SO_4^- to retard pitting depends on the concentration of aggressive ions, such as the halides, in solution. Sometimes inhibitors are effective even under corrosion fatigue conditions.

Sodium dichromate at 200 ppm, restores the fatigue limit of 0.35% carbon steel immersed in water with 25 ppm each of sodium chloride and sodium sulphate[120]. At stresses above the fatigue limit a longer life is obtained using this inhibitor than for the steel in air. No such protection is obtained with this inhibitor when the supply of oxygen to any part of the surface is restricted so that localized corrosion is induced.

The normal air fatigue limit can be regained in mild steel for completely deaerated water or 3% Na Cl solution[123]. This shows that adsorbed water alone is not harmful to fatigue life of mild steel below the fatigue limit: it also shows that the chloride ion does not affect the fatigue limit unless accompanied by the presence of oxygen. The presence of the chloride ion alone in deaerated solutions is, however, sufficient to lower fatigue life at stress levels above the fatigue limit[123]. During the fatigue of a quenched and tempered 1035 type steel in 5% Na Cl solutions it has been found that hydrogen sulphide is not particularly damaging in the absence of air[124]. Carbon dioxide, however, was found equally damaging in the presence or in the absence of air for this steel[124]. Mild steel fatigued in aerated 3% Na Cl solution shows almost immediate formation of intrusions and extrusions at the surface without prior formation of pits[123]. Corrosion pitting in 13 Cr steel is associated with crack initiation even in the most

dilute aerated solutions of NaCl[125]. The size of pits from which cracks originate are found here to be of the order of 1μm and to increase in size considerably as the concentration of NaCl is increased[125]. Halides generally cause pitting corrosion of high alloy chromium and chromium-nickel steels[125,126]. Of the group of halogens the chloride ion is most frequently found in practice and concentrations of 3×10^{-4}M are critical for these steels[125, 126]. The chemical and electrochemical reactions in a pit are described as working active-passive cell reactions[126-128]. The cell exists, as shown in Fig. R.9, as the result of aeration differences or chloride penetration through the passive layer formed on these steels. The base of the pit is enriched with halide and relatively starved of an oxidising agent for the repassivation process. The area of surface metal around the pit is relatively well supplied with oxygen and becomes the cathode while the base of the pit dissolves anodically. Concentration of damaging species near the base of a pit or tip of a crack are likely to be quite different therefore from that in the bulk solution. Dissolution at the base of a pit (Fig. R.9) causes migration of chloride to the pit site, which in turn produces increased dissolution: the process is thus self-stimulating, or autocatalytic[127]. It is well established that[126-128] metals susceptible to pitting have increased dissolution rates in the presence of chloride, whereas some metals, e.g. some titanium alloys, resistant to pitting corrosion are largely unaffected by chloride ion concentration. Further discussion on mechanisms of pitting and application to fatigue are left for section 2.7. This section is concerned only with the observed effect of this

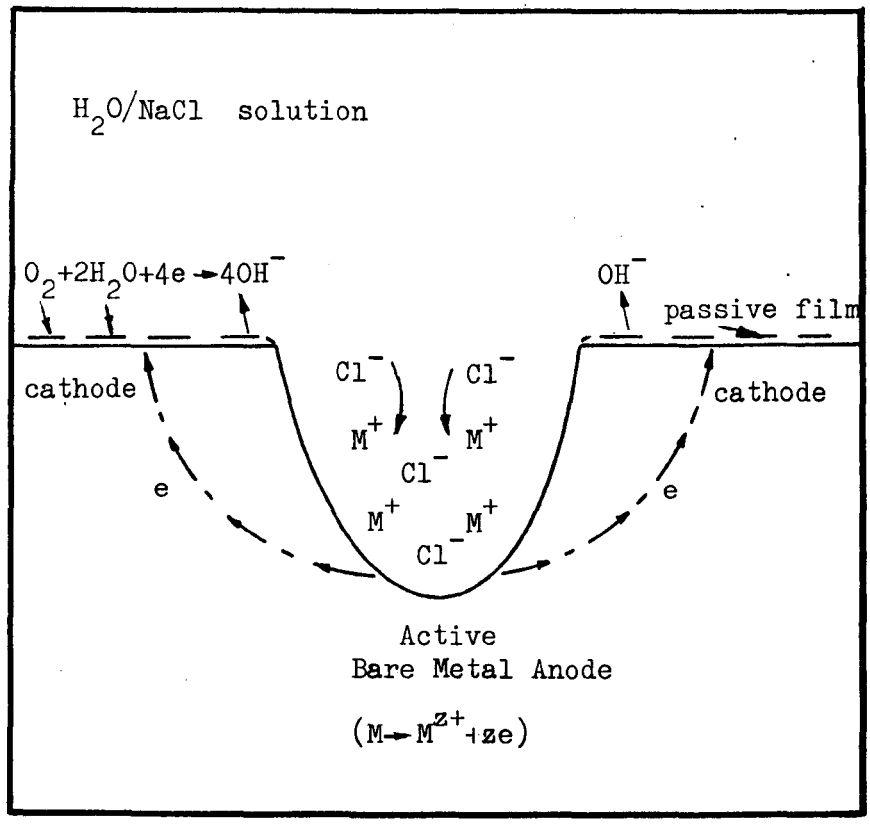

Figure R.9 Schematic illustration of a growing pit

damaging species as a variable in fatigue. Titanium 8 Al - 1 Mo - 1V alloy has been found to form a monolayer of passive oxide film, preventing the alloy from further attack, in less than 5 ms in 1N $NaNO_3$ solutions. The time taken for a similar monolayer of oxide in 1N NaCl solutions was however found to be in excess of 38 ms[129]. The chloride ion was in this case more damaging than the nitrate. During fatigue the effect of the chloride ion is often found to be alloy-composition or frequency dependent. Ti-6Al-4V, Ti-6Al-3V-1Mo, Ti-6Al-6V-

2Sn-1Cu-0.5 Fe, Ti-7Al-2.5Mo alloys have no degradation in fatigue crack propagation resistance in 3.5% salt water environment at 0.08 Hz[130]. Ti-7Al-2Cu-1Ta alloy however is quite markedly degraded by chloride ions during fatigue[130]. For Ti-6Al-6V-2Sn and Ti-6Al-4V alloys, owing to the increasing ability to form a passive film at the crack tip, crack growth rates decrease with decreasing frequency in solutions containing chloride or bromide ions[131]. A transition stress intensity ΔK is also found, above which corrosion fatigue crack growth is increased with decreasing frequency. This reversal in frequency effect is the result of stress corrosion cracking at the higher stress intensities in the presence of chloride or bromide ions[131]. The addition of Na_2SO_4 with these alloys produced frequency independent behaviour, yet in distilled water crack growth rates increase with decreasing frequency. It is very apparent from all these results that damaging species cannot be easily isolated in their effect. They are variables which are often dependent on many other mechanical, metallurgical, and environmental variables for resultant action.

2.6.3 Temperature, Velocity, Viscosity and Volume Ratio

The influence of temperature on corrosion fatigue processes has been investigated by several researchers and the results have often been at variance with previous work. It seems that the differences in material tested and the method of testing as well as the specific environment may explain the differences in results obtained. For example, mild steel at 55 MN/m^2 stress amplitude with an artificial sea water drip environment has been tested at 15, 25, 35 and 45°C[117].

Compared with 15°C, a 24% reduction in 10^7 endurance stress was found at 45°C but only a 3% difference at 25°C. The increasing temperature was more damaging here, although within temperate climatic ranges the effect is small. The same tests in air showed no appreciable effect even at 45°C[117]. Another test, at low and moderate stress amplitudes, on steel wires immersed in 0.1 M NaCl has produced somewhat different results[118]: life was increased slightly by increased temperature from 23°C to 35°C followed by a decrease in life at 50°C to values slightly below the lives obtained at 23°C. At high stress amplitudes there was found to be no change in life at 35°C. but some 11% increase in life was obtained at 50°C. The results of this series of tests[118] were explained at the time as being the balancing result between increased penetration power of the chloride ion with decreased concentration of dissolved oxygen depolarizer as temperature is raised. Drill rod material was also tested in 2.5% NaCl solutions[118] and showed definite improvement in fatigue life at 82°C compared with 27°C. In this case it was thought that improved life was the result of a more uniformly distributed pitting attack at the higher temperature. The pits produced were also much shallower at high temperatures than at lower temperatures so that the ratio of cathodic to anodic areas was higher at lower temperatures. The temperature of the material in the vicinity of a crack tip has been measured, using fine wire thermocouples[132], so that the heat dissipated during the cycling of a low carbon steel could be investigated. Temperature changes in the region of 3°were recorded which varied with frequency of test and stress amplitude. Initial temperature rise occurred with cyclic load, followed by constant readings

and a final increase in temperature near specimen fracture. The difference between the temperature effect variation in aqueous environments and the lack of a temperature effect in air fatigue, up to 45°C, was later suggested[37] to be the result of an environmental cooling effect: crack tips, having a higher local temperature[132], being more effectively cooled by immersion than in drip or spray-type tests. The effect of a large electrolyte to specimen volume ratio is that of a constant temperature heat sink for the metal. Viscosity of electrolyte and relative velocity may also influence this temperature effect.

The main reasons for a temperature effect are likely to be due to the influence of temperature on the activity of damaging species and, for aqueous solutions, the solubility of oxygen. In distilled water, for example, the oxygen content of air-saturated water reduces from 14.16 mg/l at 0°C to 8.11 mg/l at 25°C[133]. The severity of attack by the environment is likely to increase with temperature for fatigue in the same way as chemical corrosion in stress-free materials: however, the effect is also likely to be limited or even reversed owing to reduced solubility of oxygen in aqueous environments with increase of temperature. Fatigue action also results in crack pumping of liquid environments and where the diffusion coefficient is low, mechanical movement by load oscillation could dominate the process of active species supply. Stirring of electrolytes can change the otherwise static situation of diffusion controlled active species transport, to one of relative velocity control. Agitation of the solution

can help to uniformly supply oxygen to the metal surface and also to prevent local heterogeneities in the solution: the tendency if any for local pitting attack is thereby reduced. Liquid environments can assist Stage I growth, perhaps by displacement of fretting debris[134], even when they are essentially inert: the effect is increased with decrease of liquid viscosity and increase of cyclic frequency[65]. These effects of relative velocity and viscosity have not received much attention but are generally thought to be relatively small. A review and list of results obtained for many materials in fatigue at temperatures below and above atmospheric values has been made[135]. Reference to the electrochemical influence of these variables is made in the following sections. For small natural fluctuations in atmospheric temperature, however, the overall effect on fatigue life seems small. For this reason close control of test temperature near atmospheric values has usually been neglected.

2.6.4 Current Density and Potential

The effect of applied cathodic currents has received considerable attention. The early work,[32, 33] discussed in section 2.1.2, was based on the interpretation of the electrochemical contribution to corrosion fatigue by means of Evans-type polarization diagrams (Fig.R4). Fig. R.10 illustrates cathodic protection of a material by suppression of the corrosion current as follows:-

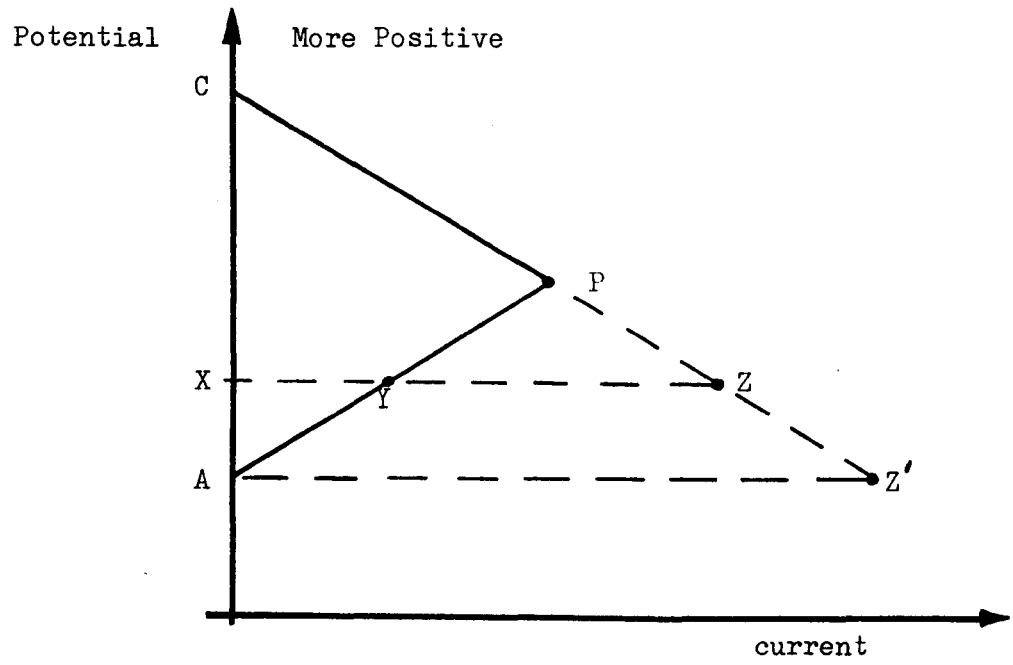

Figure R.10

Schematic Cathodic Polarization

The effect of an applied cathodic current YZ is to depress the cathodic potential below P to a value X corresponding to the position Z. The corrosion current is thus reduced to XY. In the case of the cathodic potential being reduced to the original unpolarized potential of the anode A, the corrosion current is entirely suppressed. In this case the applied cathodic current AZ′ is responsible for the polarization of the cathode exactly to the more negative potential of the anode. The effect of small cathodic currents in neutral K Cl solutions

was found to produce slight decreases in fatigue life[33]. However, as the magnitude of the applied cathodic currents was increased, life was steadily lengthened until a corrosion fatigue limit was established similar to that found in air for steel[33]. With increasing cathodic currents, increased life was accompanied by a decrease in the number of cracks found in the test specimens and a reduction of the amount of iron going into solution. At the limit, when life became infinite, no cracks were found and no iron went into solution. A lower fatigue limit than that obtained in air was established which was a function of applied cathodic current. It was also found that less current was required to establish a fatigue limit at the lower cyclic stress amplitudes than at the higher ones. In acid solutions, where polarization effects are a predominant feature, some improvement in fatigue life was also found with applied cathodic currents[33]: no fatigue limit was found for steel in 0.1 N HCl solution. However, later work has shown a fatigue limit for mild steel in both neutral and acid solutions under cathodic polarization[123, 136]. The protection afforded by applied cathodic currents has been shown to be proportional to current density[137], up to a maximum of 1 amp/cm^2. Anodic currents were also shown to decrease fatigue life to the same extent. Applied currents to materials during corrosion fatigue can thus protect completely in somesolutions and at least certainly modify the fracture process in others.

Further modification of the electrochemical reactions possibly occurs with pH variation and this is discussed in Section 2.6.5. Much of the work in the past has suggested that the greater the cathodic polarization, the better the fatigue resistance. This has been shown not always to be the case,

however, since at potentials where a significant amount of hydrogen is liberated from solution and absorbed by the metal, embrittlement may occur. An optimum value of potential resulting from cathodic polarization for the protection of steel in sea water has been established[138]. It has also been shown that the protection in this case results from inhibition of the initiation stage. Crack propagation rates have sometimes been shown to decrease slightly during cathodic protection and fatigue, but more often than not there is little or no benefit[138]. Δ Ko in brine has a value substantially lower than in air, and yet in brine with cathodic protection ΔKo is slightly higher than in air[139]. A pipe-line X-65 steel (0.16 C) fatigued in tension with 3.5% NaCl solution showed maximum environmental enhancement of fatigue crack growth at the lowest frequencies and at the highest ΔK values. Crack growth rates in this steel were fifty times that of air with cathodic protection at - 1.04 V SCE but only ten times that of air if fatigued at a free corrosion potential of - 0.68 V SCE ($\pm$ 30mV free variation)[140]. Generally it seems that cathodic protection usually enhances life in corrosion fatigue on smooth specimens or small well made components without cracks, but can dangerously increase fatigue crack propagation rates and so shorten life for pre-cracked specimens or large structures containing flaws.

Anodic currents applied to mild steel during fatigue in 3% NaCl result in improved life up to 30μA/cm^2. Between 30 and 300μA/cm^2 fatigue life is constant and at higher anodic currents than 300μA/cm^2 fatigue life is drastically reduced[135]. The anodic behaviour of metals such as 18/8 stainless steels and titanium alloys is somewhat different. Such metals exhibit passivity under certain conditions as schematically illustrated by Figure R.11

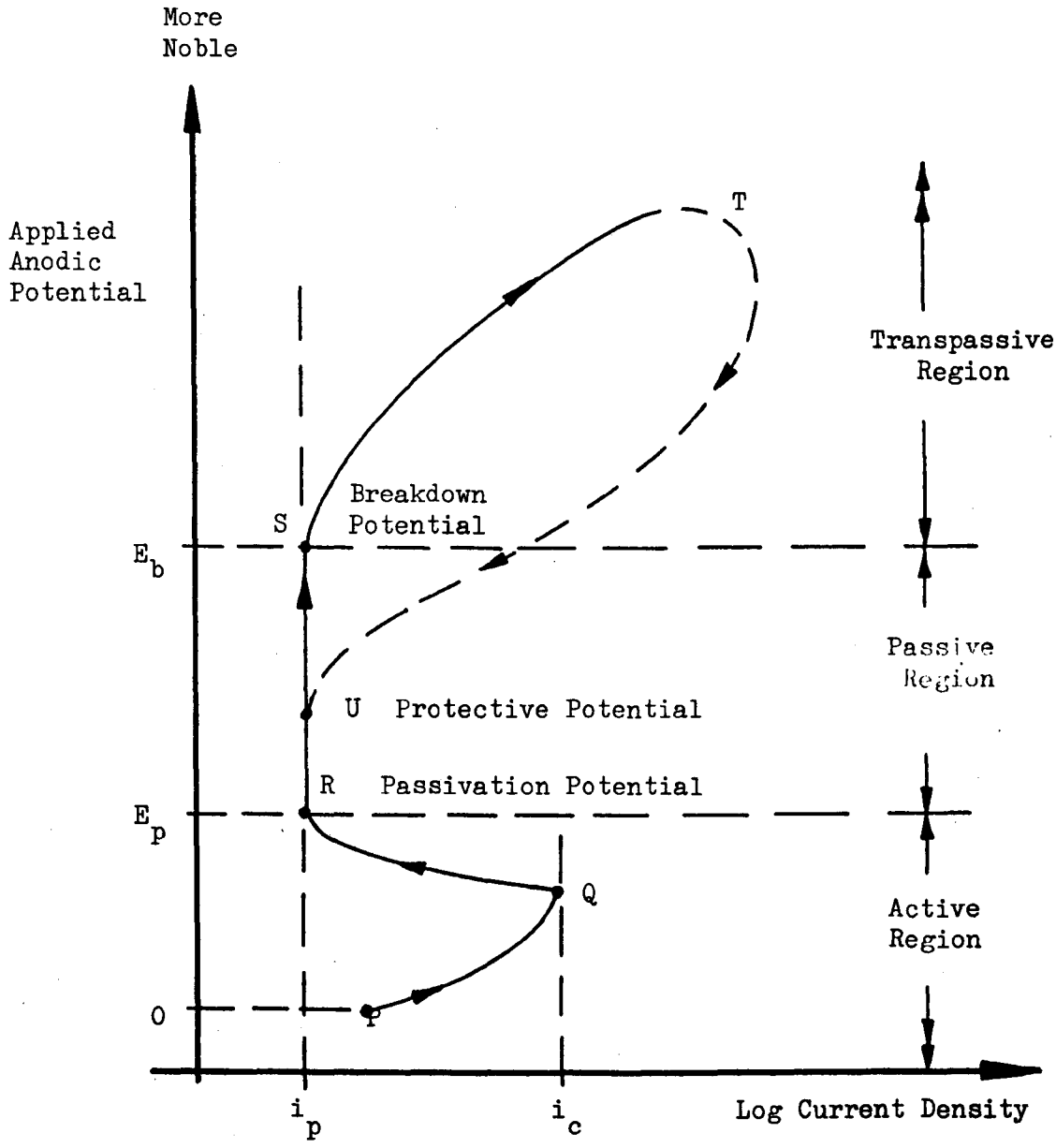

Figure R.11 Schematic illustration of anodic polarization for materials exhibiting passivity (determined potentiostatically)

As the applied anodic potential is increased from zero at P, the current density also increases indicating increased corrosion. At point Q an oxide film, formed on the metal surface, is responsible for a fall in current from i_c. This passive oxide film protects the metal from corrosion so that the rate is reduced to the passive current density i_p indicated by R. The potential E_p at R is known as the passivation potential, and further increases in anodic potential are not accompanied by any significant change in corrosion rate until the breakdown potential E_b is reached at point S. The passive film then no longer so effectively protects the metal and a rapid increase of corrosion occurs. If polarization is reversed in this transpassive region, the curve may follow a different path T until a protective potential is reached in the passive region at point U. The active region path PQR may also be rather different in the reverse direction.

Anodic polarization curves potentiostatically determined for stress-free metal/electrolyte systems are reproducible if conducted with due care and attention to standard conditions[141]. Such potentiostatic or potentiodynamic curves may then be modified to assess the effect of stress in general and fatigue in particular. For example, the rest potential, that is the potential that a metal will itself develop when immersed in an electrolyte, is important. If this lies within the passive region, the metal will resist corrosion in that electrolyte: the application of fluctuating stress and/or stirring of the electrolyte could affect this rest potential radically. Stainless steels, for example, generally have a breakdown potential in saline solutions ranging from 200 to 550mV SHE and this appears

to be influenced by residual surface stresses and surface finish [135, 142-144]. The rest potential measured for En 58J in 0.17M NaCl, O_2 free at 37°C is 400 m V SHE and this is typical for stainless steels so that rest potentials border on breakdown potentials. Over a period of time a rapid fall and rise of potential between 150 mV and 400 mV SHE in oxygenated isotonic saline has been recorded for this reason indicating breakdown and oxide film repair[144]. It has been stated that it is usually not possible to distinguish between the fracture surface from corrosion fatigue in a stable passive state and a fatigue fracture in an inert environment[142]. Passivity is thus a major factor to be considered for corrosion fatigue behaviour and variables which affect the passive state are critical. It has been shown that the aggressive chloride ion, discussed earlier in section 2.6.2, in fact reduces the passive region by lowering the breakdown potential as well as increasing the passive current density so that the rate of corrosion is greater. These two electrochemical effects are enhanced as the concentration of chloride ions is increased[143].

The potential/current density curve obtained for anodic polarization of a specimen during fatigue is also often greatly modified from the standard curve (Fig. R.11) under static conditions. This is illustrated in Fig. R.12 where the passivation potential and the corresponding reduction in current density in the passive region are non-existant in the extreme case. The concentration of oxygen in solution, temperature, viscosity and velocity can also similarly considerably modify the potential/current density curve produced under standard anodic passivation conditions[141]. The effect of imposed potentials is

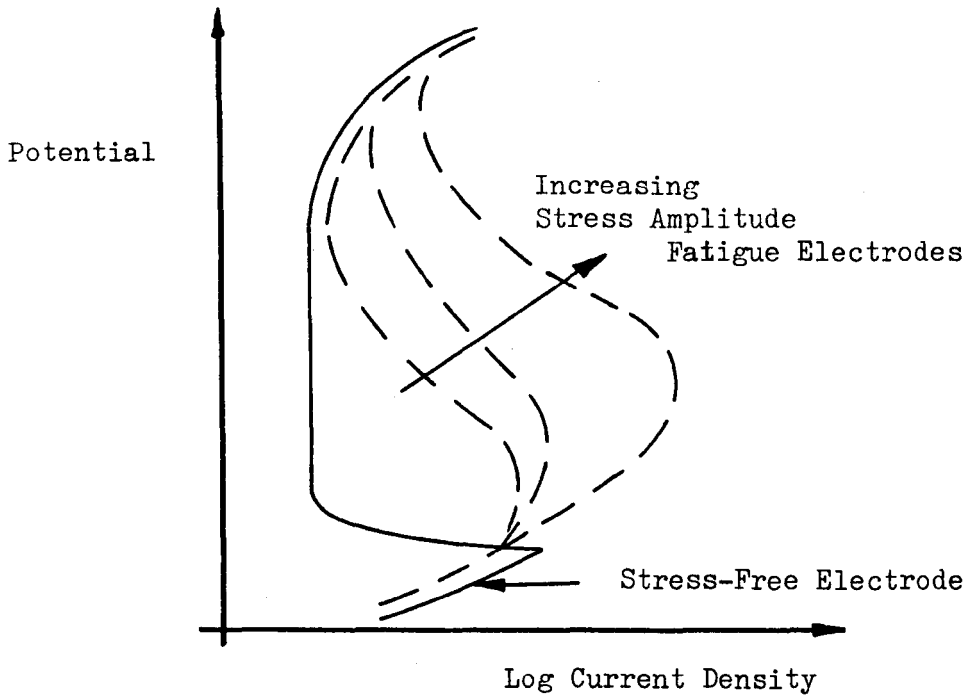

Figure R.12 Schematic anodic polarization curves for stress-free and fatigue loaded electrodes

thus frequently difficult to predict and also to interpret even when recorded in laboratory tests.

The freely corroding potential measured during the aqueous corrosion fatigue of a metal alloy is frequently found to vary with both applied amplitude and time[144, 145]. Open circuit potentials have been measured for many materials and three basic types of curve found, as shown in Fig. R.13 Curve "a" represents the behaviour of a material which rapidly forms a stable oxide film in the given environment. Curve "b" shows the initial formation of an oxide film as the potential rises, followed by pitting corrosion and a sequence of film breakdown (b′) and repair processes with time. The material

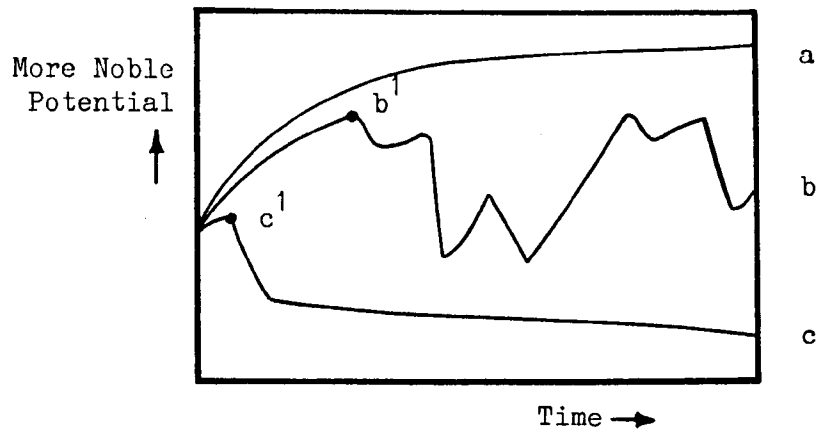

Figure R.13 Schematic potential-time curves (after Hoar & Mears[144])

behaviour illustrated by curve "c" is that of general corrosion: the freely corroding potential in this case falls rapidly (c^1), after initial surface layers are removed, and then becomes quite stable. Materials exhibiting stable passive film formation, such as that shown in Fig. R.13 curve "a", for stress-free corrosion are also desirable for fatigue applications[146]. Curve "b" materials are very unpredictable in behaviour while those following curve "c" such as mild steel are more certain. It is well established[145] that, after an immediate tendency towards the repair of imperfections in the film when the solution is introduced to the metal surface, the potential will fall (at c^1 Fig. R.13) for these materials. The time which elapses before the potential begins to fall is termed the film-life, and is related to the intensity of the corrosive action as well as to the magnitude of applied cyclic

stress as shown in Fig. R.14

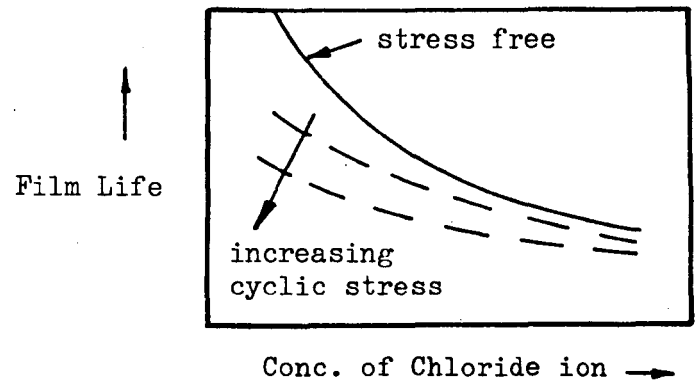

Figure R.14 Schematic representation of the influence of a damaging species and stress amplitude on film life as determined by a fall in potential (after Gould and Evans[35])

Film life is longer with less corrosive solutions and with lower cyclic stress amplitudes.

It has been observed that, for materials such as mild steel, the approximate air fatigue limit is regained if the uniform corrosion rate is sufficiently low[147]. For example, tests have been carried out on 0.18%C steel exposed in deaerated 3% NaCl and anodically polarized at selected current densities. Uniform corrosion rates in excess of the natural corrosion rate in aqueous solution were found to be proportional to the current density. A "critical" current density was found for this steel/environment system to be $2\mu A/cm^2$. Below this value 10^7 endurance fatigue life was established. This critical current density, equivalent by Faraday's Law to a rate of 5 m d d ($Fe \rightarrow Fe^{++} + 2\bar{e}$) was independent of stress, within the range tested[147]. Further cathodic polarization tests also confirmed that this critical corrosion rate was not sensitive to pH or to the anion type. Furthermore, it

was not found necessary to attain zero corrosion rate in acid solutions in order to extend fatigue life to $>10^7$ cycles provided the corrosion rate was below the critical value: the critical rate being approximately the same in all these solutions[147]. Similar tests on other materials have also shown critical corrosion rate effects although generally the rate is influenced by pH. The critical corrosion rate is a fundamental factor to be considered for corrosion fatigue. It appears to be basically a material constant but unfortunately it is also a function of specimen size and geometry in a given environment[135, 147].

The influence of cyclic stress and strain in modifying the electrochemical behaviour of a metal surface has also been investigated. Patel et al[148] have recorded current transients synchronised with loading frequency under potentiostatic control. Cyclically fluctuating currents have been observed and explained in terms of local depassivation or dissolution of the metal surface in phase with the applied cyclic stress[108, 148]. Cyclic stress may generate active/passive cells on the metal surface which can lead to earlier crack initiation than for fatigue in inert environments. The influence of wave-form and frequency on potential variation during a single cycle has been found to be closely related to fatigue life[149]. The shorter life often observed in tests with long rise times (periods of increasing strain) is suggested[149] as being the result of greater ability of the potential to more closely follow the strain: the range of potential variation per cycle is thereby increased. Shorter lives were related to small variations in potential. No frequency effects

were found when the potential of the specimen during a cycle followed the applied strain magnitude exactly. Current density or potential effects are thus sometimes considered as fundamental predetermined variables which are imposed on the system, and sometimes these electrochemical factors are measured and used as a means of detecting changes in other variables.

2.6.5 The Influence of pH

Potential/pH diagrams have been constructed for pure metal/water systems based on the original 1945 publication and now extended in the "Atlas of Electrochemical Equilibria" works by Pourbaix[150], This work is based on the formulation of the thermodynamic equilibria of all the reactions possible in a given system as a function of two independent variables. The Pourbaix diagram for the iron-water system at 25°C is shown in Fig. R.15 simplified and shaded to show the zones of corrosion, immunity and passivation[150].

These regions are determined from Fig. R.15 according to the following practical definitions: corrosion zones are regions where the activity of metal cations, anions, or complex anions $>10^{-6}$ g ion/l; immunity zones are regions where the activity of metal ions $<10^{-6}$ g ion/l and oxides, hydroxides, etc., are thermodynamically unstable with respect to the uncombined metal; passivity zones are regions where solid metal compounds are thermodynamically stable and in equilibrium with activity of metal ions $<10^{-6}$ g ion/l; while the underlying metal is thermodynamically unstable. The arrowed lines, marked 1 → 2 and 3 → 4 on Fig. R.15 are results to be discussed later in Sections 4.4. to 4.7. and 5.1.

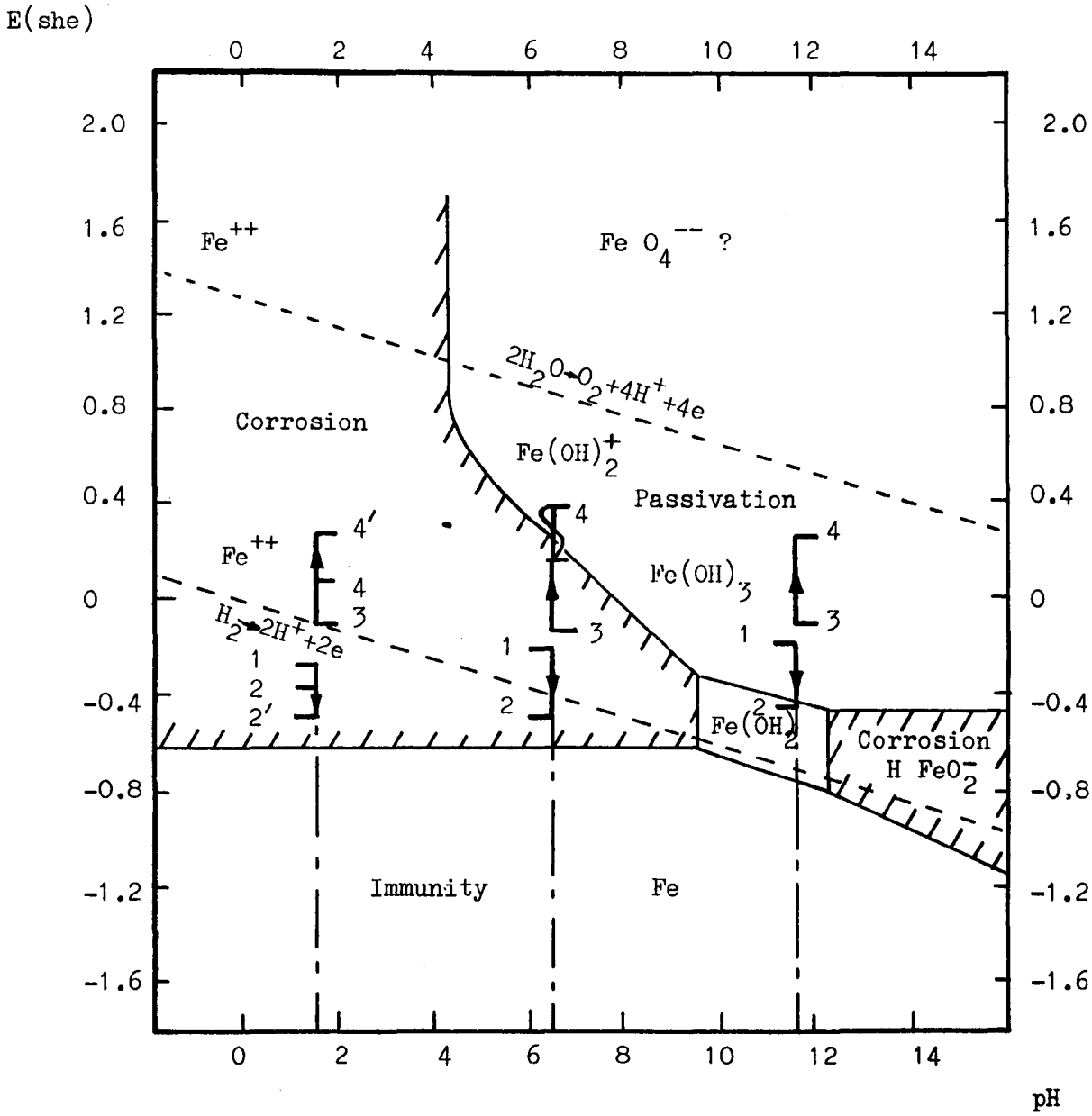

Figure R.15 Potential-pH equilibrium for the Fe/H_2O system at 25°C

Electrochemical considerations must take into account three factors: thermodynamic, kinetic and structural. Thermodynamic studies alone, or in combination with kinetic studies, are insufficient to define the behaviour of the system:

structural studies are a necessary concomitant. The scale of relative equilibrium potentials gives a degree of "thermodynamic nobility" but a knowledge of kinetic parameters and the influence of structural factors is required in addition to arrive at "practical nobility" scales. For those metals whose ionic exchanges at 25°C in aqueous media are rapid, the behaviour is in accordance with thermodynamic predictions. For those metals whose ionic exchanges are slow, on the other hand, the divergence between the thermodynamic nobility and the practical nobility is sometimes very great. The influence of anions in the practical case is critical. Structurally anions are a factor to be considered in cathodic deposition or as selectivity factors in anodic attack. Kinetically anions, as essential constituents of the metal solution double layers and catalysts of ionic exchanges or destroyers of the surface layers, are a major feature. Practical systems are usually multiple electrode systems in which several reactions can occur simultaneously so that kinetic aspects are not so simply studied as in the case of bimetallic systems, where a single well-determined reaction occurs at each of the two electrodes present.

The diagrams only at present concern pure metals and therefore cannot give direct information about the behaviour of alloys. The corrosion behaviour of alloys will in general differ from that of pure metals with regard to all three factors mentioned above. However a knowledge of the thermodynamic properties of the major constituent metals of an alloy can sometimes enable predictions to be made regarding the conditions for passivation or otherwise for the alloy. For this reason relevant Potential - pH diagrams are included in section 2.8

for the materials selection review. Use may also be made of such diagrams to investigate local environments within pits, or other such minority areas of a specimen surface. There is a considerable amount of evidence[151-157] which shows that changes in electrode potential, pH and solution composition occur within pits. The pH and potential have been measured at the tips of propagating cracks in high strength steels for various bulk solution pH values and conditions of external polarization[151-157]. The results, when plotted on a Pourbaix diagram for the Fe/H_2O system, clearly showed that the crack-tip pH is virtually independent of the bulk pH and is determined solely by the electrochemical reactions occuring within the confines of the crack. Further, it was found that irrespective of external polarization conditions, the crack-tip potential in these tests[151-157] invariably settled at a value just below the hydrogen line (see Fig. R.15) defining the limit of thermodynamic stability of water. It was also found in these experiments that crack growth stopped when either pH or potential were controlled so that crack tip conditions were maintained above the decomposition of water line. Generally it was found that the pH in pits or near crack tips is more acidic than the bulk solution when under anodic control. When the bulk solution is very acidic, however the crack-tip pH can be lower but also sometimes much higher: for a bulk solution at pH = 2, crack tip pH values have been measured ranging between approximately 1.5 and 10.5 depending on the external polarization [152-154]. Cathodic control, in contrast to anodic control, usually results in crack-tip pH values which are higher than in the bulk solution. Changes in the pH value with pure iron

of up to 7.5 units have commonly been observed[158] across an anodic site together with a potential shift of up to 150 mV more negative in the centre. Such changes have been observed sometimes prior to any corrosion being observed.

Restriction of oxygen supply in crevices of all sorts can also lead to pH values appreciably lower than that of the bulk solution. Zapffe[159] found that after fracture trauma local pH values may decrease from neutral values to between 5.3 to 5.6 for human body fluid: as healing took place, the pH gradually returned to the normal 7.4. Local and general working pH may thus vary with time and affect the corrosion fatigue performance of implant metal alloys. Stainless steels have been immersed in near neutral pH solutions and local crevice values of pH = 1 are possible if oxygen is restricted[159]. The fatigue performance of stainless steel is satisfactory in neutral pH solutions but shows a drastic decline at pH 4 and less[160] (also see Section 2.8). With decreasing pH value, the critical current density i_c (Fig. R.11) required for the passivation process increases. The depassivating pH of stainless steels, for example, is a critical factor[161]. The corrosion fatigue strength in this case decreases when the pH value decreases[142]. For example, an 18/9 austenitic stainless steel requires a minimum passivation current density of 500 $\mu A/cm^2$ in sulphuric acid solution of pH 1, while passivation takes place naturally in the applied currentless state in solutions at pH 4.6. The corrosion fatigue strength at 10^7 cycles for the pH 1 solution has been recorded as 206 MN/m^2 and at pH 4.6 it is 245 MN/m^2 [142]. A 0.48% C steel

in aerated water, adjusted to a pH value greater than 12, has been shown to exhibit a fatigue limit which was attributed to the formation of a protective passive layer at this pH, reducing the corrosion rate below the "critical" value[123, 162]. The pH value of a bulk solution or of any local environment within pits, crevices or cracks is thus a fundamental factor affecting the type of corrosion possible; since this factor is also frequently indirectly responsible for the corrosion kinetics and structural selective attack, pH is a variable of paramount importance for corrosion fatigue studies.

2.7 The Development of Modern Theories and the Present Understanding of Corrosion Fatigue Mechanisms

2.7.1 A Systems Approach

A study of the variables discussed in section 2.6 together with the ways in which they have been found to inter-relate in the process of corrosion fatigue is most valuable in the formulation of possible mechanisms. Fig. R.16 is an attempt by the author to correlate these variables on a systems-type diagram. The boxes and lines shown in full illustrate the inert environment situation: mechanical and metallurgical variable factors interact with each other ('A'), as the result of forward path and feedback (indicated by double lines and arrows); the inter-action of 'cyclic load' and the 'basic material' (paths 'E' and 'F') result in 'fatigue', which causes changes in the basic material (feedback path 'F'); further feedback paths indicate resultant changes in metallurgical variables ('D'), mechanical variables ('C'), and cyclic load ('B'). The boxes and lines, shown dashed, together with the diagram in full lines (as discussed above)

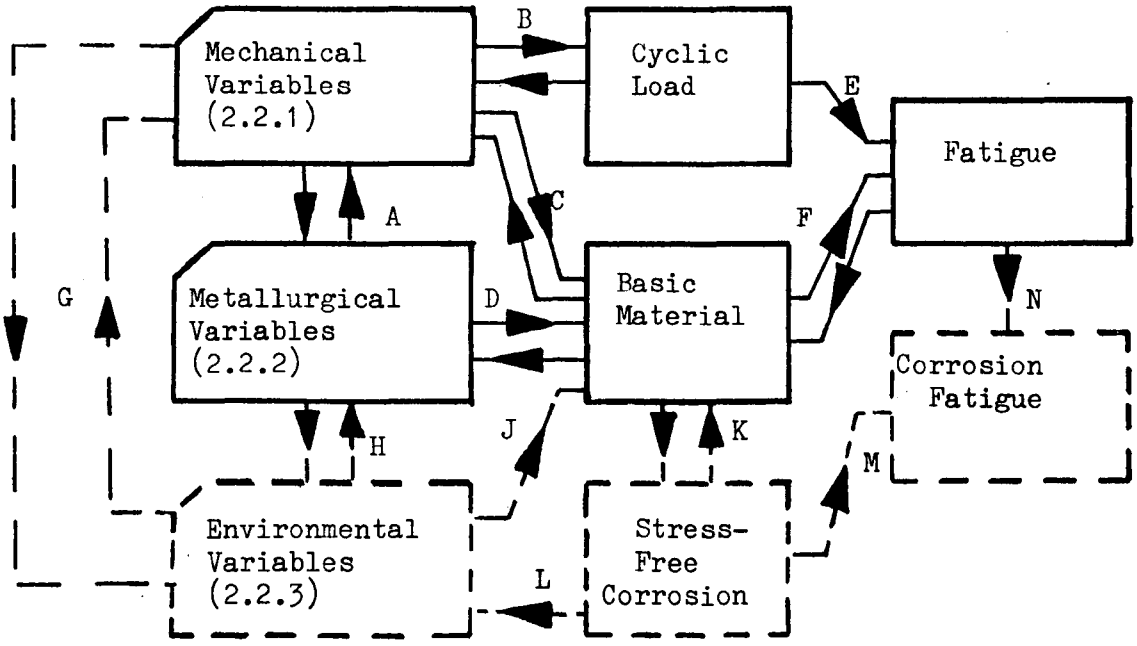

Figure R.16 A Systems Diagram Relating Interaction Paths In The Process of Corrosion Fatigue

illustrate the new system for corrosion fatigue: environmental variable factors inter-act with both mechanical and metallurgical factors (paths 'G' and 'H'); reaction with the basic material ('J') and inter-actions ('K') result in 'corrosion', which in turn can affect the environment (feedback path 'L'); the process of corrosion fatigue is then the conjoint action of fatigue and the environment (paths M and N).

Note, from Fig. R.16, that the environment can affect the process of fatigue in at least two different ways resulting in quite different corrosion fatigue behaviour. If the predominant effect of corrosion is a feedback effect, via

path L, all the input variables will be likely to be affected, so that processes such as embrittlement and stress corrosion may be possible. If, on the other hand, the predominant effect of corrosion is a forward path M, the conjoint action of inputs M and N may result in corrosion fatigue. Fig. R.16 provides a 'skeleton' on which to hang some mechanisms; it is, however, likely to prove to be far too simple a model. Fig. R.17 schematically shows some possible S/N curve types resulting from corrosion fatigue. Curve (a) represents fatigue in vacuo or in an inert environment; curve (b) shows

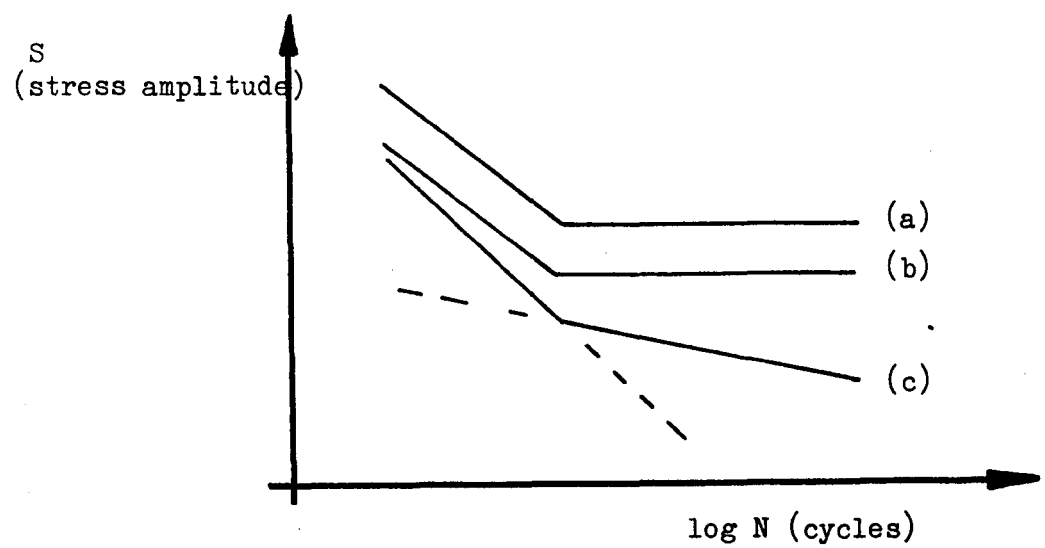

Figure R.17 Possible Fatigue Curves

reduced fatigue life above a reduced fatigue limit; while curve (c) illustrates, what is commonly referred to in the literature as, "true corrosion fatigue". It is a requirement of any proposed mechanism to explain in each case, why a fatigue limit exists (curve (b)), or alternatively, why such a limit is absent (curve (c)).

A "Fatigue of Metals Refresher Course" organised by the Institution of Metallurgists in 1955, reviewed the results of work then available and firmly established, in a paper by Waterhouse[134], the conjoint nature of corrosion fatigue. It was suggested also then that the processes of fretting corrosion and corrosion fatigue had much in common, so that the fretting may assist crack nucleation and hence lead to fatigue. In the following sections a review will be made of the many mechanisms which have been advanced, firstly for "purely mechanical" fatigue and then for "corrosion" fatigue, in the light of more recent studies.

2.7.2 The Mechanical Aspects of Fatigue Crack Initiation

A mechanism of fatigue in vacuo or inert environments cannot, by definition, involve corrosion processes. Such a mechanism must therefore have a purely mechanical and metallurgical basis and, while it represents a special case of a more general corrosion fatigue mechanism, it should provide a better understanding of fundamental processes.

Landgraf[40] has reviewed the mechanical response of metals to repeated strains and Fig. R.5 of Section 2.4.1 was used to illustrate a summation of elastic and plastic strain resistance. Fig. R.18 (a) shows the strain resistance of three idealized metals, using a plot similar to Fig. R.5, Fig. R.18 (b) compares the stress-strain responses of the three metals. A "rule of thumb" has been noted[163, 164] that most metals when subjected to a strain amplitude of 0.01 will

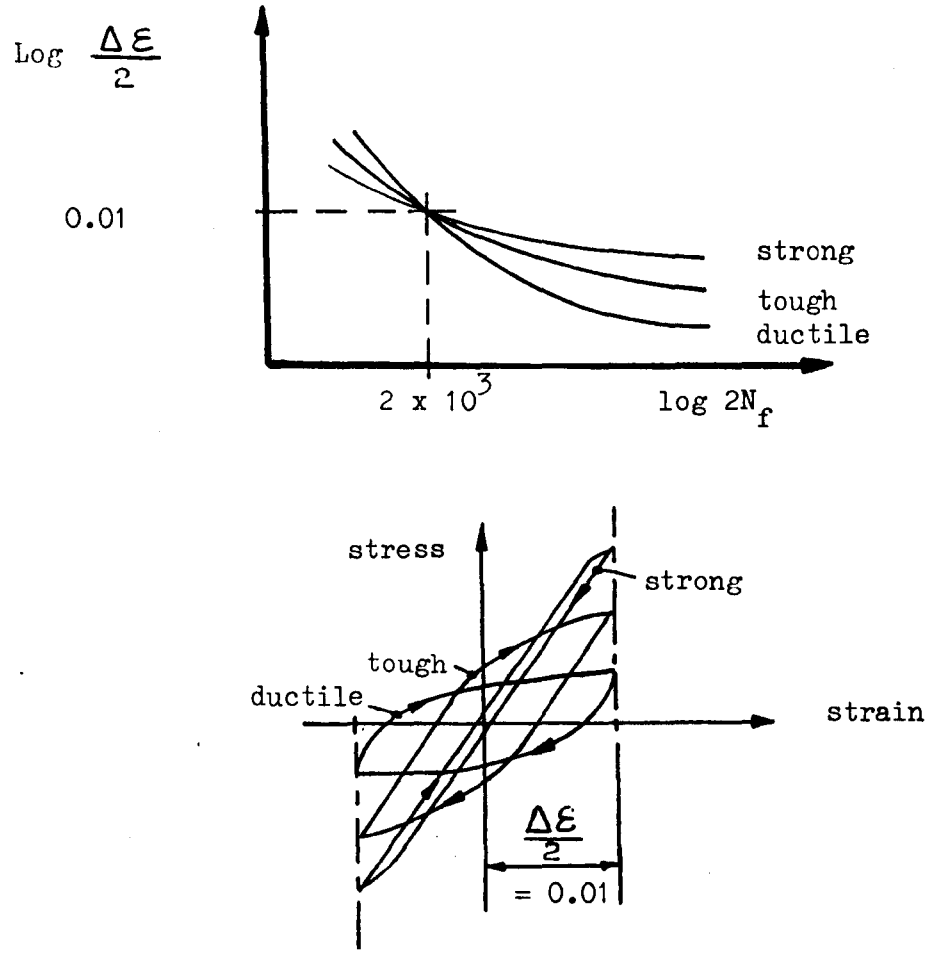

Figure R.18 Schematic representation of the cyclic strain resistance of idealized metals due to Landgraf[40]

fail in approximately 2000 reversals. This is a convenient position, where the curves cross on Fig. R.18 (a), to distinguish between high and low cycle fatigue. The relative materials rankings will depend upon this distinction: ductile metals offer maximum strain resistance in the low cycle region, while strong metals are superior at high cycle lives, and tough metals are shown to exhibit good overall strain resistance. Strong metals resist imposed strains elastically on the basis of strength, while ductile metals resist imposed strains plastically on the basis of ductility. Overall behaviour

may be predicted, by equation (i) of Section 2.4.1., and for notched material equation (vi) may be used indicating that resistance to fatigue is dependent upon the product of stress and strain resistance.

Crack initiation is known to occur in regions of metal where strain is concentrated or localized[83, 165] and a large number of specific dislocation models have been developed to describe the nucleation of fatigue cracks: most models inherently rely on the onset and localization of plastic deformation by slip; leading to crystallographic notching of the metal surface. When considering such models, where cracks are actually nucleated, it is the implicit assumption that there is some stress amplitude below which plastic strain is negligible. It is to be concluded, therefore, that an intrinsic fatigue strength limit exists in all materials below which fatigue can never occur.

Fig. R.5 shows the strain/cycle curve becoming horizontal at $\Delta\varepsilon_i/2$, corresponding to a fatigue limit stress $\sigma_i = \Delta\varepsilon_i . E/2$. Feltner and Morrow[166] have given evidence for the existence of this limit σ_i which is termed a microyield stress. Fig. R.19 schematically shows their results: at some small inelastic strain (say 10^{-5}) the anelastic strain, which is non-damaging, is equal to the plastic strain. The stress amplitude σ_i corresponding to this magnitude of inelastic strain has been found to be nearly identical to the fatigue strength limit: that is, fatigue will not occur at applied stress amplitudes less than σ_i, the microyield stress. This concept of an intrinsic fatigue strength limit for all materials is contrary to some beliefs and long life tests are required to establish

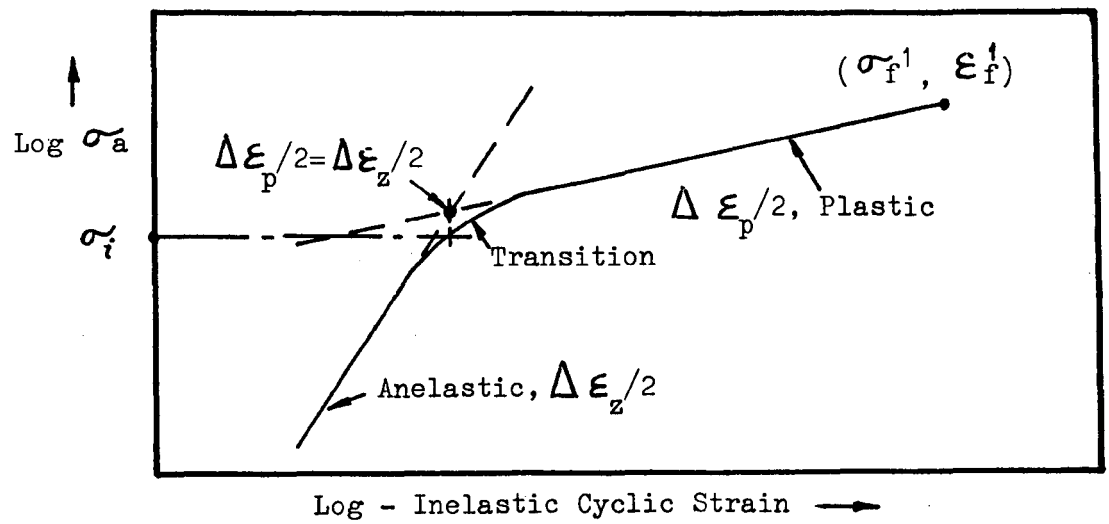

Figure R.19 Variation of inelastic cyclic strain with stress amplitude (after Feltner and Morrow[166])

the facts: some metals, such as aluminium alloys may not show a transition 'knee', establishing the existence of σ_i until lives in excess of 10^9 cycles have been endured.

Data for low carbon steels fatigued above and below the fatigue limit, shows essentially the same slip band structure, although lower stresses produce less slip[24, 167]. The mechanism producing the fatigue limit is not generally therefore that of preventing the formation of slip bands or the elimination of shallow cracks from the root of PSB's. On the other hand Helgeland[168] and Roberts[169] have both shown that, in the ideal case of the single copper crystal, there

is a stress of about 30 MN/m^2 below which persistent slipbands (PSB's) will not form; and Feltner et al[88,170] see this stress as equivalent to the microyield stress . The reason why PSB's form still remains to be clarified.

Feltner[88] has described what is generally accepted as the process of PSB formation. During initial rapid hardening of crystals under fatigue a dense dislocation debris, much of it in the form of dislocation dipoles, forms uniformly over the material : that is a debris-hardening mechanism is operative[170]. PSB's are formed as the debris structure becomes locally unstable, so that local stresses become large enough to cause local softening. Cyclic plastic deformation is then confined to reversible PSB's not only on the surface, but also in the interior[172, 173]. Catastrophic localized degeneration of the previously uniform dislocation structure occurs, during this cyclic strain-softening process, where plastic strain is concentrated. This highly localized plasticity originates at the surface and propagates into the material along adjacent primary glide planes, producing a dislocation cell structure containing twist boundaries.

Slip band growth has been studied by Avery et al[174] and an average rate of approximately 160 dislocations per cycle emerged on the planes with the highest resolved shear stress[42, 174] it was also established that slip bands develop in "bursts" of slip which were not uniformly resolved in each cycle. Watt et al[175] also confirmed this mode of slip band growth in bursts, by recording intervals of zero development on copper. He polished off 55 μm from the surface of saturation-hardened material, which then showed an incubation period during

cycling before slip bands reappeared at the surface.

It was shown[176] also that crack initiation in copper single crystals may be postponed significantly by orienting so that the slip vector on the primary glide plane was parallel to the surface of a bending specimen: the development of PSB's by displacements on the secondary glide systems took considerably longer. Avery and Backofen[177], Grosskreutz[178], Laird and Duquette[179], as well as Lukas and Klesnil[180], have historically reviewed the various mechanisms advanced for fatigue crack nucleation via dislocation mechanisms of slip band formation.

Electron microscopy has been used to show that, after the initial fatigue hardening process has levelled off, the dislocation structure in the material consists of tightly packed, slightly wavy, elongated clusters of edge dislocation dipoles[172, 181, 182]. Crystals containing PSB's have been clearly shown to have a two phase dislocation structure: material in PSB's consists of a 'ladder' or 'wall' structure of primary dislocation dipoles, whereas the matrix material (not in a PSB) consists of a more loosely organised structure of dipoles. Fig. R.20 schematically shows the PSB ladder spacing 'd' as well as the intrusions and extrusions developing on the surface within a PSB. The state of the crystal surface here once established would have little influence on the slip processes within the slip band. PSB's have also been observed as having a highly regular hexagonal honeycomb structure of dislocation cells, extending to only approximately 200μm below the surface[181]: the C axis has been identified as

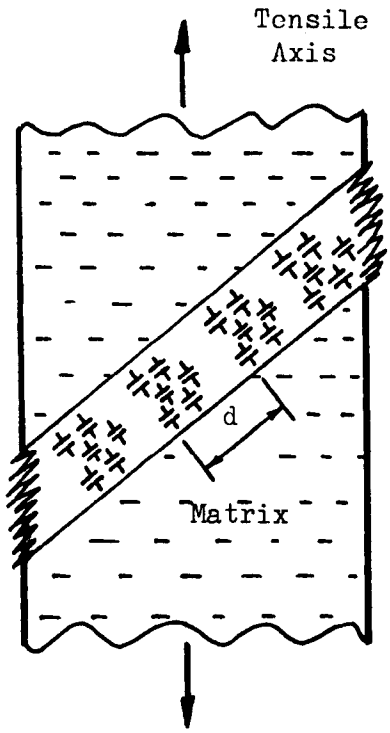

Figure R.20 showing schematic dislocation dipoles, intrusion and extrusion development on a PSB

always normal to the plane of the slip band[172]. Kuhlmann-Wilsdorf and Nine[183] have suggested how cyclically shakendown, quasi-equilibrium, dislocation structures could form inside PSB's.

A very recent review of fatigue by Laird[171] concludes that work has been done on most f.c.c. metals and alloys to show that a true fatigue limit exists in each case, and that the fatigue limit is associated with the formation of PSB's. If the stress is not high enough to form PSB's, then no fracture will occur. This behaviour for f.c.c. metals and alloys is not, however, generally found for other metal structures. Mild steels (as already discussed) together with iron, have a fatigue limit well above the stress required to form PSB's.

Why is the behaviour so different from f.c.c. metals? When viewed by optical microscopy it is reported that PSB's in iron and copper appear quite similar, yet the dislocation behaviour of the two metals is very different: the difference being not just that due to the interstitial solutes, although these are known to be valuable in raising the fatigue limit[88, 171]. As discussed in Section 2.5.3, very little is known about the fatigue behaviour of h.c.p. structures: twinning and grain boundary cracking complicates crack nucleation mechanisms[184, 185], although it has been established that fatigue life is still governed by cracks that originate at the surface[186]. Similar complications arise in rhombohedral metals[8, 185] where cracking at deformation induced twin boundaries and along cleavage planes may occur during fatigue.

Roberts[169] has shown that for copper, as the strain amplitude is increased, the entire metal surface becomes covered with PSB's. This observation is thought, by Laird et al[101], to indicate a tendency towards intergranular initiation of cracks in polycrystals at high amplitude cyclic strains, rather than the transgranular initiation usually found at more moderate cyclic strains. Evidence exists[187] to show that in the single-phase materials, alloying with substitutional atoms to achieve a more planar slip mode character produces a more homogeneous slip distribution, as well as a greater tendency to reversible strain hardening. It was noted in Section 2.5.2 - 2.5.4, that both reversibility and homogeneity of slip play important roles in crack initiation, with the worst combination being heterogeneous, non-reversible slip. The severity of the notch-peak surface topography is enhanced

by this combination so that cracks may be sooner nucleated.

Steel specimens having transverse holes show the first appearance of PSB's at lower stresses than for plain specimens owing to the stress concentration[24]. It has also been established that, on account of the cold working effect during drilling of holes, the crystallites adjacent to the edge of the hole are strengthened so that slip does not start immediately at the hole edge, but at a distance of about 70 μm from it[24]. During fatigue the slip lines then propagate towards the hole. The same phenomena of PSB formation and propagation is observed in notched and unnotched specimens. The first traces of slip have been observed after only 0.05 to 0.3% of the total life cycles, being faster in time with increasing cyclic stress level[24]. Initiation of PSB's is highly dependent on the shear strain, and cracks always start on the slip planes with the highest resolved shear stress[42].

With few exceptions, fatigue crack nucleation is confirmed by experiment as a purely surface phenomenon[23, 88, 170]. The mechanism of crack nucleation and the mechanism whereby PSB's are formed are clearly related, and in the particular case of f.c.c. metals and alloys a common mechanism may be shared which is responsible for the fatigue limit. A practical difficulty exists in observation of the crack nucleation process. How quickly do cracks form from the increasingly complicated surface structure of PSB's, as the fatigue cycles are accumulated?

McClintock[188] has shown that a Bauschinger effect, which is an integral part of plastic deformation regardless of molecular mechanism, is required for concentration of

reversible cyclic plastic deformation inside PSB's. Since dislocations terminating at a clean metal surface will move under a lower stress than those internal dislocations that are anchored at both ends[26], preferential surface deformation results. Residual stress formation at the surface is thus likely, which in turn may result in a substantial Bauschinger effect. This effect and an effective recovery process seem to be the only two vital ingredients for the developments of PSB's.

Argon[189], when reviewing surface effects on fatigue crack initiation, points out that the production of PSB's is not enough for the nucleation of cracks: a mechanism is also required for the production of damage or degradation of slip band cohesion. Without such a damage mechanism, only intrusions could possibly lead to continous crack production due to notching. Since the established facts show that intrusions are sometimes completely absent[98, 172], and also that crack nucleation commonly occurs at the extrusion boundaries[23, 24, 189], a damage mechanism must be present. Argon[189] sees a clue to the required mechanism of fatigue damage in high temperature fatigue, where diffusion and plastic deformation result in a continuous decrease in density[190]. The resultant porosity is seen to be preferentially concentrated inside PSB's to form cracks, as vacancies condense on dislocation structures. At temperatures below the diffusion range where visible porosity is not found in PSB's, submicroscopic porosity could still exist. The existence of the extrusion itself is seen as proof of porosity, and the result of swelling in the PSB's by vacancy production[191-193]. This mechanism is general and would of course also apply to glassy polymers as well as crystalline solids. Intrusions would

negate this damaging process, but could be explained by the brittle subsurface fracture of isolated extrusions. Experimental work[194, 195] has firmly established the presence of subsurface pores in PSB's. The pores observed are always surface connected and, for low amplitude fatigue stressing and at cycles $\geq 10^6$, a series of tubular holes is found extending in the deepening PSB's perpendicular to an irregular embryonic crack front[195]. Recent observations[196] that dipoles in the cyclically hardened material are largely of vacancy type, is seen by Brown[197] to suggest that PSB's are accompanied by macroscopic internal stresses which can strongly influence crack nucleation and growth. The vacancy production mechanism would therefore appear to be not only possible, but also most probable of the major mechanisms advanced for fatigue crack nucleation.

A further recent development in the understanding of crack nucleation mechanisms has been introduced by Freudenthal[198]. He suggests that there are in fact two major fatigue mechanisms: one referred to as 'plastic fatigue', and the other as 'elastic fatigue'. 'Plastic fatigue' refers to all the work discussed so far where materials scientists have concentrated on annealed metals with simple crystal structures. Such materials have little or no initial elastic range so that fatigue here is caused by stress cycles that continually impose cyclic strain of the kind occuring when yield is exceeded. A mechanism of 'plastic fatigue' has therefore been evolved which assumes that the behaviour of more complicated structures, resulting from alloying or cold work for example, is still one basically

of the 'plastic fatigue' of 'weak' points. 'Plastic fatigue' is suggested by Wood[199] to be a special case mechanism which will not apply to metals generally. Load bearing structures require strong metals with extensive elastic ranges, and they are meant for use primarily under stresses confined to this range. These materials are nevertheless just as susceptible to fatigue as the simpler plastic metals, yet they do not produce the massive post-yield strain, when cycled well within the elastic range.

An alternative mechanism described as 'elastic fatigue' has been proposed to account for materials such as titanium, where a fatigue failure at amplitudes considerably less than half its elastic range occurs without any sign of slip. 'Elastic fatigue' results in a transgranular shear microcrack suddenly nucleating in an otherwise flat and featureless surrounding; no visible slip disturbances occur during this sub-yield strain fatigue. Quite literally, on the face of it, 'elastic fatigue' appears to have little in common with 'plastic fatigue'. There is a grey area for some metal alloys, where it seems arguable whether 'elastic fatigue' may still be 'plastic fatigue' arising in occasional weak localities within the structure. Steel and McEvily[200], however, provide experimental evidence, from a Ti-6Al-4V alloy to indicate fatigue failure by a distinctive mechanism characterized by a slipless and apparently brittle mode of crack initiation: such materials have been termed pseudo-elastic[198]. It was concluded[200] that crack initiation in this pseudo-elastic metal alloy was the result of internal stress-intensification in the high cycle range, rather than the surface PSB formation

responsible in 'plastic' material; the restricted ability to cross slip in this alloy was considered responsible for a strongly path dependent dislocation content and behaviour under given cyclic conditions; a process of cyclic softening, a pronounced Bauschinger effect, and a high rate of cyclic hardening in a given hysteresis loop was observed, which was considered also to be importantly involved in the crack nucleation process of this alloy. Benson, Grosskreutz and Shaw[201] also worked on Ti-6Al-4V and found crack initiation in h.c.p. α-grains by a slip-band mechanism at stress amplitudes above the fatigue limit but, under cyclic stresses near the fatigue limit, fatigue cracks initiated at the interface between h.c.p. α and b.c.c. β-grains without detectable slip. It therefore seems that the distinction between 'plastic' and 'pseudo-elastic' materials can be made only in low-stress, high-cycle fatigue.

2.7.3 The Mechanical Aspects of Fatigue Crack Growth

Fatigue crack growth laws were discussed in Section 2.4.2 In this section an attempt will be made to answer the question why a crack of a given length should grow under a cyclic stress whose magnitude is far less than that required in static tension to propagate the crack? Fig. R.21 helps in placing a scale to various views of fracture. Crack growth rates of practical interest range from the threshold up to about 10^{-3}mm per cycle. On purely physical grounds a crack cannot grow less than about 4×10^{-7}mm per cycle since this

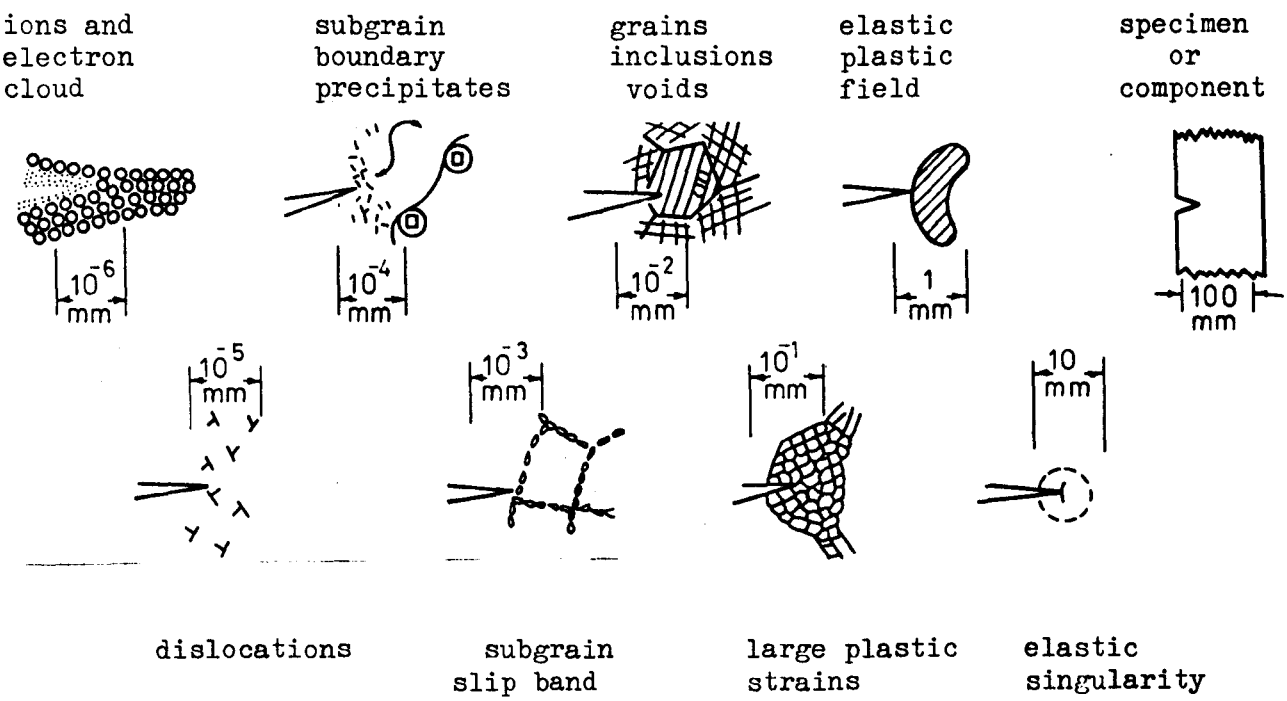

Figure R.21 Schematic Illustrations of Fracture when viewed at Different Scales (After Pook[47])

is the order of one lattice spacing. On a macroscopic scale, of say 10^{-1}mm, a metal can usually be regarded as a homogeneous continuum.

As discussed in Section 2.1.3, the process of fatigue crack growth has been defined by Forsyth[38, 39], as illustrated in Fig. R.22. Stage I cracks grow from slip generated nuclei

along planes of maximum shear stress until a certain critical depth is reached. Stage I crystallographic growth, or microcracking along slip places, is then replaced by stage II crack growth along planes perpendicular to the maximum tensile stress; that is, noncrystallographic growth. Wood[165, 194]

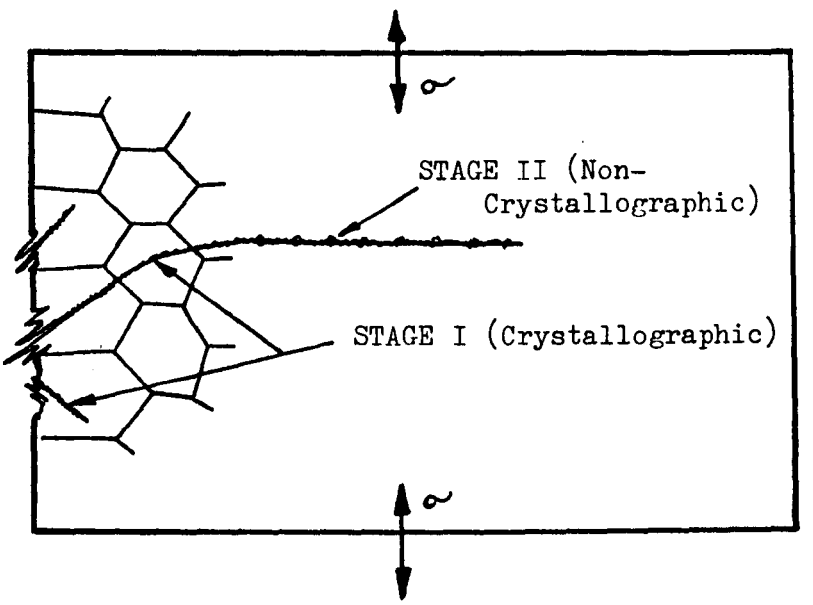

Figure R.22 Schematic Diagram showing the different stages of crack growth as defined by Forsyth[38]

has also distinguished between high-strain, low-cycle fatigue, and low-strain, high-cycle fatigue, on the basis of the slope of the S/N curve as well as the type of damage produced by various load levels. He showed a transition in behaviour at approximatley 10^5 cycles, and a high-strain fatigue has been regarded ever since as a quite distinct mechanism from that responsible for fatigue at low strain. Plumbridge and Ryder[202], examining the metallographic evidence, however, see no justification for the separation of high and low cycle

fatigue: they conclude that there is adequate evidence to show that both high and low cycle fatigue results in the production of cracks growing in stage I and stage II modes. The only reason for differentiating between high and low cycle fatigue, in an inert environment, would be that of distinguishing between the relative proportions of fatigue life spent in the initiation, stage I, and stage II crack growth modes. High-strain cycling in many materials results in large proportions of the total cycles to failure being spent in extending stage II cracks[203].

Crack propagation from notched structural members will, depending on the severity of the notch and specimen geometry, be essentially stage II propagation in most cases. Owing to the major engineering interest in large strong structures containing inherent flaws, and the comparative simplicity of observation, stage II crack growth has been extensively studied[43-51] using pre-cracked specimens: viewed in the light of linear elastic fracture mechanics, great progress has been made. A mechanism of stage II growth, involving a repeated plastic blunting process at the crack tip, appears to be widely accepted. Fig. R.23 is a model by Laird[204], as presented by Grosskreutz[178], which is strictly applicable only to ductile materials under moderate to large fatigue load amplitudes. During the tensile part of the load cycle, large plastic strains at the crack tip cause localized slip on the planes of maximum shear. At maximum stress, yielding occurs to the extent of the plastic zone, r_p. Reversal of the strain forces the crack faces together, but the new surface created during tension is not completely rehealed by reversal slip. The slip during the compression occurs mostly on new

planes so that the crack tip takes on a folded appearance with "ears". After completion of the compressive half cycle, the crack tip is re-sharpened and the sequence can begin all over again. Laird[204] based this model on a synthesis of many

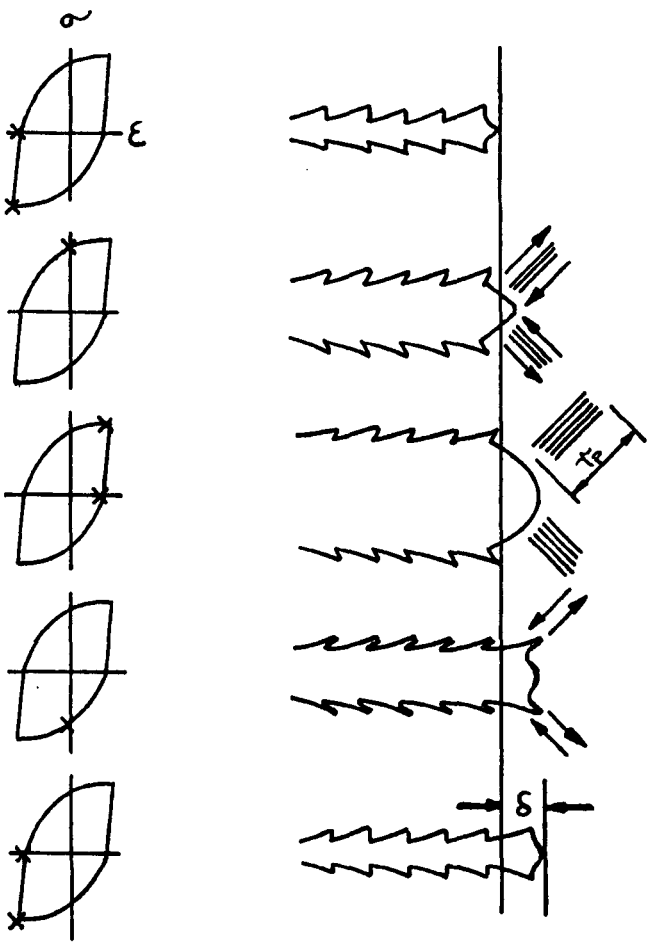

Figure R.23 Fatigue crack growth by the plastic blunting mechanism (model by Laird[204]). Drawings at left indicate points on the cyclic hysteresis loop for which the crack-tip geometry obtains. r_p is the plastic zone size measured along planes of maximum shear (after Grosskreutz[178])

photographs of cross sections taken through the crack tip of pure aluminium at various positions of load cycle. This

repetitive process accounts for the regular pattern of growth striations and, since there is a lack of dependence on any specific dislocation mechanisms, the model is capable of generalization. Other mechanisms[67, 188, 193, 205] have been advanced but are essentially also plastic blunting mechanisms, with specification of the slip processes involved. In the case of a truly brittle cleavage crack, Tyson and Alfred[206] have reviewed crack propagation models on the atomic scale and suggest that, since this is only possible in a crystal if the stress required to rupture atomic bonds at the crack tip is reached before the shear strength of the latticeis exceeded the tensile stress at the tip of a brittle crack must be of the same magnitude as the theoretical tensile strength of the material. Continuum mechanics may be used, albeit with some difficulty and great care, in some cases. However, for reasons now to be discussed, fallacious estimates of fatigue life often result from the indiscriminate use such methods.

Sufficient elastic energy must be released during stage II crack growth to provide the energy required to create new surfaces, and any plastic zones which accompany the creation of those new surfaces. Stage II crack growth occurs because of the resharpening of the crack tip with each cycle and not as a consequence of any progressive structural damage. However, as reviewed in Section 2.5.1 - 2.5.5, the microstructural variables have some effect on the blunting mechanism, so that crack growth rates can be different at the same cyclic stress amplitude in materials of different structure. A crack will remain dormant, in an inert environment, if the increment of

local growth during any stress cycle is less than one atomic lattice spacing, so that new surfaces cannot be created, or if some mechanism is operative which prevents resharpening of the crack tip.

Experimental evidence, during the examination of stage II cracks, shows that the material immediately adjacent to and ahead of a crack contains the dislocation morphology characteristic of high strain fatigue cycling of bulk specimens[207, 208]. If this is indeed so, then the cyclic stress-strain curve determined for bulk material should be applicable to the plastic zone. Additional, more recent, evidence, however, suggests that another zone within 1 to 2μm of the crack tip may be far more important[178, 209]. Material in this inner zone may deform in ways not observed in normal bulk deformation. It has been observed, for example, that very dense dislocation clusters are present just below the fracture surface of a high-strength aluminium alloy, yet if as little as approximately 5μm is removed from the surface the clusters are not found[209]. Observations near the fracture surface of pure aluminium and copper have also shown extremely dense dislocation structures, together with highly misorientated subgrains much smaller in size than ever observed in bulk deformation[208, 210, 211]. Grosskreutz[178] sees such evidence pointing to the existence of enormous plastic strains in the region immediately ahead of a crack, the magnitude of which is never approached in bulk samples, even at ductile necking. Since the mechanical

properties of such highly strained material are quite unknown, the indiscriminate use of bulk material continuum mechanics in treating crack-tip material deformation is hardly justified.

It is still not certain also exactly how fatigue striations are formed. Wanhill[212] considers that they are created only as the stress is increased from its minimum value in each loading part of the cycle. Laird, on the other hand, takes the opposite view. He concludes in a recent review discussed by McEvily[125] that striations are created during the unloading portion of each cycle. The latter view is supported by experimental evidence from the fatigue striations created during the unloading portion of each cycle for PVC. For this material it was observed that striations were the result of a depression formed as the localized region behind the tip was compressed. A corresponding lateral expansion of material at the crack tip could also be seen during unloading. Lynch[213] sees the formation of striations on fatigue-fracture surfaces as evidence of a two-part process. Compressive deformation, during unloading brings the opposite crack faces closer together and deforms the fracture surface immediately behind the crack tip. The next tensile half cycle reopens the crack and produces another increment of growth. This model for striation formation accounts for the smooth appearance of the first part of a striation and the coarse slip step on the second part of a striation[204, 214]: it also accounts for the deformation bands beneath the fracture surface[215]. The influence of symmetry and the number of slip systems operating at the crack tip on the appearance of the striations, which have been noted [216],

would also be expected from such a model.

Two types of striation are commonly found and are capable of resolution at crack growth rates of the order of 10^{-5} mm per cycle[217]. Forsyth[109] defines 'ductile striations' as characteristic of a normal 'soft' material fatigue fracture. Enough plastic deformation occurs at the root of a crack in this case during each stress cycle to produce a series of parallel step lines, perpendicular to the direction of crack progress. Crack progress and striations in this case are often strongly grain orientated. 'Brittle striations', on the other hand are characteristic of a 'hard' material fatigue fracture, where less plastic deformation occurs at the root of the crack per cycle so that growth is more brittle: the characteristics of cleavage develop and a series of circumferential step lines appear representing the advancing crack front, together with 'river' markings radiating from a narrow crack origin. Electron fractography has been used extensively[218] to analyse the fracture surface topography of most engineering materials, and while these two basic striation types are often identified, striations not clearly identified as belonging to either group, or the complete absence of any striations, is also a common occurence. It is not at all clear whether the models so far proposed for striation formation do indeed always operate, being subjected only to growth rate modification according to material properties.

Tomkins [219] has studied factors which might modify the crack tip material in the fatigue of high strength metals, and so affect the basic mechanism of stage II growth in these materials. He noted that at the lower applied strain level, high strength metals had improved fatigue properties; that is

decreased crack growth rates and increased endurance, consistent with their decreased plastic strain range for a given applied stress range. At high applied strain ranges, however, he noted that endurance is drastically reduced and that the simple power law relation of the Coffin-Manson form (approximating to the 'plastic' line of Fig. R.5, Section 2.4.1) is not operative for the strong metals. The intervention of 'fast' fracture at the highest plastic strain levels could easily account for this behaviour. However, the most dramatic difference in the behaviour of strong metals occurred at the lower plastic strain levels. Tomkins[220] showed that the stage II mechanism operates but that secondary fracture features are also present in electron fractography studies of high strength steels. Secondary fracture evidence was also found on the fracture surfaces of aluminium alloys tested in high strain fatigue by Erhardt and Grant[221]. Microcracking occurs within the flow bands formed at the crack tip. Fig. R.24 schematically shows how the stage II model, based on the Tomkins shear decohesion mechanism[205] variant of the general Laird[204] model (Fig. R.23) of plastic blunting, is modified for strong metals.

The effect of microcracking on the amount of crack growth per cycle is that of inhibition of the lateral development of the flow bands. The overall crack tip displacement here is similar to the ductile case but a smaller proportion of it is accommodated by increase in flow band width and the shear decohesion is higher than for the ductile model. Tomkins reports[219] that this secondary cracking is seldom observed

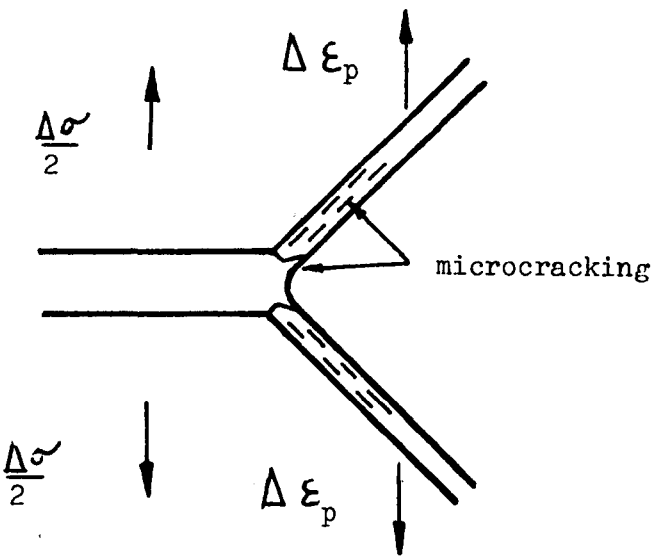

Figure R.24 Modified model for Stage II crack growth analysis for high strength metals (After Tomkins[219])

in the regions of stage I fracture so that the ductile model of stage II crack growth, which is also thought to apply to ductile materials during stage I growth, should hold for high strength metals during the early stages of growth: this is borne-out at low strain levels, where most of the life is spent in stage I crack growth.

It seems generally agreed[204, 213, 222] that the essential difference between Forsyth's stage I growth, at 45^0 to the metal surface, and stage II growth is that only one shear plane is operative at the crack tip during stage I, whereas both planes operate in stage II. This is strongly supported by direct observations of the dislocation structures at stage I and stage II crack tips in copper single crystals by Klesnil et al[211, 223]. Stage II cracks have also been observed, at

low stress intensities, to revert to stage I crack growth[39]. Stage I cracking in f.c.c. metals has been usually found along (111) planes, which is in accord with a shear mode of failure[224] and therefore supports the idea of a single stage I and stage II mechanism. Furthermore, it has been reported in a few cases[225-227], that growth striations have been observed in stage I growth. These stage I growth striations were similar to the stage II markings but tended to be somewhat finer. The rate of growth in stage I is, as discussed in Section 2.4.2, likely to be too small for observation by conventional techniques. Fractographic examination of stage I fracture surfaces is also difficult, since these areas are small and it is hard to replicate the very fine features, if any, likely to be present.

Luther and Williams[228] conclude that, when considering the mechanism of fatigue in an inert environment, the material may be considered as a testpiece composite with a relatively weak surface layer. This model of fatigue was concerned principally with the attainment of a condition of plastic instability. When the weak surface layers becomes plastically unstable, stage I cracks will form, and only when the crack tip attains a condition of plastic collapse will stage I growth change to that of stage II.

2.7.4 The Conjoint Aspects of Corrosion Fatigue Crack Initiation

The environment and surface oxide present on a metal surface both exert a large effect on the formation of PSB's and the nucleation of fatigue cracks therein. This fact was generally discussed in Section 2.6.1. It is hoped here to

review some of the proposed mechanisms responsible for the shortening of fatigue life relative to that obtained in a vacuum. During the fatigue of a metal the mechanical model, whereby PSB's are generated, has the inherent possibility of producing newly produced slip steps or fracture surfaces free of absorbed gas, which can therefore be crack rewelded on reversal of the load. The higher fatigue life generally found in a vacuum is usually ascribed to 'clean' slip steps permitting slip reversal[229]. The rupture of an oxide film by an emergent slip step, on the other hand, has long been advanced[230, 231] as a mechanism for the earlier nucleation of a fatigue crack. Fig. R.25, based on that originally

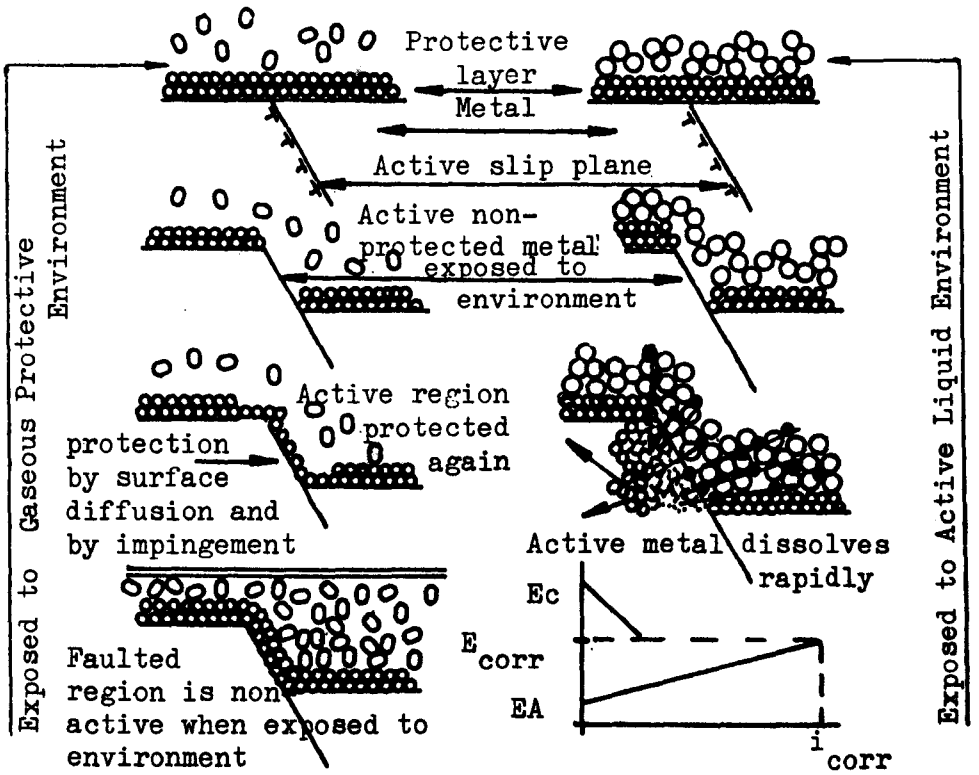

Figure R.25 Schematic diagrams contrasting the dissolution which occurs when a film is broken in air and in an aqueous environment (after Smith and Staehle[232])

Exposed metal area << area of surface oxide

produced by Smith and Staehle[232], illustrates the difference in behaviour of a metal with a protective film while the slip step process is occuring under a protective gaseous environment (e.g. air) and an active aqueous environment. Freshly exposed surfaces are reprotected almost immediately in air while metal ions, soluble in the aqueous environment, dissolve until a new film reforms. From the available data Laird and Duquette[179] concluded that for gaseous environments there is little, if any effect of environment on the initiation of cracks and that the major effect is in the propagation of cracks during fatigue. In strict contrast, aqueous environments were seen to play a significant role in the fatigue crack initiation process.

The existence of oxide films or other surface molecular layers, during aqueous corrosion fatigue, will control the movement of dislocations whose ends terminate at a metal surface. Andrade[233] has found that surface films, even when very thin, have a very marked strengthening effect on the mechanical properties of single metal crystals. He also showed that dislocation movements at the surface may carry atoms of the surface contaminant into the metal. The mechanism of film rupture is only operative provided, obviously, that the film actually ruptures, and also where the rate of film repair is not too high. Originally this mechanism was proposed by Laute[230] for steels. He found that lower test frequencies sometimes gave longer lives owing to an almost continuous film repair. This mechanism has since been supported by Simnad and Evans[33] and Ryabchenkov[231] for neutral solutions but, not,

however, for acid solutions where oxide films are soluble. Duquette and Uhlig[136] experimented with NaCl . solutions at pH 12 where steels showed passivity. The fatigue limit in the presence of this absorbed OH^- surface film was not affected and it was therefore concluded that even where films are present, the stresses generated in high cycle fatigue is not sufficient to rupture the film. Alternatively it was suggested here that, the generation of PSB's occurs at low enough rates that film repair takes place more rapidly than does significant corrosion damage due to the corrosion couple between freshly emerging metal and the film.

Preferential dissolution mechanisms have been used by Evans[234] to explain early crack initiation in corrosion fatigue. This mechanism involves the deformed areas of a metal, such as regions of intense slip, becoming more anodic than the undeformed areas. Pelloux et al[235] have recently reviewed and stressed the importance of PSB's for crack nucleation. Dissolution of the oxide layer has been shown to enhance PSB formation in some cases. Thus a film rupture mechanism could sometimes be a later development of a preferential dissolution mechanism. Parkins[236] has suggested recently also, that anodic dissolution may sometimes remove the initially fatigue damaged surface layer before cracking is initiated. It was further suggested that this process would sometimes continue until the dissolution itself, by producing a fissure, initiates cracking or until the activity decays to the point where an alternative mechanical initiation becomes possible.

Parkins found good agreement, in experiements[236] with mild steel immersed in a carbonate-bicarbonate solution held at -750 mV (SCE), for the time "t" to form a crack of 10^{-2}mm depth when crack nucleation is controlled by dissolution from:

$$t = \frac{10^{-2} Z F \rho}{i M} \qquad \text{(vi)}$$

where i = anodic current density

Z = valency of the solvated ion,

F = Faraday's constant

ρ = density of the metal

and M = molecular mass of the metal

At - 750 mV this system was at its most electrochemically active state: at -1400 mV dissolution was negligible, and at -650 and -500 mV filming of the surface rapidly followed initial dissolution, so that crack initiation times were much faster when not under dissolution control.

Deformation prior to fatigue has been found to have no appreciable effect on crack nucleation[237, 238], so that the mechanism of preferential dissolution of PSB's, resulting in premature crack initiation, is a dynamic one. Lihl[239] and Glikman and Suprun[237] suggest that the cyclic deformation of metal alloys induces slip band precipitation of impurities which then increase electrochemical reactivity. Some dynamically induced electrochemical heterogeneity mechanism is thus seen as responsible for accelerated crack nucleation. Changes in potential, in the active direction, have frequently been recorded during the early stages of corrosion fatigue e.g.[108, 144, 145]. Spahn[162] saw these potential changes as the result of localized corrosion occurring at the anodic

PSB's, and thus lends support for the mechanism of preferential dissolution. Duquette and Uhlig[136], as discussed in Section 2.6.4, potentiostatically applied cathodic potentials to low carbon steels under high cycle fatigue in various solutions. They concluded that a higher general corrosion rate does not occur in cyclically stressed steels and that polarization, as envisaged by Evans and Simnad[33], does not occur in this case. Vedenkin and Sinyavskii[240] investigated corrosion fatigue behaviour of steels under cathodic polarization in neutral and alkaline solutions. They concluded that the action of protective currents was that of changing the pH locally at the metal surface sufficient to generate a passive film and that the observed change in potential of a stressed area is a consequence rather than a cause of cracks. A galvanic couple produced by stressed - unstressed metal was not favoured as a mechanism on this evidence in situations where protective currents are applied. The presence of passive films considerably complicates the process of corrosion fatigue.

One of the earliest proposed mechanisms for crack nucleation in fatigue under aqueous environments was that of pitting[241]. As discussed in Section 2.6.2, reduced fatigue lives are usually obtained in aggressive environments where pits are formed. Mechanically, the shape of the pits formed is all important, however, corrosion induced pits tend to be hemispherical in section so that stress concentrations are not large[13]. Elongated pits have sometimes been found in failures but generally they are now regarded as the result and not the cause of corrosion fatigue cracking. That is, after nucleation and growth, cracks are broadened by corrosion[108].

Pitting, although conceivably a mechanism of fatigue in some environments, cannot be a general mechanism since corrosion fatigue of metals occurs in environments where pitting is known not to occur[33, 136]. Rollins et al[160], working with high carbon steels, showed that initial growth of pits was controlled by a corrosion process independent of cyclic frequency. The geometry of a pit altered from the corrosion induced hemispherical section, to that of an elongated pit, as a crack commenced to develop after some critical pit size was attained. The critical pit size depended on the stress level, suggesting that size necessary to produce local yielding at the base of the pit by reaching a critical stress concentration. Fig. R.26 shows that a

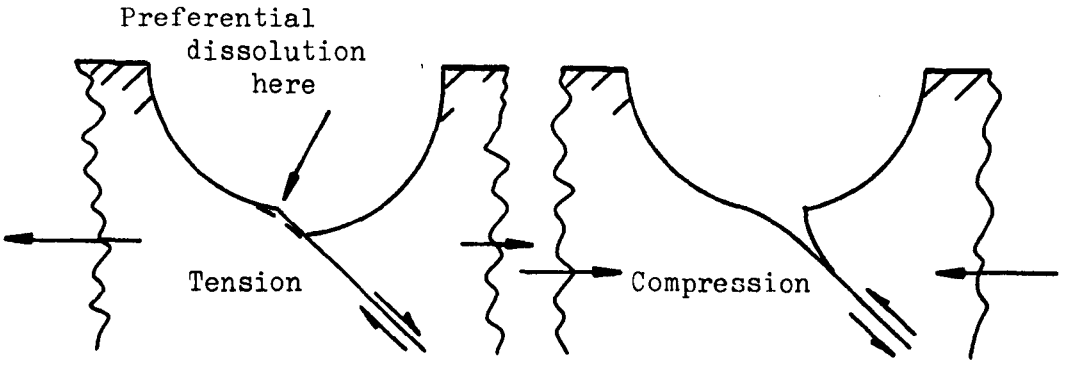

Figure R.26 schematic development of a crack at the base of a pit

crack may be nucleated by the mechanism of preferential dissolution of an emergent slip step at the base of a hemispherical pit. Since there will be little change in the stress concentration factor at the base of a pit so long as it remains hemispherical in section during growth, in fact since the radius is increasing there is a tendency for reduced

stress concentration with growth, this reason for crack nucleation is unlikely. What seems more probable, is that having reached a certain critical size, a pit ceases to grow so that a crack can then be initiated at its base by another mechanism, such as preferential dissolution of an emergent slip step, in the same way as from the surface of a material without pitting. Cracks initiate at pits simply because they are, by geometry and past history, the more active anodic sites. It is far less likely that PSB's, for example, will penetrate the cathodic surface film away from a pit. However, failure of a passive steel, for example, involves metal consumption by repassivation of slip steps rather than dissolution, and pitting may be more important here where a passive layer is destroyed by chloride ions.

Another mechanism for corrosion fatigue, first advanced by Rebinder[243], is the concept of a reduction of surface energy of a solid following the adsorption of a liquid. This Rebinder mechanism has been held by his co-workers as a general mechanism of corrosion fatigue for many years[244, 245]. Karpenko[246] later modified the Rebinder effect and proposed separate mechanisms for crack initiation and propagation: nucleation was still thought to be strongly influenced by absorbates, but propagation was thought to be more the result of an electrochemical process within the cracks. Karpenko[245] based his ideas for a crack initiation mechanism on the results of tests using mild steel in distilled water with and without 1% addition of saponine, a surface active agent. Many cracks rapidly appeared on the steel surface in the treated water and yet in the untreated distilled water they were absent. This observation, together with the results of fatigue

tests in air compared with distilled water, convinced him of the importance of surface wetting. Later work by Karpenko[246] explained the beneficial effect of surface compressive stresses as a suppression of the adsorption factor and thus supported the Rebinder effect for an initiation mechanism. However, even for nucleation, Rebinder's ideas are not entirely acceptable as a mechanism. Andrade[233], as discussed above, has demonstrated the importance of thin oxide films in strengthening single crystals. He interpreted the Rebinder effect as the action of surface active reagents penetrating between the oxide film and the metal, which thus destroyed the otherwise strengthening action of the oxide.

As discussed in Section 2.6.4, Uhlig[149, 123] has established a critical corrosion rate, below which a fatigue limit may be established. A certain small corrosion rate must therefore be maintained to nucleate a fatigue crack. For steels this rate was approximately $2\mu A/cm^2$ which is equivalent to an overall corrosion rate of only 1×10^{-4} atom layers per stress cycle: obviously this rate cannot be responsible for corrosion fatigue initiation since cracks clearly develop at rates only slightly higher than this. Selective corrosion of specific sites may, however, manage to remove small amounts of anodic material. Pyle et al[247] suggest that in order to remove one atomic layer from a step face during each stress cycle, a local dissolution rate of approximately sixty atoms per surface site per second is the minimum rate at which dissolution mechanisms could be expected to produce cracks. In practice therefore, since only very local areas of metal surface are subjected to cyclic slip, the effects on total

dissolution behaviour are extremely small and it is local dissolution only which may play an important role. Patel et al[248] have recently investigated the cyclic-plastic strain enhanced dissolution behaviour of metals, under conditions where they are immune and susceptible to corrosion fatigue failure. Under potentiostatic control, transient dissolution currents were observed at each strain reversal. These currents increased progressively with each strain cycle, where crack initiation was known to occur in practice. They also decrease progressively with continued cycling where the metal was subjected to conditions under which it was known to be immune from corrosion fatigue. Since no exceptions to this rule were found it was concluded that strain-enhanced-dissolution is an operative mechanism of corrosion fatigue crack initiation.

Spahn[142] reviewing a mechanism of corrosion fatigue in the case of passive steels, points out that failure occurs in the fully passive state if only the pH is low enough. He sees the minimum current density necessary for passivation as a prominent factor. This is supported by the fact that steels are more sensitive to corrosion fatigue failure, in the passive state, the higher the current density for re-passivation. Following the penetration of the passive layer by a slip step the local area is repassivated and, during this process, metal is dissolved. Both from a mechanical point of view and from electrochemical considerations, this 'weak-passive-filmed-notched' area is activated again and again so that a crack is eventually nucleated. Strong localization of corrosion in the passive state is observed and,

as opposed to corrosion fatigue in the active state, relatively few cracks are nucleated and lead to fracture.

Yet another mechanism advanced for the nucleation of fatigue cracks is that of hydrogen adsorption penetration into the metal lattice and consequential embrittlement. Under conditions of static stress it has long been known that some metal alloys fail because of the entry of hydrogen atoms into the lattice. An outstanding feature of hydrogen embrittlement is that it is only detectable at low strain rates, so that if a similar process is to occur during corrosion fatigue any mechanism proposed must be strain rate critical. Many mechanisms[249, 250] for the static stress hydrogen embrittlement have been advanced. Zapffe postulated that gaseous hydrogen was formed at discontinuities in steels, and that high pressures were slowly built up which eventually lead to cracking. Cottrell considered a similar mechanism, but that hydrogen atoms concentrated round dislocations and travelled with them through the lattice during strain, discharging as gas at voids or inclusions. Troiano et al[251] see an equilibrium between the hydrogen, considered harmless, in voids or lattice defects and that found in the lattice. Straining is considered to increase the capacity of the voids in the region of which multi-axial stress concentrations occur so that embrittlement is caused by the hydrogen in the lattice. Cracks found in practice are mainly intergranular and, as discussed in Section 2.6.4, hydrogen cracking is induced by cathodic polarization, since this promotes the production of hydrogen.

Karpenko[252] experimented with 0.3%C steel with cathodic

and anodic currents during corrosion fatigue: he attributed the reduction in fatigue strength to hydrogen adsorption at cathodic areas. He also concluded that corrosion fatigue could be the result of one of three mechanisms as illustrated by Fig. R.27.

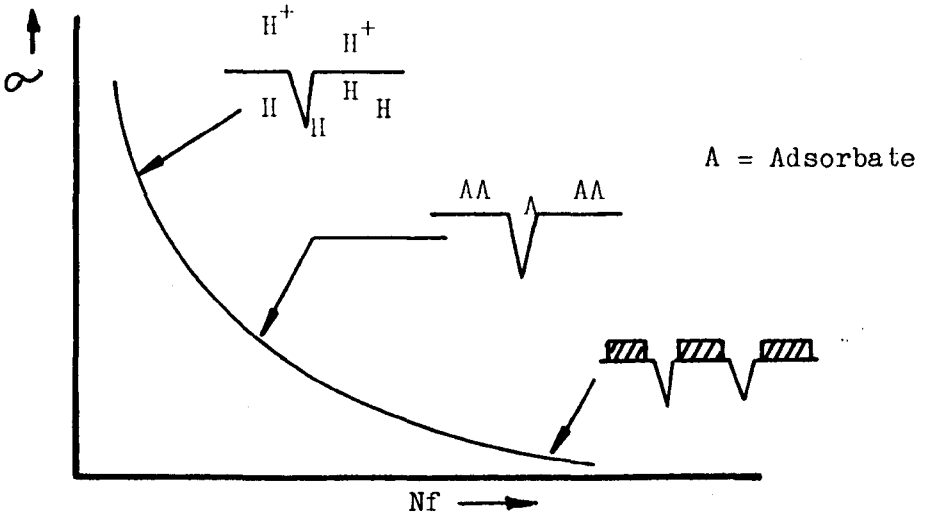

Figure R.27 Schematic diagram of Karpenko model of corrosion fatigue as a function of applied stress amplitude (Karpenko[252])

At high stress amplitudes, hydrogen embrittlement of cathodic areas dominates; at moderate amplitudes, Karpenko's earlier combined adsorption-electrochemical two-part mechanism due to corrosion at anodic areas is operative; and at low amplitudes crack nucleation and growth is considered to be mainly due to an electrochemical corrosion fatigue mechanism. Holder[253] has recently investigated fatigue crack initiation in cast steels with and without surface absorbed water. His results indicate that small amounts of water considerably

reduce the life to initiation of a crack. Hydrogen was also shown to be liberated as a crack commenced to grow. Hydrogen embrittlement was proposed as the failure mechanism and the first stage of such a mechanism has much in common with the Rebinder effect. Beachem[254] proposed a model for hydrogen embrittlement in steel in which hydrogen aided whatever deformation processes the matrix allowed. Hydrogen acts as a plasticizer in iron instead of an embrittler according to this theory: microvoid coalescence, quasi-cleavage, or intergranular cracking are made easier because hydrogen lowers the yield point stress of steel.

The effect of hydrogen on the mechanical properties of titanium and its alloys has recently received considerable attention. Beck[255] has studied occluded hydrogen resulting from the cathodic charging of Ti-8Al-1Mo-1V and Ti-6Al-4V. The resultant embrittlement of these alloys was a function of the interstitial hydrogen content rather than the amount of precipitated titanium hydride. A hydride layer, which is a hard and brittle phase, was also formed on the surface of Ti-6Al-4V by cathodically charging at -850 mV SCE. This layer should serve as loci for crack initiation, however, the presence of hydride did not impair the ductility of commercially pure Ti[255, 256]. Irving and Beevers[257] found that the hydride/Ti matrix boundary was the weakest point and is more likely to be the site of crack nucleation. A similar mechanism of hydrogen embrittlement, to that proposed by Beachem[254], seems to act also for titanium. Hydrogen is required to mobilize dislocations which pile up on hydride/Ti boundaries causing a build up of stress and hence cause crack initiation. In the static stress situation it is generally accepted that it is difficult to initiate cracking in titanium in most

environments. If therefore hydrogen embrittlement is a mechanism of corrosion fatigue crack nucleation it must owe much to the mechanical factors in the dynamic case.

Of fundamental importance, when considering any mechanism, is the nature of slip itself. Considered in Section 2.7.1 as a mechanical feature of the material considered, the details of the slip process clearly affect the effectivearea of clean material surface available for reaction. Figure R.28, after Payer and Staehle[151], schematically compares the slip step heights with the thickness of any protective film: (a) shows coarse or discrete slip where the protective film is easily broken and a relatively large amount of unprotected material is exposed; (b) shows fine or wavy slip where far less unprotected material is exposed and in some cases, where the protective film is a thick one, no fresh material may be exposed for reaction.

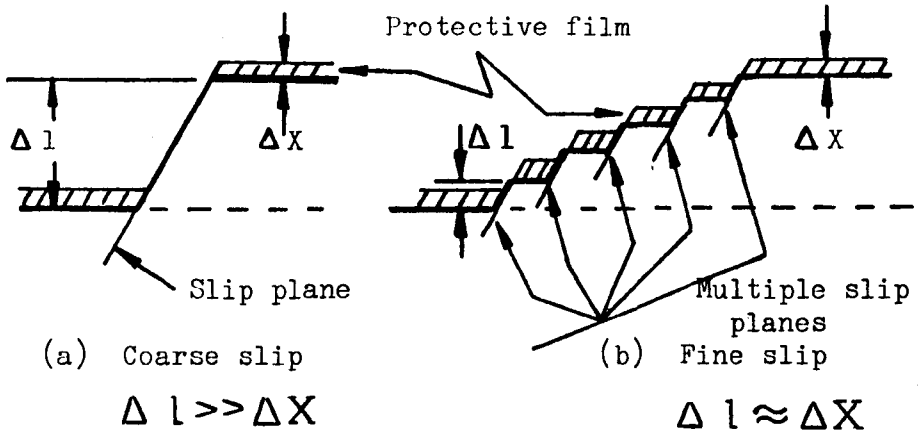

Figure R.28 Comparison of slip step heights with thickness of protective films (a) Coarse slip where step height, $\Delta l >> \Delta X$ (b) Fine slip where step height $\Delta l \approx \Delta X$ (after Payer and Staehle[151])

Latanision and Staehle[258] have shown further that the existence and properties of protective films can affect the nature of slip itself. Slip step height was found to vary significantly for filmed and non-filmed surfaces. The slip lines were spaced at distances five times greater for the non-filmed surfaces than for the filmed surfaces. Corrosion fatigue is thus shown to be a conjoint process from as early as the formation of slip lines.

Pyle et al[247] believe that slip steps must exceed a certain critical width for corrosion fatigue, which for aqueous electrolytes is 5×10^{-4} mm. It is suggested that preferential dissolution bands are at least this wide. They also propose that the height of slip steps is important in determining the fraction of depth of penetration of surface waves which may be used for subsequent crack growth. Widely spaced slip bands are found more often in fatigue specimens than in deformation of metals in simple tension and it is suggested that this is the reason why corrosion fatigue is a more general phenomenon than stress corrosion cracking.

Mechanisms for crack nucleation involving, rupture of oxide films, oxide film dissolution, preferential dissolution, general anodic dissolution, repassivation, pitting, reduction of surface energy by adsorption, critical corrosion rate, and hydrogen embrittlement, have been advanced by researchers to date. It seems almost certain that no one mechanism completely governs all situations of corrosion fatigue crack initiation. A Rehbinder type mechanism of reduction of surface energy by adsorption is attractive for crack initiation but, as discussed, it has some severe limitations. Karpenko's latest

model[252], Fig. R.27, shows a likely change in mechanism with stress amplitude which could account for the results obtained in practice and the frequent division between low cycle and high cycle fatigue studies. For the low stress amplitude region, Karpenko has claimed that corrosion is favoured by cyclic stress so that the electrode potential in highly stressed areas is lowered and the oxide film locally destroyed. The mechanisms involving preferential dissolution and film rupture are thus compatible with the adsorption-electrochemical theory in this high cycle fatigue region. It may well be that the role of a surface absorbate in aqueous corrosion fatigue is to assist in removing the outermost layer of surface atoms. This may also be important regardless of stress amplitude and the fact that this mechanism will not by itself always lead to failure. Another crack nucleation process may then follow, the mechanism of which is dependent on stress amplitude and the metal/environment couple.

2.7.5 The Conjoint Aspects of Corrosion Fatigue Crack Growth

Figure R.6 of Section 2.4.2 is reproduced in Fig. R.29 not only to show again the general form of the crack growth rate curve, but also to consider the division into three regimes and mechanisms as seen by Ritchie[53, 78] for steels. The influence of environment, and consequential conjoint action in corrosion fatigue, diminishes with increasing alternating stress intensity ΔK. Regime C is generally accepted to be uninfluenced by the environment, being the

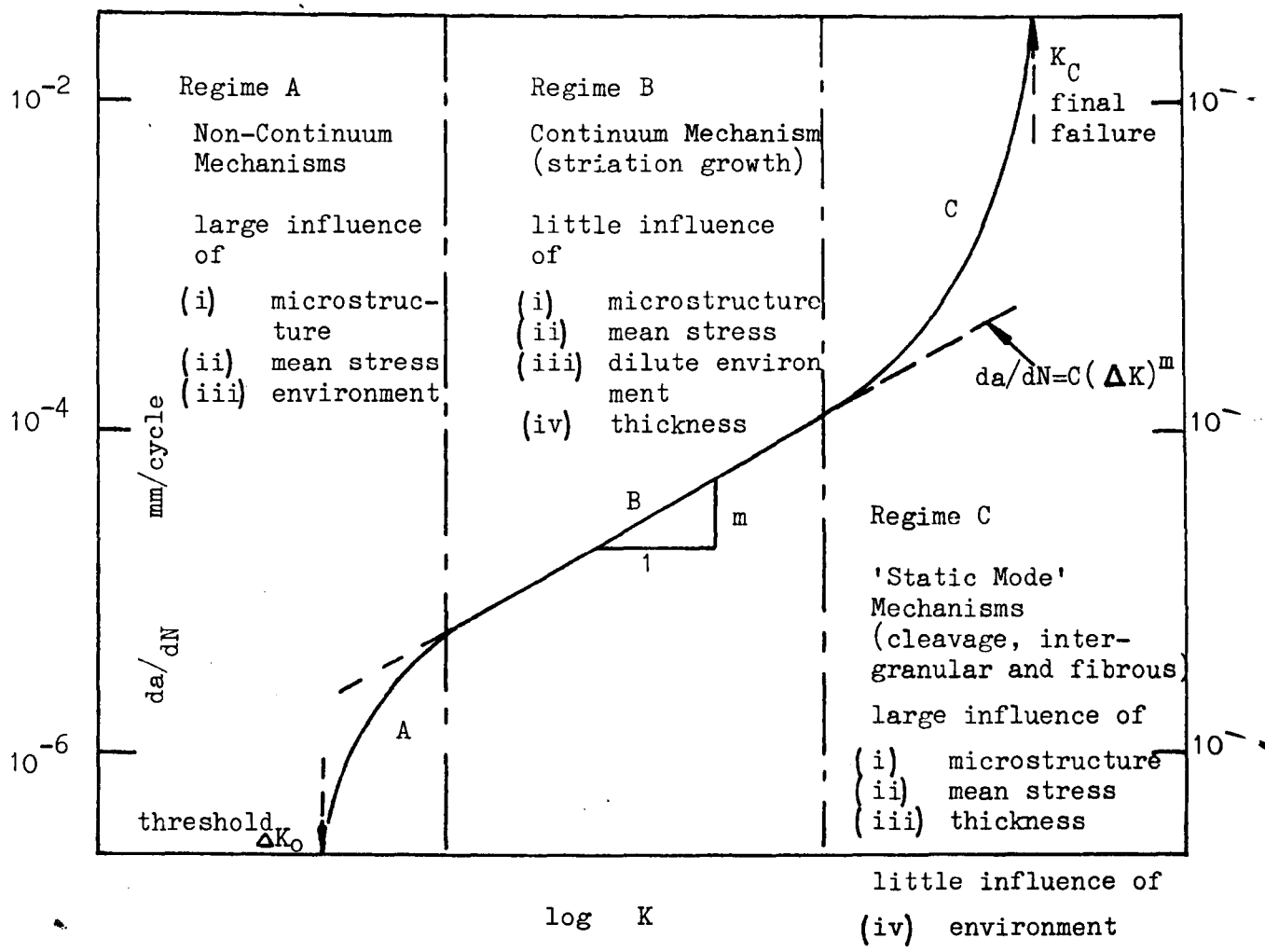

Figure R.29 Primary fracture mechanisms in steels associated with sigmoidal variation of fatigue crack propagation rate (da/dN) with alternating stress intensity (ΔK) (From Ritchie[79])

result of a mechanical "static-mode" mechanism. Regime B has been most extensively studied and, as shown in Fig. R.29, is described by the Paris-Erdogen Law[46] (eqn (ii) Section 2.4.2).

For steels, such failures are clearly by a transgranular ductile striation mechanism with some small increase in Stage II crack growth rates, over those in vacuo, resulting from the environment. Chemically aggressive environments have the greatest effect at low stress amplitudes and at low test frequencies[49, 110, 111, 112]. On the other hand, when considering the effect of some of the major variables, regime A is clearly quite different from regime B. The mechanism is a subject of some controversy and attempts at a model for the determination of the threshold ΔK_o have been mathematically complex[79]. High stress amplitude, low cycle corrosion fatigue has not been clearly separated from stress corrosion cracking in many models and in others these two processes have been combined in different ways. Wei and Landes[111], for example, add the effect of stress corrosion and fatigue while Austen and Walker[259] suggest that the two processes are mutually competitive. The latter model assumes that the crack will propagate by the fastest available mechanism pertinent to the prevailing stress intensity: implying that a corrosion fatigue crack growth curve can be constructed by combining fatigue and stress corrosion plots to obtain the fastest rate throughout. Another model would be required, however, to account for the behaviour during corrosion fatigue at the very low stress amplitudes, where neither fatigue nor stress corrosion processes alone are valid. The application of a fracture mechanics approach for a mathematical model is at present very limited in this region.

The results of Ritchie[79] are endorsed by many but by no means all researchers. Wadsworth and Hutchings[260], and

Clark[261] for example do not share the majority opinion, that the effect of the environment is more important in the early stages of crack formation than in the later subsequent propagation of such cracks. As in the case of crack nucleation the effect of environment may well be quite different in different combinations of metal, stress level, and environment, so that both groups of researchers may be correct in their opinion. Ryder et al[262], working with high strength aluminium alloys in torsion under certain liquid environments, have shown an increase in stage I crack growth rate compared with results in air, yet a decrease was observed in the growth rate during stage II cracking. In contrast to these results, however, they also showed that there was no influence of the environment on stage I growth rates for α-brass and austenitic stainless steels. Stage I crack growth is enhanced by the torsional loading in these results, however, and it could be that such results are not generally applicable to other types of fatigue loading, or mode of crack opening, whether at high or low stress amplitude. Ryder et al conclude that their results do not conform with Laird's[66] arguments that stage I and stage II cracking occur by similar mechanisms. However, in general, the various mechanisms for corrosion enhanced growth of cracks which have been proposed would be a more significant cause of crack extension when the mechanical increment is small. When, for example, the diffusion distance for the corroding medium is small, dissolution of anodic precrack slip steps will be rapid compared with the cathodic sides of a crack. As the crack lengthens diffusion distance is greater. Turbulent back-flow, in the capillary-like channels, is also more likely to occur in longer cracks so

that dissolution is impeded by the accumulation of corrosion products. Recent work by Taunt and Charnock[263] shows that the more mechanically damaging the crack, the less likely it is to have the damaging environment reaching the crack tip and hence the environmental effect is less. Shallow cracks were established as being more chemically damaging with initiation and the first stages of propagation being more chemically influenced than propagation at stage II. Transport of reactive species to crack tips by mechanical pumping of fluid by fatigue oscillations was found to be the most efficient mechanism in all practical situations. Within a long narrow fatigue crack, the supply of reactant may become rate limiting and as discussed in Section 2.6.3 - 5, the composition of the environment within a crack may be quite different from that of the bulk solution.

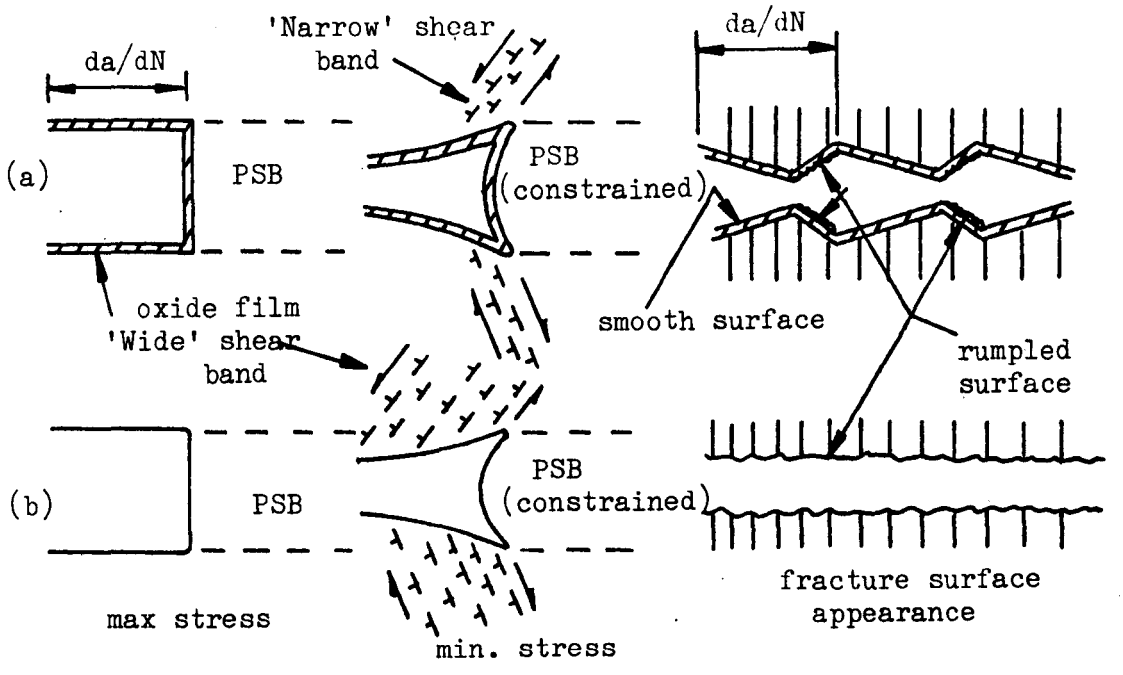

Figure R.30 Schematic diagrams showing deformation of fracture surface close to crack tip during unloading: (a) in aggressive environment producing well-defined striations; (b) in vacuum (after Lynch[213])

As discussed earlier, in Section 2.7.3, Lynch[213] has proposed a model for the formation of striations on fatigue fracture surfaces. The model adapted to illustrate the effect of aggressive environments (a) compared with fatigue in a vacuum (b) is shown schematically in Fig. R.30. Slip steps and oxide films forming on crack surfaces during stage II growth are considered to prevent reversal of interfacial shear, associated with intrusion, during the unloading part of the stress cycle. The first part of each striation is smooth and the second part of each striation is 'rumpled', containing coarse slip steps, for all aggressive environments. The environment clearly, in this model, affects striation appearance since dislocation emergence at fracture surfaces is influenced by the state of the surface. Fig. R.30 (b), shows that compressive deformation during unloading in a vacuum may produce slip over all the fracture surface formed during tensile loading, instead of confining slip to a narrow band immediately behind the crack tip as in the presence of an oxide film, so that well defined striations are not then produced[264, 265]. Schijve[266] has recorded apparently locally discontinuous crack growth at very low stress intensities and it is suggested by Lynch[213] that this is because the development of PSB's cannot keep up with crack growth. Plastic deformation is thought to occur, at very low stress intensities, by cyclic shear on planes at approximately 45^{o} to the crack plane. Although the crack opens and closes each cycle, no crack growth results until accumulation of cyclic shear produces a PSB at the crack tip. The crack advance is thus seen as one by intrusion in a similar manner to that of nucleation from a surface. Schijve[267] sees aggressive environments as

tending to keep the tensile mode of fracture throughout. Fracture surfaces from fatigue in a vacuum tend to have larger shear lips than those produced in mildly corrosive environments. For aluminium alloys for example he found no shear lip on fracture surfaces fatigued in salt water.

The model of Lynch[213], Fig. R.30, not only accounts for the formation of slip bands beneath the fracture surface[215, 216], but also for the saw-tooth profile usually found in practice[204, 214]; that is, a peak matching peak topography on opposite fracture surfaces. With such a model for corrosion fatigue it also seems possible that a secondary fretting mechanism might operate within a growing crack during the compressive half cycle. The mechanism of fretting is stated by Waterhouse[268], after much research, to contain three basic processes:

(a) continuous removal of oxide films from metallic surfaces, which then quickly produce more oxide,

(b) mechanical removal of metal without oxidation and

(c) abrasive action by oxide debris formed in (a) or by subsequent oxidation of metallic debris formed by (b).

In the usual metal surface frettage situation, the manner in which fatigue cracks may be initiated has been widely discussed[269]. Waterhouse has stated that oscillatory tangential relative movement often only occurs on part of the area of contact between two surfaces, and that fatigue cracks originate at the boundary between slip and non-slip regions. In the absence of applied surface frettage, the mechanism of fretting corrosion

is obviously not directly applicable to crack nucleation in corrosion fatigue. Within the confines of a growing fatigue crack, however, the mechanism of fretting corrosion could possibly operate on a miniaturised scale. In the absence of oxygen, only process (b) is possible and the damage rate would be much slower. In more aggressive environments the peak to peak contact of striations, particularly under mode II and III type crack opening, could result in the striation 'damage' profiles which have been reported in some cases[204]. A secondary fretting mechanism during crack growth in corrosion fatigue is not inconsistent with Lynch's model[213] for primary advancement of the crack front. Further, it might be considered possible that, by secondary removal of metal and oxide debris behind the crack, the crack tip is more effectively resharpened during the compressive half cycle.

The Rebinder effect of adsorption and reduced surface energy has also been advanced for aqueous passive state corrosion fatigue as a mechanism of crack growth[244]. The reasoning for the adoption of this mechanism for growth, as well as for nucleation, of cracks follows a study of the "physicochemical mechanics of metals". When a fatigue microcrack forms, the aqueous environment is drawn in by the capillary forces. However, even before the crack has filled with liquid, the surface-active molecules penetrate into the crack by migration along its walls. The adsorptional penetration of the surface-active molecules into the crack will proceed at a fairly high rate and in all cases considerably higher than the rate of the capillary movement of the liquid. The adsorption of the surface-active molecules on the walls of cracks during

their growth reduces the surface energy. Further development of plastic slip and loosening of the metal is facilitated by the reduced work of formation of new surfaces. The adsorption layers will also prevent crack closure during the compression part of the load cycle. There is a complete lack of correlation between adsorption factors and dwell-time under load for passive metals, at any given frequency and amplitude. For this reason adsorption factors can account for the formation of a distinct fatigue limit, as shown by curve (b) in Fig. R.17 of Section 2.7.1. The time factor at a given frequency and amplitude is highly significant, however, in active state corrosion fatigue so that curve (c) is produced and the adsorption factors in this case are in no way sufficient to account for this behaviour. An adsorption mechanism might nevertheless be responsible for the first stages of crack growth in Fig. R.17 curve (c), as well as for the behaviour of curve (b), in the same manner for crack nucleation as discussed in Section 2.7.4. Later in the process, when the corrosion products exert wedging pressure on the crack walls and thus increase the crack tip stresses, another mechanism must prevail. Using isoamyl alcohol adsorption to suppress the corrosion factor in the passivation of the inner surfaces of microcracks, Rebinder et al[244] have shown that the S/N curve does indeed change from the true or active corrosion fatigue behaviour, depicted by curve (c) of Fig. R.17, to that of passive behaviour depicted by curve (b). Rebinder et al[244] refer to curve (b) as an "adsorption fatigue curve", and see this mechanism as an explanation of why the increase in general corrosion observed when an anodic potential

is applied to a system does not intensify corrosion fatigue. The adsorption-fatigue effect is virtually independent of general corrosion processes and over-all increases in system potential do not change the potential difference between the bottom of a crack and its walls. It is this latter potential difference which determines the rate of crack growth of fatigue microcracks.

Corrosion fatigue crack propagation is seen by many researchers[247, 270] as a mechanical mechanism modified by an environmental contribution which is largely due to metal dissolution. Pyle et al[247], for example, see the process as initial dynamic plastic deformation during the tensile half cycle, allowing localized dissolution at step edges on the crack front, followed by reversed slip during the compressive half cycle which sharpens the crack front. Reapplication of the tensile stress then results in either further plastic deformation and dissolution or mechanical propagation by brittle fracture. They see the balance between these two alternatives depending upon the stress intensity at the crack tip and the mechanical properties of the metal. Support for this view is to be found in the brittle striations observed frequently in practice[227, 262, 271-273], and originally thought to be the result of hydrogen embrittlement effects only. Preferential dissolution of newly bared metal at the advancing yielding front of a crack while the static sides become oxide-covered, so that the anode current density there is very much less than at the crack front, is a common

mechanism advanced for corrosion fatigue as well as for stress corrosion cracking. The difference between these processes is usually accepted to be the dynamic aspect in fatigue. Crack growth at high stress levels is enhanced, so that fatigue failure results even in metal/environment systems where stress corrosion cracking does not occur. At the lower stress amplitudes the crack closure is responsible for the resharpening of a crack, whereas corrosion in the static case causes crack blunting.

The possibility of hydrogen embrittlement as a mechanism for corrosion fatigue initiation processes was discussed in Section 2.7.4. An increasing number of researchers also see hydrogen embrittlement as the major mechanism for the growth of fatigue cracks in many metal/environment combinations[79, 140, 274-276]. The mechanism basically involves the production of atomic hydrogen at the crack tip by, for example, reactions of the type

$$Fe + H_2O \rightleftharpoons FeOH^+ + H^+ + 2e,$$

$$2H^+ + 2e \rightleftharpoons 2H$$

The stress gradient ahead of the crack tip then, according to Misawa[274] among others, drives absorbed hydrogen atoms into the metal lattice. Troiano[275], for example, considers that such hydrogen is accumulated at the region of maximum hydrostatic tension, resulting in a reduction of the cohesive strength. Vosikovsky[140] has compared crack growth rates at cathodic and free-corrosion potentials for pipe-line steels in salt water and distilled water environments. He has compared such results also with the crack growth rates in a hydrogen gas environment. In each case he found widely spaced brittle

striations, showing the signs of quasi-cleavage fracture. This steel is not susceptible to stress corrosion crackings and his investigations suggested that the main mechanism responsible for growth acceleration during corrosion fatigue was hydrogen embrittlement.

Cleavage crack propagation is known to result from the suppression of glide or reduction of binding energy, or both, by chemisobed hydrogen[277, 278]. Vosikovsky[140] proposed a discontinuous, two stage crack-propagation mechanism, to explain the substantial differences found in brittle and ductile striation spacings. Favourably orientated grains were thought to have failed by a brittle striation mechanism ahead of the main crack front. The remaining grains then create ligaments which fail either by ductile striations or ductile tearing when exposed to higher strains further behind the crack tip. A balance between the two fracture processes is thought to exist, so that the ligaments left behind the crack front restrain the growth of cleavage and, in turn, the fracture of surrounding material increases the strain on unbroken ligaments. A further possibility of the additional effect of some anodic dissolution to dissolve these highly strained ligaments was seen by Vosikovsky[140], based on the work of Krafft and Mulherin[279] in stress corrosion cracking of high strength steels. Such a three-part mechanism could explain why, under certain conditions, the crack growth rate for free corrosion is sometimes found to be faster than that at cathodic potentials, where the effective hydrogen pressure at the crack tip is higher.

Okada et at[280] have used acoustic emission techniques to study stress corrosion cracking mechanisms in stainless

steels under 3% NaCl aqueous solutions. Such methods can differentiate between hydrogen embrittlement, when acoustic signals are produced, and active path corrosion, when no signals are detected. Their results showed that martensitic stainless steels crack by hydrogen embrittlement but that ferritic stainless steels and AISI type 304 stainless steel propagate cracks by active path corrosion. A similar test under fatigue would be interesting, and it seems highly probable that although hydrogen embrittlement can operate regardless of the applied potentials[281], it may not generally operate for all materials. However, the cracking process in corrosion fatigue does seem weighted towards hydrogen cracking. Smith et al[153] have shown that, apart from the thermodynamic conditions at the root of a growing crack always being favourable for the discharge of hydrogen in steels, significant hydrogen is indeed absorbed. They also demonstrated that crack tip pH in steels is independent of bulk pH, being determined solely by the electrochemical reactions occurring within the confines of the crack. They further demonstrated that the crack tip potential, irrespective of the conditions of external polarization invariably falls below that defining the limit of thermodynamic stability of water (see Potential - pH diagram for Fe/H_2O system in Figure R.15, Section 2.6.5). It is therefore apparent that crack tips in steel, and probably many other materials, are always at potentials where water would decompose to provide a source of the hydrogen necessary to enter the metal to promote failure. Control of pH or potential within the crack, not bulk values, was achieved by Smith et al[153], so that local conditions remained above those for the decomposition

of water and this resulted in zero crack growth rates.

Doker and Munz[282], working with titanium alloys in 3.5% NaCl solutions, see hydrogen-assisted cracking as the basis of a corrosion fatigue crack growth mechanism. They found a significant effect of dwell-time under load, which is said to be indicative of hydrogen embrittlement, and very little effect of rise time, indicating that dissolution effects were small. As a consequence of the high repassivation rate of titanium alloys, hydrogen is though in this case to be produced only at the very tip of a crack. The concentration of hydrogen surrounding the crack tip is therefore small but nevertheless sufficient to change the properties of the material ahead of the crack tip.

A number of mechanisms have been proposed, and briefly discussed in the last few sections, for the physicochemical interactions which govern metal fractures after some period of cyclic stressing in an aggressive environment. A list was made of the major mechanisms for nucleation of cracks in Section 2.7.4, and this section shows that any of these mechanisms could equally apply also to crack propagation, although embrittlement arising from corrosion generated hydrogen is frequently considered the most dominant mechanism here. It appears that a combination of almost all these mechanisms, depending on the metal/environment combination, stress amplitude, and the stage of growth, may be applicable. It is really no wonder that a mix of such diverse mechanisms should produce results which are difficult to interpret. For example, if crack closure resharpens the crack front, does corrosion

prevent this and give rise to a crack blunting mechanism, or does hydrogen cause more cracking ahead of the crack to accelerate cracking? Addition of damage, superposition of damage, and fastest damage path, have all been used as a basis for a mathematical model of the conjoint behaviour but with limited general success. At the present time it seems that the best that may be hoped, for in the near future, is a broad classification of metal/environment combinations with their individual dominant corrosion fatigue mechanism at each stage of life.

2.8 Surgical Implant Metals and Alloys

2.8.1 The Use, Requirements and General Properties of Surgical Implant Metals and Alloys

Historically, many metals and metal alloys have been used since the introduction of gold to dentistry and surgery in the sixteenth century[283]. In the early 1900s, stress-raising features were recognized and eliminated from the steel plates then used as implants. This redesign of implant plates greatly reduced the incidence of mechanical failure, which was very common at the time: corrosion was, however, still a major problem.

The most commonly used implant material in Britain at the present time is stainless steel complying with the British Standard Specification En 58J (BS 970, 1449, 1554 & BS 316 S12), or with the American Specification AISI 316L or 317, These steels are fully austenitic and also contain approximately 3% Mo for increased resistance to chloride ion attack. The use of these materials is laid down by the British Standard on Surgical Implants (BS 3531). The steel is usually cold worked to produce a tensile strength of 760 to 900 MN/m^2 but strengths of up to 1380 MN/m^2 are possible[284]. Rockwell 'C' hardness of 28 to 35, with a grain size of 6 to 7 on the ASTM scale, is usual from a three-quarter hardening process. The Armco Steel Corporation of the U.S.A. have carried out stress corrosion tests in human serum on implants made of AISI 316 stainless steel[285]: no evidence was found to support an earlier report by Zapffe[159] that this material is susceptible to stress

corrosion cracking. AISI 316 steel , apart from having a very low material cost compared with other implant materials, is easily shaped and worked at low cost. These steels have superior strength and fatigue resistance to the cobalt based alloys which were introduced in 1937, just before the 316 type stainless steels. A range of cobalt based alloys was developed for high temperature work in jet engines, which is loosely called Vitallium: the composition is approximately 25 to 30% Cr, 5 to 7% Mo, small quantities of C, Si, Mn, Fe, and the balance Co[286]: British Standards (BS 3531) also covers this material. Apart from an alloy containing tungsten which can be wrought, Vitallium and other Co-Cr-Mo alloys are available only in the as-cast form which can limit their application. Many difficulties[287] have been experienced in the production of this range of alloys when fabricating complex shapes. It is difficult to prevent the occurence of large grain size[288]. The intrinsic corrosion resistance of Vitallium type alloys, however, is generally accepted to be higher than that of stainless steels.

Although these two major types of material are a very considerable improvement on the corrosion resistance, combined with strength, of implants previously used, numerous failures do occur from both mechanical and corrosion causes[283]. Since the use of metallic components in prostheses for permanent replacement of human structures is increasing, with advances in surgical technique, the need to develop new alloys having a service life in excess of the life of the individual patient is urgent.

Titanium is a relatively new implant material[289], having

been introduced by amendment to BS 3531 Standards in 1964. It is now becoming widely used for implants[290, 291], as it is the most inert material yet produced for use in the relatively pure state or, alternatively, as an alloy. A further very important advantage is that there is a tendency for bone to fuse with titanium[292, 293]. The problem of subsequent loosening of the implant is thereby alleviated. Tensile strengths up to 770 MN/m^2 can be obtained with annealed titanium T160[294]. Some concern has been expressed about the low modulus of elasticity, which is approximately half that of stainless steel[295]. Some surgeons believe a high modulus of easticity is desirable so that maximum rigidity is obtained in the fixation of long bone fractures[295]. However, since there is a greater difference in elastic moduli between all metal implants and bone (bone is 5 to 19 GN/m^2 and bone cement only 3 GN/m^2), the lower elastic modulus of titanium at some 107 GN/m^2 would seem adequate. Generally it is the relative movement between implant and bone which is important so that from an engineering point of view, the lower elastic modulus can be viewed as a step in the right direction: that is, more nearly matching the properties of bone. In order to take advantage of this implants may well have to be redesigned, in shape and method of fixation, when working in titanium. The gross mismatch of elastic moduli between implant and bone is an important factor in the failure by subsequent loosening, so frequently recorded in the past: fretting corrosion is also a very likely result of incompatible elastic moduli. Density of bone and bone cements is approximately 1 g/cm^3, so that

titanium at 4.4g/cm^3 has a great advantage over stainless steel with 7.8g/cm^3.

It is reported that smooth specimens of titanium in aqueous environments have a fatigue strength not significanly different from that found in air [269-299]. No instance of crevice attack have been reported below 93°C for titanium and stress corrosion cracking does not occur [300-301]. For precracked specimens, on the other hand, both stress corrosion and enhanced fatigue crack growth have been observed in aqueous environments [296-299,302]. The property of titanium to be easily fabricated by normal workshop methods in the manufacture of implants, rather than by methods involving casting techniques, is indeed fortunate: such precision made implants should not be 'pre-cracked'. Titanium is therefore easily the most compatible material for bone replacement so far produced for implants. Various alloys of titanium have been developed, mainly for the aircraft industry, which are also finding a future as implant materials. The major types in use today are T318, having 6% Al, 4% Va; T680, with 11% Sn, 4% Mo, 2.2% Al, and 0.2% Si; and T550, with approximately 2% Sn, 4% Mo, 4% Al, and 0.5% Si. These alloys all have a comparable corrosion resistance to the relatively pure titanium, but they also have greatly improved mechanical properties [290,291]. According to the manufacturers of these alloys[290], every requirement of implant surgery can be covered using titanium and its alloys. Many thousand such implants have been used during the last decade and a half with some considerable success [290]. How these implants will behave, however, during the normal life-span of a recipient is of course not yet known.

Metallurgical examination of failed implants, by Scales

et al [303,304], and later by Brettle and Hughes [305], has shown that corrosion fatigue is a common cause of the failures which do occur. Transcrystalline cracks are usually found in stainless steel implants. Intercrystalline cracks have also sometimes been found in stainless steel having a high carbon content and also a low molybdenum content. Such steels are now avoided. Fischer and Zitter [306] recommended that low carbon steels or, alternatively, steels stabilized with titanium and niobium should be used to avoid intercrystalline cracking. As far as fatigue performance at human body stress amplitudes is concerned, however, no suitable metallic implant material has yet been found which is in anyway a match for bone.

Galante et al [307] have recently examined fractured femoral stems in cast cobalt-chromium alloys (Müller prostheses), and also forged 316L stainless steel (Charnley prostheses). All the surfaces of these stems exhibited fatigue striations and some, of each material, had fractured by corrosion fatigue within two years of implantation. Charnley [308] has had experience of some 7000 patients and reports that the femoral stem fracture rate is practically zero for patients under 64 kg in weight, but can reach 6% for patients over 90 kg. He suggests that the primary cause of this stem fracture in fatigue, is a defective technique in the use of bone cement which can leave half the length of the stem unsupported: increased stress levels are thus produced. Weightman [309] provides evidence to support this view. He has shown that stress levels for a properly cemented prosthesis femoral stem, in both cobalt-chromium alloys and stainless steel varies, according to design, between 22 and 72 MN/m^2 when supporting

a load equivalent to four-times body weight. Maximum tensile stress at the same load when distally clamped half-way along the stem, however, increased to 145 MN/m^2 for the Charnley design.

'In vivo' measurements in human subjects, at a walking pace of 1.3 m/s, of the hip load for a person weighing 75 kg have produced cyclic peaks up to 1.8 KN [310]. A person weighing only 44 kg still produces peaks of 1.2 kN when walking. The maximum load on a hip prosthesis has been both calculated and measured. It is found to be greatest when descending a step (of 21 cm height) and the magnitude of the load in this case can reach between 6 to 8 times body weight. [310] Human limbs which have been repaired with metallic implants can undergo a very large number of stress reversals in the course of one day. Hicks [295] has estimated that 5000 to 10000 reversals are to be expected per day or up to 3×10^6 cycles per year. Such a figure over the course of an 'active' 8 hour day results in a fatigue frequency of approximately 0.2 Hz average. Rest periods and faster 'walking' paces, for example, of up to ten times this frequency are, however, to be expected. Even greater frequencies could result from the movements of younger, more athletic individuals. However most of the corrosion fatigue data obtained so far, for implant materials has been at frequencies greatly in excess of human frequencies. The further development of new alloys for implants can only really be the result of a study of the relevant dynamic performance. The following tests are therefore required:

(i) corrosion fatigue at realistic 'human movement' frequencies

(ii) fretting corrosion between implants, bone and fixed components, and

(iii) wear between metal joints and high density

polyethylene or other materials for socket inserts.

All these results will need to be evaluated before a new alloy can be recommended for service.

Waterhouse [268] has reviewed some of the observations made on implants, removed from patients, to suggest that fretting corrosion does in fact occur. A review of laboratory tests has also pointed to the fact that fretting corrosion is the most important factor in the failure of implant fittings, where the possibility of relative movement between screws and plates cannot be eliminated in practice. From this point of view the 64Co - 30Cr - 6Mo Alloys used at present are seen by Waterhouse [268] as the safest materials to use as implants. Titanium alloys hold out a promise of improved corrosion fatigue performance but are generally suspected of much greater susceptibility to fretting corrosion and wear at joints. Unless, therefore, a new titanium alloy or a new surface treatment is developed which is proved to be fretting corrosion resistant the inherent improved corrosion fatigue performance cannot be utilized. Alternatively, it may be that new surgical techniques for fixing, for example by adhesives only instead of screws, might entirely remove the possibility of fretting damage at metal-bone junctions: work in this field is progressing steadily [311,312]: acrylic cement is now commonly used, for example, in the fixing of artificial hip joints: ceramics and polyethylene are also being studied for fixation[312]. The matching of implant mechanics to that of the skeleton in order to avoid loosening, known as isoelastic implants is being actively pursued[312].

If such methods are indeed successful, the development of implant metal alloys can be concentrated on wear resistance to the working-joint and corrosion fatigue performance only: the standardization of implants could therefore be simplified. At the present time there are, for example, over 100 different types of total hip implants on the market [312].

2.8.2. The Corrosion Behaviour of Surgical Implant Metals and Alloys

Fig. R.31 shows the reactions which may occur at the surface of an implant metal in contact with body fluids and tissue. Since all the alloys used will be passivable with the inherent danger of breakdown of the oxide film to the active state, both processes are shown. The extremely thin passivating layer can be damaged easily when fitting and also subsequently chemically and by mechanical rubbing in areas of relative movement. Breakdown to the active state most certainly always occurs therefore and must be allowed for when recommending an alloy for service. On account of a relatively large cathodic surface and a small area of film breakdown, a very undesirable acceleration of the localized corrosion process occurs during corrosion fatigue. Apart from the obvious early nucleation of fatigue cracks, a localized accumulation of dissolved metal ions is more unfavourable for the surrounding body tissue than a uniform distribution of corrosion products.

The active state is produced after mechanical removal of the passivating metallic-oxide layer, and metal dissolution then occurs together with repassivation reactions at the damaged surface.

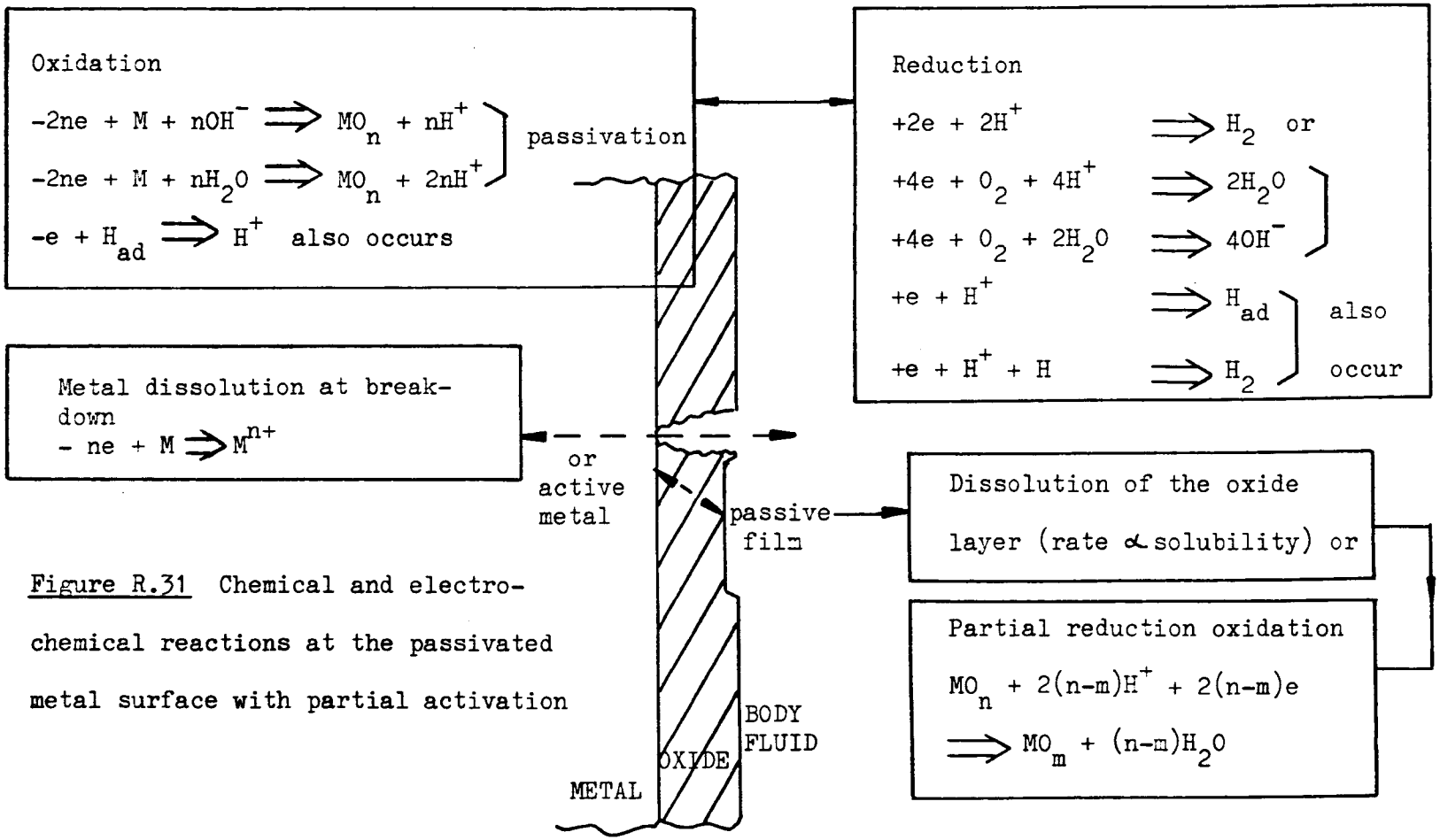

Figure R.31 Chemical and electrochemical reactions at the passivated metal surface with partial activation

Because the total electrons absorbed by the implant material, by reduction of the hydrogen ions and the dissolution of oxygen, must equal the total released electrons resulting from metal dissolution and repassivation, these reactions do not depend entirely upon the electrochemical properties of the metal: reaction kinetics is also significant. Implant surfaces must repassivate rapidly, after damage to the oxide, to inhibit the active dissolution of metal. The potential of the associated oxide electrode should therefore exhibit a high negative value. Redox potentials of oxide - electrodes, for example Ti/TiO_2 =-1.5V SCE at pH = 7, may serve as a guide but, as pointed out by Schaldack and Hull [313], mixed potentials that are not foreseeable can become established in practice.

Electron conductivity of an oxide is an important factor to be considered. Titanium oxide, for example, is non-electron conducting but can become capable of conducting electrons as the result of alloying. The diffusion of oxygen in titanium oxide is the limiting function and the reason generally accepted for the unexpected slow repassivation rate of pure titanium. An improvement in performance of titanium under conditions of fretting corrosion, for example, should result from an alloy having increased electron conductivity in the oxide layer. Materials such as stainless steel and cobalt alloys have electron conducting passive oxide layers, so that the repassivation rate is determined primarily by the velocity of the reduction/oxidation reaction at the surface, i.e. the passing of electrons through the solid/electrolyte interface. In the passive range, anodic current densities in the range 10^{-6} A/cm^2 for stainless steels,

ranging to below 10^{-9}A/cm^2 for the more passive alloys of titanium are found [313]. When stainless steels or nickel alloy undergo pitting, the initial breakdown occurs very rapidly and the current density increases 10 to 100 fold within a few seconds. Thereafter, the current density will fluctuate as the film heals and then suffers breakdown at some other site. The current density for the cobalt based alloys attains a passive current density that then remains constant. The titanium alloys, however, continue to show a decrease in their passive current densities with the passage of time; a behaviour which is most desirable for implants that must remain 'in situ' for many years.

It is helpful here now to take a look at the thermodynamics of corrosion as established by Pourbaix [150], by studying the domains of passivation on the relevant Potential - pH diagram, where available, for implant materials. The potential - pH diagram for the Fe/H_2O system was produced in Fig. R.15 adapted from Pourbaix [150]. As discussed in Section 2.6.4, there are many complications and limitations to the application of Pourbaix diagrams. Stainless steel, for example, is likely to be a very complex resultant of the properties of the constituent metals. However, a knowledge of the thermodynamic properties of the products of attack of the constituent metals is sought here, so that the likely passivation conditions for implant alloys may be predicted.

Fig. R.32 shows the potential - pH diagram for the Cr/H_2O system in solutions containing chloride [150]. It is clear that chromium is a very base metal, as its domain of stability lies considerably below that of water. This diagram, when compared with a Pourbaix diagram for solutions not containing chloride [150],

shows increased solubility of the hydroxide. Hence chromium is more easily attacked in chloride solutions and the region of passivation is drastically reduced to a narrow band between 7.9pH and 8.7 pH, that is, outside the normal range for implant environments. The arrowed lines on Fig. R.32 to R.34, marked 3 → 4 and 5 → 6 are results to be discussed later.

Fig. R.33 shows the potential - pH diagram for the Ni/H_2O system. Since the domain of thermodynamic stability for nickel has a small zone in common with that of water, it can be considered to be a slightly noble metal: certainly it is more noble than iron or chromium. The diagram for cobalt is very similar to this diagram for nickel and is not considered here separately: nickel is slightly more noble than cobalt. It is unfortunate that, in the case of nickel, there is much experimental evidence as reviewed by Pourbaix [150], which is not in agreement with the theoretical diagram of Fig. R.33. Generally tests in the upper regions of the theoretical corrosion domains do not result in corrosion, and in the predicted passive domain there is often in fact no corrosion in practice. The theoretical diagram seems therefore to be a very conservative prediction of the passive domain. It is further unfortunate that the behaviour in the presence of chloride in the solution is not yet available as a potential-pH diagram.

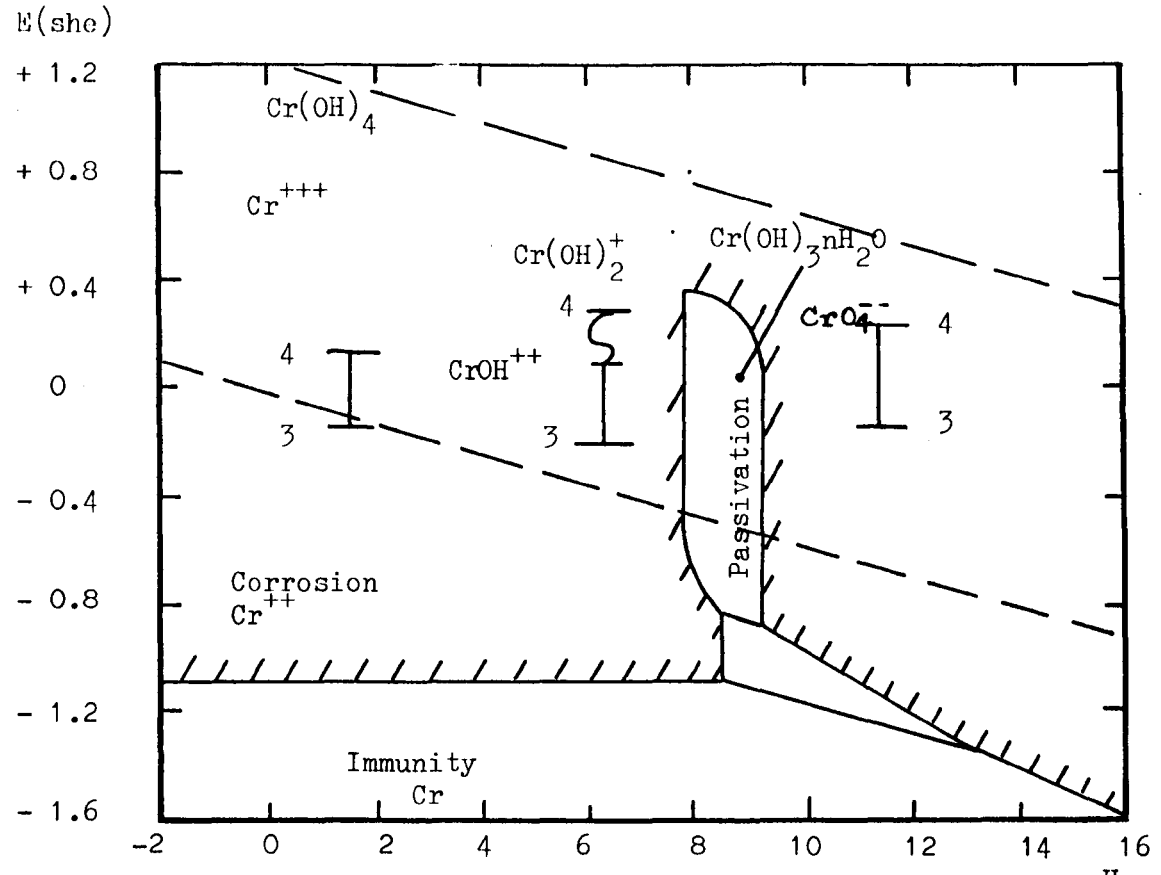

Figure R.32 Potential pH diagram for the Cr/H_2O system in solutions containing chloride

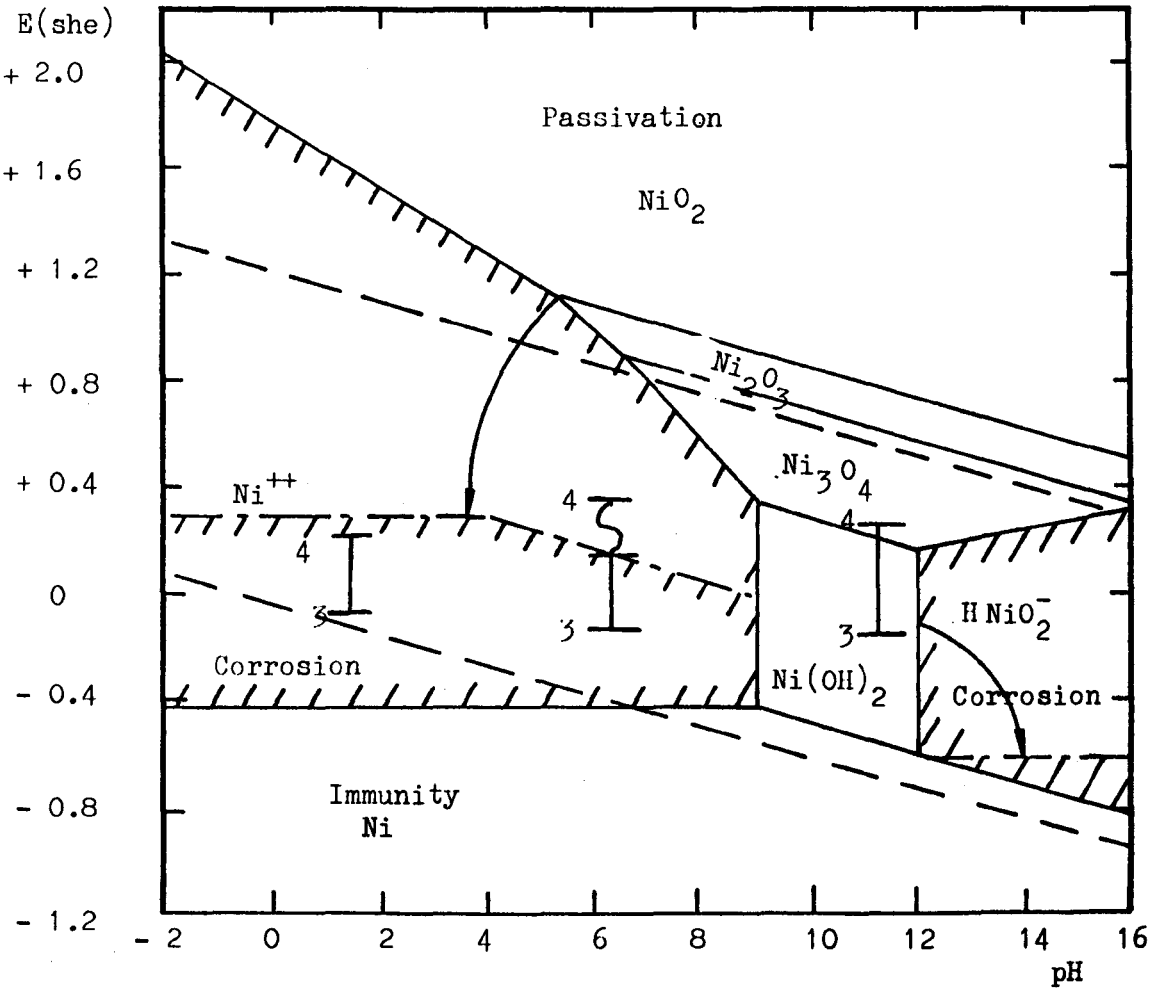

Figure R.33 Potential - pH diagram for Ni/H_2O system (practical results show reduced corrosion domain-←)

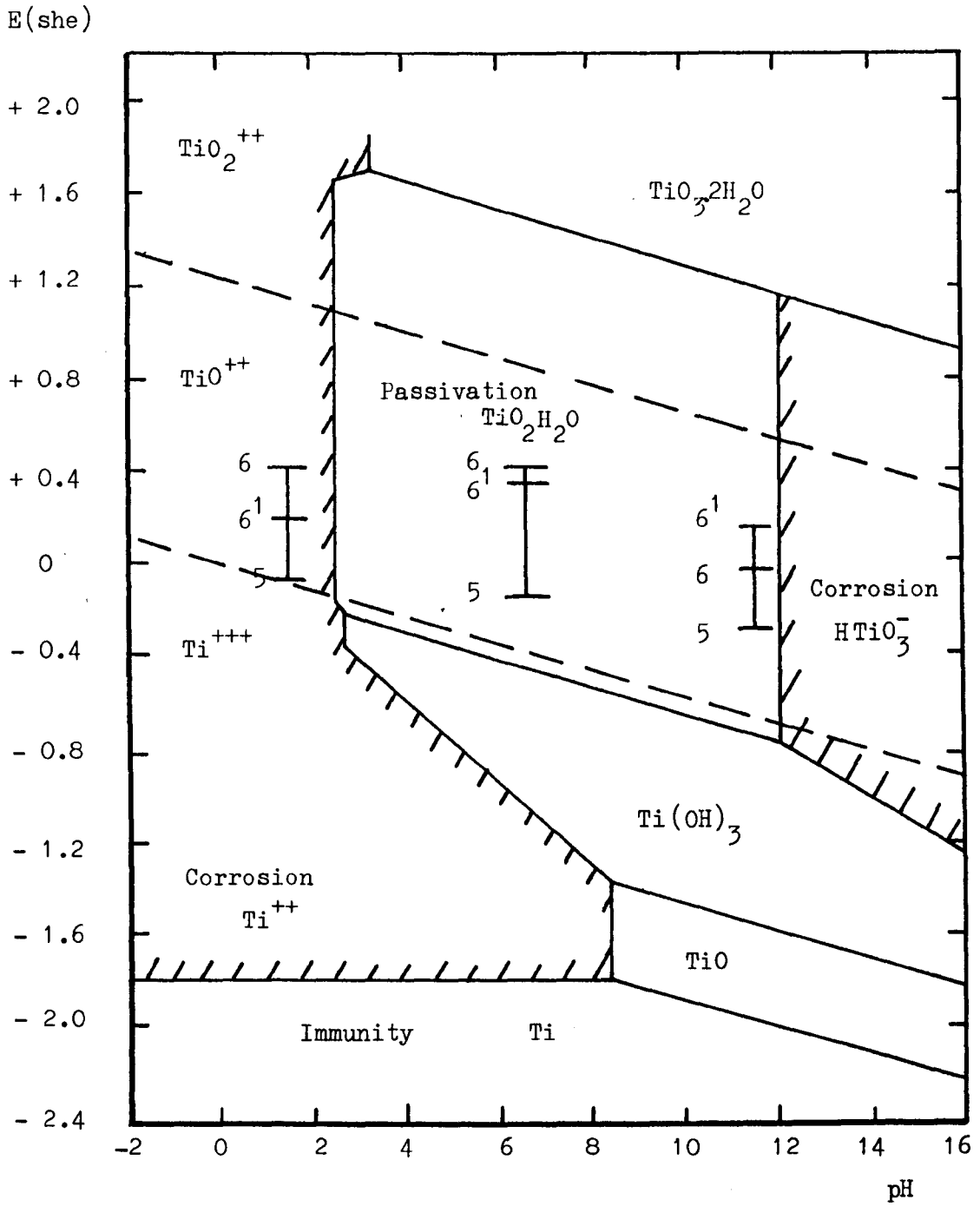

Figure R.34 Potential - pH diagram for Ti/H_2O system

Fig. R.34 shows the potential - pH diagram for the Ti/H_2O system. Titanium is clearly not a noble metal since its domain of thermodynamic stability lies well below that of water: the relatively high electrode potential exhibited by titanium is entirely the result of the passivating oxide film on its surface. The domain

of passivation at the potentials normally recorded (in the vicinity of OV she) is large, showing possible corrosion at pH 2.5 or less and pH 12 or more.

The environment, in which surgical implant alloys are required to perform satisfactorily, is a mix of human body fluids such as blood, plasma and lymph, all containing a considerable concentration of chloride ion. Testing 'in vivo'[283], or in a substitute living system, is practised sometimes when events in the dynamic living system must be observed, and which would otherwise not be found. Most commonly, however, 'in vitro' testing, externally in laboratories, is employed. For convenience and simplicity simulated body fluids are used for 'in vitro' testing. Hanks's physiological solution [314], is one such solution which is a fairly close imitation, from the chemical aspect, of the fluid in muscle and bone. The composition is as follows:

	(g/l.)
NaCl	8.00
$CaCl_2$	0.14
KCl	0.40
$NaHCO_3$	0.35
glucose	1.00
$MgCl_2.6H_2O$	0.10
$Na_2HPO_4.2H_2O$	0.06
KH_2PO_4	-
$MgSO_4.7H_2O$	0.06
NaH_2PO_4	0.10

Hoar and Mears[144] have used Hanks's solution in an electrochemical behaviour study of corrosion - resistant alloys, intended for use as surgical implant materials. A much simpler

0.17M sodium chloride solution, with additional carbonate and phosphate to buffer it at pH7.0 was also used. The latter simpler solution gave results very similar to those found in Hanks's solution. It was also found that, without the buffering, specimens in 0.17M sodium chloride generally maintained a potential of 50 to 100 mV more positive than their counterparts in the buffered solution. An electrolyte of isotonic saline, suitably buffered, thus appears to be an appropriate substitute for body fluids. The pH of body fluids is normally neutral [314] but due to fracture trauma and operative shock, as well as locally in crevices, the pH can for a time become very acidic [62, 159] and is thought to approach unity. Experimentally pH2 has been recorded [311] with consequent active corrosion of stainless steel implants. The aggressivity of body fluids with respect to all implants can be best compared [315] on the basis of potential - pH diagrams corresponding to a redox potential of - 150 to + 100 mV. Hoar and Mears [144] describe some 'in vivo' measurements of potential from implants in goats and humans. After some difficulty with scratching of the implants and consequent repassivation behaviour complications, it was found that implants generally maintain potentials quite close to those of the same alloys in Hanks's solution at 37°C. Finger pins used in the repair of human digital ligaments were observed 'in vivo' and the results indicated that the steady state potentials of unscratched implants are

0.20 to 0.30V (she) for 18Cr - 10 Ni - 3 Mo stainless steel

0.30 to 0.40 V (she) for 27 Cr - 7 Mo - balance Co (Vitallium)

0.45 to 0.55 V (she) for titanium

These potential ranges are then of particular interest for testing

'in vitro' during corrosion fatigue. However, some degree of abrasion between fixing screws, bone and implants is bound to occur during the implanting operation. Film breakdown as the result of scratching of the metal surface is very probable in practice so that a wider range of potentials is also of interest. Since scratching of these implants generally immediately lowers the potential by several hundred millivolts, [144] a range of potentials suitably lowered, should be examined for fretting and corrosion fatigue studies.

In 0.17M sodium chloride solutions, breakdown of passivity was found, by Hoar and Mears[144], to occur with the generation of electrobrightened pits at 0.20 to 0.50V (she), approximately 0.90 V(she), and 20 to 30 V, respectively for stainless steel, cobalt based alloys, and titanium alloys. Hoar and Mears[144] conclude that stainless steels and nickel alloys are unlikely to resist all breakdown by pitting when exposed to body fluids indefinitely. A very recent review article by Jordan et al [316] showed evidence for fatigue failure in stainless steel bone screws, intermeduallary rails, a spinal brace, and in cardiac pacemaker leads. Such failures in corrosion fatigue are primarily the result of the passive film breakdown which can nucleate fatigue cracks. Hoar and Mears[144] further state the cobalt-based alloys have a better performance and may well withstand exposure to body fluids for very long times. Unfortunately they would also produce a slow passage of cobalt into the environment by cation transport through a passivating oxide film. They also further conclude that titanium and especially some of its alloys should withstand exposure to body fluids for an indefinite period. There would, however, be an extremely small passage of titanium into the environment transported in a similar manner to that found for cobalt.

What is required is an insoluble oxide so that no transference of metal to the environment occurs. Few if any oxides are completely insoluble, and over a period of perhaps many years in the case of an implant, transference may be appreciable. It is important to consider in this respect, notonly how much metal may eventually be found in body tissues, but what metal will be found: is the metal particularly dangerous to health? The possible migration and accumulation of certain metal ions in vital organs of the body has to be studied by the medical profession. Some metal ions are much less well tolerated by the body than others and cause a more severe reaction. Brettle [287], in a survey of the literature on metallic surgical implants, advances this as the reason why some mild steel implants, inserted during the earlier treatment of fractures, caused little discomfort to the patient although showing gross corrosion. Chromium and particularly nickel is more objectionable because it can cause bone necrosis and inflammation [317]. Cobalt is also a cause of concern owing to the long term concentration in vital body organs resulting from ion migration [317]. At the present time, there is no metallic material available which is free from toxic elements, and which might be useful as an implant material. Tests with implants of CoCrMo -, FeCrNiMo - alloys and titanium in vivo have shown that only titanium has properties suitable for surgical implants in human subjects [293].

2.8.3. The Corrosion Fatigue of Surgical Implant Metals and Alloys

The corrosion fatigue of metals in general has been

Material	Smooth Specimens			Notched Specimens	
	In Air 10^8	In Saline 10^7	In Saline 10^8	In Air 10^8	In Saline 10^8
Titanium Base					
1. T160 (CP Titanium)	247 (370+)	268 (180*)	268 (320+)	116	89
2. T318 (Ti-6 Al-4 V)	378 (490-)	469 (248*)	433 500-	137	130
3. T550 (Ti-4 Al-4 Mo-2 Sn fully heat treated)	278		326	113	86
4. T551 (Ti-4 Al-4 Mo-4 Sn fully heat treated)	261		261	96	96
5. T680 (Ti-22 Sn-4 Mo-$2\frac{1}{4}$ Al)	344		295	126	100
Stainless Steels					
6. 316 S 12 (Annealed)	240 (230#)	206 (400*)	203 (190#)	103	75
7. 316 S 12 (20% cold worked)	440 (700#)	372	337 (530#)	123	106
8. 316 S 12 (High nitrogen annealed)	268		203	72	68
9. Duplex stainless steel (25 Cr-5 Ni)	399		340	143	106
Cobalt Base					
10. Co-Cr-Mo alloy (as cast)	247		234	137	48
11. Co-Cr-Ni-W Wrought alloy (annealed)	440		364	179	127
12. Co-Cr-Ni-W Wrought alloy (cold worked)	385		268	144	89
13. Co-Cr-Ni-M Wrought alloy (NP35N cold worked)	310		310	179	120

Table R.1 Fatigue strength of implant materials at AWRE in MN/m^2 at 10^7 and 10^8 cycle endurance limits, using Amsler Vibrophore ≏100 HZ after Hughes et al[318]. Also, + T130 Smith [319], * Jordan[62], - Smith and Hughes[322], and # Smith and Hughes[320]. Data in brackets refers to rotating bending tests.

discussed at some length in the previous sections. The next step is to review the corrosion fatigue research which is of particular relevance to the metals and metal alloys now in use for implants. The results shown in Table R.1, presents the data for smooth and circumferentially 'vee' notched specimens (k_t=4) for a variety of implant materials researched at AWRE by Hughes et al [318] and Jordan [62]. This comprehensive list of 10^8 cycle endurance limits for surgical implant alloys may be taken as a basis from which to assess the relative performance of each material. Hughes et al [318] used an Amsler Vibrophore machine at frequencies of around 100Hz and a 0.17 M NaCl solution at pH 7.4 with free access to oxygen. Smooth specimens of stainless steel (316S12), 20% cold worked, are clearly shown to have a high air fatigue strength which is reduced by 23% in saline. The wrought alloy of Co-Cr-Ni-W has the same high air fatigue strength and is reduced by 17% in saline. The titanium alloy T318 on the other hand, although possessing a lower fatigue strength in air than the other two materials, shows a 15 % increase in strength in saline: at 433.5 MN/m^2 it is easily the best performance at 10^8 cycles in a saline solution. The notched results are not so clearly defined into material classes, but it can be seen that a reduction by 70% occurs in fatigue strength in saline solutions because of the notch for T318: this material has still the best performance, however, but the difference is not so remarkable in the notched condition. Other results [62,319,320,322] which have been obtained in subsequent work at AWRE by alternative methods of testing are also included on Table R.1., in brackets and keyed for reference. These results often show some considerable

differences in corrosion fatigue performance, the reasons for which will now be discussed.

The influence of frequency and cold work on the fatigue strength of a 316 stainless steel in 0.17 M saline was investigated by Smith and Hughes[61, 319, 320, 321]. Using rod-shaped specimens in rotating bending tests over the range 1 to 60 Hz, the fatigue strength of material cold drawn to give a hardness of 387 HV was found to be independent of the test frequency for this mode of stressing. It was proposed therefore that accelerated tests at 30 Hz would be in order for such tests instead of the 1 to 2 Hz of natural body movements. Such raising of test frequencies is of course useful, but it remains to be shown whether a more realistic 'flexing-deformation' load application can also be speeded-up.

The effect of cold working the material was found to reduce the fatigue endurance for stainless steels in saline at 10^7 cycles, from 700 MN/m^2 in air[320], by some 24%. Since the corresponding reduction in the annealed condition at 140 HV was 17%, from 230 MN/m^2 in air it could be argued that cold working resulted in a larger drop in fatigue strength from air to saline solutions. The resulting endurance limit for the cold worked material is nevertheless some 179% improved in saline solutions, compared with 204% improved for fatigue in air, over the annealed material. Differences between the Amsler tests and those obtained by rotating bending were not significant for the stainless steels in the annealed condition. The considerable differences between the results for the two methods of testing the cold work material, however, illustrates the interdependence of residual stress,

structure, and type of applied stress. Cold work clearly increases the resistance to fatigue in bending, where the maximum applied stress is at the worked surface, more effectively than in direct tension.

Jordan[62, 316] has investigated the frequency dependence of stainless steel, titanium (T160), and titanium alloy (T318) when they are all in the annealed condition. Fig R.35 shows the results obtained in rotating bending in 0.17M saline

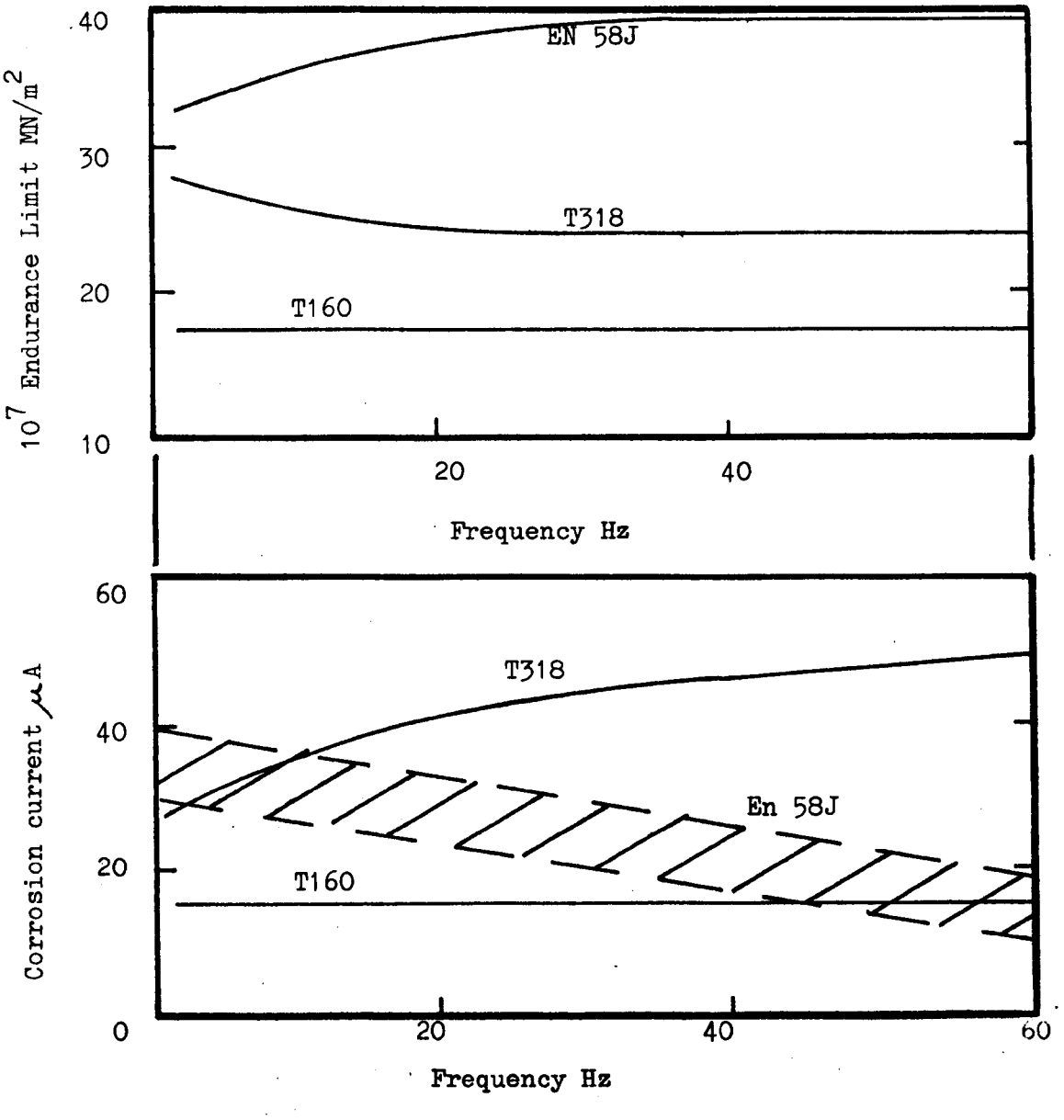

Figure R.35 The variation in fatigue strength and corrosion current with frequency in a 0.17M saline (after Jordan[62])

at pH 7.4, between 1 and 80 Hz. Smith and Hughes[61, 320, 321] found no effect of frequency for cold worked stainless steel, but Jordan[62, 316] found that in the annealed condition some 11% reduction in 10^7 endurance limit was obtained at the lower frequency. T318 showed an increased limit at the lower frequency of approximately 8%, while the commercially pure titanium T160 exhibited complete independence of frequency. As discussed in Section 2.4.6, the corrosion fatigue performance of many materials is improved as the frequency increases, reducing the time for corrosion. The behaviour of the titanium alloy T318 is therefore rather surprising and indicative perhaps of a different mechanism of failure to that which operates for the stainless steel, at low stress amplitudes. At the high stress amplitudes, however, the behaviour of T318 regarding frequency was similar to that of the other materials so that a longer life was obtained at the lower frequencies[322]. Figure R.35 shows also a corresponding plot of corrosion fatigue current for these materials under potentiostatic control, in the range 1 to 80 Hz, as recorded by Jordan[62]. The currents were measured at stress levels equivalent to their 10^7 endurance limits at each frequency. These results mirrored the effect of frequency on the endurance limit previously recorded; that is, a constant current for T160; decreasing current with decreasing frequency for T318, in accord with increased endurance at lower frequencies; and increased current for stainless steel at lower frequencies corresponding to the reduced endurance.

Jordan[62] reports also that the 10^7 endurance limit of 400 MN/m^2, (Table R.1), for annealed stainless steel bars in rotating bending was very high in comparison with the result

of 206 MN/m^2 he had previously obtained using the Amsler Vibrophore. Conversely, endurance limits at 10^7 cycles were very much lower for both T160 and T318 annealed materials in saline under rotating bending than those obtained in Amsler tests. The stainless steel performance was concluded to be affected by grain size and the opposite behaviour in titanium was thought, by Jordan to be the result of differences in specimen surface finish:all material was tested as received and the finish of T160 and T318 was very poor. At first sight it is difficult to see why, if the surface finish had such an effect on the titanium as to be responsible for differences in corrosion fatigue performance between bending and direct stress application, it would not also have a similar effect on the stainless steel. However Bapna et al[323] report, after a study of the influence of surface finish on the fatigue life of stainless steel, that this factor has very little effect for stainless steel. This result confirms the findings of Jordan, although it might still be thought surprising to some researchers as surface finish on all steels has generally received much attention in the past. It is no doubt a question of degree, so long as a surface score mark does not become a stress raising notch. Such findings regarding the relative unimportance of surface finish are also quite in accordance with those obtained for mild steel[108] in distilled water fairly recently. Differences in grain size, specimen size, load application and type, as generally discussed in Section 2.4 and 2.5, do result here in different corrosion fatigue performances for these implant materials. These conclusions serve to emphasize the importance of obtaining as

close a resemblance to the implant service conditions, with each variable, as possible.

The rate of crack propagation in stainless steel is slightly faster in saline than in air. Colangelo[324], at high stress intensities, as well as Wheeler and James[325], over a more moderate range of square-wave stress applications, both obtained this result from their work. Since Hughes et al[318] have shown so clearly that the fatigue strength decreases substantially in saline solutions for the case of small, smooth, type 316 specimens, it is apparent that the initiation period is shortened in the presence of chloride ions.

Further work by Jordan[62] to investigate the effect of pH of saline on the 10^7 cycle endurance limit, for the 20% cold worked type 316 stainless steel smooth specimens, showed that this limit was reduced progressively from 372 MN/m^2 at pH 7.4 to 344 MN/m^2 at pH 4.5. A drastic fall in the endurance limit to 179 MN/m^2 then followed at pH 2.5. Tests on commercial purity titanium in the annealed state, for comparison, showed a reduction in 10^7 endurance which was quite modest; from 268 MN/m^2 at pH 7.4 to 244 MN/m^2 at pH 2.5. Such results could account for the now common observation[305] that stainless steel implants fail by corrosion fatigue more frequently in practice than cast Co-Cr-Mo or titanium components. The results of the laboratory tests so far conducted, at normal pH values, do not reveal deficiencies in corrosion fatigue preformance for implant materials when the body fluids become locally acidic. It is unlikely that any substantial improvement, in the corrosion fatigue performance of materials other than titanium alloys, can be made as the result of new manufacturing techniques. It is the promise of improved

corrosion fatigue performance over a wider range of pH for implants which makes any further improvement in the mechanical properties of titanium alloys worthwhile.

The titanium alloy T318 (Ti-6Al-4V) has received considerable attention in the aircraft industry, since it combines good corrosion properties with a high strength and low weight. Unfortunately much of this research generally, and in particulr with respect to fatigue, is not directly applicable to implants. However, it is useful to consider the work which has been done to discover the effect of microstructure, produced by various heat treatments, on the fatigue properties of this alloy. Figure R.36 is a section of the

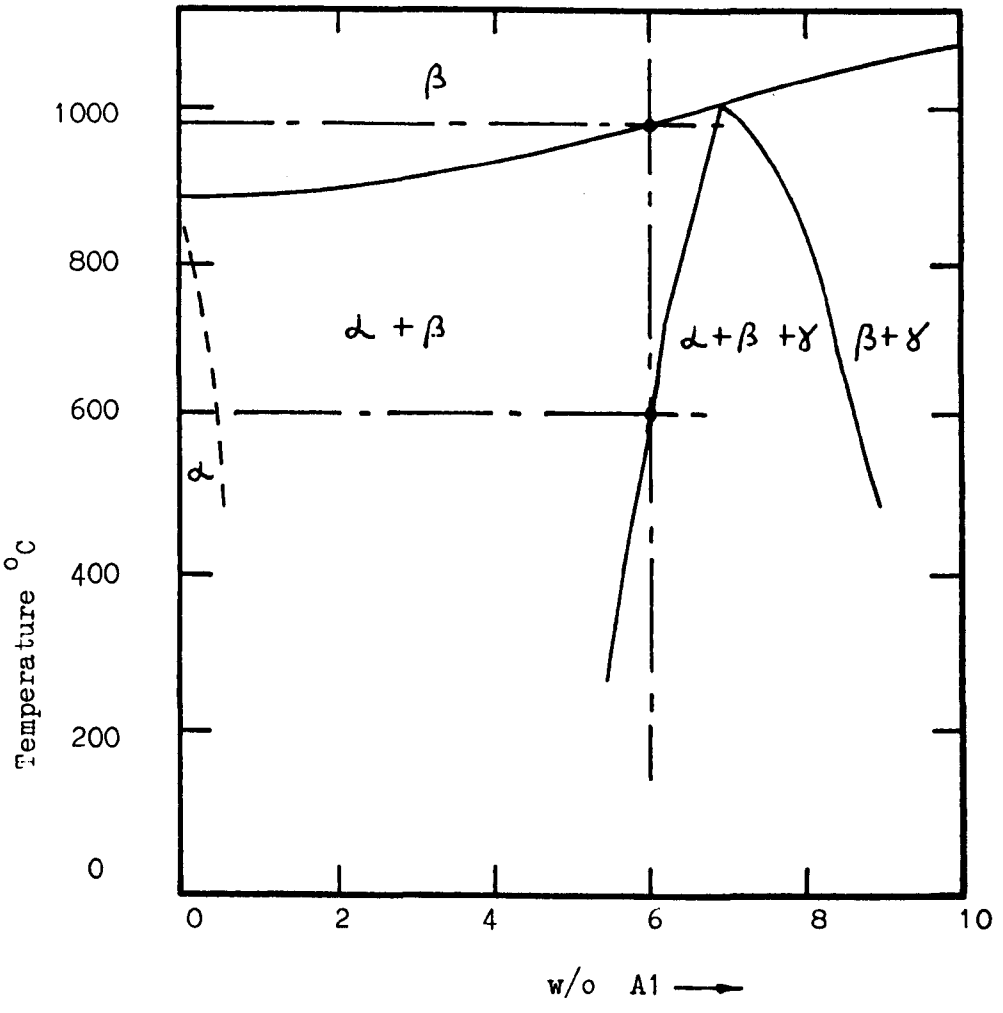

Figure R.36 Vertical Section of the Ti-Al-V Phase Diagram at 4 w/o V

Ti-rich end of the Ti-Al-V tenary phase diagram, from which it is seen that a 6% Al alloy has a single β phase structure above about 990°C. Cooling from this temperature produces a two-phase structure consisting of a hexagonal α phase which is rich in titanium, and a body-centred cubic β phase. A third γ phase ($Ti\ Al_3$) should exist at temperatures below about 600°C according to the phase diagram, in Figure R.36 but in practice the microstructure of this 6% Al alloy is found to consist of large α grains with approximately 10 to 15% β phase present.

Bartlo[326] has varied the temperature of annealing in the $\alpha+\beta$ region and obtained different relative proportions of the α and β phase. Subsequent thermal treatment experiments by Bartlo[326], which were later confirmed by Lucas and Konieczny[327], showed that grain coarsening lowered the fatigue strength of both smooth and notched specimens. The α grain size was shown to be important in respect of high cycle fatigue: a reduction from 18μm down to 5μm produced an increase of 134% in life at 10^8 cycles. Lucas[328], and Bowen and Stubbington[329] have found improved fatigue life by increasing the amount of deformation, during component manufacture, in $\alpha+\beta$ region. Reduction in the β grain size followed by refinement of the α grain size was considered advantageous. Lucas[328] and Broichhausen and Kann[330] investigated the effect of β-forging at 1038°C and at 1093°C. The lower temperature β-forging was found to have much better fatigue properties than similar $\alpha+\beta$ forged material at 968°C, yet the higher temperature β-forged material was only marginally better. Again the reason for this result was explained in terms of the quite different microstructures obtained in each case. The lower

temperature β-forged material, exhibiting the best fatigue performance, had much finer α platelets, within the prior β grains, than those found at the higher temperature. Grain size is all important for air-fatigue performance and for high frequency corrosion fatigue.

So far as corrosion fatigue data is concerned, very little information is available which is directly relevant to the implant situation.

Waterhouse and Dutta[331] examined the corrosion fatigue behaviour of T130 and T318 alloy in a 1% sodium chloride solution and compared the behaviour with that in air as a basis for a study of fretting.

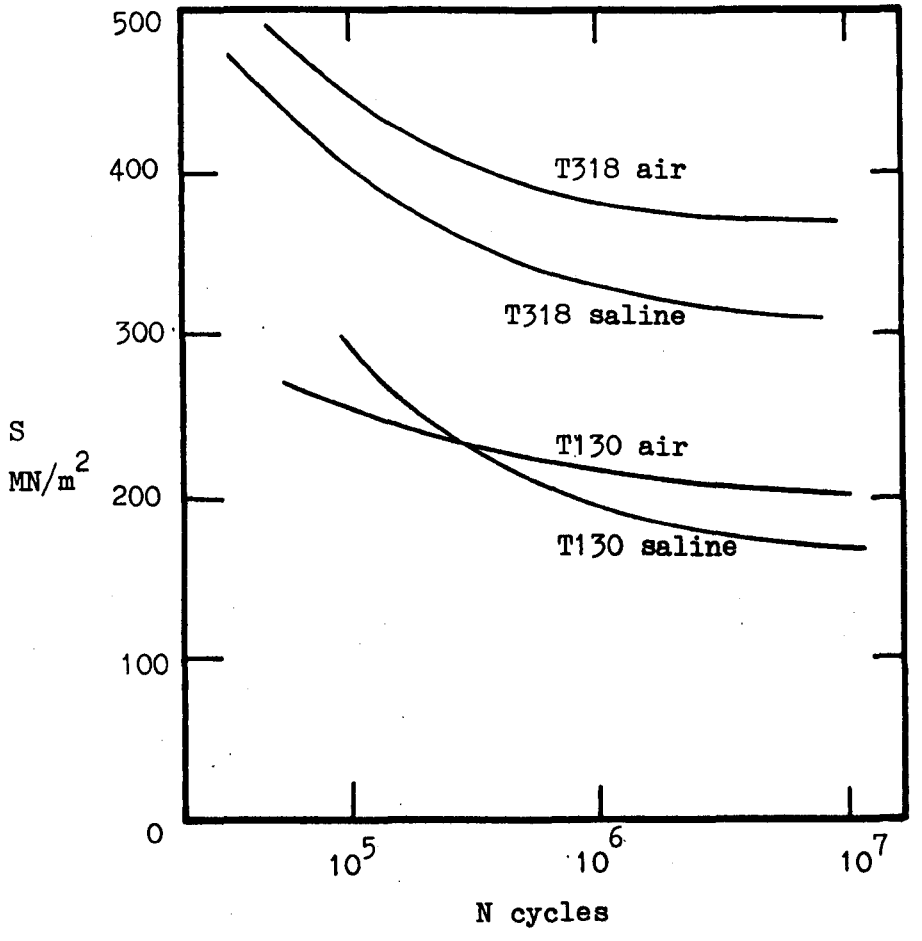

Figure R.37 The Effect of Saline on Fatigue of Ti-6Al-4V alloy (after Waterhouse and Dutta[331])

A four-point-loading rotating-bending fatigue machine was used in this work. Figure R.37 illustrates the results which clearly show a decrease in fatigue strength at all stress amplitudes for T318 when fatigued in saline. However, T130 results showed a 'cross-over' in the curves. Rather different results were obtained for T318 by Hughes et al[318] for smooth specimens tested using an Amsler machine. Fatigue performance at 10^8 cycles in this case was slightly improved, in a similar 0.17 M saline solution, over that recorded for air. Notched specimens were found, by Hughes et al[318], to behave similarly in air and in saline, suggesting that it is the nucleation of a crack which is most affected by the environment. Centre-notched plate bend specimens tested by Judy et al [332] in a 3.5% saline solution also behaved similarly in air and in saline: the crack growth rates were the same. A Ti-7Al-2Nb-1Ta alloy, however, was found by these workers to be extremely crack-rate sensitive to environment. Dawson and Pelloux[131] measured the crack growth rates for Ti-6Al-4V and found rather different results to those of Judy et al: the presence of chloride ions, as discussed in Section 2.6.2, was found to increase fatigue crack growth. The different results which have been obtained, both for total life of smooth specimens and crack growth rates for pre-cracked specimens of this Ti-6Al-4V alloy, show that corrosion fatigue performance is strongly dependent upon the method of testing. It would therefore be useful if more tests were conducted with appropriate variables for implant applications.

Potentiostatic control was used by Jordan[62, 315] to

investigate the effect of applied anodic and cathodic potentials on the corrosion fatigue of T160 and T318. The results are shown in Figure R.38. A feature of both materials was the local minimum value of the endurance limit between 0 and approximately -200 mV (cathodic). A local maximum endurance for T160 occurred at approximately -2000 mV (cathodic): other turning points and local maxima for T318 were not established outside the range ±2V. The fall in endurance found for T160 at potentials more negative than -2000 mV were attributed to the effects of hydrogen evolution. At potentials above about 1000 mV (anodic) film breakdown and pitting occurred resulting in a wide scatter in the endurance values for T160. The equilibrium domains as indicated by Pourbaix (see Figure R.34) are of interest and are included in Figure R.38. Smith and Hughes[322, 333] using rotating bending for stressing T318 alloy in 3.5% saline, however, found no significant effect on fatigue strength of applied potentials of -1400 mV to +1400mV (SCE). Smith[319] has also tested titanium specimens which had been anodised in a 5% phosphoric acid solutions. An oxide film of approximately 1600 Å was found to consistently result in a longer fatigue life in saline than specimens tested in the as-ground condition.

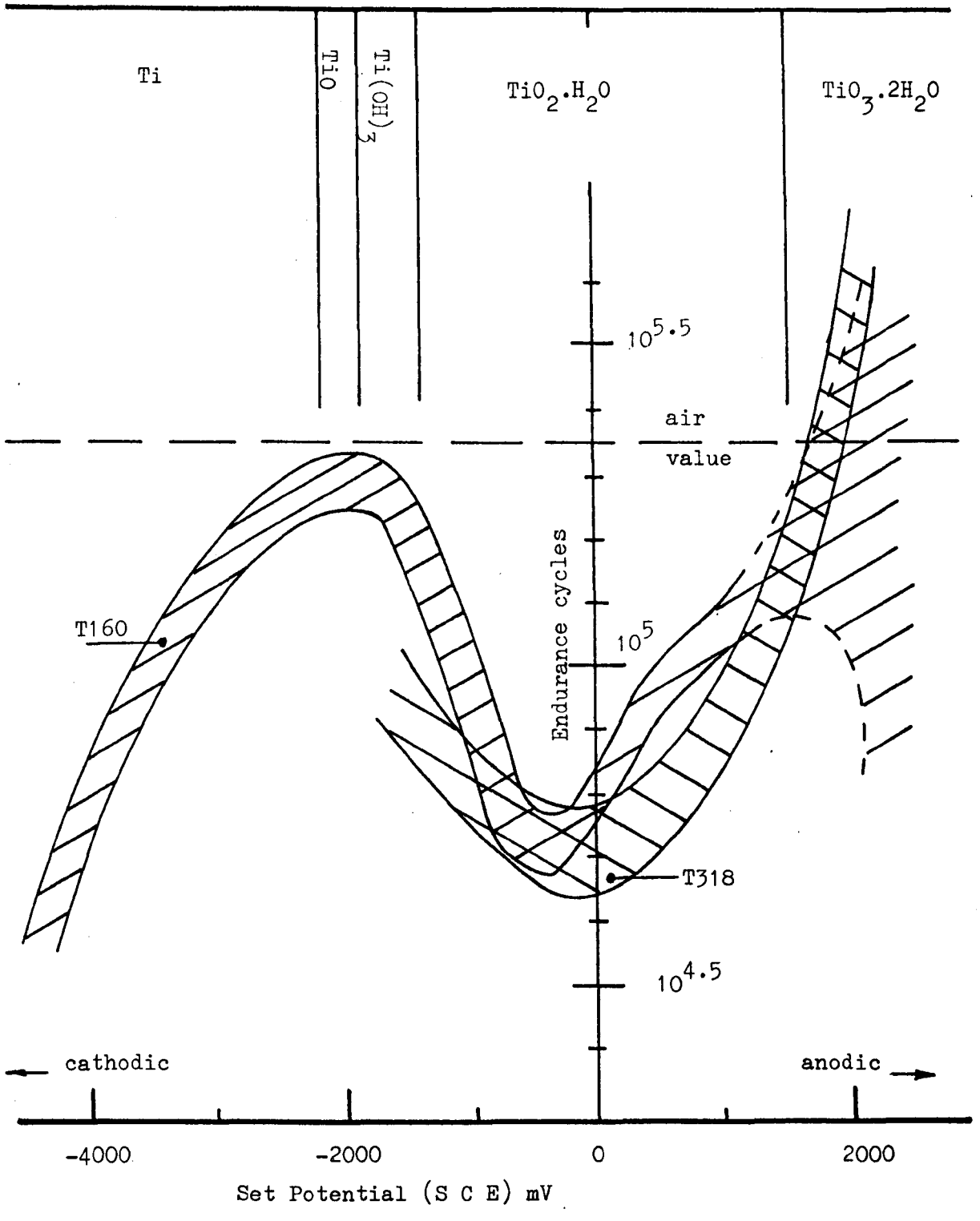

Figure R.38 The effect of applied potential on the fatigue endurance of T160 and T318 in neutral 0.17M saline solution (results from Jordan[62] presented in modified form) at 50 Hz and constant stress amplitude.

3. EXPERIMENTAL TEST PROGRAMME

3.1. Background and Object of the Test Programme

3.1.1. General Background to the overall Test Programme

The present programme of work was initiated as the result of discussions between two groups of researchers at a conference of corrosion fatigue at U.M.I.S.T., organized by C.A.P.A./I.Corr.T, on the 3rd and 4th April, 1973. A paper [108] entitled "Low Frequency Corrosion - Fatigue of a Carbon Steel with Stress Concentrations in Distilled Water", which was an account of work carried out at the Hendon site of Middlesex Polytechnic by Booker and Whitaker, was read by the present author. Another paper [318] entitled "Corrosion - Fatigue of Surgical Implant Materials: Test Methods at A.W.R.E." which described the work undertaken on behalf of the Department of Health and Social Security at the Atomic Weapons Research Establishment, Aldermaston, by Hughes, Jordan, and Orman, was also presented. Subsequent discussions between the authors of these two papers indicated that co-operation in some further research could be fruitful.

Most of the corrosion fatigue work at A.W.R.E. had been conducted at high frequency, and it was required to confirm the predictions which had been made for implant material behaviour at more realistic frequencies. It was also desired to resolve doubts about the validity of the test method of load application by employing a more typical mode of stressing/straining for implants. A test facility, similar to the one originally designed by the author for work on mild steel, which would provide reversed bending fatigue at a typical walking pace was thought to be the most attractive solution. It was therefore decided to redesign and build such test rigs, to the authors specifications, at three sites: A.W.R.E.; Middlesex and City of London Polytechnics.

A supply of implant metals and metal alloys from A.W.R.E., for the production of specimens at Middlesex Polytechnic, was agreed so that the same materials could be tested on the different sites undertaking this research. Separate programmes of research to be performed at each site were agreed so that, although each site programme was independent and could progress at its own pace, it was hoped that the separate results obtained finally would be mutually enhanced.

3.1.2. General objectives of the test programme at Middlesex Polytechnic.

The overall objective of this research was to investigate the behaviour of some surgical implant alloys during corrosion fatigue in simulated body fluids. The influence of drilled holes necessary for the fixation of some implants, and of variations in the environment was particularly of interest here.

Previous work [108,318] had investigated the relative interactions of mechanical strain and metallic corrosion during the conjoint action of corrosion fatigue. An interaction theory had been developed for implant alloys at A.W.R.E. [318] and, concurrently, also by the author for mild steel [108]. It was hoped in the present work to establish a more general theory of such interaction effects. Specific combinations of material and environment were planned to be investigated with this objective in mind. Mild steel, austenitic stainless steel (type 316), commercial purity titanium (T130), and titanium alloy Ti-6Al-4V (T318) were all considered.

The first of these materials tested was considered because it was naturally non-passivating and could therefore be used as a basis of comparison in contrast to the behaviour of the characteristically passivable implant materials. The environments for each material were chosen to be 0.17M saline, which could be adjusted to produce three selected pH conditions (1.5, 6.5 and 11.5), together with distilled water, and tests in air for comparison.

The influence of strain amplitude, geometric stress concentrations, salinity, and pH on corrosion fatigue performance was particularly sought.

3.2. Experimental Facility and Procedures

3.2.1. Design of the test rig and details of specimens

Surgical implants frequently take the form of plates, through which holes have been drilled for the purpose of fixing them to human bone. The most common form of the stressing applied to such bone plates is that due to bending. A specimen for corrosion fatigue testing in bending of not too dissimilar size and proportion was therefore seen as highly desirable. Fig.1 shows the plate specimen design and the method of applying load by flexing the plate. Specimens were of an "hour glass section" waisted design, with some specimens having a hole drilled through the plate at mid-position, as shown in Figure 2. Location dowels and bolts were used to secure each end of the plate specimen to support legs (Fig.1). The clamping support legs were manufactured from the same material as the specimen under test, i.e. stainless

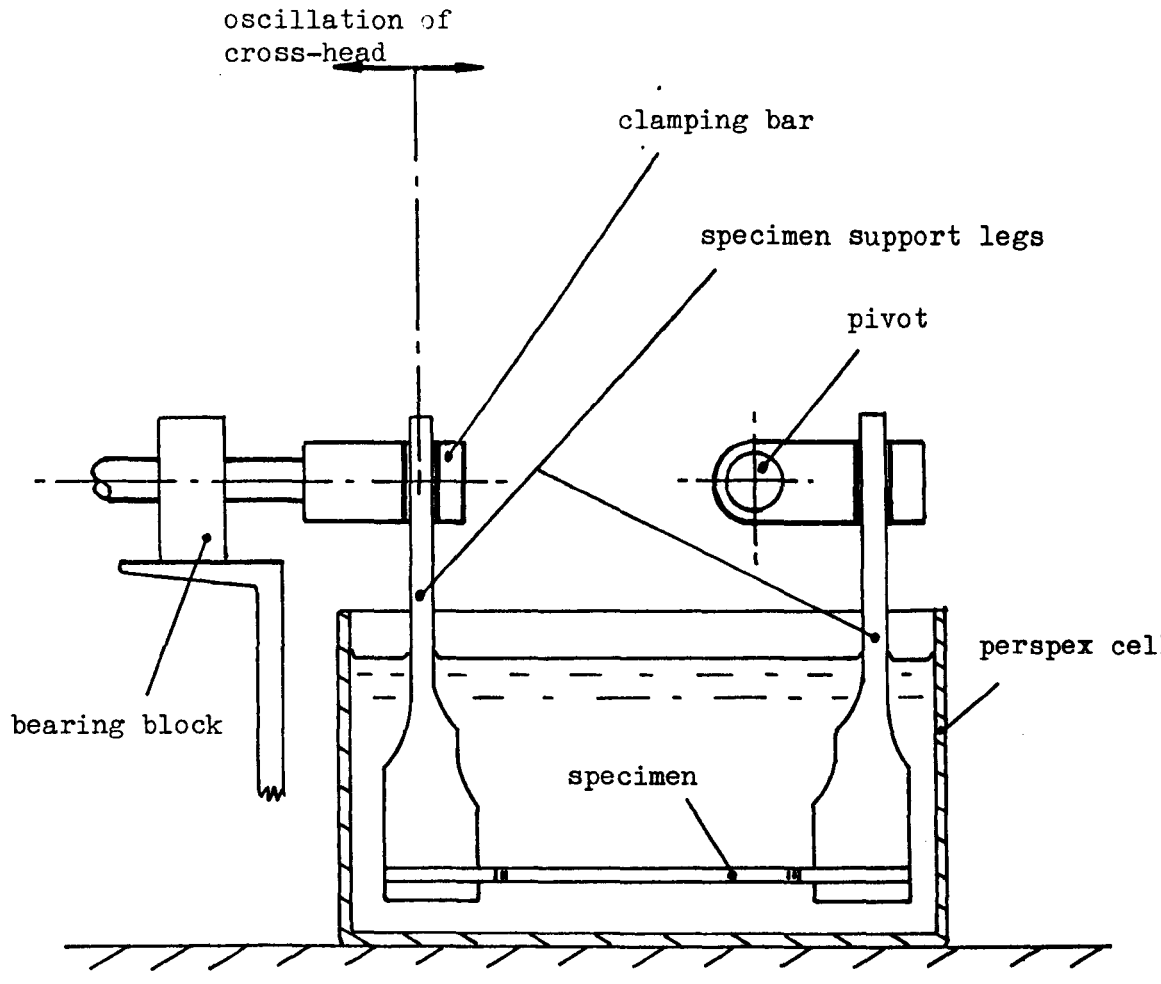

Figure 1 Schematic diagram showing one cell of a rig for testing flat plate specimens by reversed bending

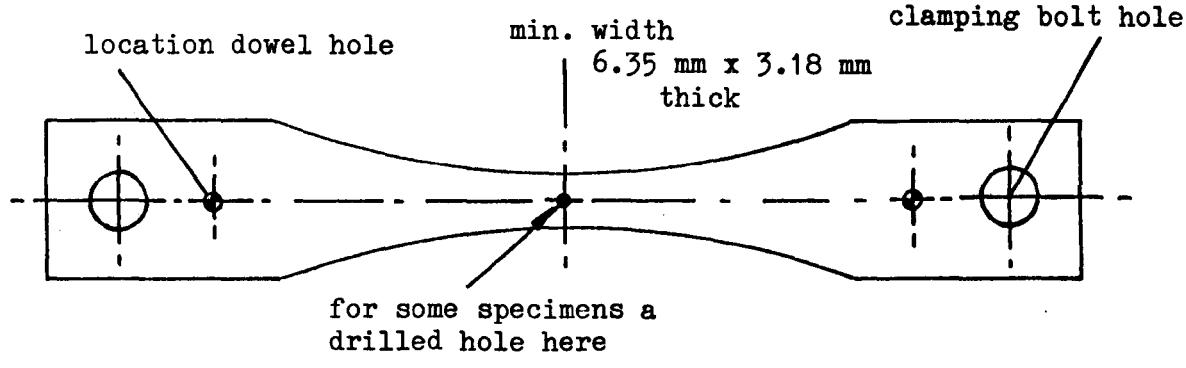

Figure 2 Design of flat plate fatigue specimen

steel for stainless steel plates and titanium for titanium plate specimens; dissimilar metals in contact were thus avoided. One leg was firmly clamped to the crosshead of the rig (Fig.1) while the other leg was free to pivot with the oscillating motion of the crosshead. The design thereby produced a reversed bending type of loading; the specimen was flexed so that its surface went through a tension-compression-tension cycle.

A much cheaper and simpler form of specimen was used for mild steel tests. As reported in earlier work [108], the U-bend form of specimen and reversed bending method of straining has been proved in distilled water corrosion fatigue studies: such a specimen is illustrated in Fig. 3, cold rolled to shape. Owing to the action of the pivot, the position of maximum stress and resulting fracture occured at 15° from the centre of curvature, as shown in Fig. 4 (a). The position of the drilled hole in these specimens is shown in Fig. 4(b).

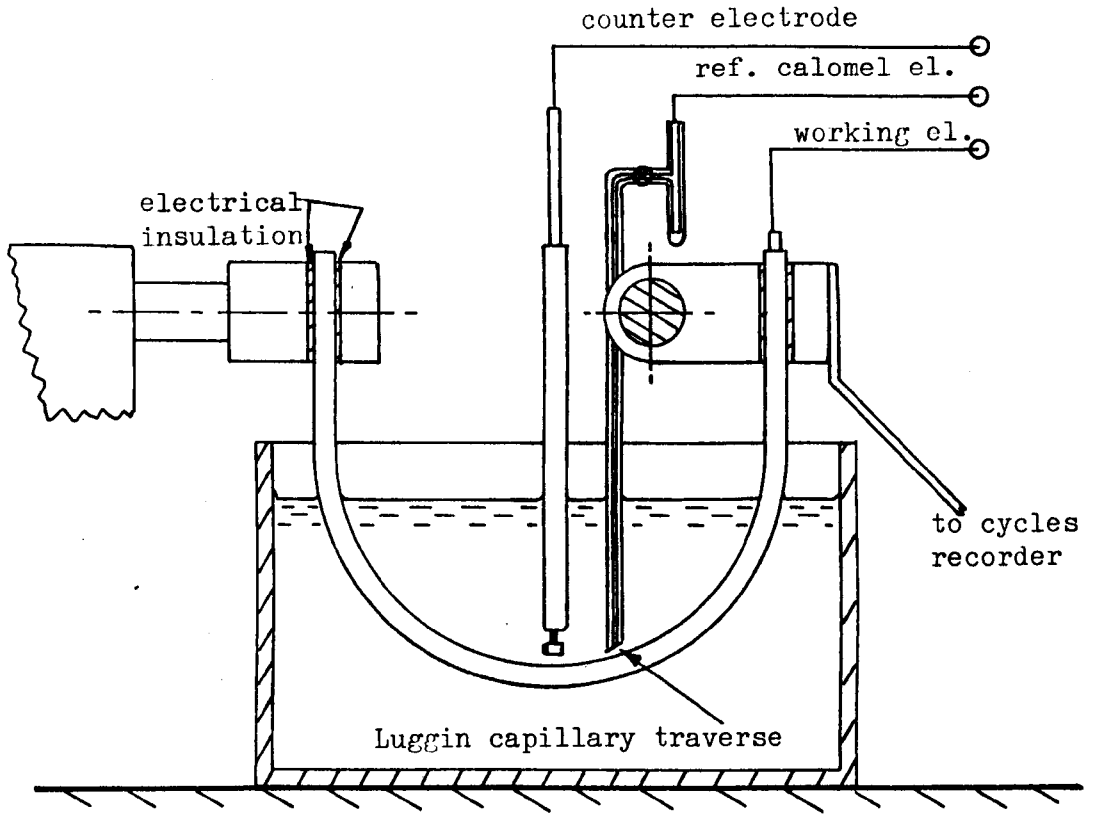

Figure 3 Showing U-bend type specimen and electrodes

Figure 4(a)

Showing the position of fracture "A" through which holes were also made on some specimens

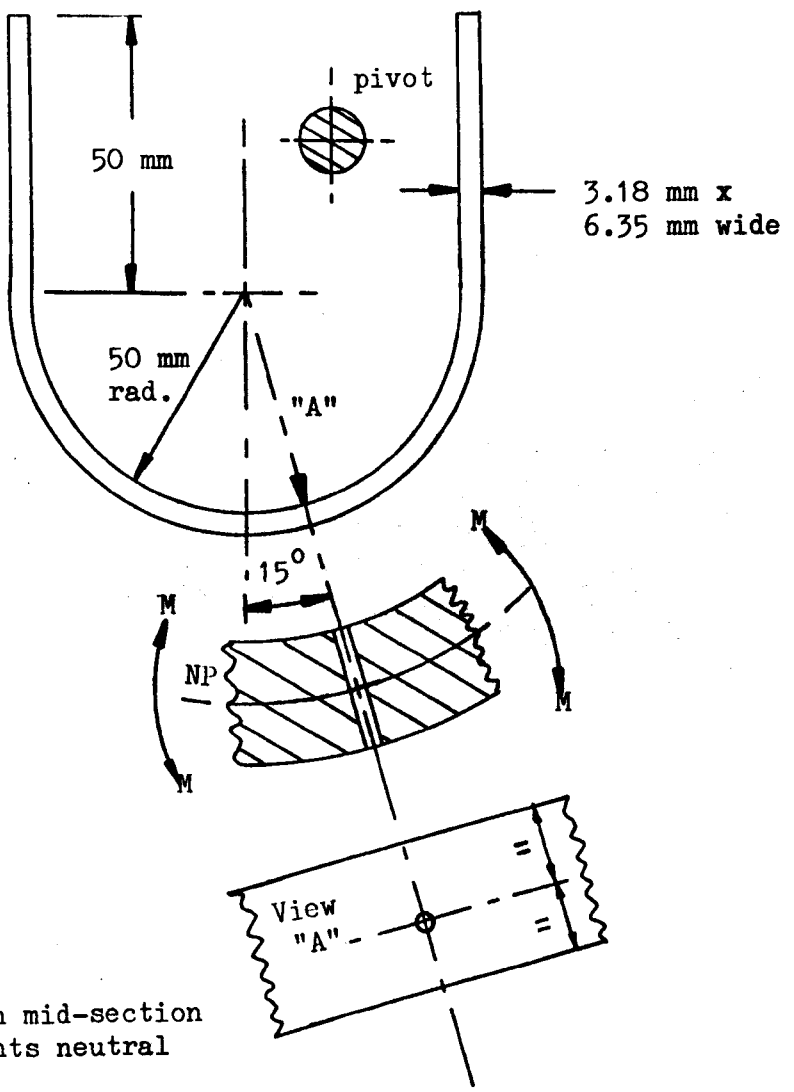

Figure 4(b)

Showing hole through mid-section at "A". NP represents neutral plane of bending

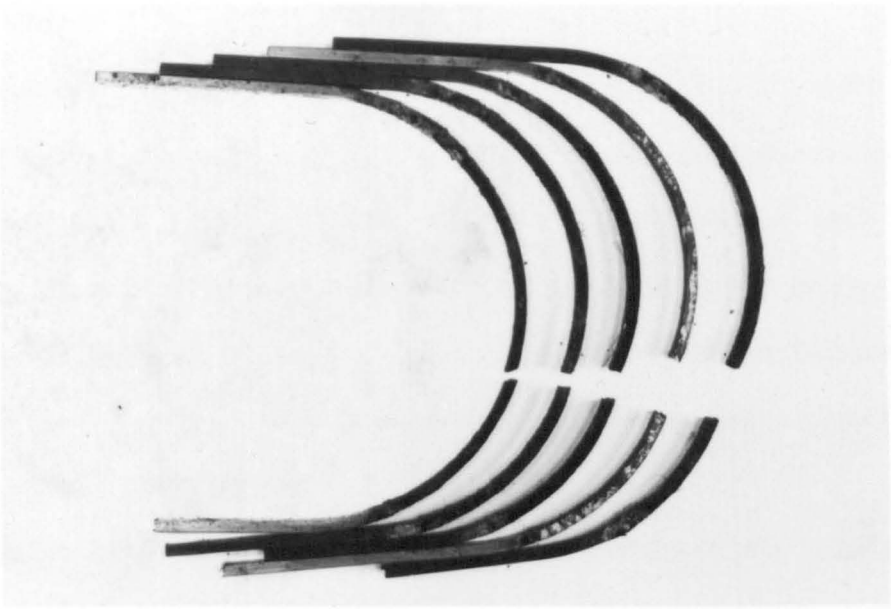

FIGURE 5

Typical fractured mild steel specimens (x0.73)

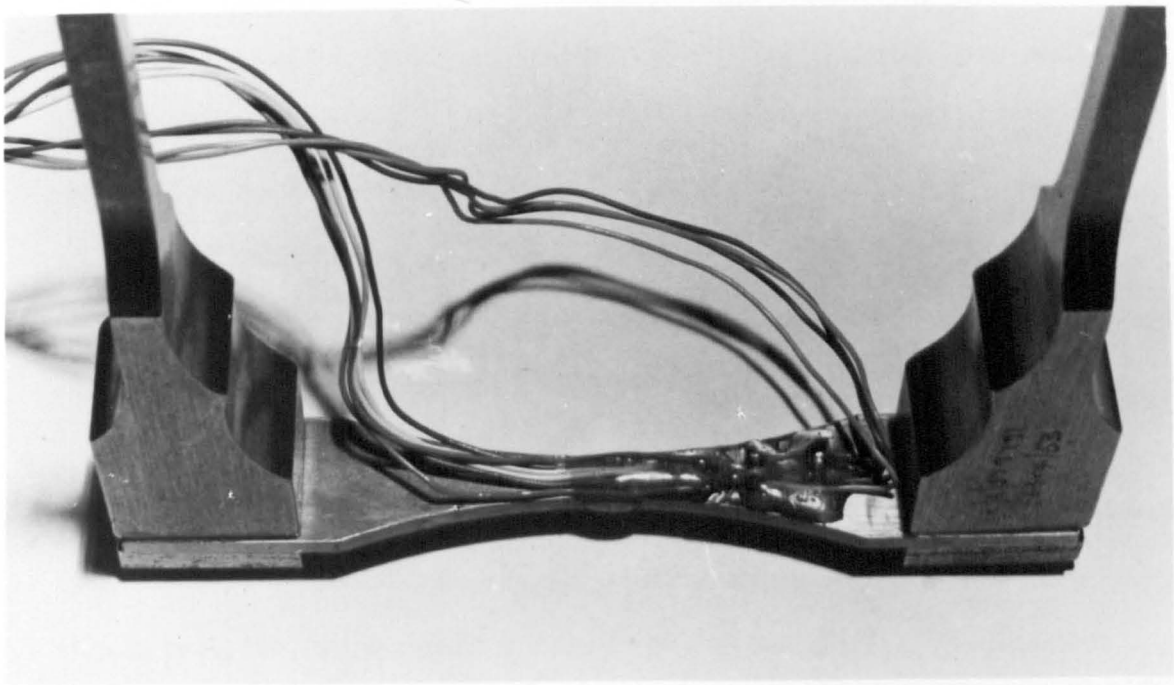

FIGURE 6

Plate-type titanium specimen with clamping legs and strain gauges for test machine setting.

Fig. 5 is a photograph of some of the U-bend mild steel specimens after fatigue fracture in distilled water, illustrating the consistent position of failure: within $\pm$ 3 mm of that indicated in Fig. 4(a) and (b). Strain gauges attached to dummy specimens verified that the maximum stress occurred at the concave surface being 4% greater than that occurring at the convex surface for all applied strain ranges.

Although these U-bend specimens were highly suitable for the bright mild steel bar material, the flat plates supplied for the testing of implant materials could not be conveniently fabricated into this shape. The complication of support legs with immersed clamping was therefore necessary for these materials. Fig. 6 is a photograph of a stainless steel plate specimen, clamped between stainless steel support legs, showing (but obscured by protective coating) a line of five strain gauges. These gauges were each of 0.3 mm gauge length and enabled a profile of the plate flexure under load to be recorded while setting-up the test rig. Similar setting or calibration specimens were used for each material tested, in order to establish the maximum strain produced during each cycle of the test rig.

The test rig facility, designed and built by the author for use at the Middlesex Polytechnic is shown, in part, by the photograph Fig. 7. Two machines, each powered by a three-phase 1 BHP 1425 r.p.m. electric motor, were bench mounted to provide oscillating motion to a cross-head ram. The cross-head was driven by an eccentive arrangement (diagramatically illustrated in Fig. 1), at a constant

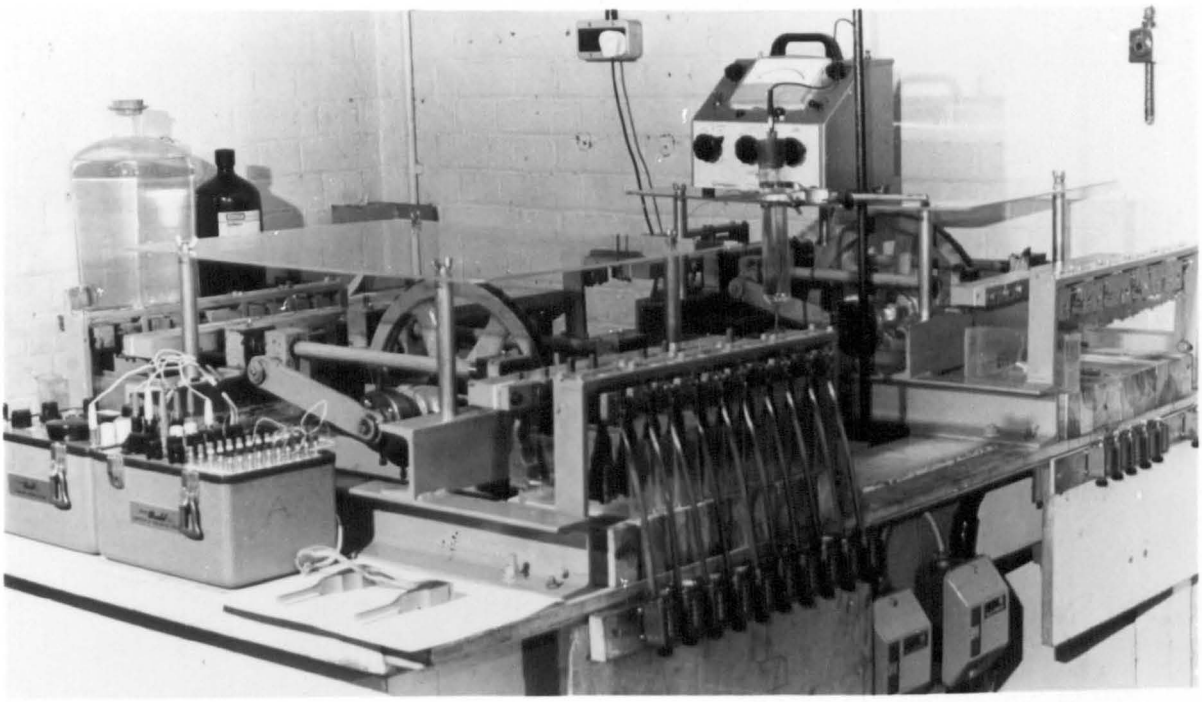

FIGURE 7

General view of test machines (mini-potentiostat and electrodes not shown).

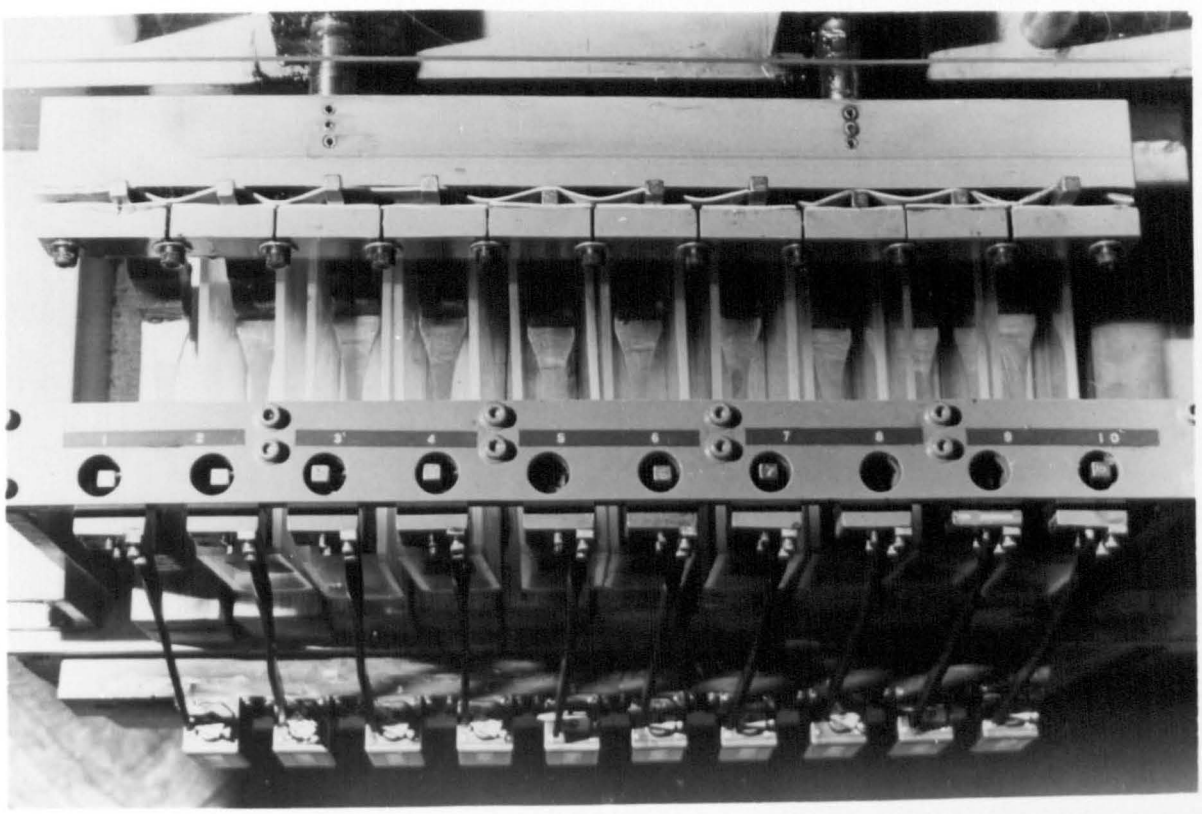

FIGURE 8

A view of one of the machine rams with 10 plate-type specimens and mechanical counters.

frequency of 1.7 Hz(5.4×10^7 cycles/year): a typical walking pace and suitable frequency therefore for the testing of human surgical implant materials. A continuous adjustment of crosshead stroke was made possible by the eccentric drive, from zero up to a total movement of 75 mm. Once adjusted to produce the required specimen strain this eccentric was locked so that a constant strain load test facility was provided. Fig. 8 is a photograph showing one of the machine rams. Each machine had two such rams, one on either side of the eccentric drive for balance and parallel motion. Each ram provided the fatigue load for 10 specimens so that a total test facility was provided for 40 specimens on test together. In view of the comparitively low frequency it was advantageous to fatigue this number of specimens simultaneously. Although all 20 specimens on test in a particular machine had the same cross-head stroke, the strain produced on each specimen was further adjusted separately to any desired level, within the stroke range, by the height of the support legs in the ram. A cycle recorder was provided for each specimen on test operated mechanically by an arm attached to the rocking pivot clamp: at specimen fracture this arm came to rest so that the cycles to failure were recorded. A check on the strain waveform produced by this fatigue machine facility showed that the cycle was within 2% of being sinusoidal for all possible specimen positions.

Each specimen, whether of the plate-type or U-bend, was contained separately in its own environment by a perspex test cell.

Insulated, both electrolytically and electrically, from its neighbour and the test rig (see Figs 3 & 8), each specimen was immersed in its own separate electrolyte. The liquid surface was freely assessible to oxygen, and the whole solution subjected to a stirring motion during the test as the result of specimen flexure and movement of the support legs. The open system was also readily assessible to observation of the specimen surface for crack imitation during corrosion fatigue tests. Standard saturated calomel reference electrodes, Luggin capillary traversing tubes, platinum counter electrodes, etc., were all positioned in racks over each specimen on test to record electrochemical data.

3.2.2. Design of mini-potentiostats

A multi-channel mini-potentiostat was designed specifically for use in this work. Fig. 9 shows the circuit diagram. This design was a modification of the potentiostat circuit designed by Smith and Hughes [333], after the one first published by Green et al [334], for controlling a single specimen under test. The multi-channel design was produced here for six specimens to be held at different potentials throughout the duration of a fatigue test. Consultation with Bloyce and Jithoo [335] showed that any number of specimens may be controlled at the same time at different potentials in this way, by the addition of further operational amplifiers to the basic circuit. This mini-potentiostat was produced at Middlesex Polytechnic, in printed circuit form, capable of applying potential in the range - 1500 mV to +1500 mV, with reference to

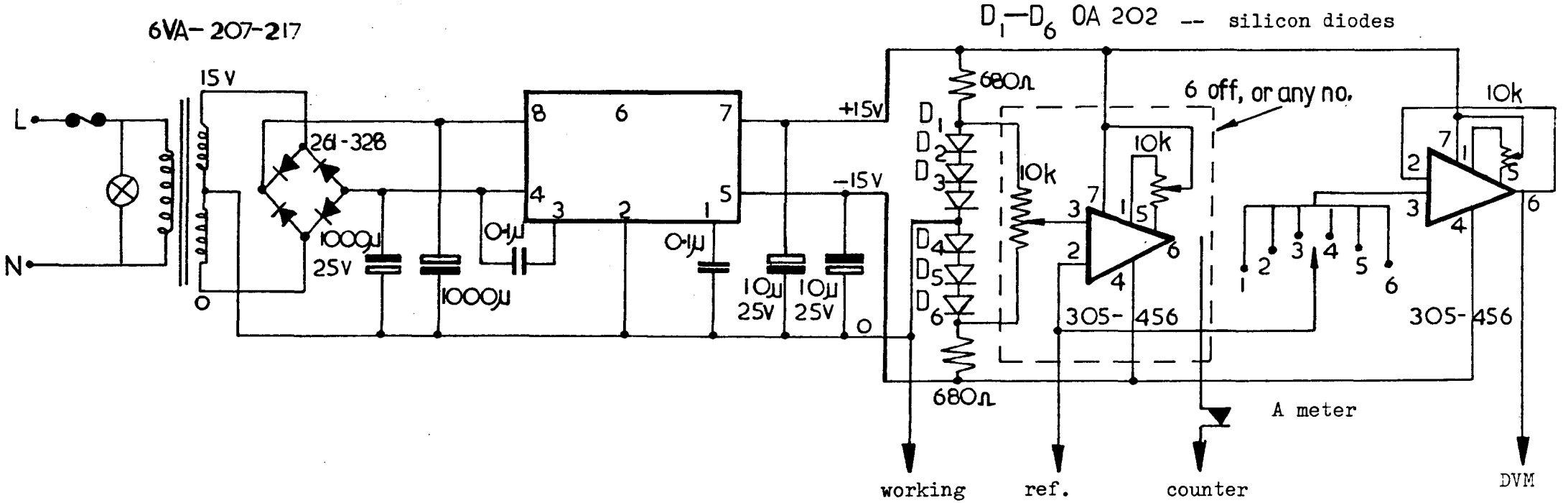

Figure 9 Circuit diagram of mini-potentiostat

a standard saturated calomel electrode. The potential applied to each specimen was capable of being independently and continuously varied within the range. A digital milli-volt meter (DVM), as shown in Fig. 9, was used to record the potential applied. The polarizing current was then registered by a micro-ammeter in series with the platinum counter electrode provided for each specimen.

3.2.3. Specimen material properties

Mild steel specimens were of good commercial quality (G.C.Q.) 0.25%C steel, as rectangular bar (3.175 x 6.350mm), in the bright drawn condition. Lengths of bar were cut and rolled around a 50 mm radius roll former to produce the U-bendspecimen shape.

Stainless steel type 316 S12 was used having the following analysis 0.048%C, 1.81% Mn, 2.4% Mo, 11.9% Ni, 16.7%Cr, 0.032% N_2 0.36% Si, 0.03% P, 0.018% S, balance Fe. Specimens were machined from sheet material which had to be previously cold-rolled approximately 20% to give a thickness of 3 mm.

Commercial purity titanium T130, analysed at 0.032%C, 0.064% Fe, 0.032% N_2, 0.180% O_2, 0.0018% H_2, i.e. approximately 99.7% pure Ti, was made into plate specimens as described for the stainless steel.

Titanium alloy T318 was analysed as follows: 6.38% Al, 4.23% V, 0.05% Fe, 0.006% H_2,balance Ti. This alloy was produced as plate specimens after a 20% cold-rolling, in common with the other implant materials tested.

Mechanical Properties	Mild Steel	S316	T130	T318
Young's Modulus GN/m^2	207	188	107	107
Tensile Strength MN/m^2	660	745	675	1071
0.1% Proof stress MN/m^2	509	600	556	925
0.2% Proof stress MN/m^2	-	680	620	980
0.5% Proof stress MN/m^2	585	729	660	1005
Percentage Elongation	9.9	26.0	17.0	5.0
Percentage reduction area	10.5	45.0	47.0	27.0
Hardness HVD (BS427)	205	289	260	340
Density g/cm^3	7.9	7.9	4.51	4.42

Table 1. Experimentally determined mechanical properties of 20% cold worked test materials.

3.2.4. Test environment

As discussed in Section 2.8.2. several solutions have been used to simulate body fluids. The behaviour of metals, in a simple 0.17M sodium chloride solution has been shown to be similar to that in Hanks solution and 'in vivo'.[144] A solution used in many tests at A.W.R.E. Aldermaston[62] for surgical implants was used also in this work:

sodium chloride	9.935 g
hydrated sodium carbonate	0.034 g
distilled water	1 litre

This simple 0.17M saline solution was made-up in 20 litre

bulk quantities, and air was allowed to bubble through the solution for several days. The saline was then stored for about a month before use.

The pH of the saline solution, when used in the perspex corrosion fatigue cells on the test rig, was found to remain constant at pH 6.5 as the result of the Na_2CO_3 buffer. Evaporation of solution from the open system during fatigue was countered by topping-up to the original level at frequent intervals, using distilled water (also pH 6.5).

Other solutions at pH 1.5 and pH 11.5 were produced for this work by addition to the 'standard' saline solution of either H_2SO_4 or NaOH. The pH 1.5 saline required a weekly adjustment of pH during fatigue testing. In the case of mild steel, for example, the pH would otherwise drift slowly to about 4. The pH 11.5 solution also required periodic adjustment to prevent a drift towards pH 9.5 over a period of about ten weeks. The addition of H_2SO_4 or NaOH was decided upon because it was not desired to change the chloride ion concentration from one solution to another. It was for this reason also that no further NaCl was added to any solution during test. These values of pH were chosen to investigate the behaviour of the surface films obtained, with reference to the most relevant Pourbaix diagram available, over a wide range. The pH 1.5 was of course very relevant to the required performance in corrosion fatigue of surgical implants.

3.2.5. Experimental procedures

Strain gauged specimens of the appropriate material under test were loaded into position on the test rig after being connected to multi-channel half-bridge circuit strain recorder, with temperature compensating dummy gauges, and all gauge readings set to zero. The height of the support leg, or U-bend datum leg, above the cross-head ram was initially set to 10 mm and the eccentric drive adjusted until the required stroke was produced, as indicated by the strain range recorded by the gauges. The eccentric drive was then locked. Any necessary adjustment of the mean strain to zero was then obtained by movement of the rocking arm pivot bar support before locking. Having set the nominal reversed bending strain amplitude for all specimens at 10 mm height above the ram, this height was adjusted down to zero and up to 25 mm while recording the change in strain amplitude. Any desired strain amplitude for testing was established according to this setting height.

The perspex test cells were then arranged in position containing the required saline solution, distilled water, or, in the case of tests in air, omitted. Final adjustment of solution level could only be made after positioning of the specimens at the required height. Wooden blocks were used to adjust the height of the test cells. Any electrodes required were then positioned. In the case of potentiostatic control, the required potential was set first on a 'dummy' specimen of the same material before application to the test specimen. This procedure helped

to prevent delay and surface damage resulting from establishing control at the correct potential at the start of fatigue.

All specimens were bench-finished after machining so that the direction of the fine surface grooves produced to 6/0 grade emery paper ran parallel to the direction of the applied stress. The surface finish within the hole was left in the simple "as drilled" condition. Consideration was at one time given to improving the surface finish within the hole by spark machining and/or electro-polishing. Such finishing methods were, however, considered unlikely in practice and would have involved champering of the highly stressed top surface corners. Hand finishing across the top and bottom of the hole was seen as the best and most realistic method of preparing the initiation site at either side of the hole [108]: the surface of the material within the hole itself was considered relatively unimportant. Plate specimens were coated with Dunlop 'Thixotropic' adhesive and bolted to their support legs. Two days were allowed for the clamped joint to cure before the whole assembly, except for the test gauge length of exposed specimen, was coated with a protective polyurethane elastomer. Produced by Berger Chemicals of Newcastle, this was a two-coat pack (PR1531) primer and (PR1535) elastomer. The object here was to obtain protection from corrosion of the entire immersed areas of support legs and clamped regions of the specimens on test. U-bend specimens were similarly coated, leaving only a total test surface area of 1000 mm^2 exposed in the region of maximum strain. This area was prepared for test immediately

prior to loading into the rig: swabbed with carbon tetrachloride finely abraded with emery by hand (in a direction paralled to that of the applied stress), swabbed again with acetone, rinsed with distilled water several times; each specimen was then positioned in its electrolyte and clamped in the rig.

During the corrosion fatigue test checks were made continuously at first, then hourly for the first eight hours, followed by "as frequently as possible" over the remaining weeks of test, of the following events:

(a) the appearance on the surface of a fatigue crack, number of cycles and time before final fracture;

(b) the appearance of the electrolyte, pH change; and oxide debris;

(c) the freely corroding potential established or otherwise during fatigue; or

(d) the current density variation with time under potentiostatic control.

Following the fracture of specimens, optical and transmission electron microscopy facilities were used at Middlesex Polytechnic to assess the mode of fracture. The results, particularly with respect to carbon coated replicas produced for TEM studies, were further checked by using the facilities at the City of London Polytechnic. Scanning-electron microscopy studies were also conducted to cross-check the results, previously obtained by TEM, using the SEM facility at A.W.R.E. Aldermaston. Specimens which had endured test lives in excess of 10^7 cycles

were also examined for signs of fatigue cracking and, by means of a tensile test, any changes in the mechanical properties were checked. Some repeat tests were made of specimens which had failed in fatigue, and at various percentages of corrosion fatigue life these specimens were removed for tensile testing.

4. RESULTS AND DISCUSSION

4.1. Fatigue Data

4.1.1. Air Fatigue Data

Although a reversed constant strain amplitude load was in fact applied to all the specimens in this work it was thought more useful, for comparison with the results of previous work, to plot the results in a conventional S/N manner rather than ε/N diagrams. All lines through S/N data were plotted using a least squares method of determining the best line from the data available. Statistically, the data was unfortunately of necessity limited for any one material environment combination, although some 550 specimens were tested in total. However, the high order of precision obtained for most of the data is an important confidence factor. Fig. 10-13 show the results obtained for fatigue in air using respectively, mild steel, stainless steel (S316), commercial purity titanium (T130), and titanium alloy (T318). The key included on the diagrams indicates the results for plain smooth specimens, and those for specimens having a 2 mm diameter hole at mid-section or, alternatively, a 1 mm diameter hole. The air fatigue limits obtained are tabulated, together for comparison with corrosion fatigue data, to be examined later in Table 1. Certain other differences in the air-fatigue behaviour of the four materials tested were, however, noted at this stage. Apart from the obvious higher fatigue strength of plain specimens of T318, the titanium material generally developed a fatigue limit

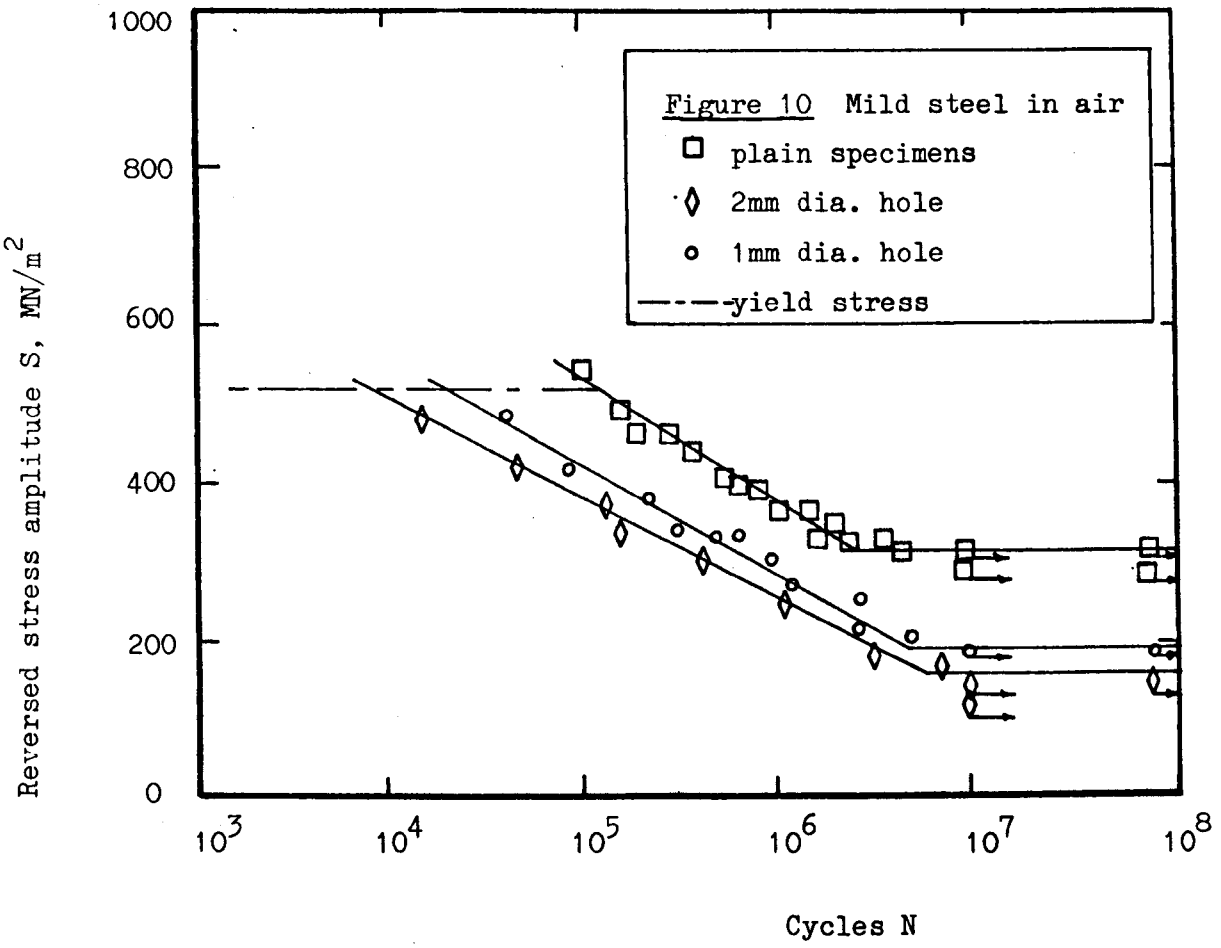
Figure 10 Mild steel in air
plain specimens
2mm dia. hole
1mm dia. hole
yield stress
Reversed stress amplitude S, MN/m^2
1000
800
600
400
200
0
10^3
10^4
10^5
10^6
10^7
10^8
Cycles N

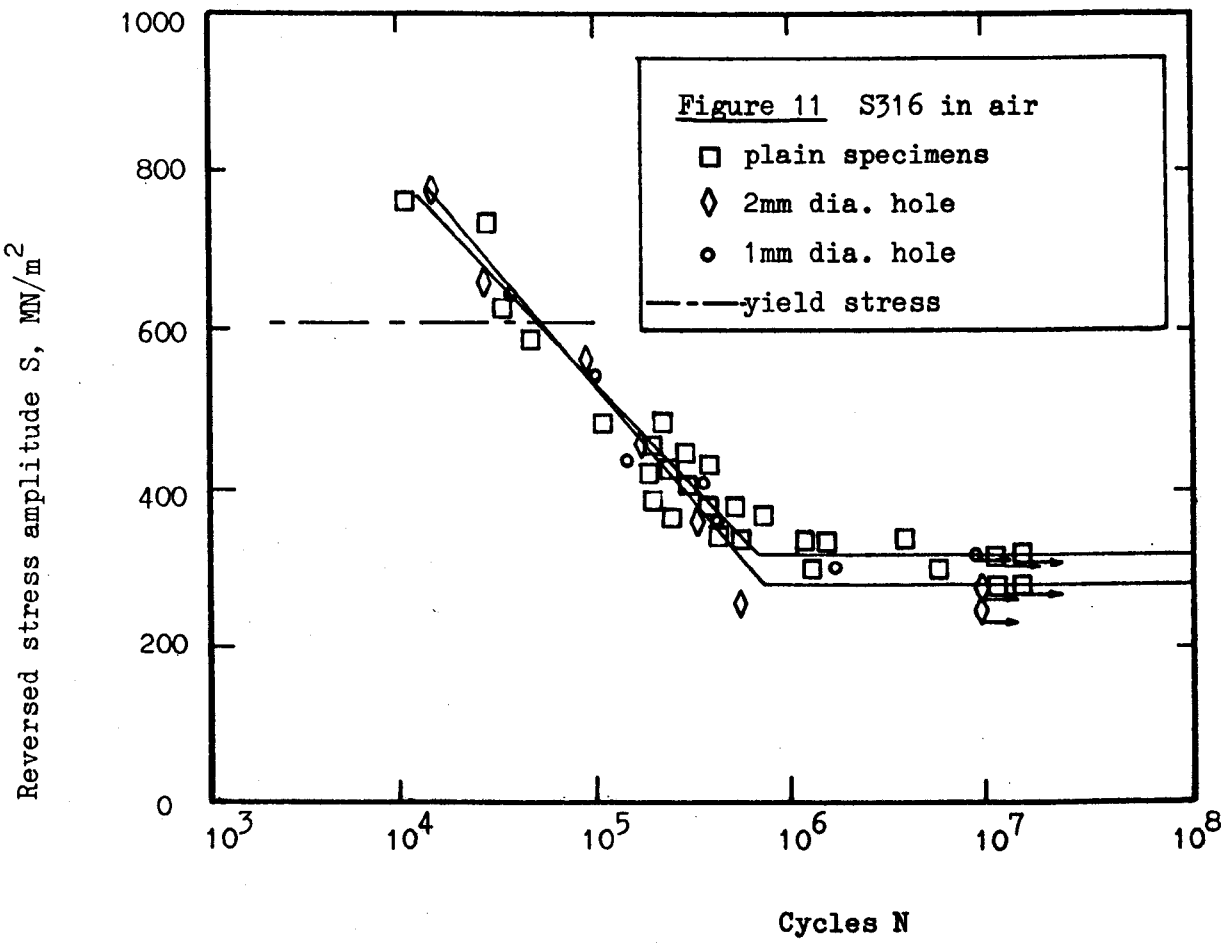
Figure 11 S316 in air
plain specimens
2mm dia. hole
1mm dia. hole
yield stress
Reversed stress amplitude S, MN/m^2
1000
800
600
400
200
0
10^3
10^4
10^5
10^6
10^7
10^8
Cycles N

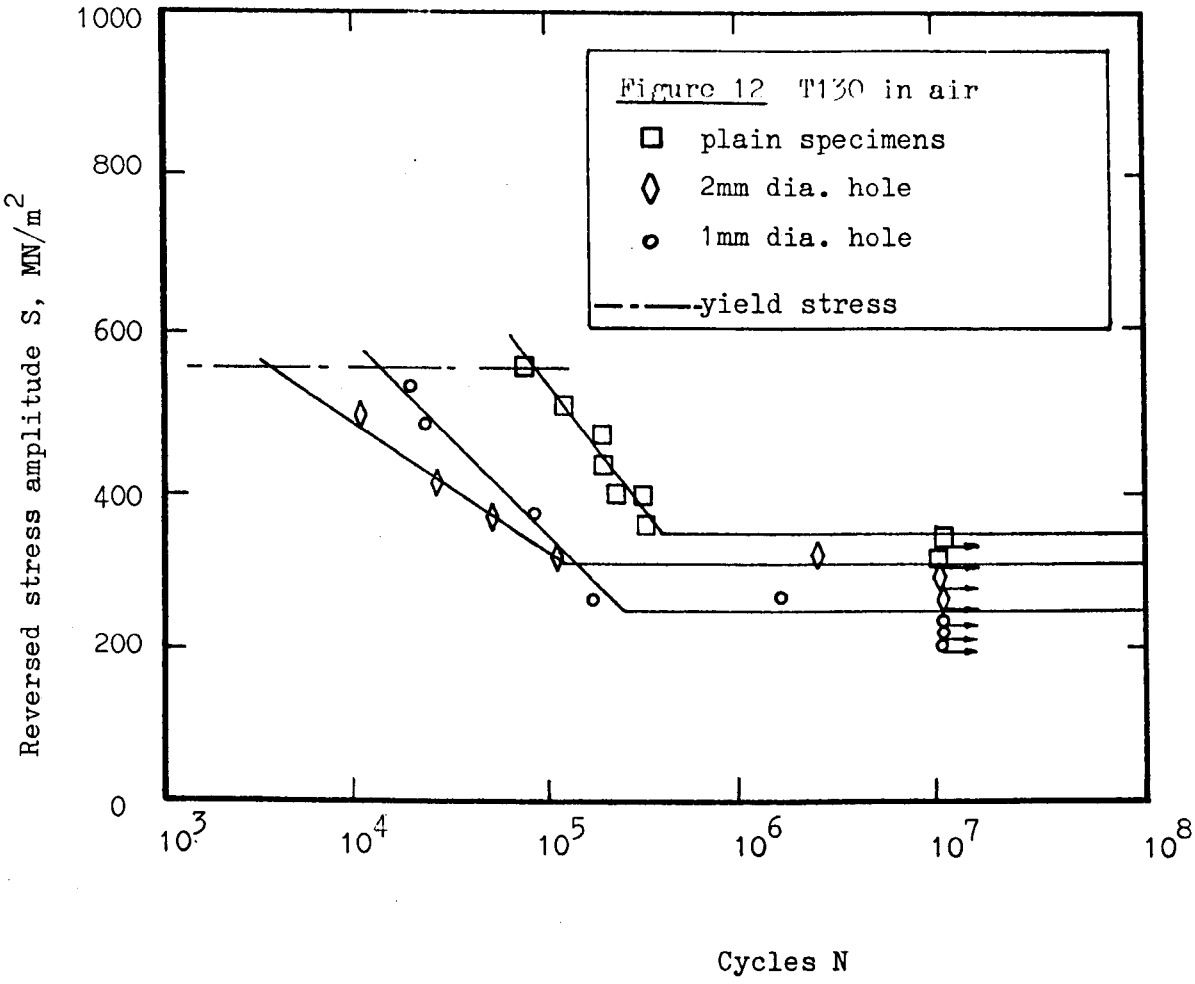
Figure 12 T130 in air
plain specimens
2mm dia. hole
1mm dia. hole
yield stress
Reversed stress amplitude S, MN/m^2
1000
800
600
400
200
0
10^3
10^4
10^5
10^6
10^7
10^8
Cycles N

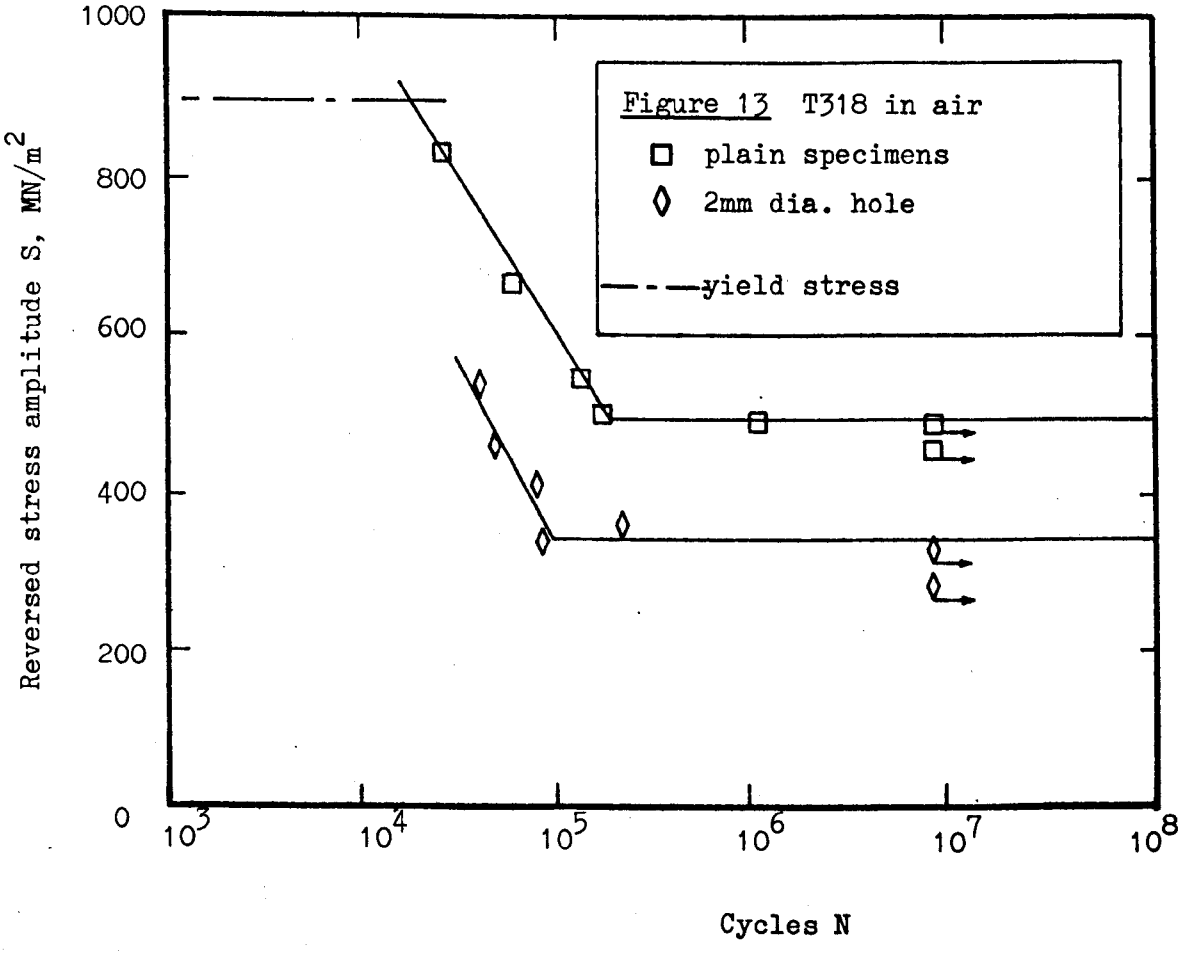
Figure 13 T318 in air
plain specimens
2mm dia. hole
yield stress
Reversed stress amplitude S, MN/m^2
1000
800
600
400
200
0
10^3
10^4
10^5
10^6
10^7
10^8
Cycles N

earlier than that for the steels. This was consistent with the steeper S/N slope obtained for titanium compared with the steels at applied stress amplitudes above the fatigue limit as follows:

mild steel in air $S = 1368 - 171 \log N$ MN/m^2 ——(1)

S316 " " $S = 1838 - 261 \log N$ MN/m^2 ——(2)

T130 " " $S = 2214 - 338 \log N$ MN/m^2 ——(3)

T318 " " $S = 2607 - 402 \log N$ MN/m^2 ——(4)

The data obtained for specimens with holes showed that the same size hole, and therefore the same nominal geometric stress concentration factor, produced very different results from the respective plain specimens data in each of the four materials tested. The strains measured in these specimens, with strain gauges covering the whole width on either side of the hole, represented the average strain, and not the maximum immediately next to the hole due to stress concentration. The stress amplitudes plotted for this data therefore represent also the average peak stress in the surface of the specimen in bending. Identical results for a specimen with a hole to those obtained for the plain specimen in the same material would therefore indicate zero stress concentration and no effect of notching. S316 clearly showed a high tolerance to notching due to drilled holes both above and below the fatigue limit. This tolerance or otherwise, to notching will be discussed later. The results for a 2 mm diameter hole were established as follows:

mild steel 2 mm hole in air $S = 1027 - 131 \log N$ MN/m^2 ——(5)

S316 " " " " $S = 1986 - 292 \log N$ MN/m^2 ——(6)

T130 " " " " $S = 1139 - 166 \log N$ MN/m^2 ——(7)

T 318 " " " " $S = 2271 - 384 \log N$ MN/m^2 —(8)

Comparison of equations (2) and (6), for example, showed a similar result for S316. The results for 1 mm diameter holes for S316 were also similar to those obtained for plain specimens and 2 mm hole specimens. Mild steel, on the other hand, clearly showed that the smaller hole was less damaging, while T130 results showed a change-over with the smaller hole being more damaging at the lower stress amplitudes. No data was obtained for T318 with 1 mm holes but the 2 mm hole was clearly very damaging to this material.

4.1.2. Corrosion fatigue data for mild steel

The results for mild steel corrosion fatigue tests are shown in Figs. 14 to 17.

Fig. 14 shows the S/N data for mild steel in distilled water (pH 6.5). The yield stress/endurance values obtained in air are included as a chain-dashed line for reference. The plain specimen results demonstrated three rectilinear 'rate of damage' branches with a particularly large scatter area 'knee' between the lower pair:

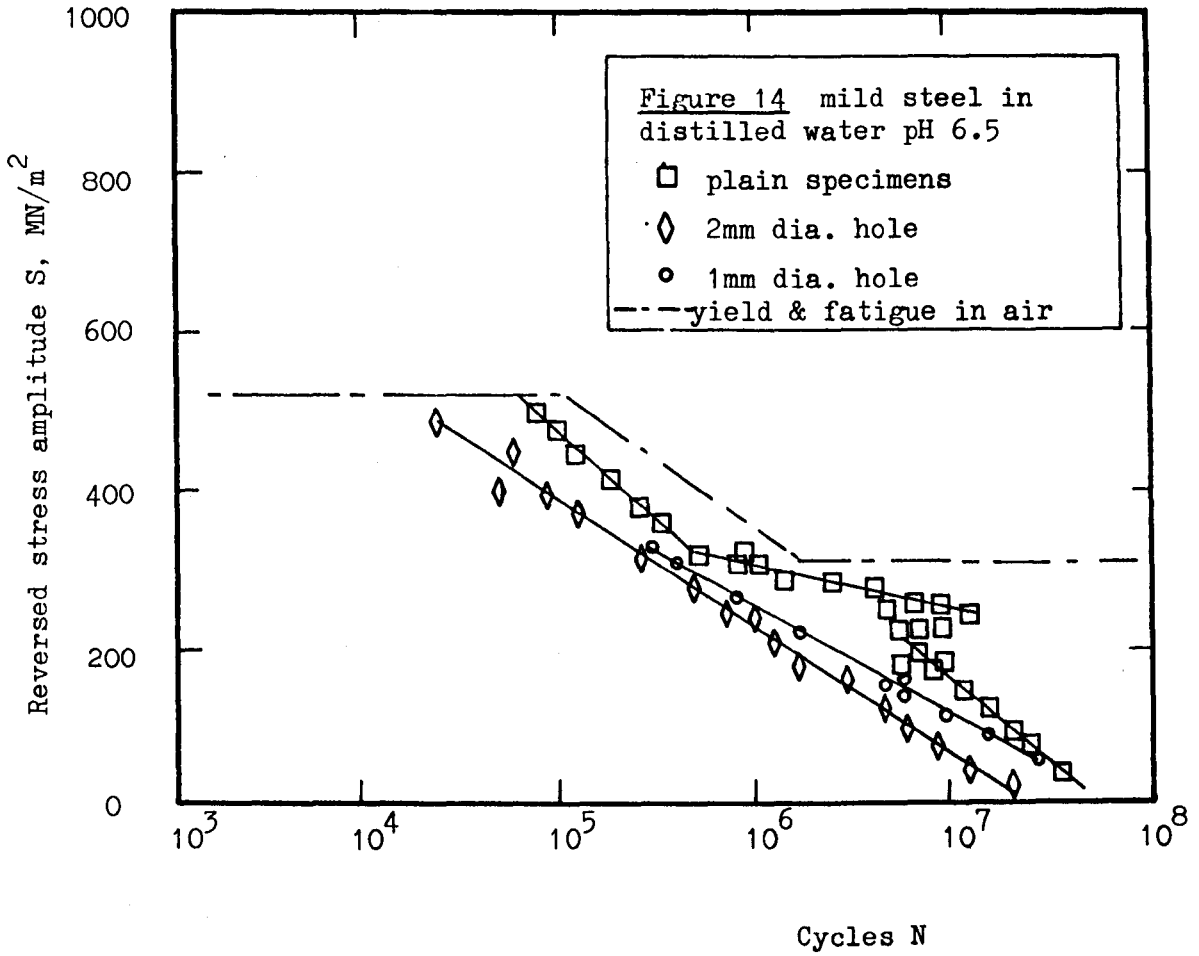
Figure 14 mild steel in distilled water pH 6.5
plain specimens
2mm dia. hole
1mm dia. hole
yield & fatigue in air
Reversed stress amplitude S, MN/m2
1000
800
600
400
200
0
10^3
10^4
10^5
10^6
10^7
10^8
Cycles N

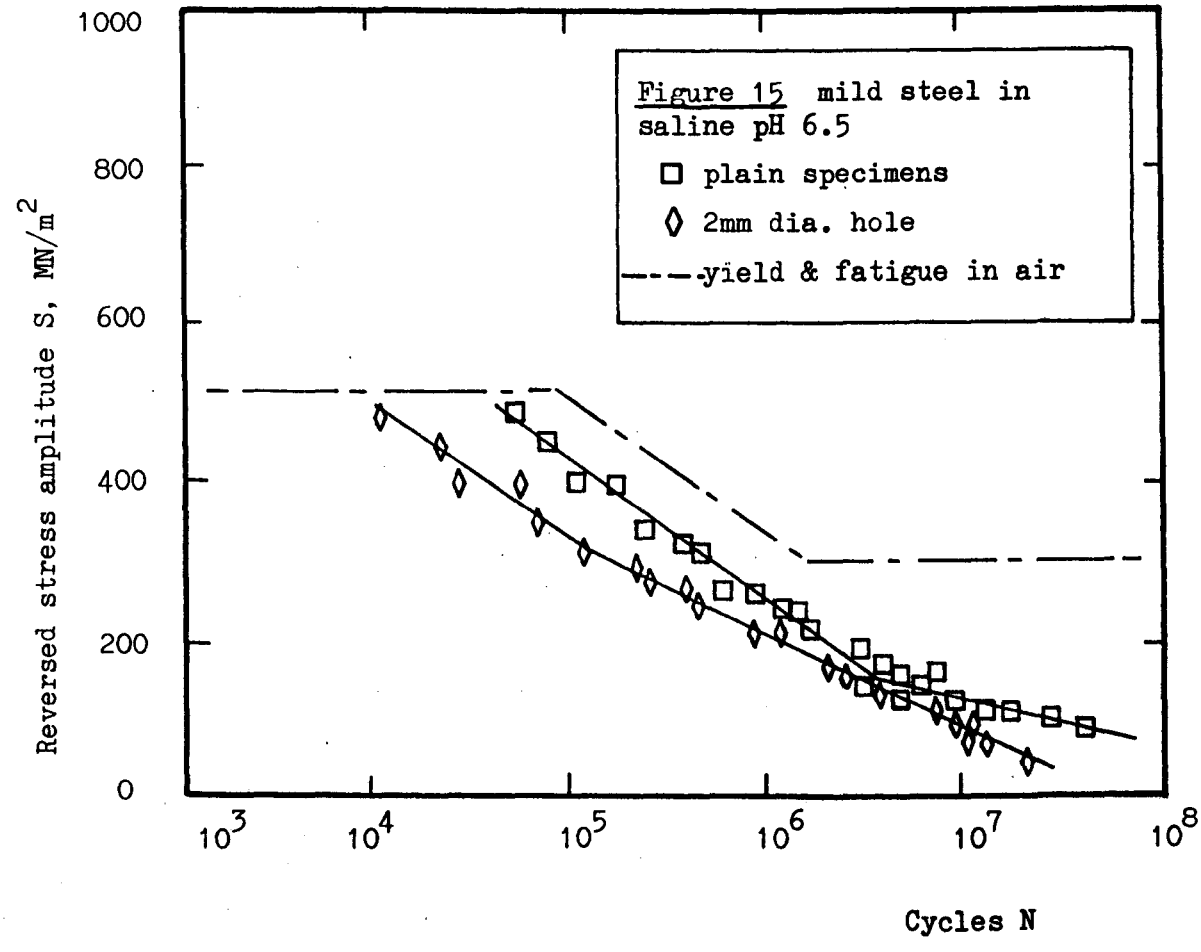
Figure 15 mild steel in saline pH 6.5
plain specimens
2mm dia. hole
yield & fatigue in air
Reversed stress amplitude S, MN/m2
1000
800
600
400
200
0
10^3
10^4
10^5
10^6
10^7
10^8
Cycles N

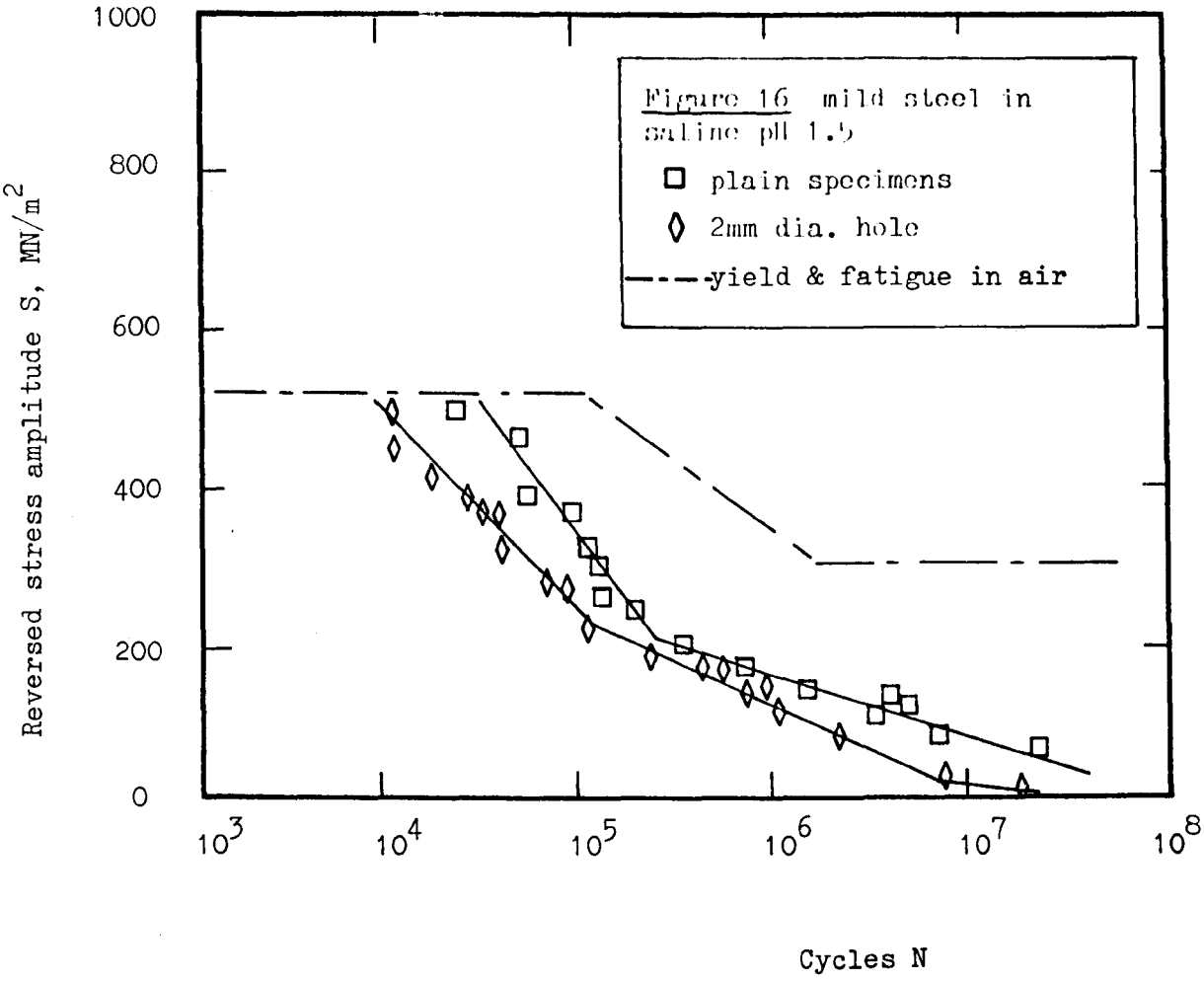
Figure 16 mild steel in saline pH 1.5
plain specimens
2mm dia. hole
yield & fatigue in air
Reversed stress amplitude S, MN/m^2
1000
800
600
400
200
0
10^3
10^4
10^5
10^6
10^7
10^8
Cycles N

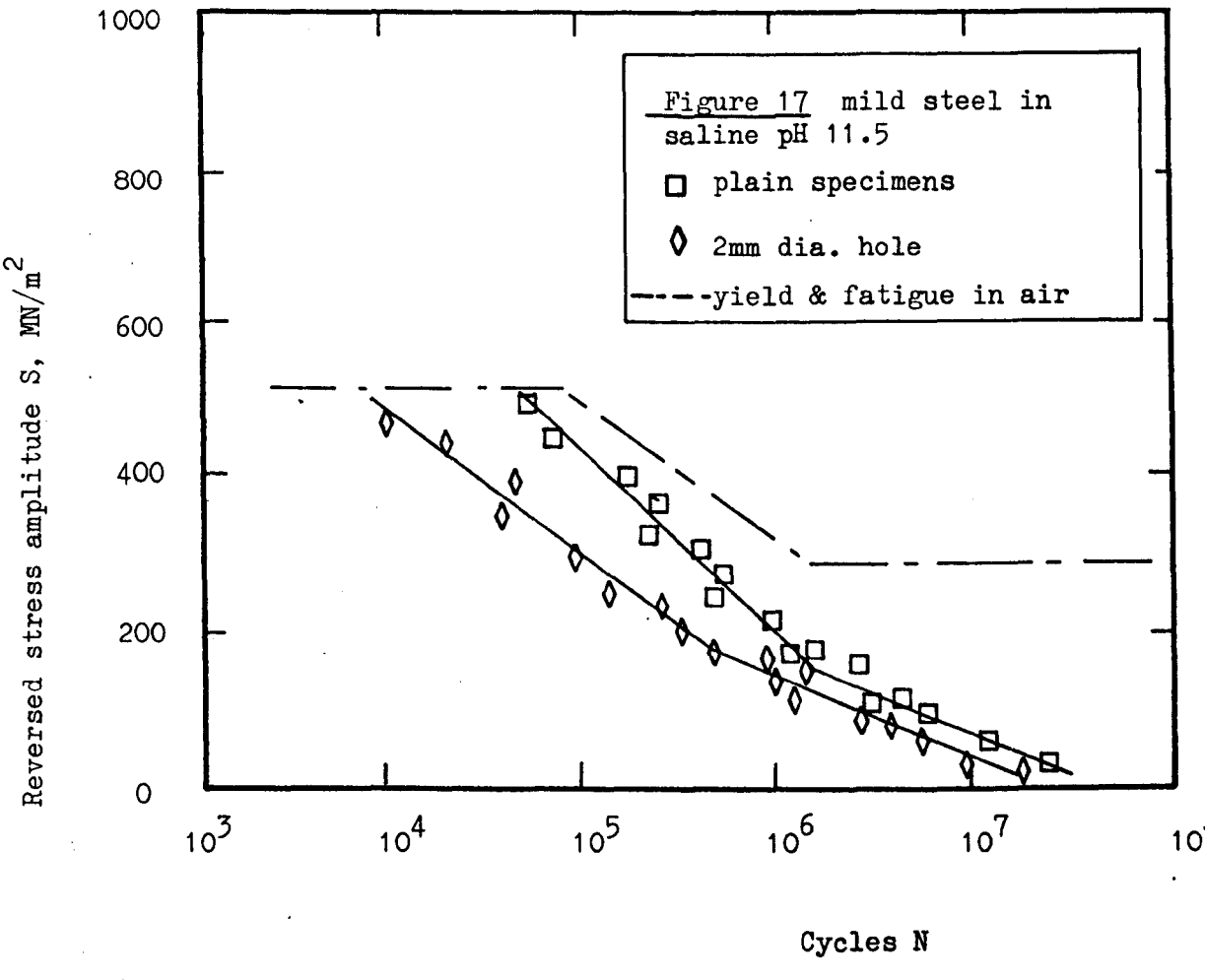
Figure 17 mild steel in saline pH 11.5
plain specimens
2mm dia. hole
yield & fatigue in air
Reversed stress amplitude S, MN/m^2
1000
800
600
400
200
0
10^3
10^4
10^5
10^6
10^7
Cycles N

$S = 1652 - 293 \log N$, for $S \geq \pm 350$ MN/m^2,

$S = 664 - 61 \log N$, for $\pm 190 \leq S \leq \pm 350$ MN/m^2, and

$S = 1660 - 217 \log N$, for $S \leq \pm 190$ MN/m^2

(9)

The upper and lower rates are similar and quite different from that produced in the median range. In contrast to this behaviour for plain specimens, the results for 2 mm hole specimens produced a single rate for mild steel in distilled water:

$S = 1133 - 151 \log N$ (10)

Once again the 1 mm diameter holes were less damaging for mild steel

The results for mild steel in saline are shown in Fig. 15. for pH 6.5. Plain specimens produced a two-branch rectilinear "rate of damage":

$S = 1313 - 176 \log N$, for $S \geq \pm 150$ MN/m^2, and

$S = 549 - 60 \log N$, for $S \leq \pm 150$ MN/m^2

(11)

This result in saline pH 6.5, is similar to the upper two rates in distilled water (comparing equations (9) and (11)). The results in saline pH 6.5, for a 2 mm hole, however, this time produced a two-part rate also:

$S = 1155 - 165 \log N$, for $S \geq \pm 310$ MN/m^2, and

$S = 918 - 118 \log N$, for $S \leq \pm 310$ MN/m^2

(12)

The saline pH 1.5 results for mild steel are shown in Fig. 16.

For plain specimens:

$$S = 2010 - 337 \log N, \text{ for } S \geq \pm 200 \text{ MN/m}^2, \text{ and}$$
$$S = 649 - 83 \log N, \text{ for } S \leq \pm 200 \text{ MN/m}^2. \quad (13)$$

For 2 mm diameter hole specimens, at pH 1.5:

$$S = 1500 - 253 \log N, \text{ for } S \geq \pm 235 \text{ MN/m}^2, \text{ and}$$
$$S = 840 - 121 \log N, \text{ for } S \leq \pm 235 \text{ MN/m}^2 \quad (14)$$

Failure occurred down to stress aplitudes < 3 MN/m^2

The two stage rate result was also found in Fig. 17 for pH 11.5 but the slope of the first part rate was considerably less steep than that for pH 1.5. The long term life, at low stress amplitudes was however not so different because the second part slope was greater for pH 11.5 than for pH 1.5. For plain specimens at pH 11.5:

$$S = 1547 - 222 \log N, \text{ for } S \geq \pm 150 \text{ MN/m}^2, \text{ and}$$
$$S = 789 - 101 \log N, \text{ for } S \leq \pm 150 \text{ MN/m}^2 \quad (15)$$

For 2 mm diameter hole specimens, at pH 11.5:

$$S = 1231 - 184 \log N, \text{ for } S \geq \pm 180 \text{ MN/m}^2, \text{ and}$$
$$S = 778 - 104 \log N, \text{ for } S \leq \pm 180 \text{ MN/m}^2. \quad (16)$$

As expected, no fatigue limit was found for any solution in the corrosion fatigue of mild steel.

4.1.3. Corrosion fatigue data for stainless steel 316

The results for stainless steel under various conditions of corrosion fatigue are shown in Fig. 18 to 21. Corrosion fatigue limits were established in each case. Fig. 18 is the result of fatigue of S316 in distilled water. Plain specimens of S316 produced a single rate of damage above the fatigue limit, of:

$S = 1388 - 183 \log N$, above a fatigue limit of $\pm$ 33 MN/m^2 ___(17)

This is a better performance in distilled water than in air (fatigue limit $\pm$ 310 MN/m^2) at low stress amplitudes. At the higher stresses endurance was, however, less than for air. The 2 mm hole specimens produced similar endurance lives to those obtained with plain specimens at the higher stress amplitudes but clearly showed reduced endurance at lower amplitudes, together with a lower fatigue limit, in distilled water with a 2 mm hole:

$S = 1810 - 273 \log N$, above a fatigue limit of $\pm$ 250 MN/m^2 ___(18)

The results for 1 mm hole were indistinguishable from those of the larger hole. The performance of S 316 in saline pH 6.5 is shown in Fig. 19. The most noticeable scatter of results

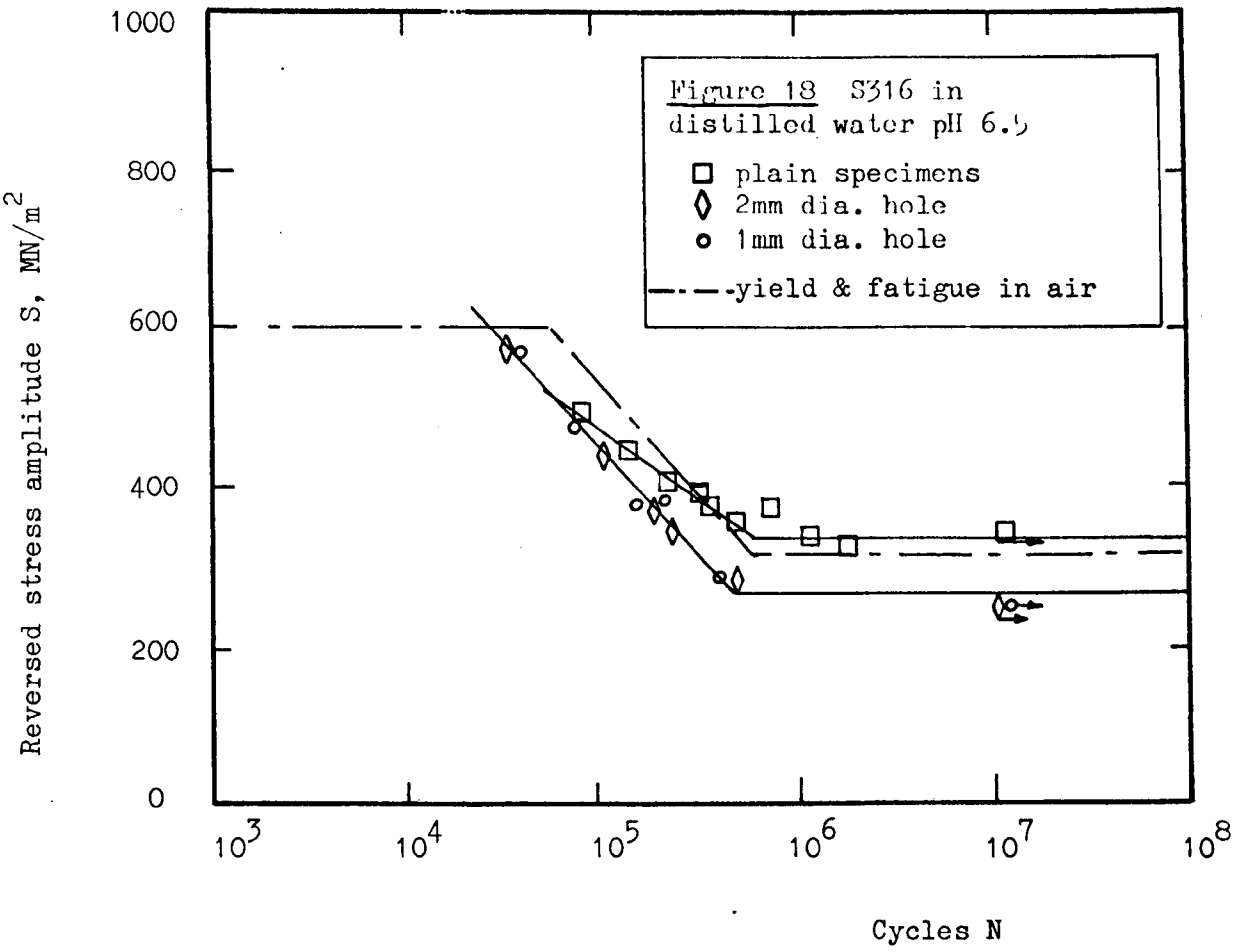
Figure 18 S316 in distilled water pH 6.5
plain specimens
2mm dia. hole
1mm dia. hole
yield & fatigue in air
Reversed stress amplitude S, MN/m2
1000
800
600
400
200
0
10^3
10^4
10^5
10^6
10^7
10^8
Cycles N

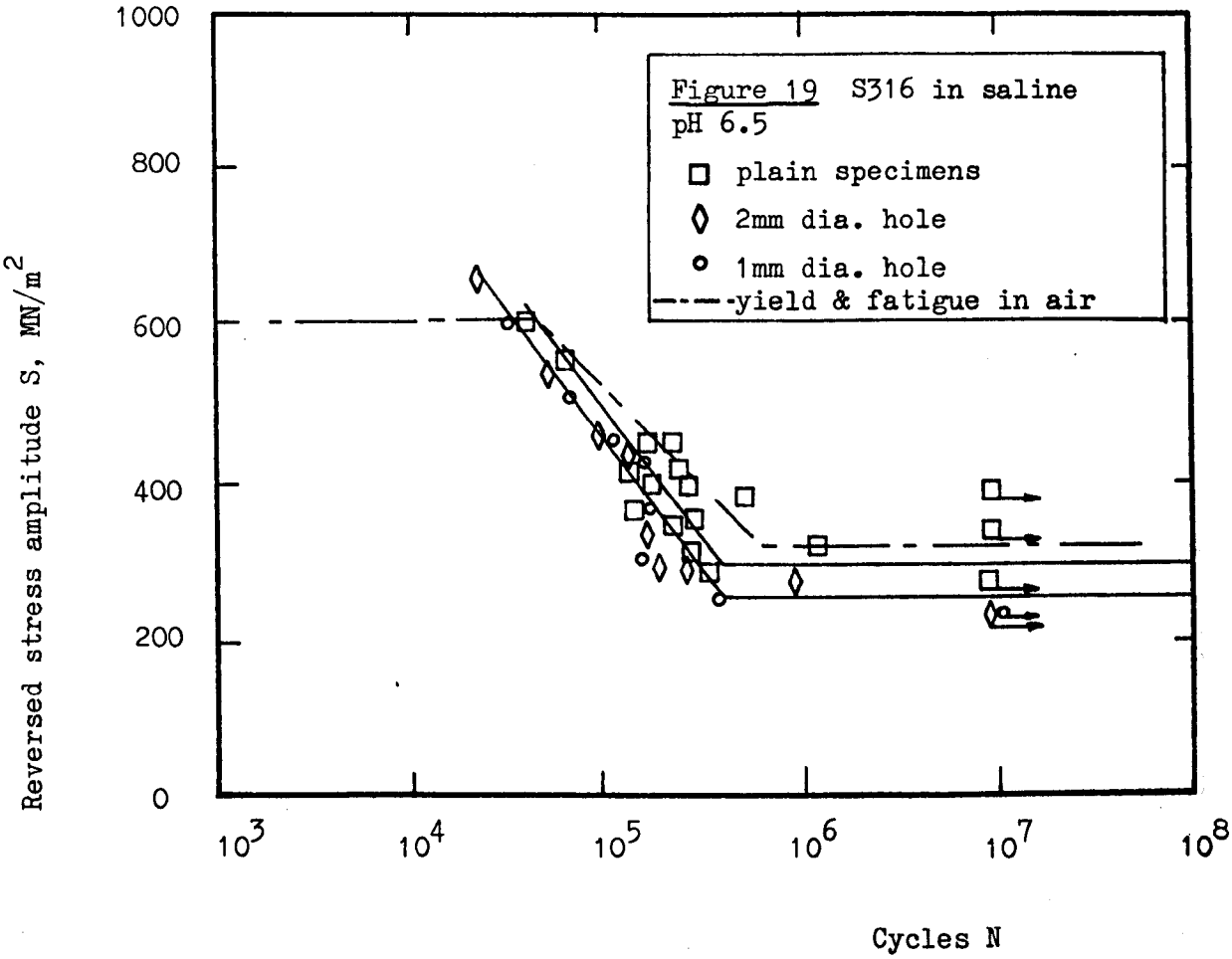
Figure 19 S316 in saline pH 6.5
plain specimens
2mm dia. hole
1mm dia. hole
yield & fatigue in air
Reversed stress amplitude S, MN/m2
1000
800
600
400
200
0
10^3
10^4
10^5
10^6
10^7
10^8
Cycles N

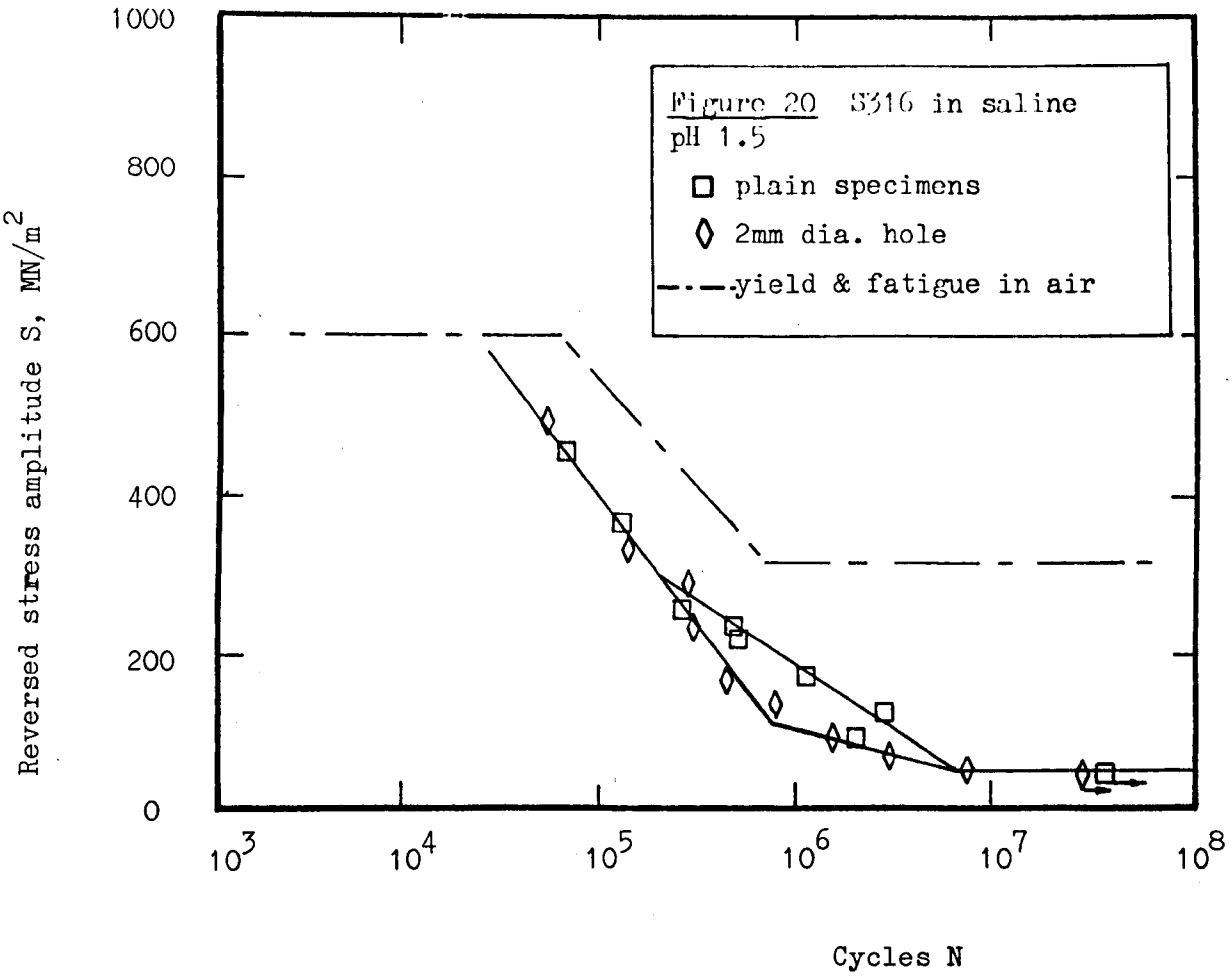
Figure 20 S316 in saline pH 1.5
plain specimens
2mm dia. hole
yield & fatigue in air
Reversed stress amplitude S, MN/m2
1000
800
600
400
200
0
10^3
10^4
10^5
10^6
10^7
10^8
Cycles N

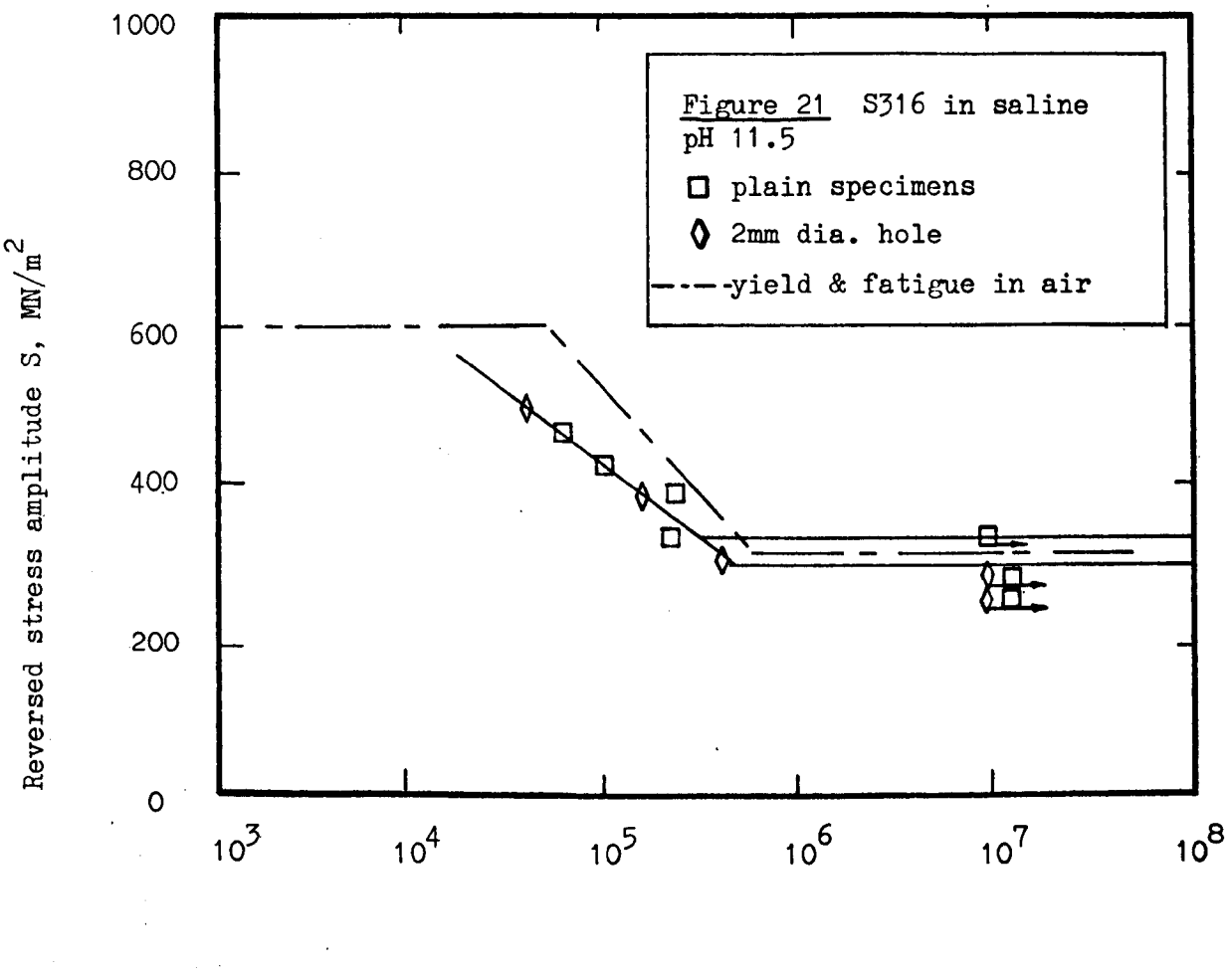
Figure 21 S316 in saline pH 11.5
plain specimens
2mm dia. hole
yield & fatigue in air
Reversed stress amplitude S, MN/m2
1000
800
600
400
200
0
10^3
10^4
10^5
10^6
10^7
10^8
Cycles N

obtained from the plain specimens here was not, however, produced in the case of 2 mm diameter, or 1 mm diameter hole specimens. The reasons for these variations in plain specimen life, particularly at low stress amplitudes in the region of the fatigue limit, were investigated and are discussed later. By comparison with the results of all other materials and conditions, this set of results was far less precise. The following equation is the best line (by method of 'least squares') which could be obtained, to represent the mean rate of damage above the "lower" or safest fatigue limit recorded for S316 in saline pH 6.5:

$$S = 2122 - 324 \log N, \text{ above a fatigue limit of } \pm 300 \text{ MN/m}^2 \quad (19)$$

The results for both sizes of hole in saline pH 6.5 were again almost indistinguishable from each other. The rate damage for the 2 mm hole in S316 immersed in saline pH 6.5 was more precise than equation (19):

$$S = 2108 - 329 \log N, \text{ above a fatigue limit of } \pm 255 \text{ MN/m}^2 \quad (20)$$

Fig. 20 shows that in pH 1.5 a fatigue limit was only obtained for S316 at very low stress amplitudes. At higher stress amplitudes no difference was found in the results for 2 mm hole specimens and plain specimens. A double rate of damage law was indicated for both types of specimen above the fatigue limit in this very aggressive environment. For plain specimens of S316

in saline pH 1.5:

$S = 1996 - 322 \log N$, for $S \geq 300$ MN/m^2, and

$S = 1166 - 165 \log N$, for $S \leq 300$ MN/m^2, above a fatigue limit of 35 MN/m^2 ——————(21)

For 2 mm hole specimens of S316 in saline pH 1.5:

$S = 1996 - 322 \log N$, for $S \geq 130$ MN/m^2, and

$S = 517 - 69 \log N$, for $S \leq 130$ MN/m^2, above a fatigue limit of 35 MN/m^2 ——————(22)

The performance of stainless steel in saline pH 11.5 is shown in Fig. 21. A single rate of damage curve, common to both plain specimens and those with 2 mm diameter holes was obtained:

$S = 1320 - 178 \log N$, above a fatigue limit of $\pm$ 320 MN/m^2 for plain specimens and $\pm$ 300 MN/m^2 for 2 mm hole specimens ——————(23)

4.1.4. Corrosion fatigue data for titanium 130

The results for commercial purity titanium, T130, during corrosion fatigue are shown in Fig. 22 to 25. A fatigue limit was established in all cases.

Fig. 22 shows that, although the fatigue limit is reduced below that in air for distilled water, a cross-over occurs in

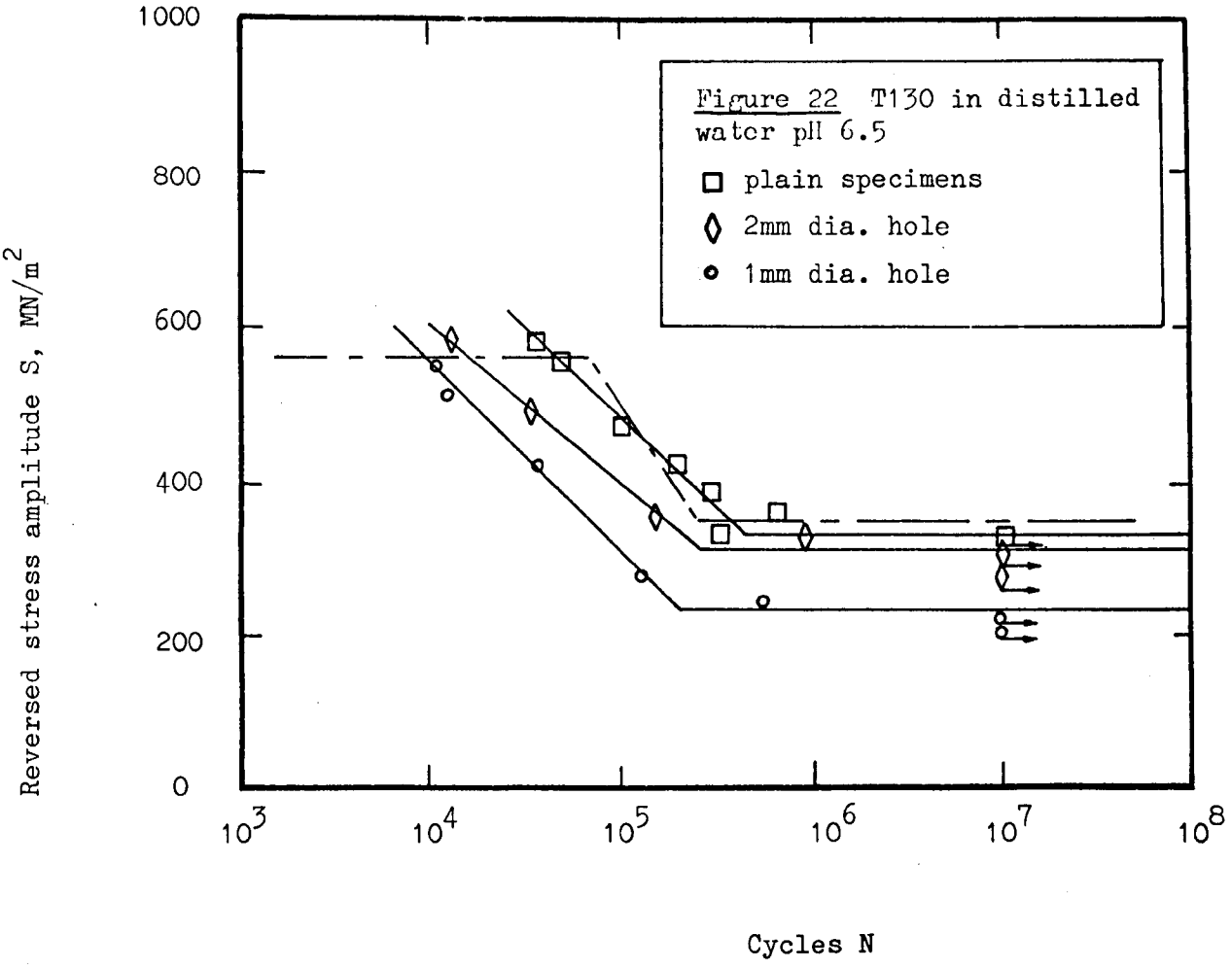
Figure 22 T130 in distilled water pH 6.5
plain specimens
2mm dia. hole
1mm dia. hole
Reversed stress amplitude S, MN/m^2
1000
800
600
400
200
0
10^3
10^4
10^5
10^6
10^7
10^8
Cycles N

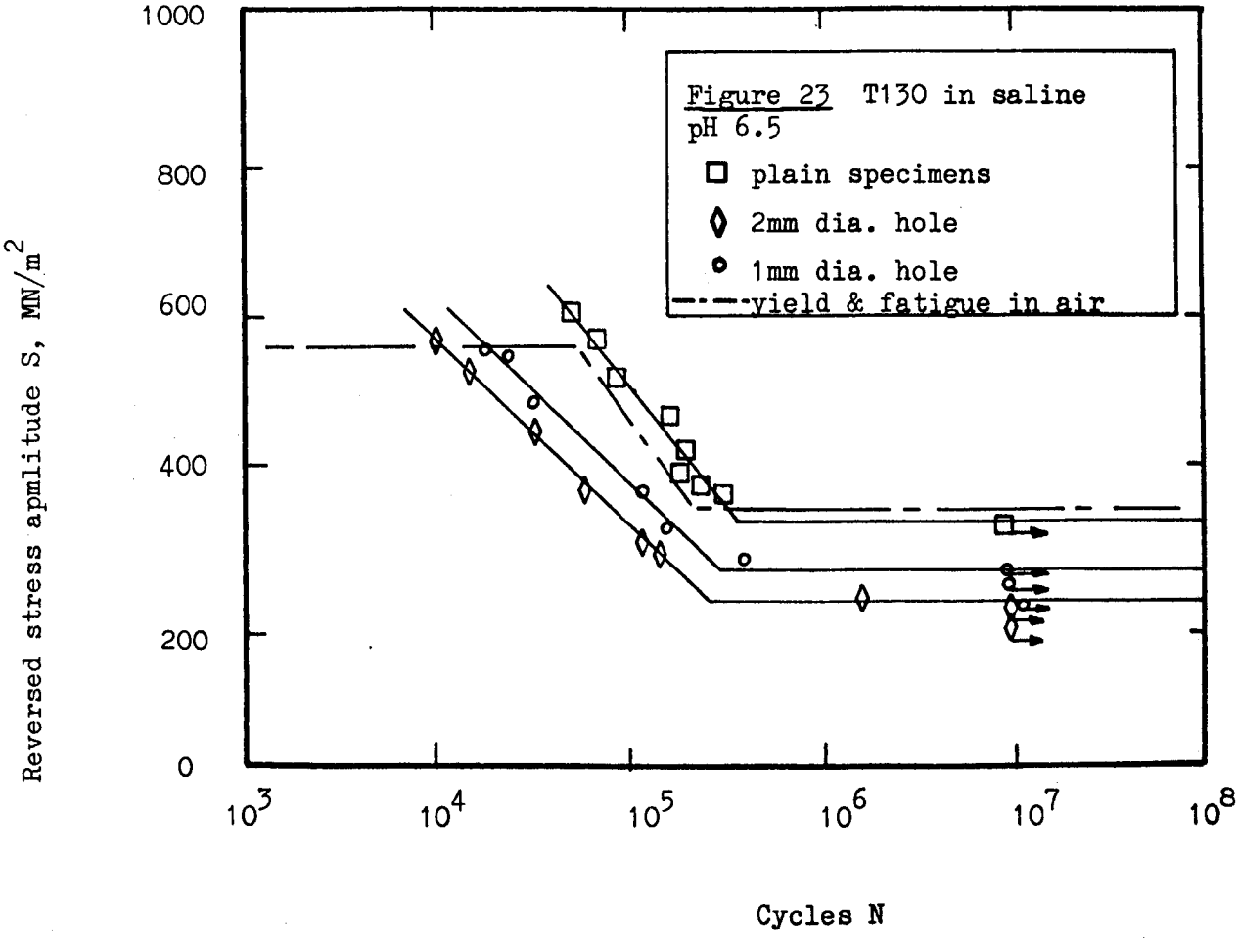
Figure 23 T130 in saline pH 6.5
plain specimens
2mm dia. hole
1mm dia. hole
yield & fatigue in air
Reversed stress apmlitude S, MN/m^2
1000
800
600
400
200
0
10^3
10^4
10^5
10^6
10^7
10^8
Cycles N

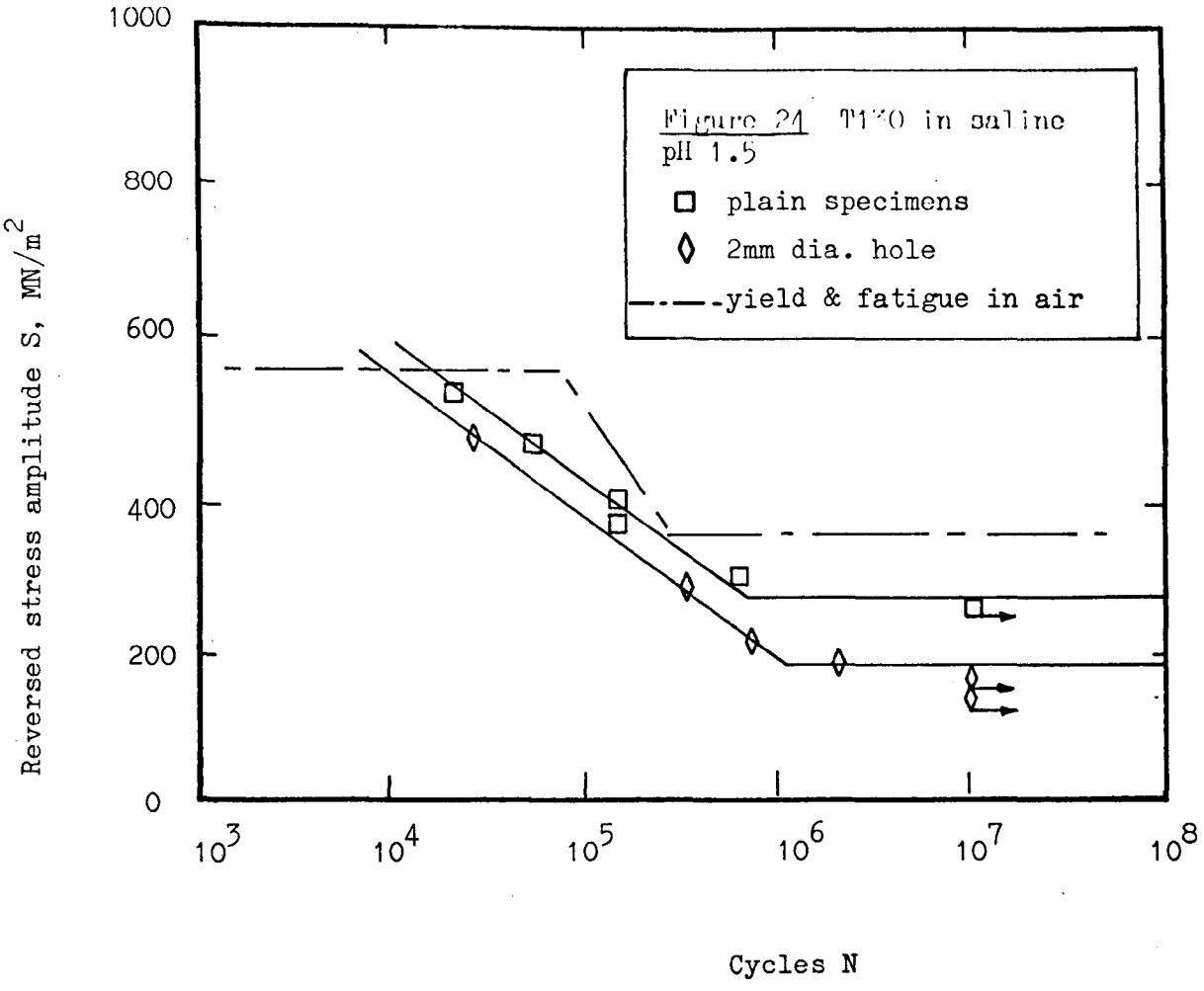
Figure 24 T170 in saline pH 1.5
plain specimens
2mm dia. hole
yield & fatigue in air
Reversed stress amplitude S, MN/m2
1000
800
600
400
200
0
10^3
10^4
10^5
10^6
10^7
10^8
Cycles N

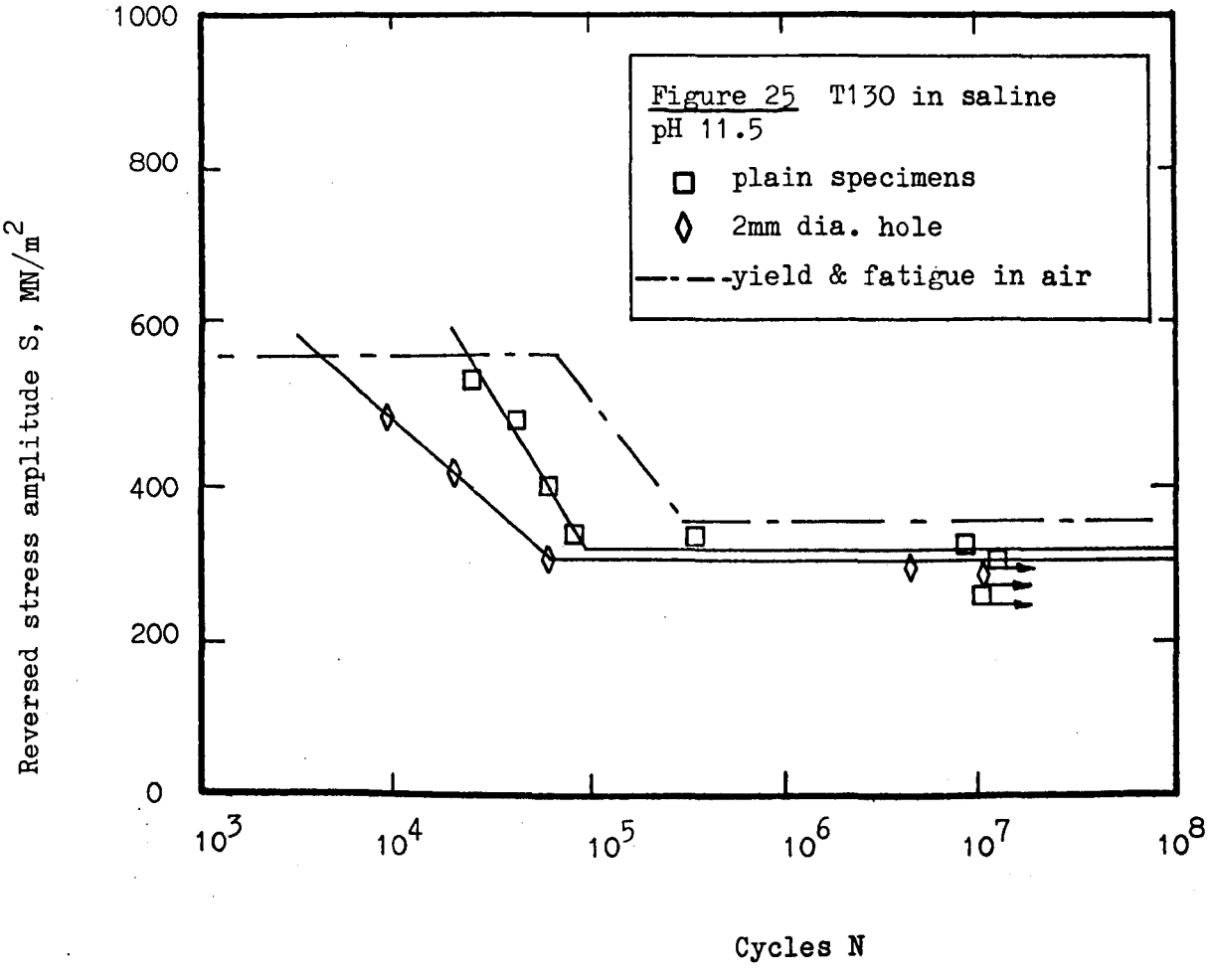
Figure 25 T130 in saline pH 11.5
plain specimens
2mm dia. hole
yield & fatigue in air
Reversed stress amplitude S, MN/m2
1000
800
600
400
200
0
10^3
10^4
10^5
10^6
10^7
10^8
Cycles N

the rate of damage law for plain specimens of T130:

$S = 1655 - 235 \log N$, above a fatigue limit of $\pm$ 325 MN/m^2 ____(24)

For 2 mm diameter hole specimens of T130 in distilled water this endurance was reduced to:

$S = 1415 - 205 \log N$, above a fatigue limit of $\pm$ 305 MN/m^2 ____(26)

The data plotted for the 1 mm diameter hole in this case showed a further reduction in endurance life over the entire range from that obtained with the larger hole:

$S = 1509 - 243 \log N$, above a fatigue limit of $\pm$ 225 MN/m^2 ____(27)

The results obtained in saline pH 6.5 for T130 are shown in Fig. 23. The performance of plain specimens was similar to that observed in distilled water and in air. The rate of damage law was steeper in slope giving longer endurance at high stress amplitudes in saline pH 6.5 than in distilled water or air. Plain specimens of T130 resulted in the following law:

$S = 2034 - 301 \log N$, above a fatigue limit of $\pm$ 340 MN/m^2 ____(28)

In contrast to the behaviour of 2 mm and 1 mm diameter hole specimens in distilled water, the relative corrosion fatigue

endurance obtained for each size of hole was reversed. The 2 mm diameter hole was found here to be the most damaging for T130 in saline pH 6.5:

$S = 1533 - 238 \log N$, above a fatigue limit of $\pm$ 230 MN/m^2 ...(29)

The result for 1 mm diameter hole specimens produced the same slope:

$S = 1585 - 238 \log N$, above a fatigue limit of $\pm$ 270 MN/m^2 ...(30)

Fig. 24 shows the corrosion fatigue behaviour of T130 in saline pH 1.5. Plain specimens had reduced endurance compared with the performance in air:

$S = 1313 - 179 \log N$, above a fatigue limit of $\pm$ 255 MN/m^2 ...(31)

The similar but lower endurance result for the 2 mm hole specimens was:

$S = 1290 - 182 \log N$, above a fatigue limit of $\pm$ 175 MN/m^2 ...(32)

representing a not inconsiderable reduction in performance.

The performance in saline pH 11.5, as shown in Fig. 25, was much improved, in comparison with that at pH 1.5, at lower stress amplitudes. Plain specimens of T130 in pH 11.5 resulted in a damage rate steeper than that for air but terminating at a

fatigue limit only just below that in air:

$S = 2206 - 359 \log N$, above a fatigue limit of $\pm$ 320 MN/m^2 ___(33)

The results for 2 mm hole specimens were of similar form:

$S = 1435 - 248 \log N$, above a fatigue limit of $\pm$ 310 MN/m^2 ___(34)

The reduction in fatigue limit, from that in air, for T130 in saline pH 11.5 was really quite small. The reduction in endurance at higher stress amplitudes for specimens with the 2 mm hole was the greatest effect of environment noted here.

4.1.5. Corrosion fatigue for titanium 318

The corrosion fatigue results for the titanium alloy T318 are shown in Figs. 26 to 29. A fatigue limit was found for all cases tested.

Fig. 26 gives the performance of T318 in distilled water. Plain specimens established a fatigue limit which was just higher than that obtained in air:

$S = 7719 - 1563 \log N$, above a fatigue limit of $\pm$ 545 MN/m^2 ___(35)

The slope of this rate damage, equation (35), is of considerable magnitude. The number of specimens tested in this region was, to say the least, sparse, but the same trend was established for T318

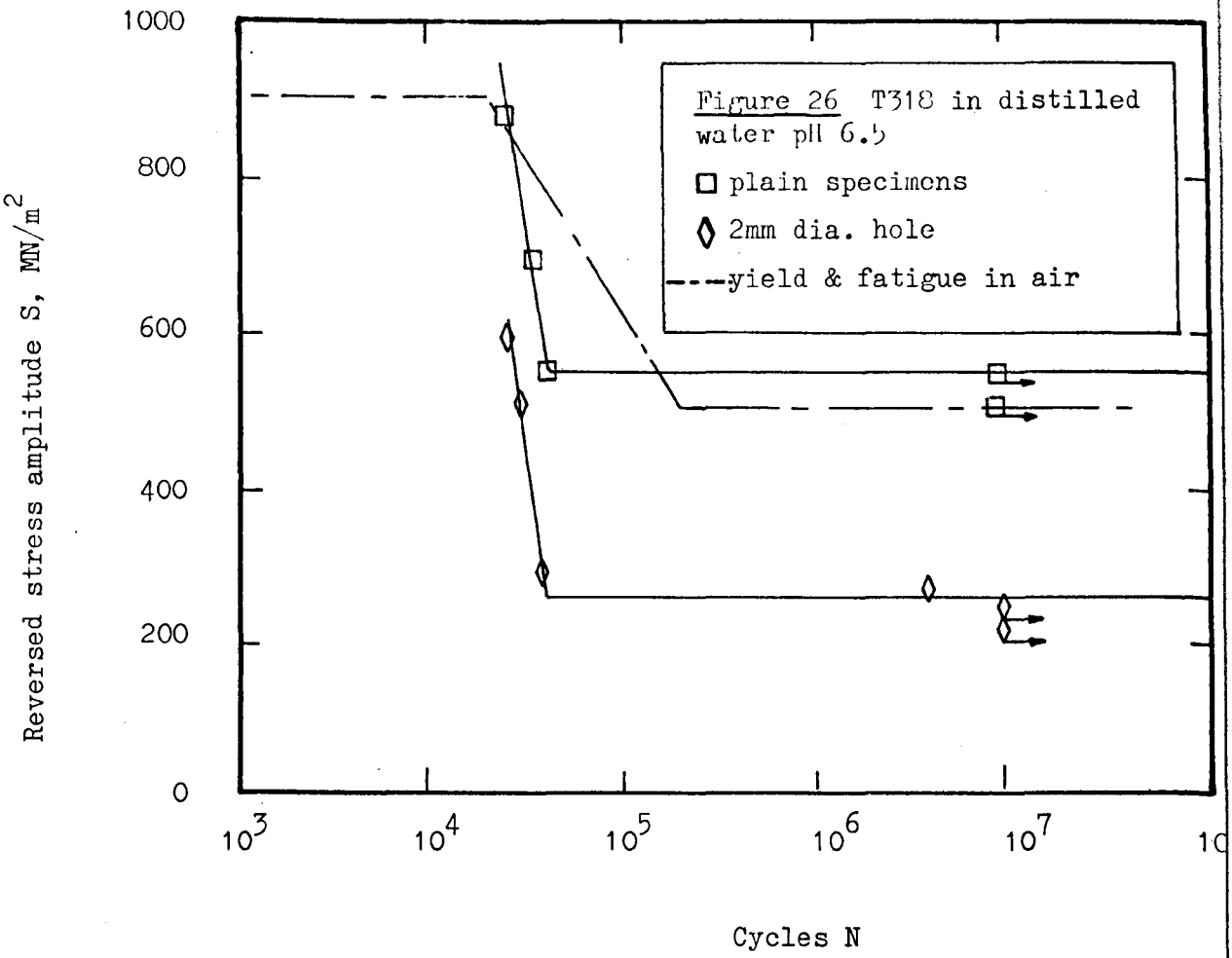
Figure 26 T318 in distilled water pH 6.5
plain specimens
2mm dia. hole
yield & fatigue in air
Reversed stress amplitude S, MN/m2
1000
800
600
400
200
0
10^3
10^4
10^5
10^6
10^7
Cycles N

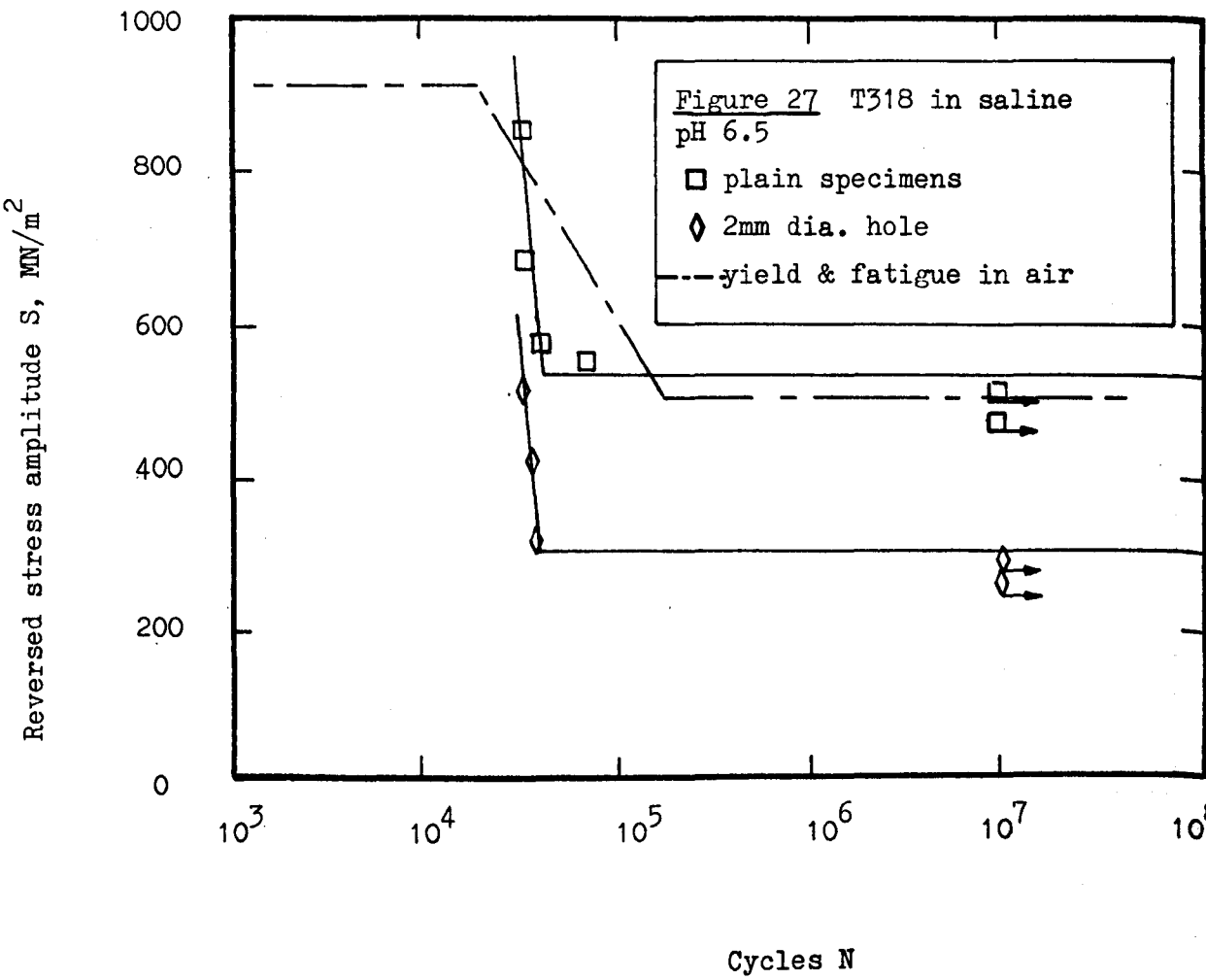
Figure 27 T318 in saline pH 6.5
plain specimens
2mm dia. hole
yield & fatigue in air
Reversed stress amplitude S, MN/m2
1000
800
600
400
200
0
10^3
10^4
10^5
10^6
10^7
10^8
Cycles N

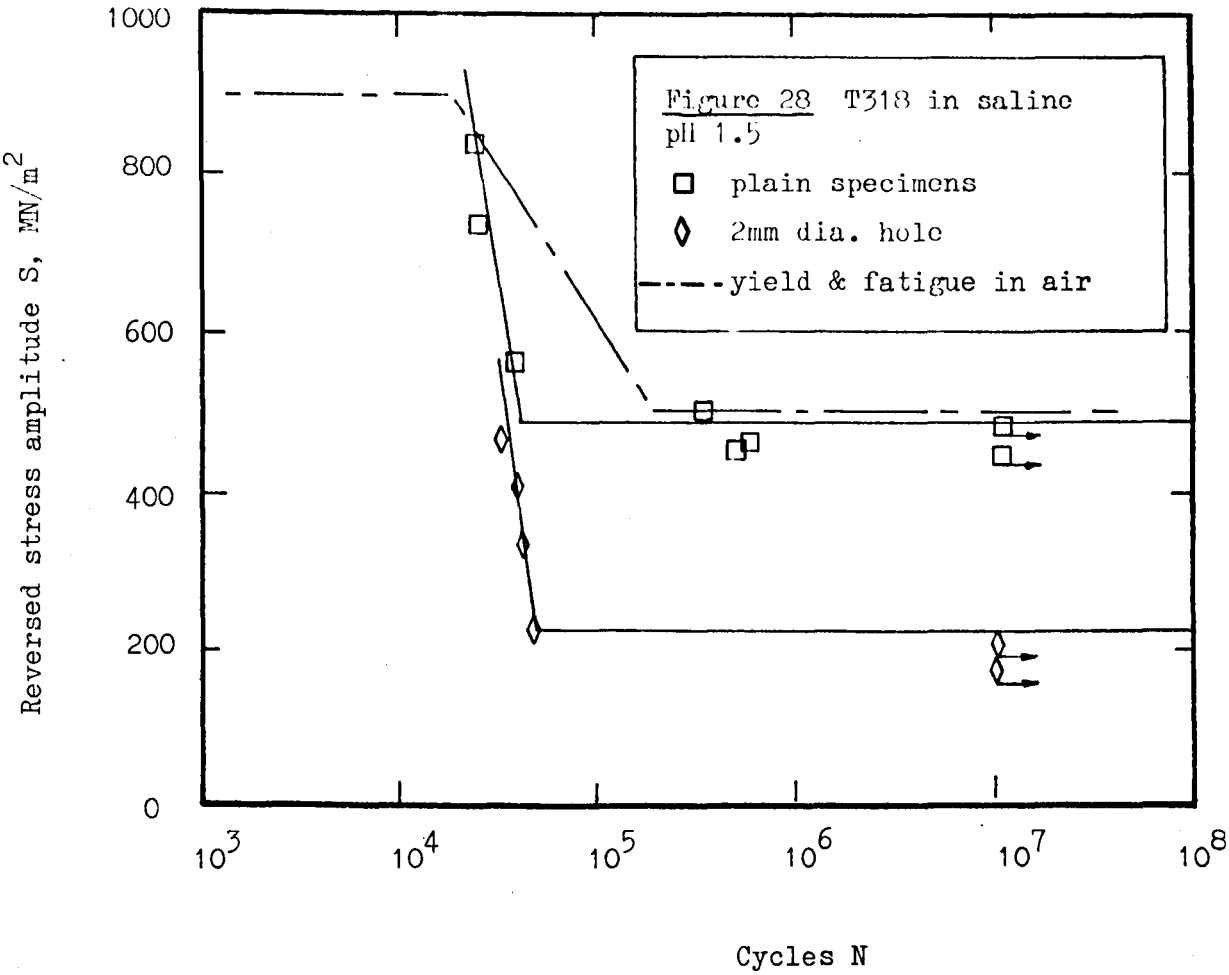
1000
800
600
400
200
0
Reversed stress amplitude S, MN/m^2
10^3
10^4
10^5
10^6
10^7
10^8
Cycles N
Figure 28 T318 in saline pH 1.5
plain specimens
2mm dia. hole
yield & fatigue in air

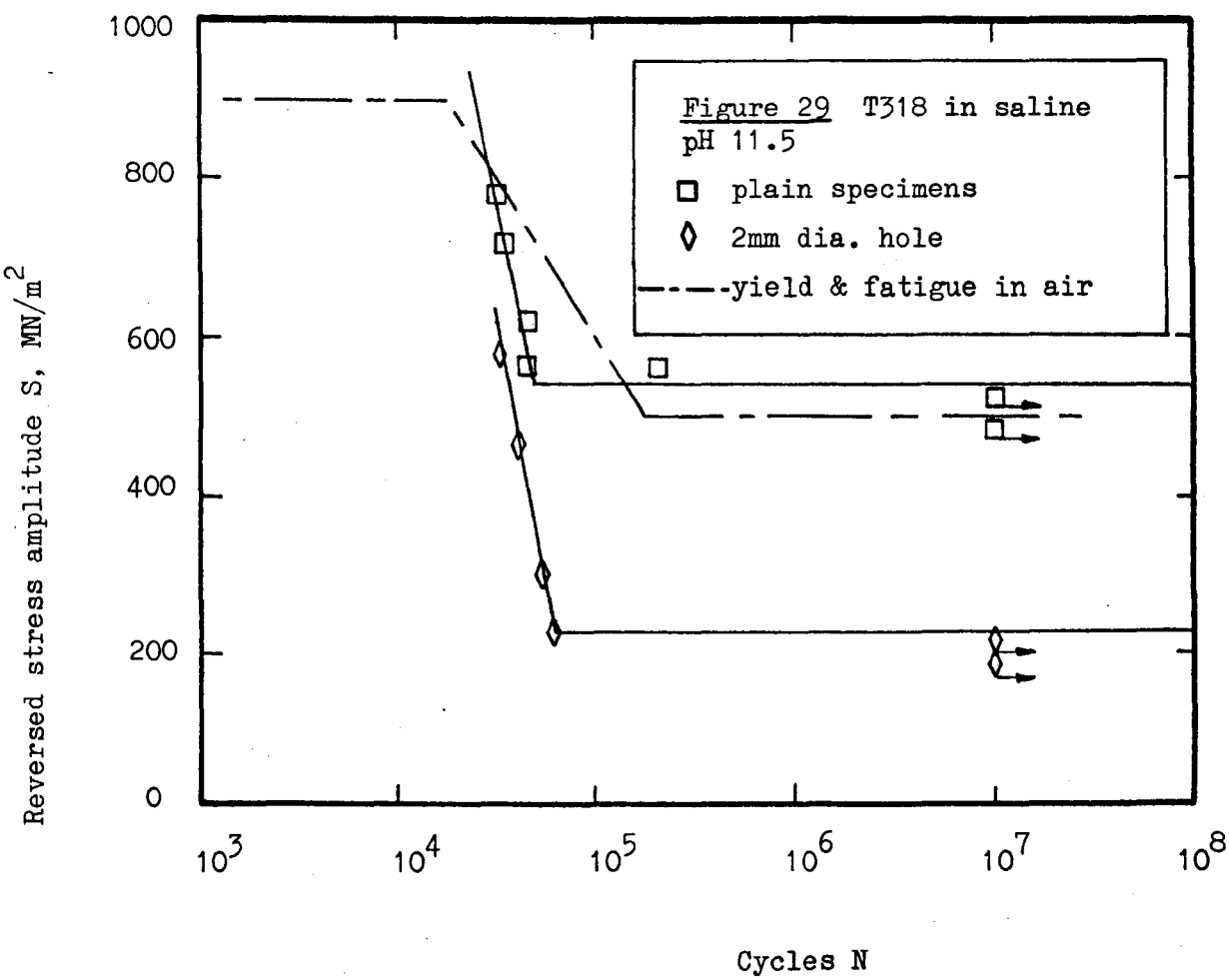
1000
800
600
400
200
0
Reversed stress amplitude S, MN/m^2
10^3
10^4
10^5
10^6
10^7
10^8
Cycles N
Figure 29 T318 in saline pH 11.5
plain specimens
2mm dia. hole
yield & fatigue in air

in all solutions tested and this fact, together with the very low scatter of data obtained, indicates some validity for results such as equation (35).

Specimens with a 2 mm diameter hole drastically reduced the fatigue limit in distilled water for T318 from $\pm$ 545 MN/m^2 down to only $\pm$ 255 MN/m^2 , indicating a large notch sensitivity for T318 here. The slope of the S/N rate damage for specimens with holes was identical to that given in equation (35) for plain specimens. The data obtained for specimens with holes above the fatigue limit was almost coincident with a continuation downward of the plain specimen result.

Fig. 27 shows results for T318 in saline pH 6.5. Plain specimens showed the following:

$$S = 14176 - 2941 \log N, \text{ above a fatigue limit of } \pm 530 \text{ MN/m}^2 \quad (36)$$

The results for the 2 mm diameter hole specimens were again found to produce the same slope for rate of S/N damage as for the plain specimens. The fatigue limit was reduced to 305 MN/m^2 in saline pH 6.5 showing less environmental damage than in distilled water.

The behaviour of T318 in saline pH 1.5 is shown in Fig. 28. For plain specimens the fatigue limit established was just less than that in air. In pH 1.5 the S/N rate law was obtained as follows:

$S = 8413 - 1724 \log N$, above a fatigue limit of $\pm$ 480 MN/m^2 ___(37)

Again the results for 2 mm diameter hole specimens produced the same rate slope so that they could almost be considered as a continuation downward of the plain specimen results. The fatigue limit for T318 was reduced to only $\pm$ 220 MN/m^2, in the presence of 2 mm holes, for saline pH 1.5.

Fig. 29 shows the results for the fatigue of T318 in saline pH 11.5. Plain specimens produced the following result:

$S = 6577 - 1282 \log N$, above a fatigue limit of $\pm$ 535 MN/m^2 ___(38)

The similar form of the results, having the same rate of damage for plain specimens, for 2 mm diameter hole specimens produced a fatigue limit of $\pm$ 225 MN/m^2 in saline pH 11.5; another drastic reduction in performance.

4.1.6. Fatigue data summary

Table 2 shows the fatigue limits, or 2×10^7 cycle endurance limits * for the materials tested as plain or 'hole-drilled' specimens in each invornment: The stress amplitude is expressed in MN/m^2.

	Air	Dist. Water pH6.5	Saline		
			pH6.5	pH1.5	pH11.5
Mild steel plain	300	72*	100*	52*	58*
" " 2 mm hole	147	8*	65*	#	23*
" " 1 mm hole	178	45*	-	-	-
S316 plain	310	330	300	35	320
" 2 mm hole	275	250	255	35	300
" 1 mm hole	310	250	255	-	-
T130 plain	345	325	340	255	320
" 2 mm hole	305	305	230	175	310
" 1 mm hole	250	225	265	-	-
T318 plain	500	545	530	480	535
" 2 mm hole	350	255	305	220	225

Table 2. Fatigue and Endurance Limits MN/m^2

* 2×10^7 cycles Endurance, # too low for recording < 3 MN/m^2, - no data. (confidence limits generally $\pm$ 2 MN/m^2 for mild steel and $\pm$ 10 MN/m^2 for other materials)

4.2. Fatigue Stress Concentration/Corrosion Interaction

For comparison with earlier analyses [108,318], a similar model and format was employed in an attempt to study the separate effects of stress concentration and corrosion during the conjoint action of corrosion fatigue.

Let:

A = Fatigue endurance of plain specimens tested in air

A_h = Fatigue endurance of holed specimens tested in air

CF = Fatigue endurance of plain specimens corrosion fatigue tested

CF_h = Fatigue endurance of holed specimens corrosion fatigue tested

The reduction in fatigue strength due to the presence of a drilled hole was considered as

$(A - A_h)/A = 1 - A_h/A = 1 - N$

where $\underline{N = A_h/A}$, the notch reduction factor ——————(39)

$(0 < N < 1)$

The corrosion effect of the environment in the absence of a stress concentrating defect was considered in an exactly analygous manner:

$(A - CF)/A = 1 - CF/A = 1 - C$

where $\underline{C = CF/A}$, the corrosion reduction factor ——————(40)

$(0 < C < 1)$

The total effect of both a hole (i.e. a notch) and a corrosive environment was thus defined as

$(A - CF_h)/A = 1 - CF_h/A = 1 - T$

where $T = CF_h/A$, the total reduction factor

$(0 < T < 1)$

and $\underline{T = N + C + I,}$ ——————(41)

where $I = f(N,C)$, $(-2 < I < +1)$ and is the interaction factor introduced to account for any synergistic behaviour.

Relating together eqns (39) to (41) it will be noted that the total reduction in corrosion fatigue performance without interaction

is given by

$(1 - T) = (1 - N) + (1 - C)$

so that $T = -1 + N + C$ and I is therefore of value - 1 when there is no synergistic behaviour. A specimen without a hole ($N = 1$) and without corrosion ($C = 1$) will have $T = 1$ in equation (41) indicating zero effect $(1 - N)$ as required in the model.

For each material the values of N,C and I, extrapolated from the S/N data, were determined at various endurance lives. Table 3 shows the tabulated values, using the 2 mm diameter hole results for N, in mild steel. The value of N was reduced with longer endurance, low amplitude stress results so that the percentage reduction in the fatigue limit due to a hole was given by $(A - A_h)/A = 1 - N = 51\%$; a higher value than that produced at higher stress amplitudes. The value of C was, with the exception of the distilled water result, similarly reduced with lower amplitude stressing so that the percentage reduction at 6×10^6 cycles endurance, for example, was 55% for saline pH 6.5 ranging to 70% for the pH 1.5 saline. The double set of results for the distilled water and the intermediate increase in values of C was the direct result of the three-stage rate of damage obtained in this case (see Fig. 14), together with the scatter of results at the "knee". In each case the value of I was negative showing that the total effect of N and C was less than the sum of the two effects considered separately. The magnitude of I generally tended toward slightly lower and more constant values with lower

mild steel in →		distilled water		saline pH6.5		saline pH1.5		saline pH11.5	
at endurance cycles x 10^{-6} ↓	N	C	I	C	I	C	I	C	I
0.1	0.709	0.896	-0.864	0.867	-0.903	0.637	-0.882	0.869	-0.941
0.5	0.708	0.833	-0.855	0.822	-0.867	0.580	-0.893	0.756	-0.963
1.0	0.703	0.910	-0.962	0.787	-0.830	0.463	-0.823	0.679	-0.904
2.0	0.627	0.910	-0.984	0.670	-0.707	0.423	-0.800	0.517	-0.734
4.0	0.503	0.850	-0.970	0.500	-0.533	0.343	-0.723	0.413	-0.609
6.0	<u>0.490</u>	0.813 0.617	-1.003 -0.807	0.453	-0.540	0.303	-0.740	0.360	-0.603
8.0	0.490	0.783 0.5[illegible]	-1.040 -0.790	0.437	-0.570	0.270	-0.760	0.317	-0.607
10.0	0.490	0.[illegible]	-0.767	0.417	-0.590	0.217	-0.707	0.287	-0.607
20.0	0.490	0.240	-0.703	0.333	-0.606	0.173	-0.663	0.193	-0.606

Table 3

Notch, corrosion and interaction factors for mild steel at various endurance lives, ref. equations (39) - (40)

Fatigue limit values underlined

S316 in →		distilled water		saline pH6.5		saline pH1.5		saline pH11.5	
at endurance cycles x 10^{-6} ↓	N	C	I	C	I	C	I	C	I
0.05	0.983	0.882	-0.978	1.005	-1.025	0.726	-0.983	0.794	-0.803
0.1	0.971	0.912	-1.030	0.994	-1.014	0.665	-0.971	0.818	-0.971
0.2	0.953	0.953	-1.080	0.963	-0.976	0.674	-1.034	0.847	-0.953
0.4	0.926	1.006	-1.152	0.929	-0.955	0.674	-1.123	0.914	-0.954
0.6	0.887	1.064	-1.145	0.968	-0.978	0.658	-1.175	1.032	-0.951
1.0	0.887	1.064	1.145	0.968	-1.032	0.535	-1.099	1.032	-0.951
10.0	0.887	1.064	1.145	0.968		0.113	-0.887	1.032	-0.951

Table 4

Notch, corrosion and interaction factors for S316 at various endurance lives
Ref. equations (39) - (40)

Fatigue limit values underlined.

T130 in →		distilled water		saline pH6.5		saline pH1.5		saline pH11.5	
at endurance cycles x 10^{-6} ↓	N	C	I	C	I	C	I	C	I
0.05	0.593	0.924	-0.754	1.025	-0.913	0.773	-0.647	0.762	-0.782
0.1	0.637	0.989	-0.812	1.077	-0.994	0.837	-0.706	0.668	-0.658
0.2	0.836	1.101	-1.038	1.167	-1.252	0.959	-0.931	0.800	-0.760
0.4	0.884	0.956	-0.956	0.985	-1.202	0.855	-1.015	0.928	-0.884
0.6	0.884	0.942	-0.941	0.985	-1.202	0.768	-0.994	0.928	-0.884
1.0	0.884	0.942	-0.941	0.985	-1.202	0.739	-1.116	0.928	-0.884
10.0	0.884	0.942	-0.941	0.985	-1.202	0.739	-1.116	0.928	-0.884

Table 5

Notch, corrosion and interaction factors for T130 at various endurace lives
Ref. equations (39) - (40)

Fatigue limit values underlined.

T318 in →		distilled water		saline pH6.5		saline pH1.5		saline pH11.5	
at endurance cycles x 10^{-6} ↓	N	C	I	C	I	C	I	C	I
0.03	0.939	0.841	-1.250	1.122	-1.244	0.902	-1.079	1.037	-1.128
0.04	0.664	0.717	-1.045	0.783	-0.993	0.658	-0.809	0.921	-0.861
0.05	0.664	0.762	-1.069	0.741	-0.978	0.671	-0.999	0.804	-0.908
0.07	0.630	0.838	-1.076	0.815	-0.976	0.738	-1.030	0.823	-1.107
0.10	0.588	0.916	-1.075	0.891	-0.966	0.807	-1.025	0.899	-1.109
0.20	0.700	1.09	-1.34	1.060	-1.150	0.960	-1.22	1.07	-1.320
1.00	0.700	1.09	-1.34	1.060	-1.150	0.960	-1.22	1.07	-1.320

Table 6

Notch, corrosion and interaction factors for T318 at various endurance lives
Ref. equations (39) - (40)

Fatigue limit values underlined.

stress amplitudes.

Table 4 for S316 showed far less of a change in all values with endurance. N values reduced with reduced stress amplitude but only showed a reduction, due to the hole, of 11% in fatigue limit. The direction of change of C was, with the exception of the pH 1.5 saline, generally the reverse of that obtained for the mild steel; showing that at the lower stress amplitudes behaviour was comparable with that in air. The behaviour of S316 in saline pH 1.5 was clearly very different, as considered in this analysis alone, and was very similar to the results obtained for mild steel. The value of C in pH 1.5 saline showed a percentage reduction in fatigue endurance of, for example, 47% at 1 mega cycle endurance yet 89% for the 10 mega cycle case; this is better than that for mild steel at 1 mega cycle of 54%, but far worse than that of 78% for mild steel at the longer life of 10 mega cycles.

Table 5 shows the results for T130 which, contrary to the other results, produced values of N increasing with the longer endurance lives. The notch effect for this material is clearly more damaging for high stress amplitudes(41% at 0.05 mega cycles) than for low stress amplitudes (at 12% for the fatigue limit). The other data for this material did not show any clear trend.

The results for T318 are given in Table 6 and again for this titanium alloy no general trend could be found for a change in the values of C and I with endurance. The value

of C near the fatigue limit simply indicated that in all solutions the performance was similar to that in air. The corresponding value for I was the highest set of values obtained and indicated the large synergistic interaction for the corrosion fatigue of T318 when holes are drilled through otherwise well behaved smooth specimens.

The statistical significance of the values of N,C, and I were examined, as previously examined in past work[318], using the multiple regression model

$$I = \alpha N + \beta C + \gamma \qquad (42)$$

Attempts to solve this equation in a satisfactory manner for all the materials tested, in all environments, were not successful. It was found, however, that the results could be divided into two main groups. The equation:

$$I = \gamma - 1.39N - 2.01C \qquad (43)$$

satisfied the titanium T130 and titanium alloy T318 in all the environments tests. Stainless steel S316 was also satisfied by this equation for all environments except for the results in saline pH 1.5. The values for γ obtained were respectively 1.39 for S316, 1.60 for T130 and 1.81 for T318.

The second group of results, for all environments with mild steel, and S316 in saline pH 1.5, were satisfied with the following alternative equation:

$$I = -0.926 - 0.048N + 1.3C \qquad (44)$$

The results of calculations based upon the solution of equations (43) and (44) are shown in Table 7. Differences

Material	Environment	I from individual experimental data	Difference in I values from equations (43)+ and (44)*
Mild steel	dist. water	-0.703	+0.065*
Mild steel	saline pH 6.5	-0.606	+0.089*
Mild steel	saline pH 1.5	-0.663	-0.062*
Mild steel	saline pH 11.5	-0.606	-0.093*
S316	dist. water	-1.145	+0.017+
S316	saline pH 6.5	-1.032	+0.096+
S316	saline pH 1.5	-0.887	+0.066*
S316	saline pH 11.5	-0.951	-0.113+
T130	dist. water	-0.941	-0.146+
T130	saline pH 6.5	-1.202	+0.028+
T130	saline pH 1.5	-1.116	+0.223+
T130	saline pH 11.5	-0.658	+0.118+
T318	dist. water	-1.340	+0.007+
T318	saline pH 6.5	-1.150	-0.137+
T318	saline pH 1.5	-1.220	+0.133+
T318	saline pH 11.5	-1.320	+0.013+

Table 7 Values of 'I' calculated from experimental data (shown in Tables 3 to 6) and compared with differences from calculated values of 'I', from equation 43+ and equation 44*

are shown between the solution of these equations and the individual experimental data given in Tables 3 to 6. The standard deviation obtained for the results from equation (43) was 0.110 and 0.078 for equation (44).

The most significant result from this analysis of the interaction between stress concentrations and corrosion was considered to be the separation, by this method alone, of the passive-filmed corrosion fatigue behaviour from those metal/environment combinations resulting in general corrosion. The slope of the function term, as denoted by its sign, relating C to I is the significant difference between equation (43) for passive behaviour and equation (44) for general or "true" corrosion fatigue.

In all eleven tested cases the diferences, shown in Table 7 between individual experimentally determined values of I and those calculated from equation (43), for passive behaviour were within twice the value of the standard deviation. For the general corrosion fatigue condition, all the five different systems tested were well within one and a half the value of the standard deviation.

4.3. Linear-Polarization Curves

A linear-polarization technique was used to determine the statically immersed corrosion rate of each material in all the environments used in this work. Within 10 mV more noble or more active than the corrosion potential, it is

commonly observed that the applied current density is a linear function of the electrode potential. Figs. 30 to 33 show the overpotential η, with the corrosion potential used as a reference point, plotted versus applied anodic and cathodic current; both scales are linear. The slope of these linear-polarization curves for overpotentials within $\pm$ 10mV, is related to the kinetic parameters of the system as follows:[336,337]

$$\Delta E/\Delta i_{app.} = \beta_a \beta_c / 2.3\ (i_{corr})(\beta_a + \beta_c) \qquad (45)$$

where

$\Delta E/\Delta i_{app.}$ is the slope of the linear-polarization curve given in mV/mA = Ω

i_{corr} is the corrosion current

β_a and β_c are the Tafel slopes of the anodic and cathodic reactions respectively.

The slope of the linear-polarization curve is mainly controlled by i_{corr} and is relatively insensitive to changes in the values of β, as shown in equation (45). An approximate solution may therefore be obtained assuming that anodic and cathodic β values of 120 mV represent the average of all corrosion systems [338]. Equation (45) then reduced to:

$$\Delta E/\Delta i_{app} = 0.026/i_{corr} \qquad (46)$$

The corrosion rate of any system may be calculated using equation (46) without knowledge of its electrode-kinetic parameters and yet with reasonable accuracy. Even for systems with activation- or diffusion-controlled ($\beta_c = \infty$) reduction

reactions, corrosion rates obtained using equation (46) differ by no more than a factor of 3 from the actual rates [338] This method of measuring the corrosion rate was considered to be of sufficient accuracy in this work and provided a basis for the relative assessment of each material/environment system. Table 8 shows the corrosion current density for each material tested in distilled water and saline. Mild steel was, as expected, quite different from the other materials when corrosion rates were compared, having a rapid $18.6\,\mu A/cm^2$ in pH 1.5 saline. It was interestingly found that the rate in pH 11.5 was indeed lower, relative to that at pH 6.5 in saline, possibly indicating a less active state. It was also interesting to find that there was practically no difference at pH 6.5 between the rate for saline and that for distilled water.

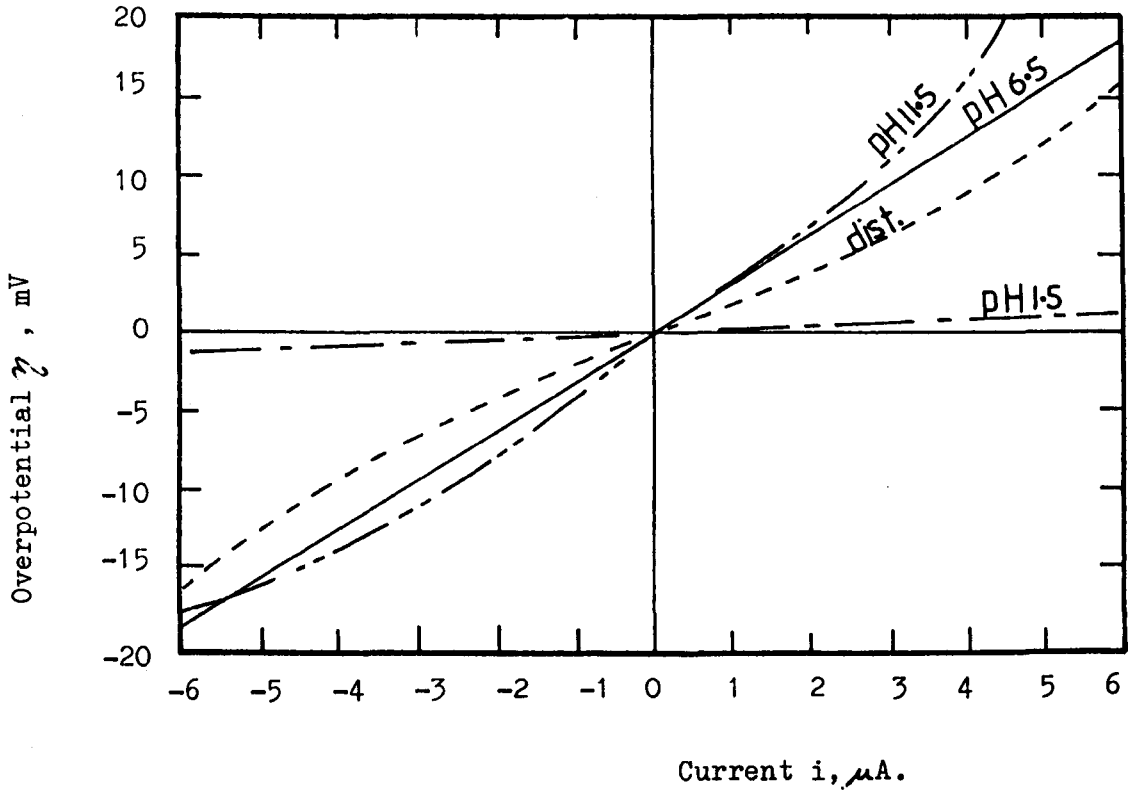

Figure 30 Linear polarization of mild steel in different environments

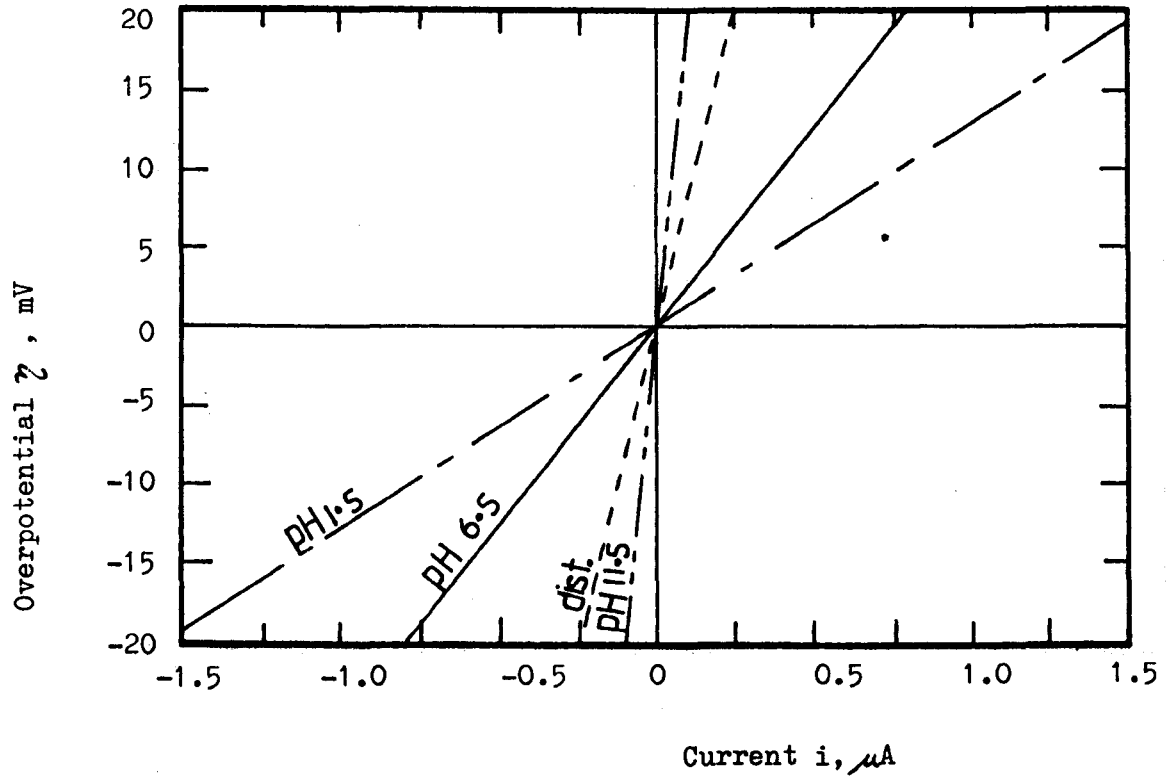

Figure 31 Linear polarization of S316 in different environments

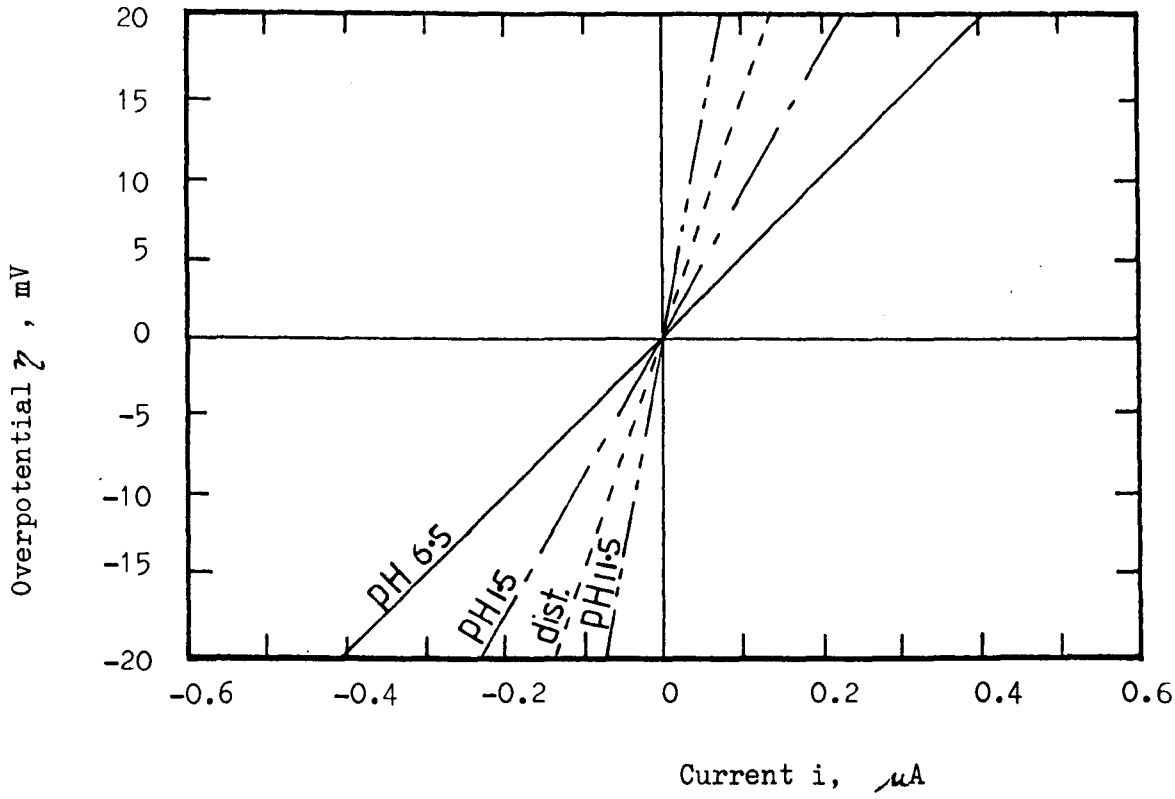

Figure 32 Linear polarization of T130 in different environments

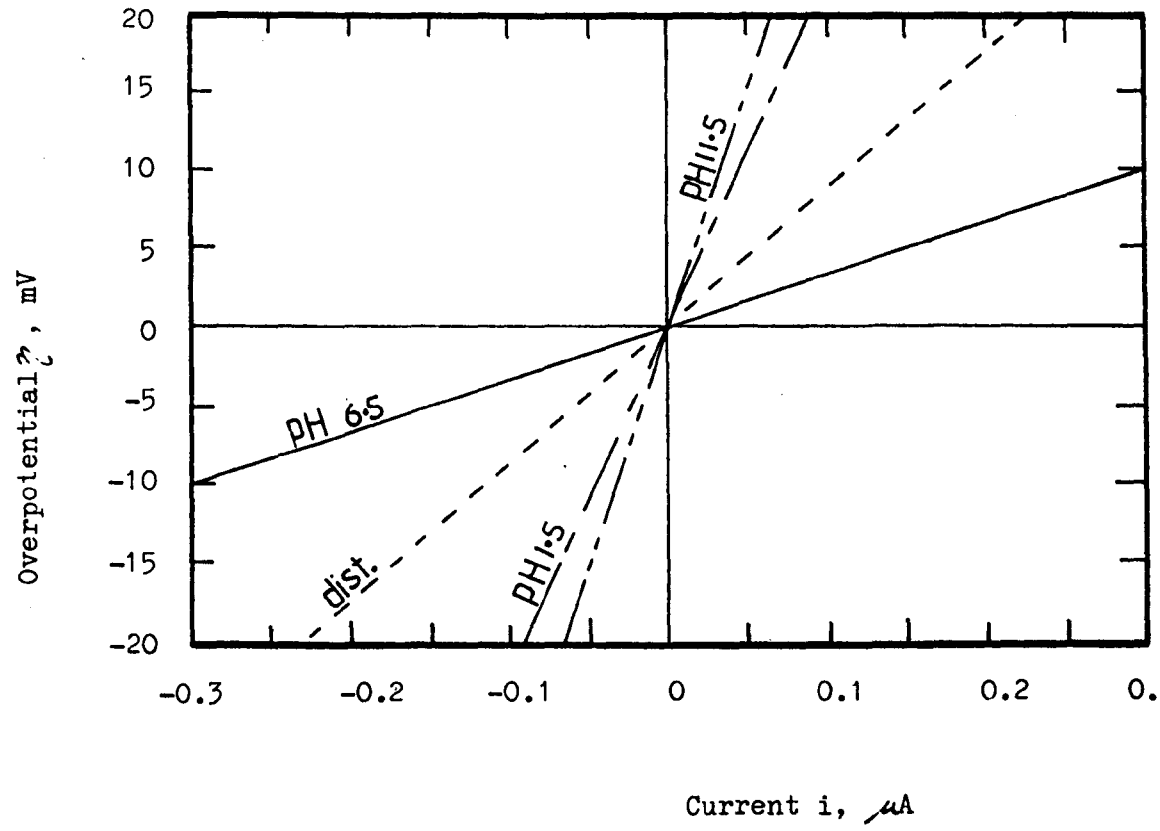

Figure 33 Linear polarization of T318 in different environments

Corrosion Current Density i_{corr} $\mu A/cm^2$				
Environ. → / Material ↓	Distilled Water	Saline		
	pH6.5	pH6.5	pH1.5	pH11.5
Mild Steel	1.03	1.04	18.6	0.743
S316	0.033	0.105	0.206	0.007
T130	0.016	0.052	0.029	0.009
T318	0.033	0.078	0.010	0.008

Table 8 Corrosion rates determined from linear-polarization curves in the $\pm$ 10 mV overpotential range (Figs. 30 to 33).

The lowest corrosion rates were found at pH 11.5 saline for all materials. The highest rate for S316 was at pH 1.5, but the titanium materials had their highest corrosion rate at pH 6.5

4.4. Polarization Data

Anodic and cathodic polarization curves were potentiostatically determined for each of the stress-free metal/electrolyte systems required in this work.

After abrading and cleaning the specimens and immersing them in the solutions a further procedure was carried out for the stainless steel specimens. Since the passive film is

present spontaniously in air and in solutions containing dissolved oxygen, it was decided to remove this by cathodic reduction [339,340] for 30 minutes at a current of approximately $200 \mu A/cm^2$. Each experiment thus started from a reduced surface and the potential was then made more positive in steps of 20 mV: the current being recorded 1 minute after adjustment of the potential. It was not thought practical to wait longer than this for the attainment of steady-state conditions. Since it was not possible to obtain a completely reduced surface on titanium specimens, except perhaps for a brief period after abrading, [129,146], measurements were taken after 5 minutes exposure to the solution in a similar way to that used for stainless steel. An air-formed TiO film of approximately 16 Å, immediately prior to test initiation, was therefore present for this material before the formation of $Ti(OH)_3$ and $TiO_2.H_2O$ passive film with reduction of hydrogen ions in solution.

Modifications to the polarization curves were recorded for the systems under corrosion fatigue. In order to differentiate between the effect of stress amplitude in the dynamic situation and stress applied in the static case, tests were also made in the corrosion fatigue rig so that specimens were held stationary at maximum and minimum stroke positions. Applied compressive and tensile stress polarization curves were thus compared with stress-free results and alternating 1.7 H_z fatigue polarization curves. Further tests were made to determine the effect of the stirring motion of the specimen in its electrolyte. These tests

comprised plotting modifications to the stress-free polarization curves, obtained previously, with specimens cycled at 1.7 Hz on the fatigue rig but having their pivot-end support legs unclamped; the specimens were thus stress-free but had approximately the same environment relative velocity as the corrosion fatigue loaded ones.

For reasons of clarity on the polarization curves, Figs. 34 to 49 presented in the following sections, only one stress amplitude is illustrated from the range of amplitudes investigated. The ringed numbers on these diagrams, e.g. 1 - 2, represent rest potential changes with time, determined as described later, for comparison in later discussion.

4.4.1. Polarization data for mild steel

Fig. 34 shows mild steel in distilled water having an unpolarized potential E_o = - 0.680 V (S.C.E.) which becomes E'_o = - 0.450 V when stirring occurs. The dynamic fatigue curve also originates at - 0.450 V when unpolarized while the statically applied tensile stress of equivalent amplitude originated at - 0.680 V. The shape of the anodic and cathodic polarization curves were found to be generally similar and stress generally was responsible for cathodic depolarization. Statically applied stress anodically polarized the system, yet fatigue loading was responsible for depolarizing the system both anodically and cathodically. The main observation here was that the movement of E_o in a more noble direction during

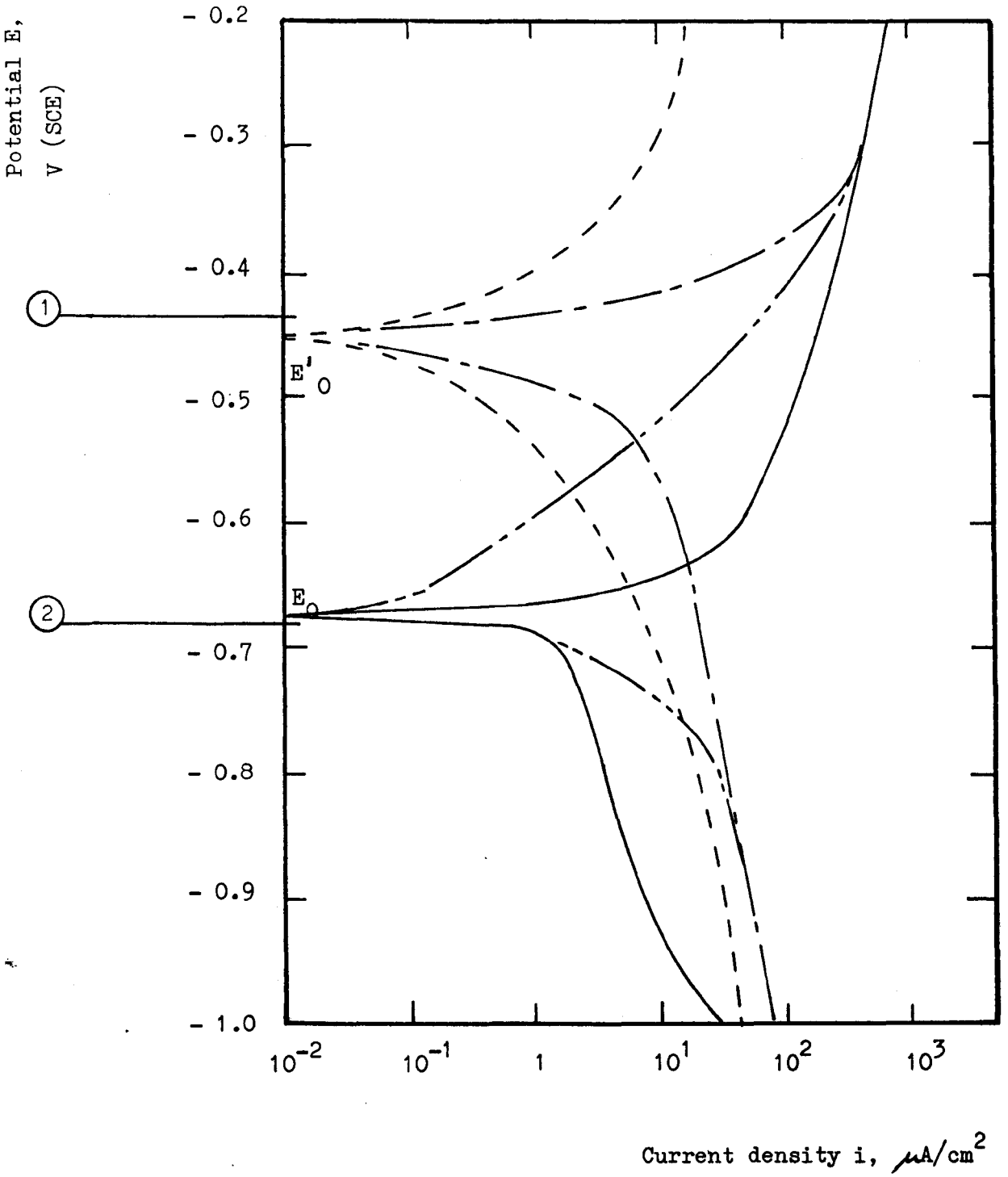

Figure 34 Anodic and cathodic polarization curves for mild steel in distilled water pH 6.5

Key:-

——————— static conditions without stress

— — — — stiring conditions without stress

——— — — static conditions with tensile stress of 380 MN/m^2

——— — ——— fatigue at ± 380 MN/m^2

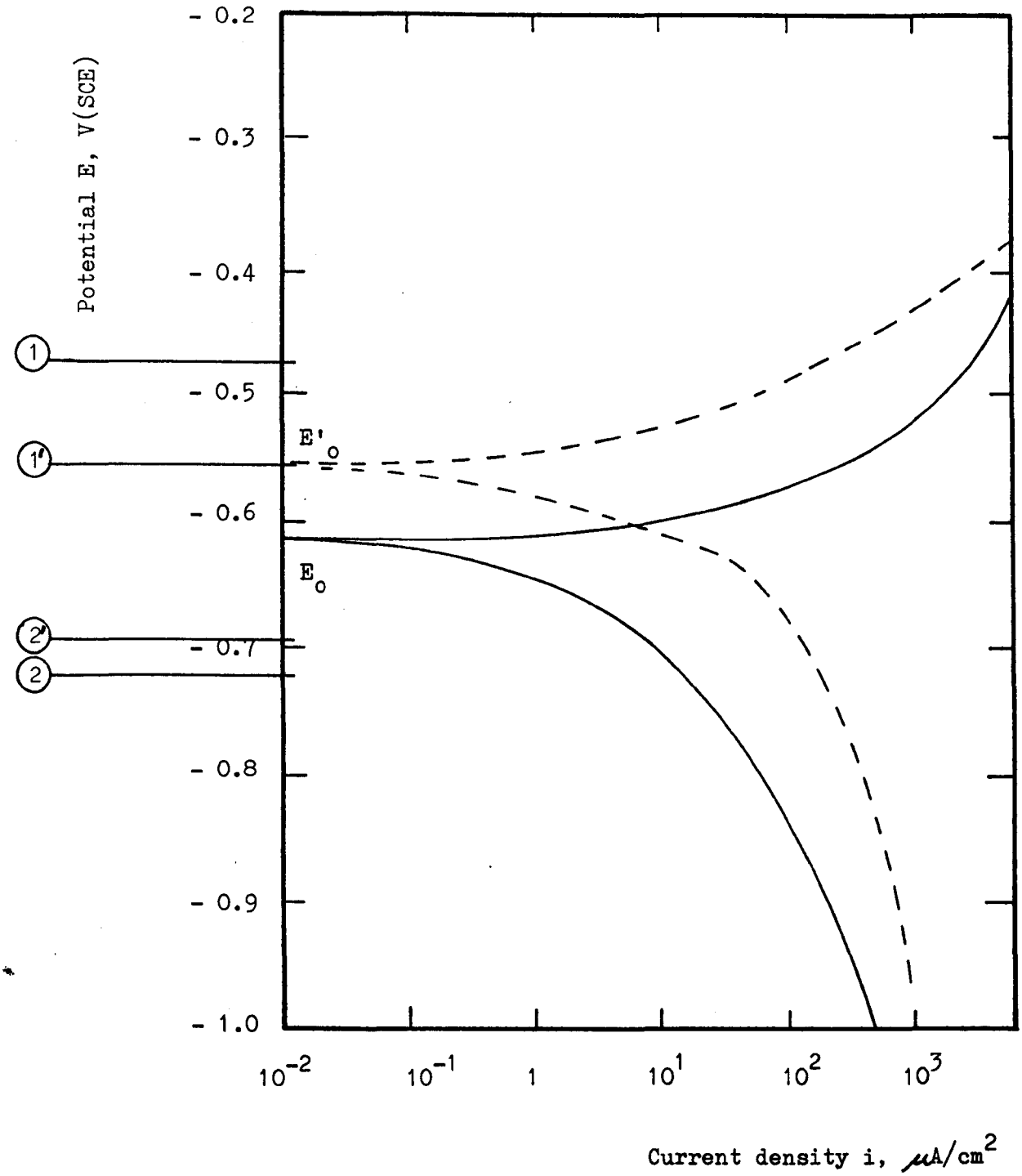

Figure 35 Anodic and cathodic polarization curves for mild steel in saline pH 6.5

Key:-

——— static conditions with and without tensile stress

- - - - - stirring conditions with and without fatigue

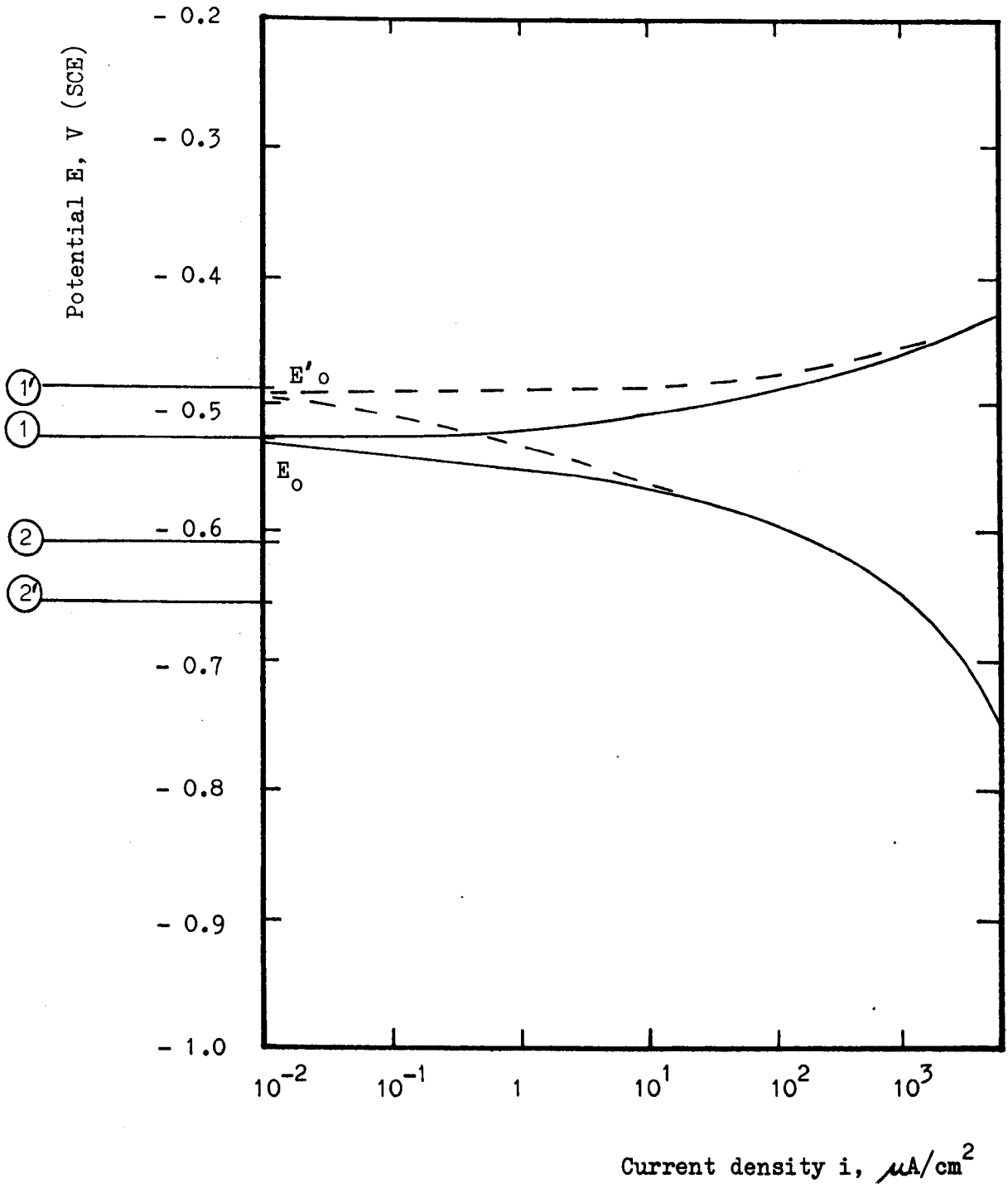

Figure 36 Anodic and cathodic polarization curves for mild steel in saline pH 1.5

Key:-

——————— static conditions with and without tensile stress

– – – – – – – stiring conditions with and without fatigue

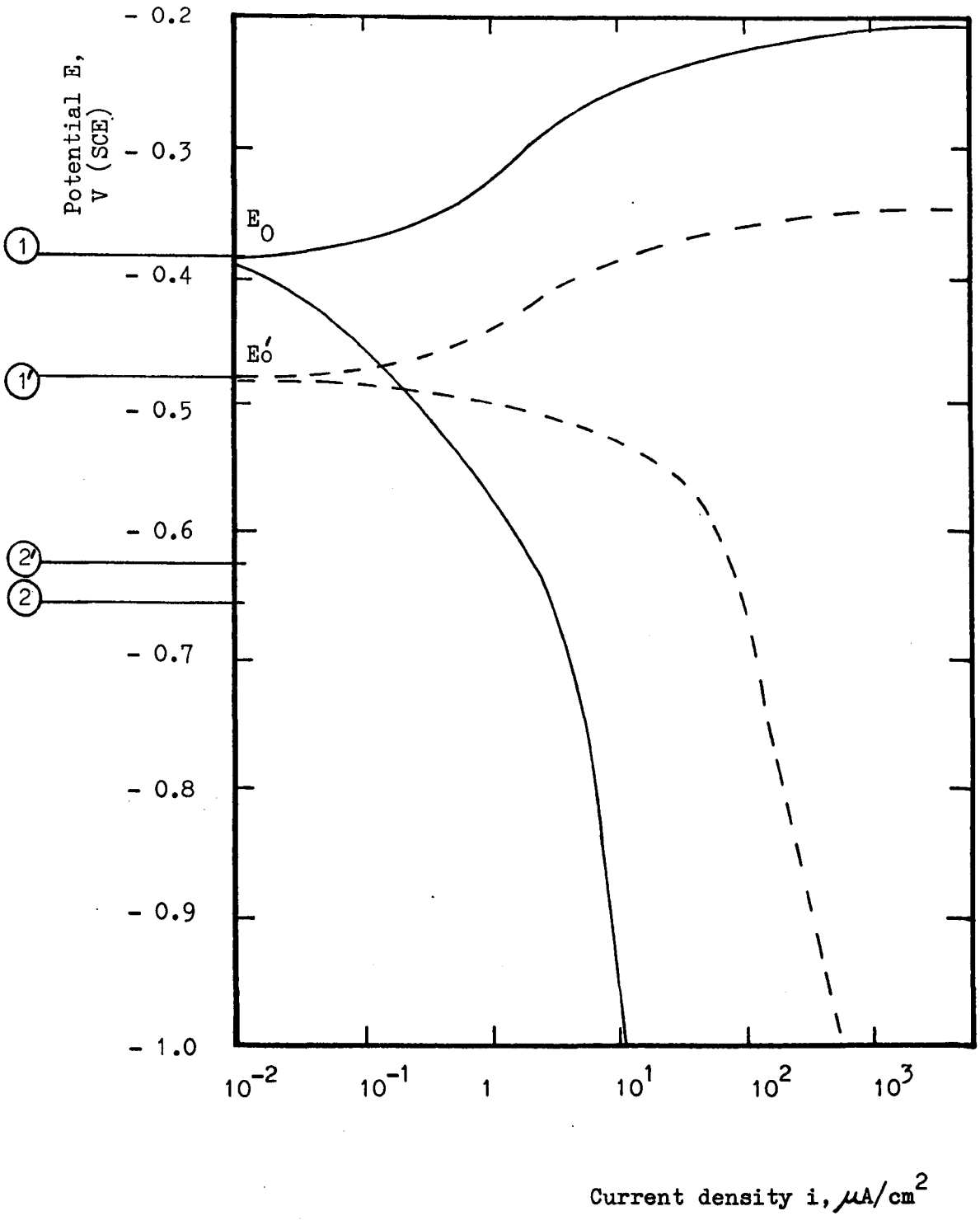

Figure 37 Anodic and cathodic polarization curves for mild steel in saline pH 11.5

Key:-

——————— static conditions with and without tensile stress

— — — — — — stirring conditions with and without fatigue

fatigue was due to the stirring action alone.

The situation seen for mild steel in saline pH 6.5 is shown in Fig. 35. The static condition E_o = - 0.610 V also moved in a more noble direction when stirred, to E_o = - 0.560 V. The movement here was much less than that observed for distilled water: the saline was also seen to act as a depolarizing agent for both anodic and cathodic reactions. The dynamic curve and the stirring curve were coincident, while the static curve was coincident with the no stress curve.

Fig. 36 gives the polarization curves for mild steel in pH 1.5 saline. E_o = - 0.520 V moved a relatively small amount in the more noble direction, to E'_o = - 0.490 V, under stirring. This system was also clearly far less polarized, at pH 1.5, than in the other solutions tested for mild steel. A grey surface film rapidly formed, on anodic polarization at approximately - 0.450 V, on which O_2 bubbles were clearly visible. This was in contrast to the rapid formation of "red"-rust observed in normal solutions of saline and distilled water. Static stress results were coincident with static no-stress results, and dynamic stresses produced the same curves obtained in stress-free stirring: that is, a small effect of stirring only was found for this system where corrosion rates were high and unaffected by the application of any form of stress.

Saline pH 11.5 produced the polarization curves for mild steel shown in Fig. 37. In this system, an unusual corrosion product in the form of green spot "fluff balls" was observed to form

rapidly on the steel surface at approximately - 0.250 V, anodically polarized. The value of E_o = - 0.390 V was more noble than that found for mild steel in the other solutions tested. The major point of interest here, however, was that, unlike the other systems, the unpolarized potential moved in a more base direction under stirring, to E'_o = - 0.480 V. Dynamic curves were similar to the stirring curves while static stress curves were coincident with the stress-free unstirred data. In this latter respect only the behaviour of mild steel in saline pH 11.5 was similar to that in solutions at pH 6.5

4.4.2. Polarization data for stainless steel 316

Figs 38 to 41 show the polarization curves obtained for S316 stainless steel. The distilled water system is shown in Fig 38 with E_o = - 0.10 V and some evidence of passive behaviour on anodic polarization in the presence of atmospheric O_2. The passive region, at approximately 0.20$\mu A/cm^2$ (active at 2.50$\mu A/cm^2$), was rather limited to + 0.10V and attempts at further anodic polarization resulted in a rapid increase in current density to saturation at + 0.40 V with oxygen evolution. With stirring the value of E'_o = + 0.03V was found, representing a small movement in the more noble direction. Stirring resulted in more effective anodic and cathodic polarization. Dynamic loading clearly showed a depolarizing effect both anodically and cathodically. Statically applied stress caused a similar effect but the curves originated at the unstirred E_o potential. Hydrogen was rapidly formed on the specimen surface at about - 0.80 V under cathodic

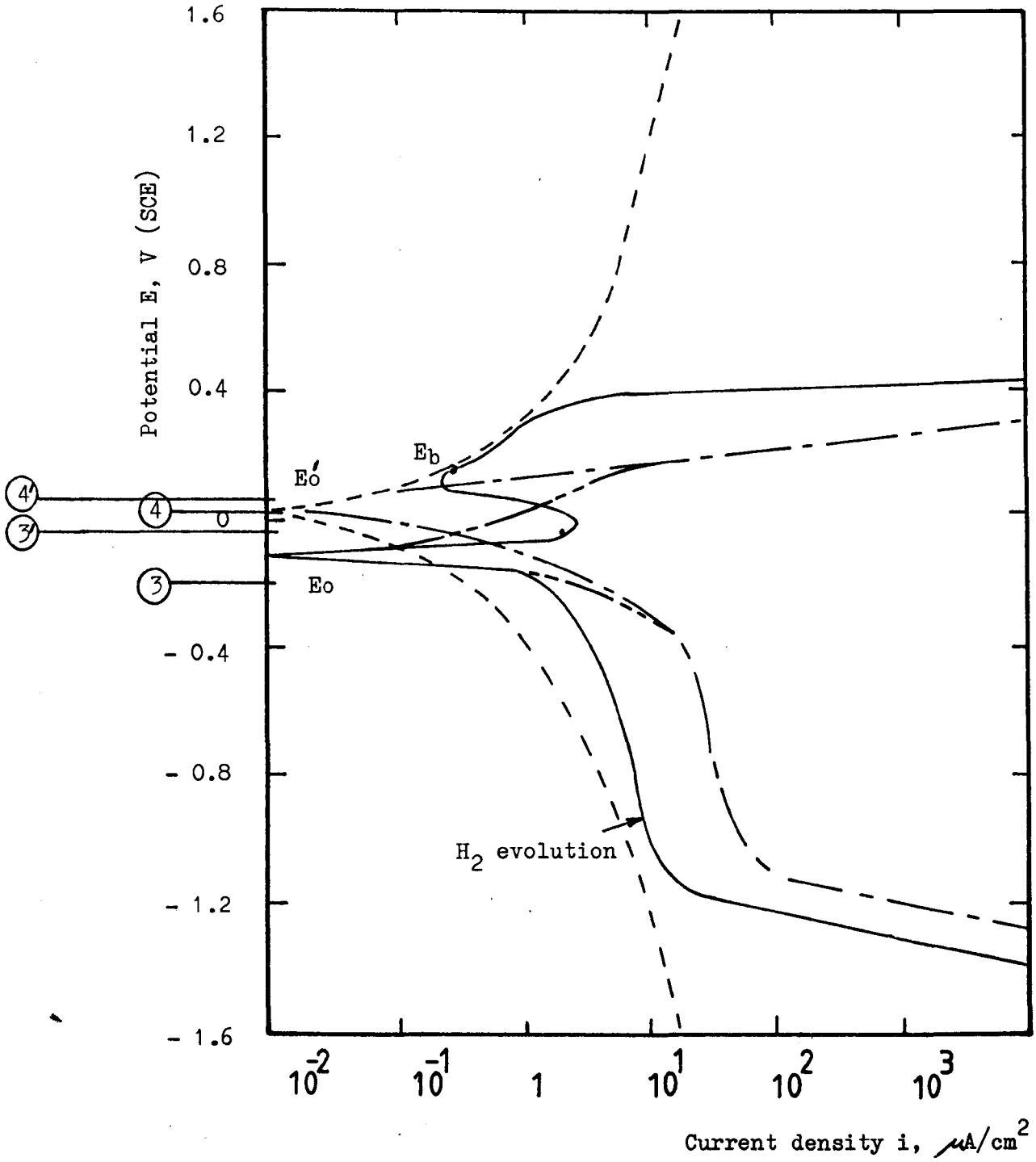

Figure 38 Anodic and cathodic polarization curves for S316 in distilled water pH 6.5

Key:-

——————— static conditions

— — — — — stirring conditions

——— — — Static conditions with tensile stress of 380 MN/m^2

——— — ——— fatigue at ± 380 MN/m^2

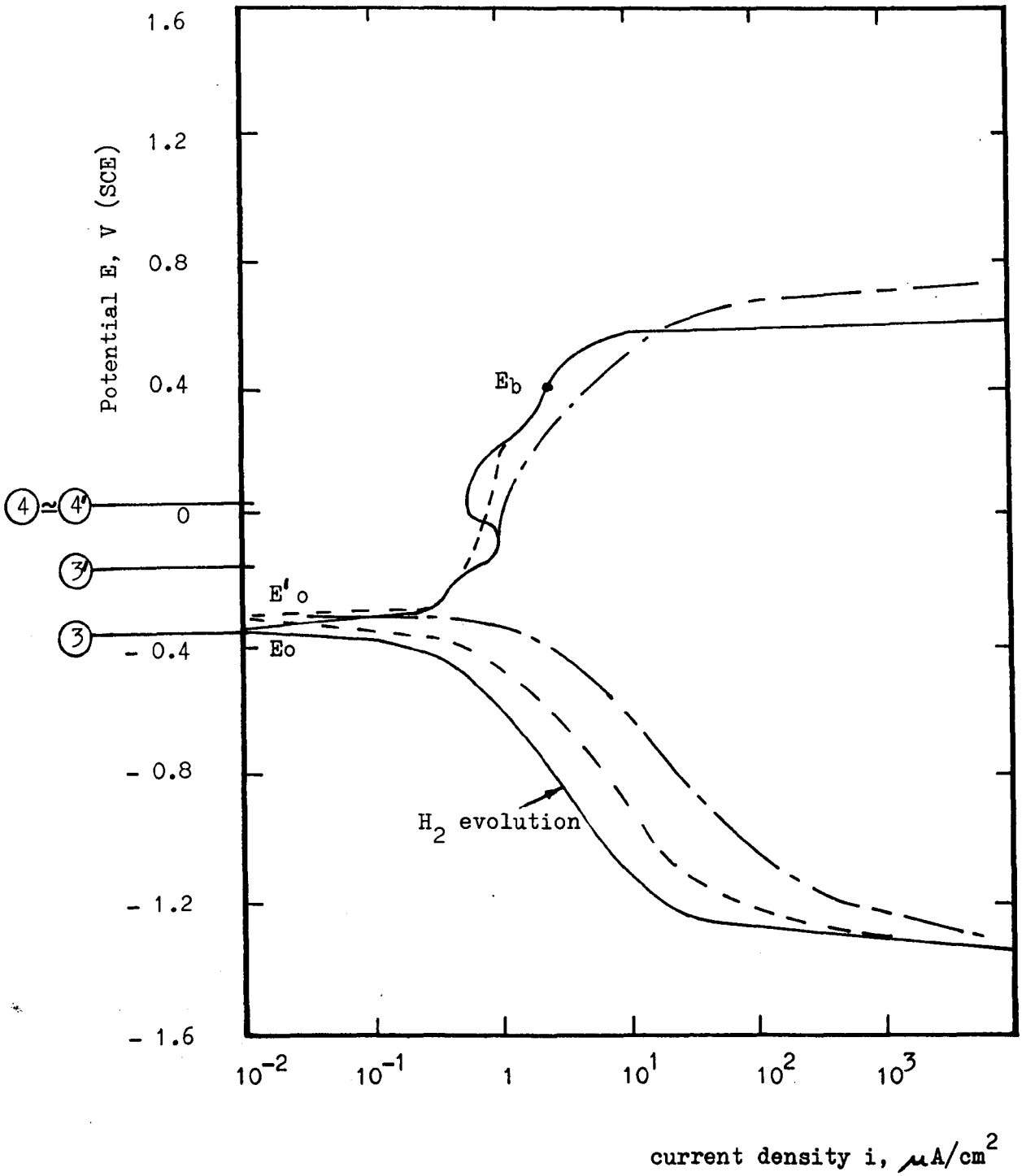

Figure 39 Anodic and cathodic polarization curves for S316 in saline pH 6.5

Key:-

——————— static conditions

— — — — — stirring conditions

——— - ——— - ——— fatigue at ± 380 MN/m^2 and static tensile stress

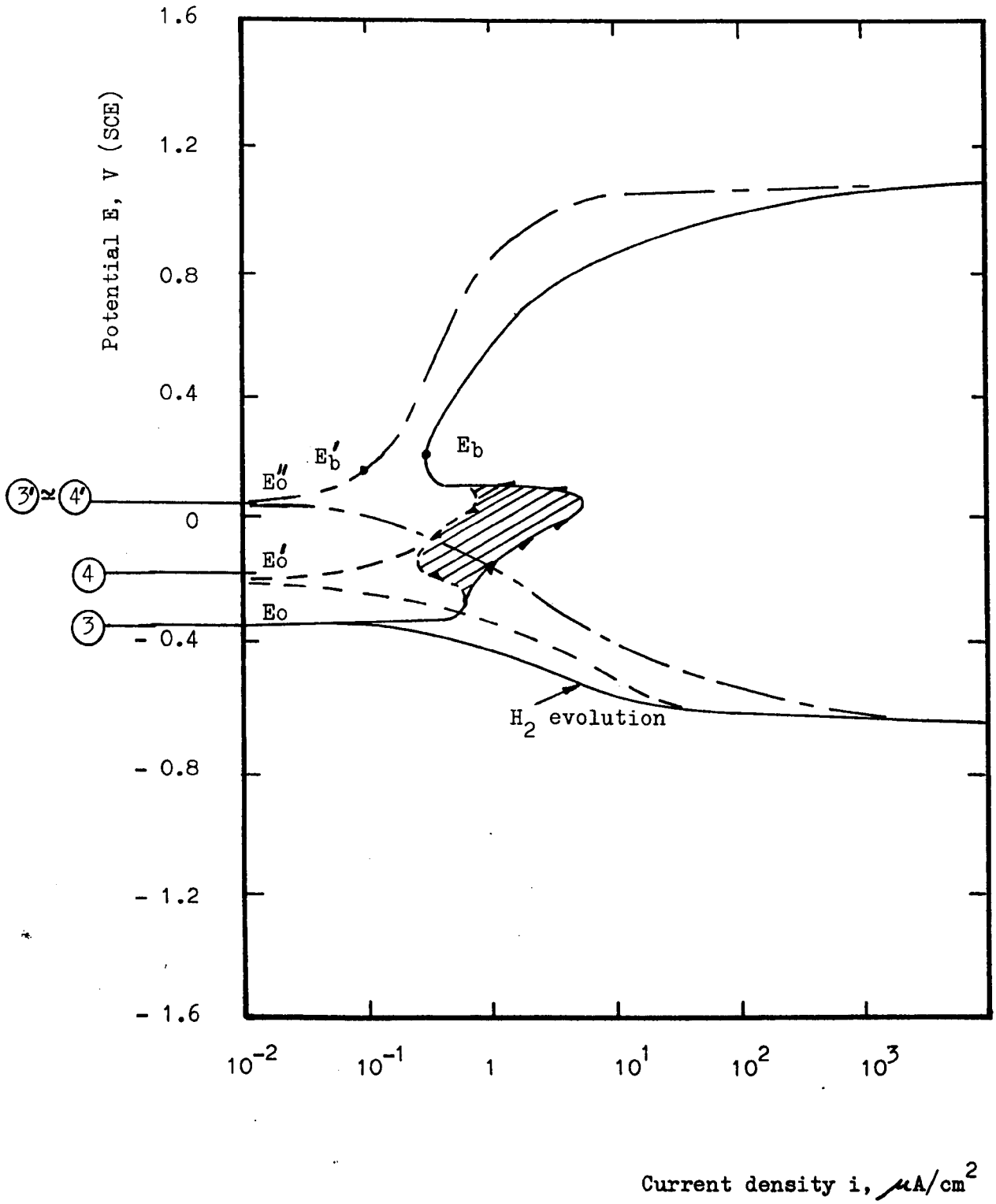

Figure 40 Anodic and cathodic polarization curves for S316 in saline pH 1.5

Key:-

——————— static conditions

— — — — — stirring conditions

——— — ——— — fatigue at ± 380 MN/m^2 and static tensile stress

shows direction of polarization differences in curves (shaded)

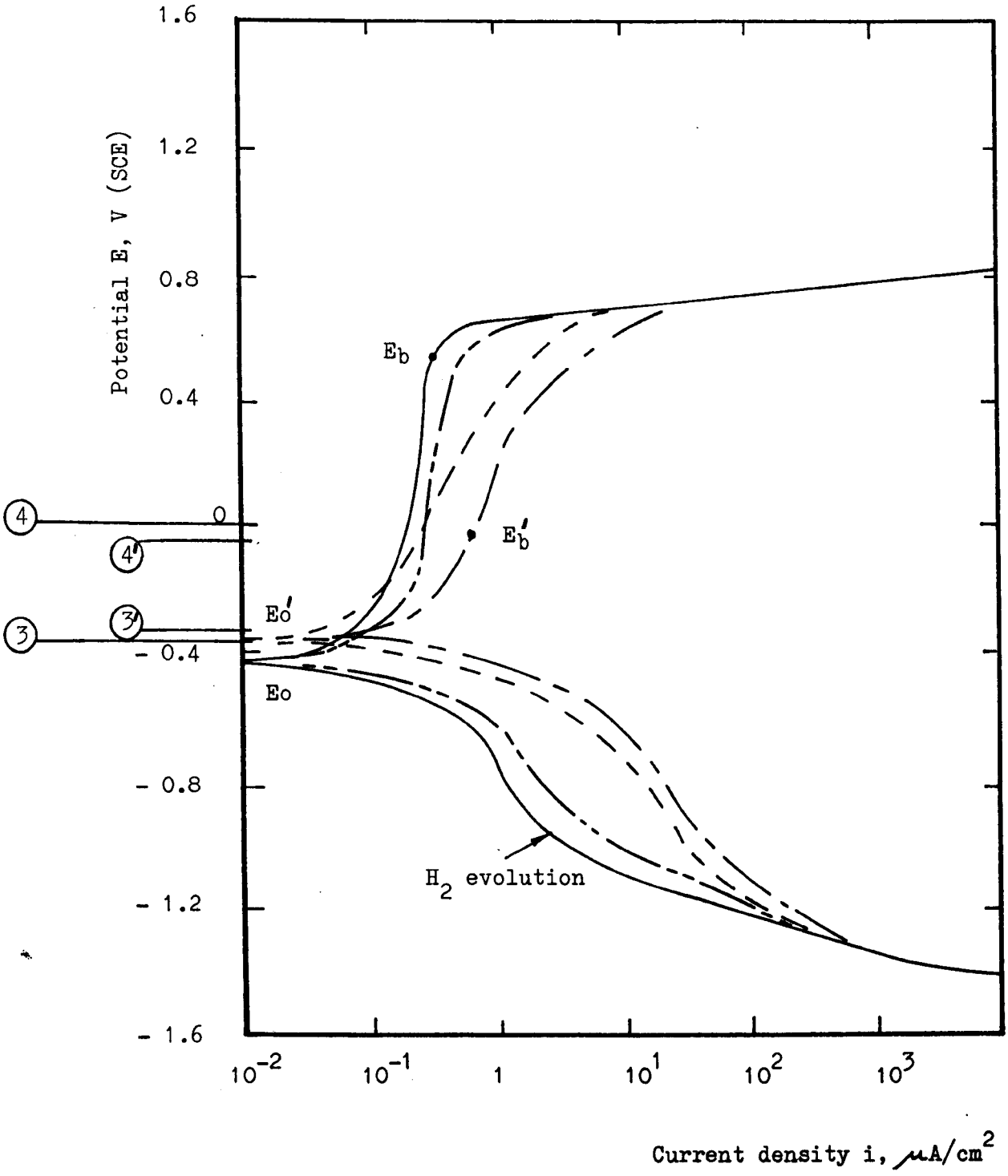

Figure 41 Anodic and cathodic polarization curves for S316 in saline pH 11.5

Key:-

——————— static conditions

— — — — — stirring conditions

— — — — — — — static conditions with tensile stress of 380 MN/m^2

— — — — — — fatigue at ± 380 MN/m^2

polarization.

The system for S316 in normal saline is shown in Fig.39. Comparison with Fig. 38 shows the relatively higher primary passive current density, at 0.56μA/cm^2, caused by the aggressive Cl^- anion: the value of E_o = - 0.35 V was also moved in the more base direction related to distilled water. "Red-rust" was clearly seen to form in this saline solution at about + 0.50 V under anodic polarization before saturation was reached at approximately + 0.60 V. Stirring only marginally changed the results for this system and, in line with this finding, static and dynamic stresses produced the same curves. Stress was more effective here in depolarizing the cathodic reactions than the anodic ones, although passivity was clearly reduced by stress.

Fig. 40 shows the polarization of S316 in saline of pH 1.5 which exhibited some instability and differences between the direction of polarization, shown shaded. The value of E_o = - 0.32 V for the reversible potential was moved to E'_o = - 0.20 V with stirring, and still further in the more noble direction to E''_o = + 0.04 V for the application of dynamic static stress. A passive current density of 0.35μA/cm^2 in the stress free, stirred or unstirred, system was reduced to about 0.16μA/cm^2 at 0.10 V with stress under anodic polarization. The corrosion-fatigue curve obtained here was, however, completely lacking the inflexion and reduction in current density which is typical of passive behaviour.

S316 in saline pH 11.5 was polarized as shown in Fig. 41. E_o = - 0.43 V for the unstirred, stress-free system, which also did not exhibit the inflexion normally associated with passive behaviour. Polarization at about 0.28 $\mu A/cm^2$ was however achieved over the anodic range - 0.10 V to + 0.55 V which was a much better passive film performance than that found in any other solution for S316. Stirring and dynamic stress, E'_o = - 0.37 V, both had depolarizing effects. It is clear that in this case the cathodic depolarizing effect of fatigue loading was approximately the sum of the static stress effect and the effect of stirring.

4.4.3. Polarization data for titanium 130

Polarization curves for titanium T130 are given in Figs. 42 to 45. The distilled water system is shown in Fig. 42, where E_o = + 0.45 V and anodic polarization achieves passive behaviour at about 3.99 $\mu A/cm^2$ between + 0.60 V and + 0.95 V. Stirring made little difference to this system but dynamic loading clearly depolarized the cathodic reactions yet static stress was hardly effective in this respect. The anodic polarization, however, was grossly affected by stress: the dynamic and static curves were initially coincidental. The current density was reduced at all potentials below that obtained by anodically polarizing without stress, 0.1 $\mu A/cm^2$ for example at + 0.80 V was increased to 3.99 $\mu A/cm^2$ when the application of stress was removed. Stress alone in this system was responsible for

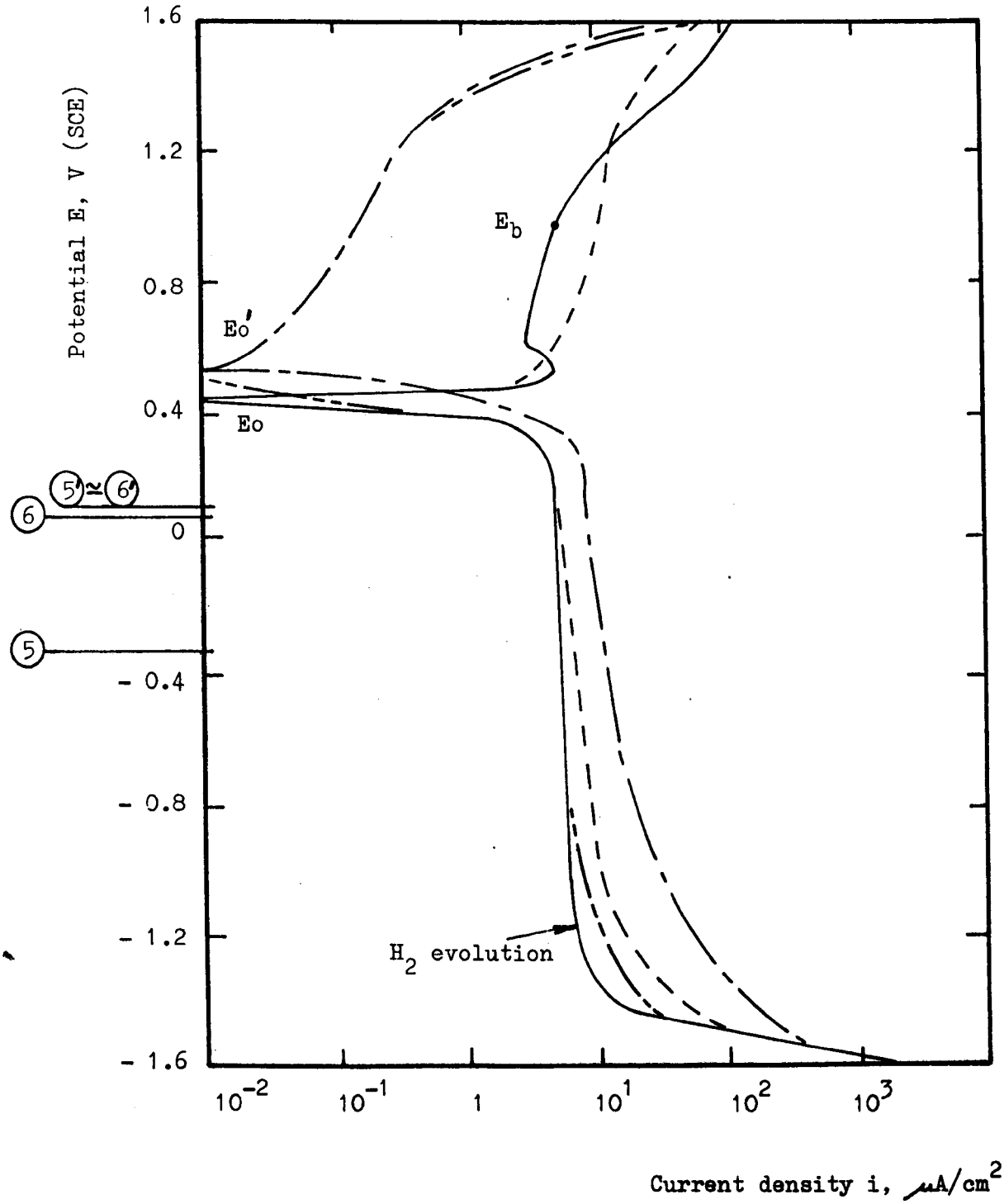

Figure 42 Anodic and cathodic polarization curves for T130 in distilled water pH 6.5

Key:-

——————— static conditions

— — — — — stirring conditions

——— — — ——— static conditions with tensile stress of 380 MN/m²

——— — ——— fatigue at ± 380 MN/m²

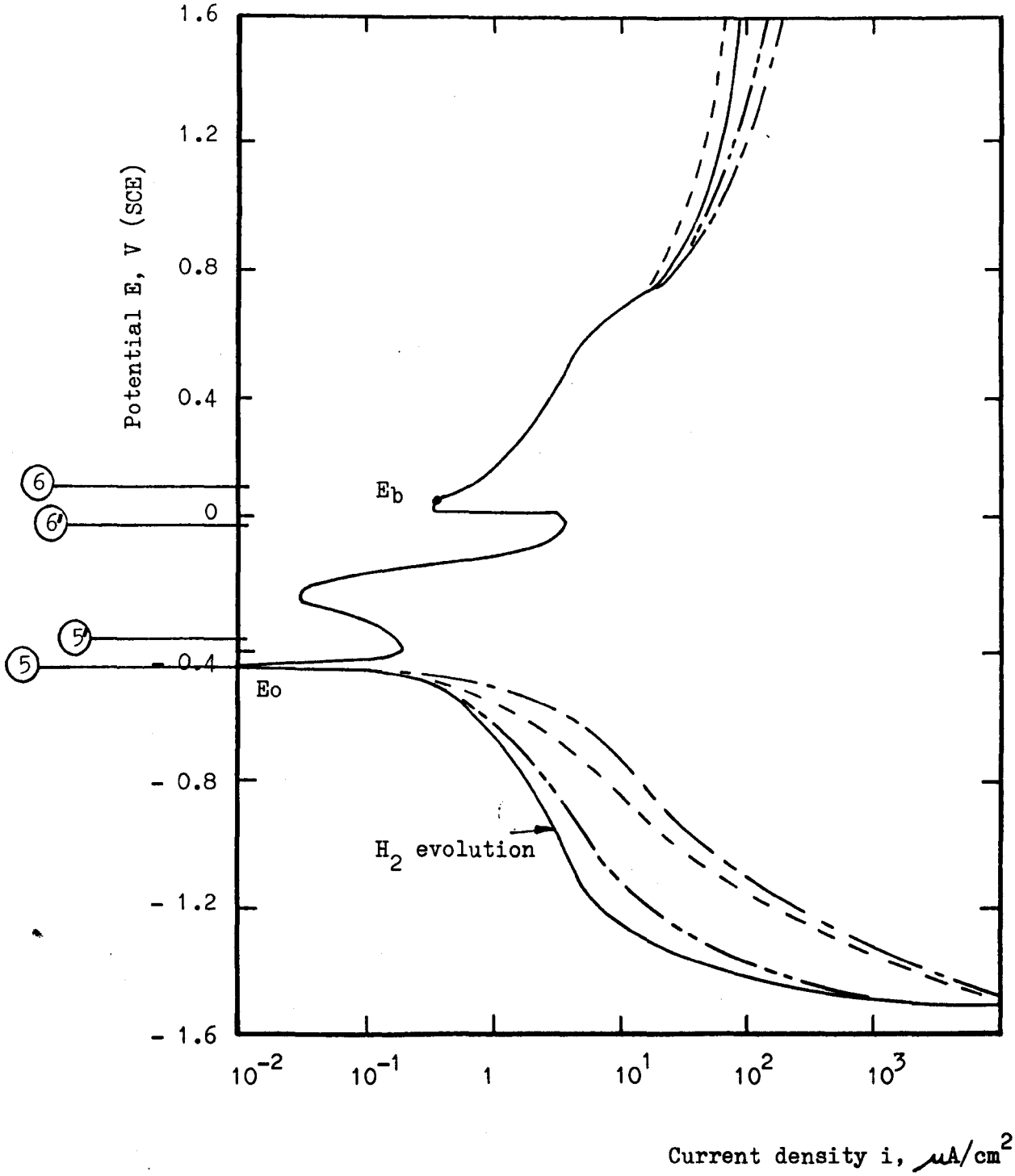

Figure 43 Anodic and cathodic polarization curves for T130 in saline pH 6.5

Key:-

——————— static conditions

— — — — — stirring conditions

——— — — ——— static conditions with tensile stress of 380 MN/m^2

——— — ——— fatigue at ± 380 MN/m^2

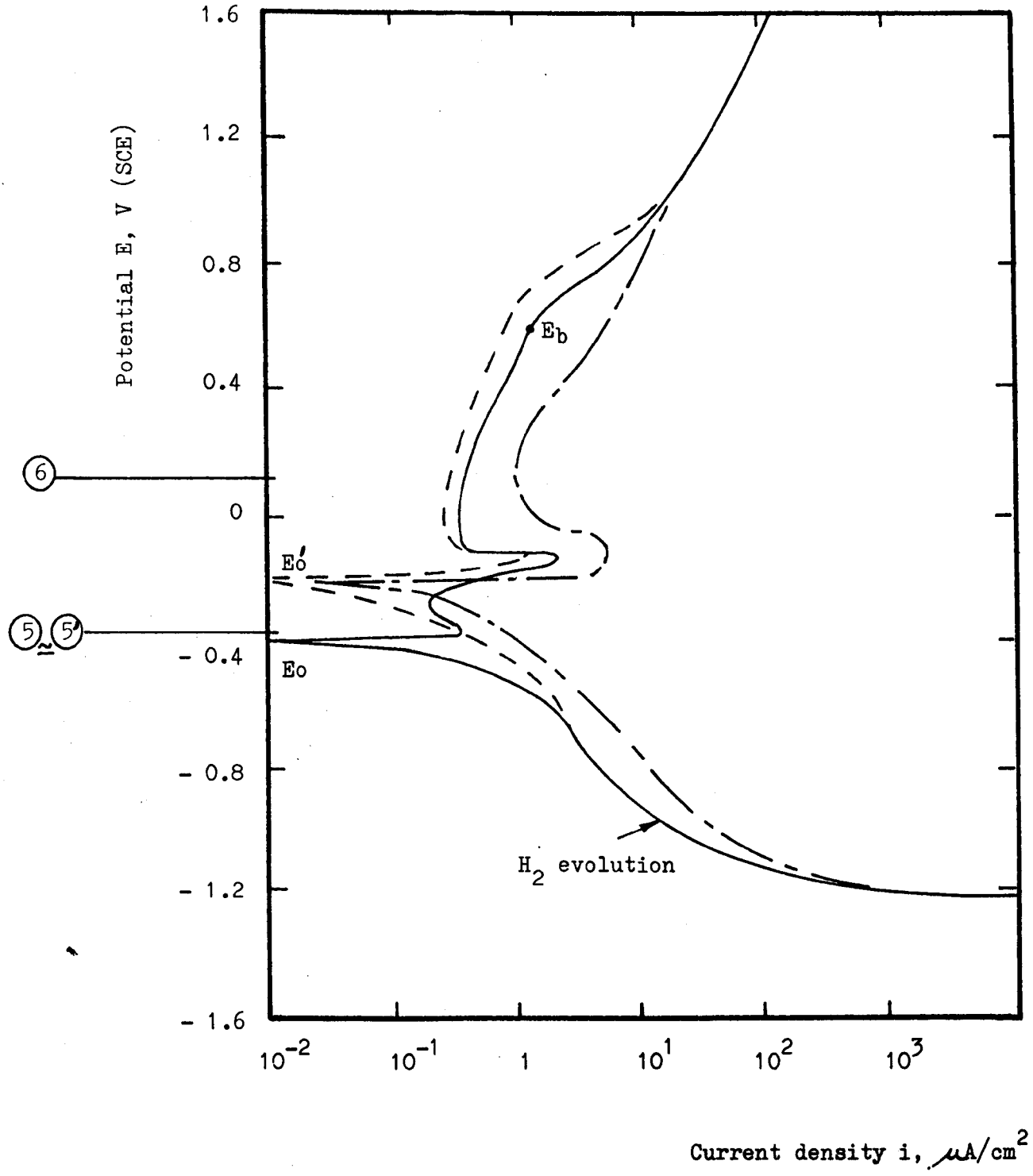

Figure 44 Anodic and cathodic polarization curves for T130 in saline pH 1.5

Key:-

——————— static conditions with and without tensile stress

— — — — stirring conditions

——— — ——— fatigue at ± 380 MN/m^2

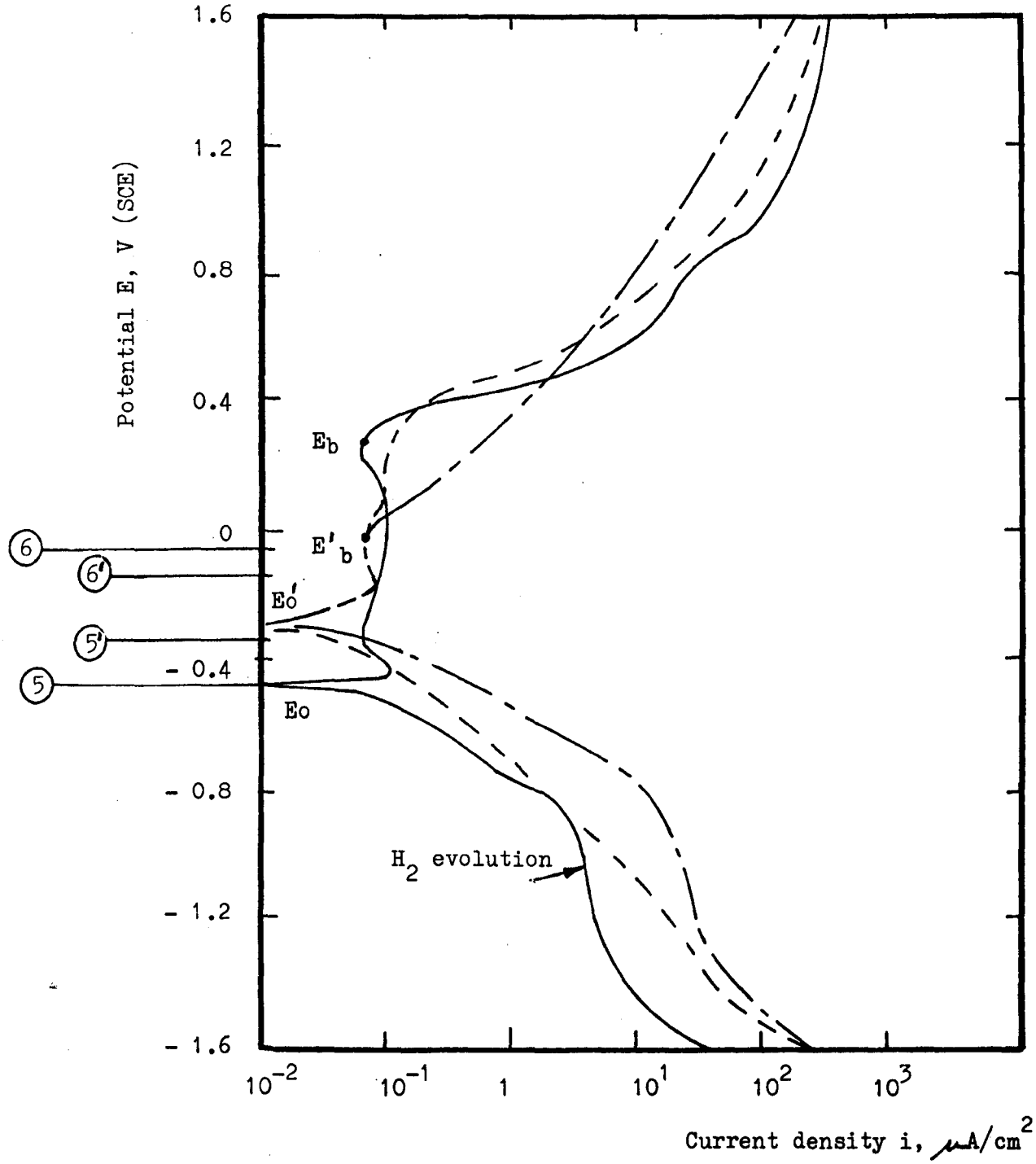

Figure 45 Anodic and cathodic polarization curves for T130 in saline pH 11.5

Key:-

——————— static conditions with and without tensile stress

— — — — — stirring conditions

——— - ——— - ——— - fatigue at ± 380 MN/m^2

raising the rest potential to E_o' = + 0.52 V.

Fig. 43 shows the T130 saline pH 6.5 system polarization curves having a common rest potential E_o = - 0.44 V. Two inflexions in the anodic polarization curve were found indicative of a change in the thickness and/or type of anodic film maintained: the first or primary passive film occurred at - 0.23 V, with as little as 0.028 $\mu A/cm^2$ current density, and the second at + 0.05 V, with more than twelve times the current density of the first inflexion. Virtually no effect of stirring or stress was found during anodic polarization although during cathodic polarization both these factors were seen to be depolarizing in effect.

The T130 - saline pH 1.5 system, shown in Fig. 44, produced a rest potential E_o = - 0.40 V. A primary passive potential of - 0.3 V, with 0.18 $\mu A/cm^2$, was followed by a secondary passive potential at - 0.10 V with 0.32 $\mu A/cm^2$. The application of stirring resulted in a more noble rest potential E_o' = - 0.20 V and the further application of a dynamic load both anodically and cathodically depolarized the system. Static stress application had no effect on the polarization results.

Fig. 45 shows the much simpler passivation behaviour of T130 in saline pH 11.5. A rest potential of E_o = - 0.48 V, followed by a passive potential range from - 0.35 V to + 0.30 V over which the current density was below 0.10 $\mu A/cm^2$, occurred during anodic polarization. Stirring was effective in raising the rest potential to E_o' = - 0.30 V. Dynamic stress was responsible

for reducing the passive range so that Eb became less noble at Eb'. Some cathodic depolarization was also found with dynamic stress.

4.4.4. Polarization data for titanium 318

The polarization curves for T318 are given in Figs. 46 to 49. The distilled water system, Fig. 46, had a rest potential E_o = + 0.4 V. Anodic polarization resulted in an initially high 'active' current density of 25 $\mu A/cm^2$ followed by a primary passive potential at + 0.60 V and 0.70 $\mu A/cm^2$ current density. Stirring and stress application had very little effect. However dynamic loading did help to establish passivity sooner and for a larger range of potentials.

Fig. 47 shows that the rest potential is reduced by the Cl^- ion (compare with Fig. 46) to E_o = - 0.41 V. A local high current density of 3.2 $\mu A/cm^2$ at zero potential, followed by one of 0.13 $\mu A/cm^2$ at the primary passive potential of + 0.06 V, was found for this system. Stirring had little effect, causing the rest potential to rise to E_o' = - 0.33 V. Stress had no effect whatsoever. "Red-oxide" was visible on the surface of the T318 above 1.0 V corresponding to current densities $\geq$100 $\mu A/cm^2$. This was completely absent from the tests in distilled water, or from saline tests with T130, and appears to be a feature of this titanium alloy and saline, when the current density exceeds 100 $\mu A/cm^2$.

The T318 - saline pH 1.5 system, shown in Fig. 48, did not

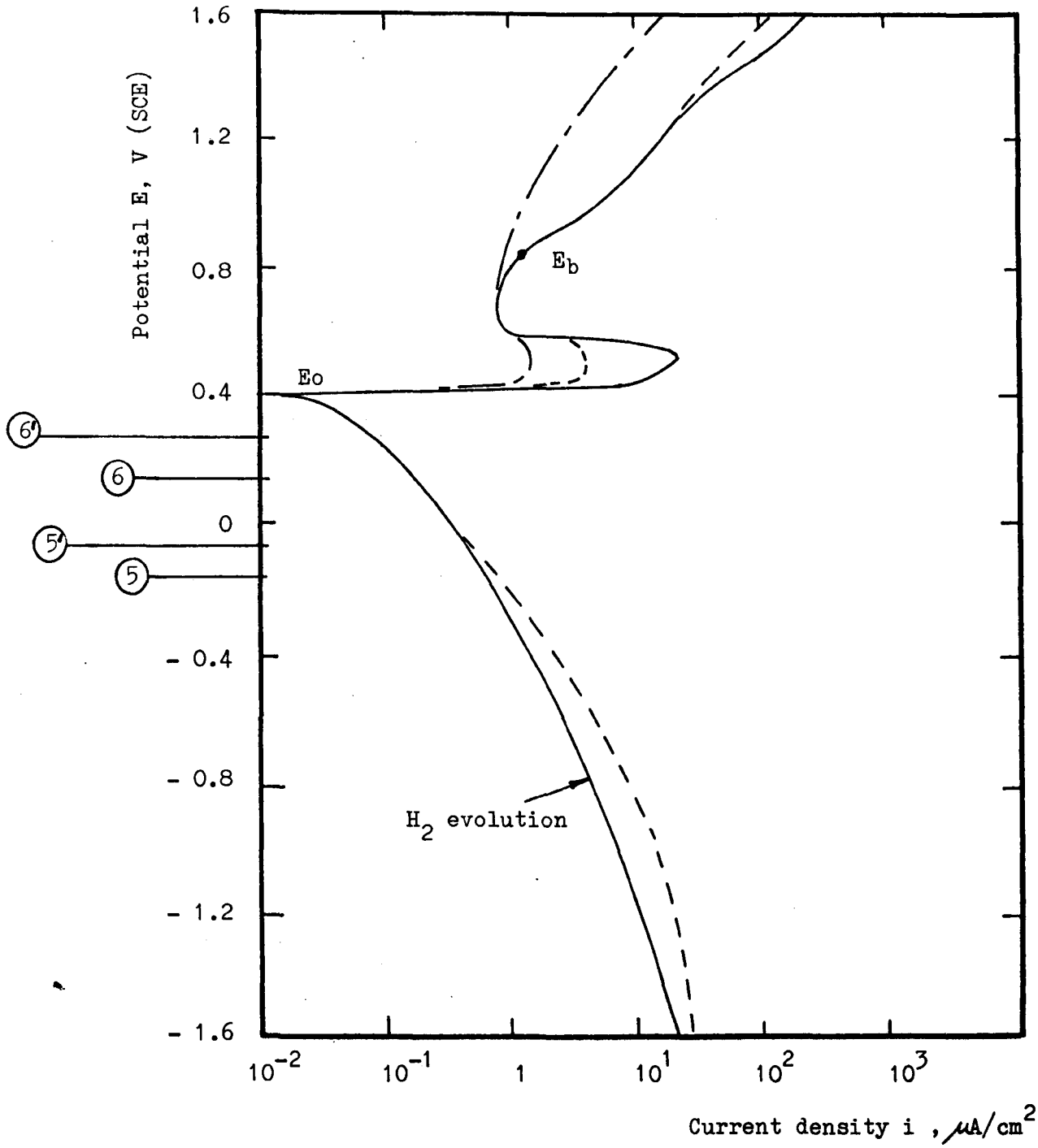

Figure 46 Anodic and cathodic polarization curves for T318 in distilled water pH 6.5

Key:-

——————— static conditions with and without tensile stress

— — — — — stirring conditions

——— - ——— - ——— fatigue at ± 380 MN/m^2

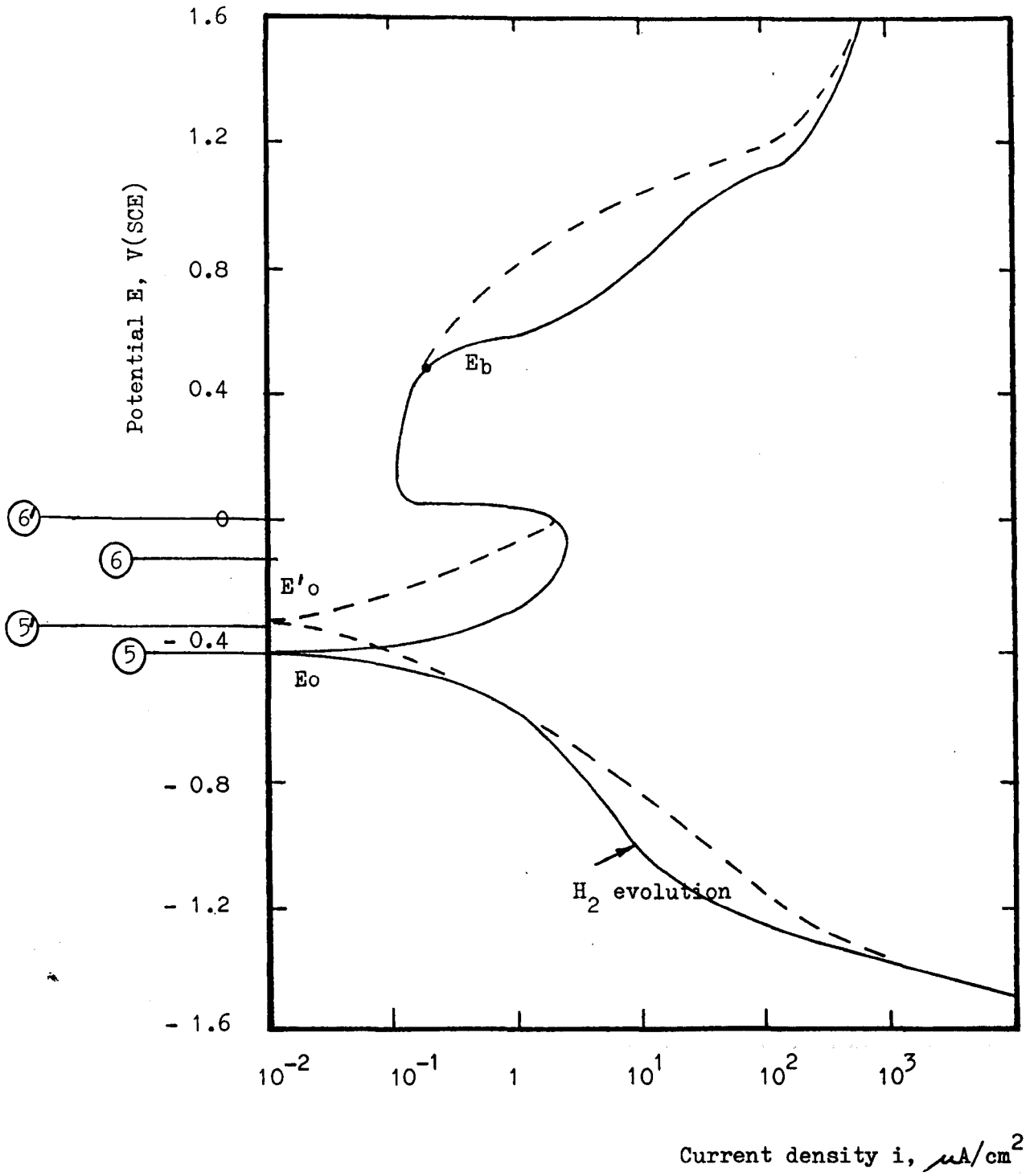

Figure 47 Anodic and cathodic polarization curves for T318 in saline pH 6.5

Key:-

——————— static conditions with and without tensile stress

— — — — — stirring conditions with and without fatigue

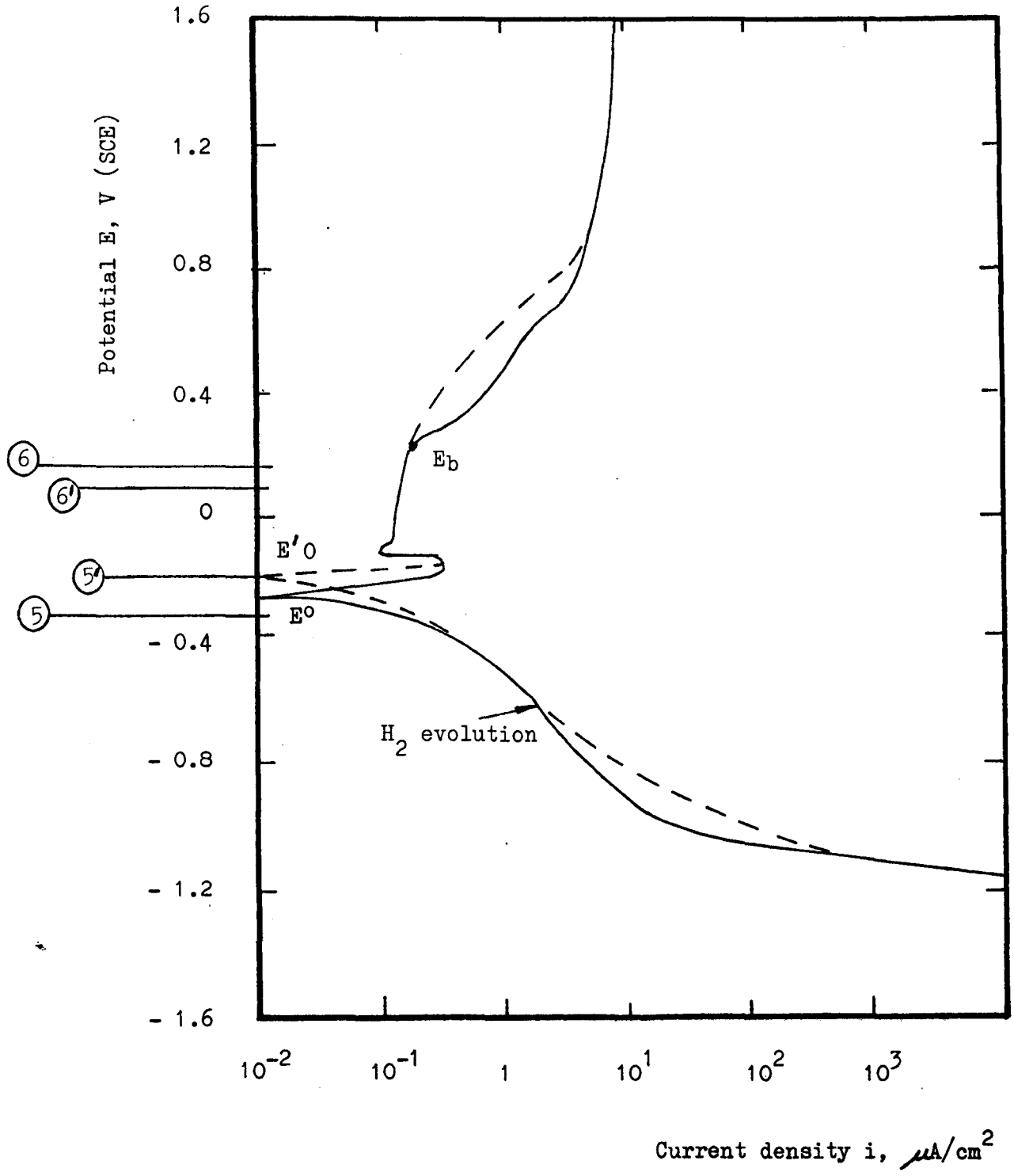

Figure 48 Anodic and cathodic polarization curves for T318 in saline pH 1.5

Key:-

———— static conditions with and without tensile stress

— — — — stirring conditions with and without fatigue

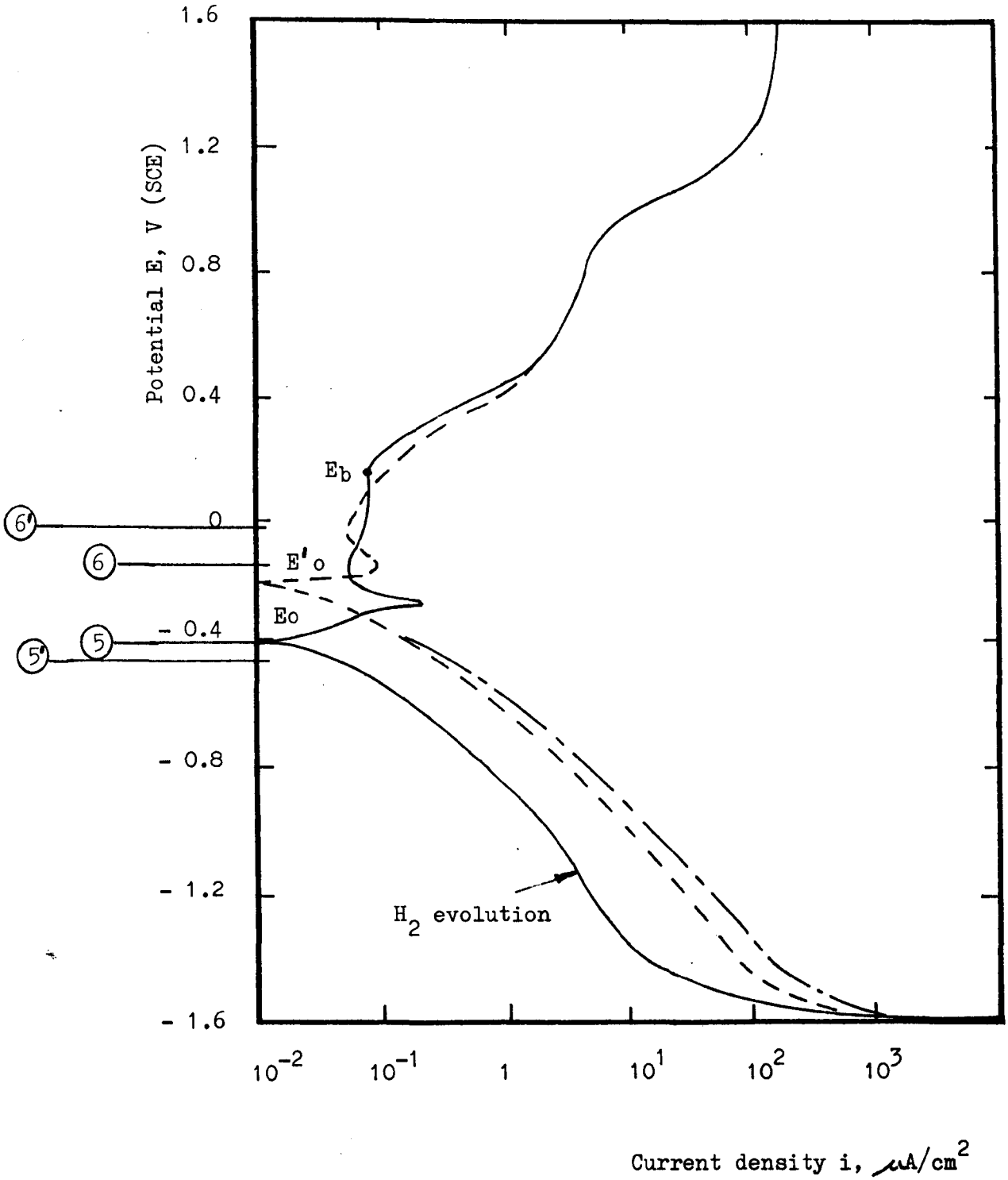

Figure 49 Anodic and cathodic polarization curves for T318 in saline pH 11.5

Key:-

——————— static conditions with and without tensile stress

— — — — — stirring conditions

— — — — — — fatigue at + 380 MN/m^2 where different from the stirring curve

show the 'red-oxide' formation at high anodic polarization potentials, but then it did not exceed the seemingly required current density over the range tested. E_o = - 0.26 V, and an initial current density of 0.45 $\mu A/cm^2$ was reduced to 0.10 $\mu A/cm^2$ at the establishment of the primary passivation potential of - 0.15 V. Stirring, again for T318 had little effect increasing slightly the rest potential to E'_o = - 0.20 V. Stress had no influence on these results.

Fig . 49 shows the polarization curves for T318 in saline pH 11.5. 'Red-oxide' was again found for this system as soon as the current density exceeded 100 $\mu A/cm^2$. Another feature in common with saline pH 6.5 was the rest potential which, at E_o = - 0.41 V, was identical. Anodic polarization past the critical value of 0.20 $\mu A/cm^2$ down to 0.05 $\mu A/cm^2$ at a primary passive potential of - 0.20 V was achieved with this system. Stirring was responsible for some cathodic depolarization and a change in the rest potential to E'_o = - 0.20V with a corresponding easier establishment of passive conditions. Again for T318 in saline, no effect was found of stress other than that of stirring action when anodically polarized. Cathodic polarization below-1.0 V with dynamic stress did, however, produce prolific 'clouds' of H_2 on the specimen surface, far in excess of that produced in the absence of stress or for any other solution tested.

4.5. Open-Circuit Potential-Time Data for Unstressed Specimens

Figs 50 to 53 show the results obtained from a recording of the open circuit potential of each material/environment combination over a period of time. As discussed in Section 2.6.4. page 69, (Fig. R13), this is a convenient way of assessing the performance of materials as poorly resistant, moderately resistant and completely resistant to a particular solution.

Fig. 50 shows the various materials changing their rest potentials with time when immersed in distilled water. Mild steel was clearly shown to be poorly resistant with a "type c" (Fig. R13) performance curve indicative of the general corrosion observed. T130 and T318 both exhibited a "type a" curve, where the surface oxide film was grown to a limiting thickness and remained intact. S316 however, was found to have a classical "type b" performance curve. Initial formation of the oxide film during the first 6 minutes of immersion in distilled water was followed by film breakdown with a fall in potential. A succession of periods of film growth and breakdown then followed with increasing amplitude of potential change for the first two weeks. Thereafter the growth/breakdown process settled down to a more limited oscillation between -5mV and -90mV.

The change in potential with time for the materials immersed in saline pH 6.5 is shown in Fig.51. Mild steel reached a more negative potential, with general corrosion, much faster than was the case in distilled water. T130 did not form

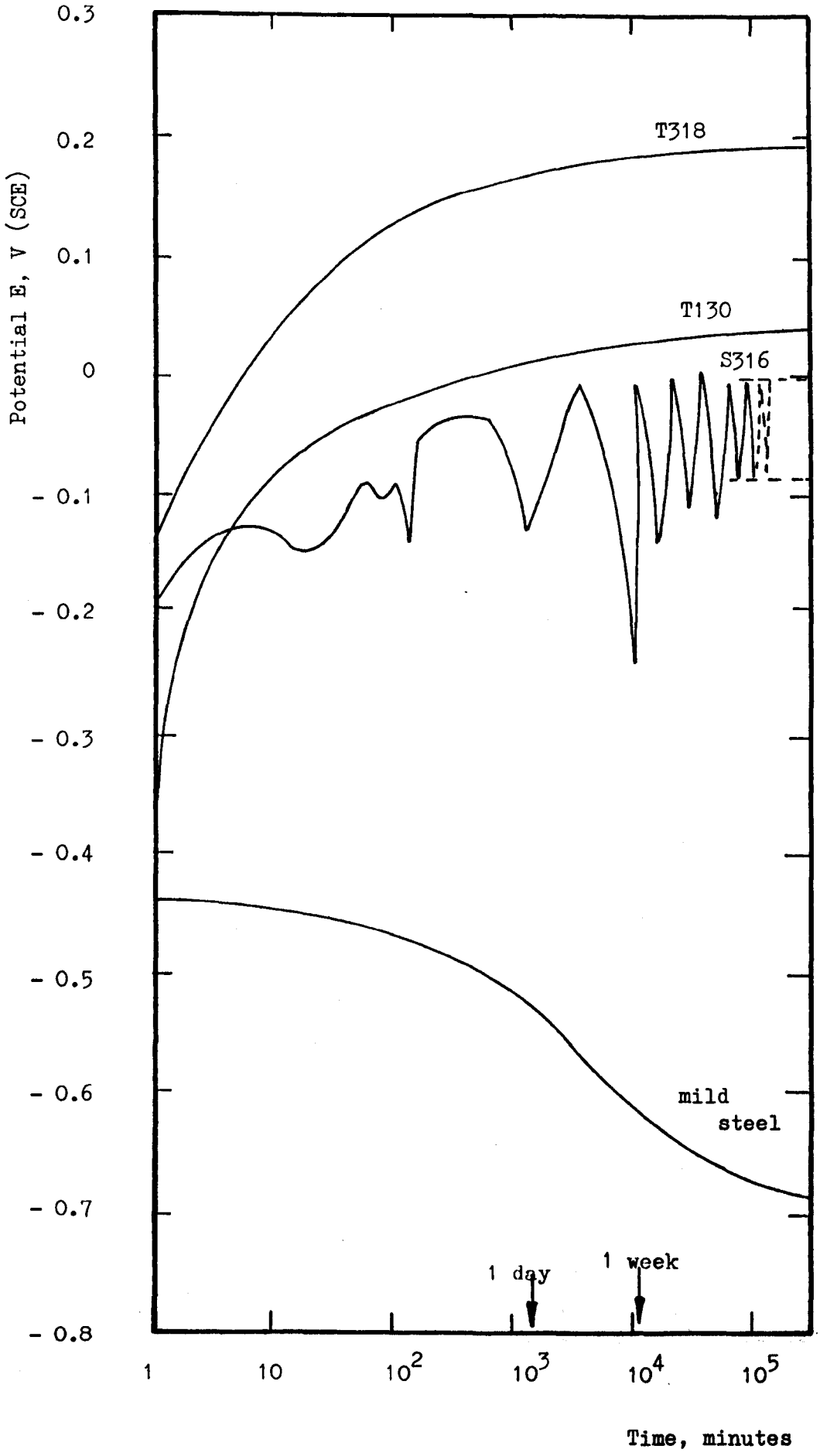

Figure 50 Potential - time curves in distilled water

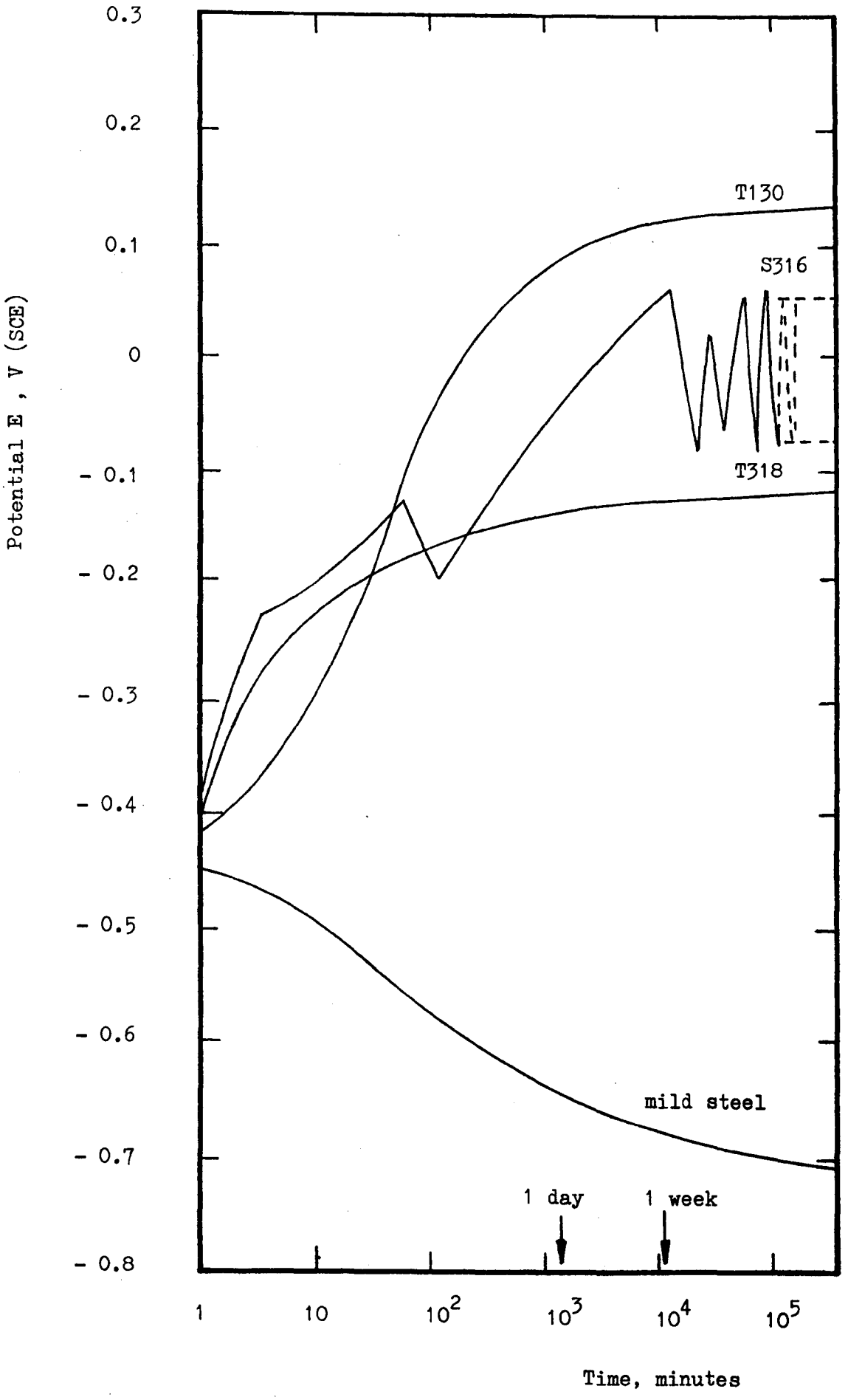

Figure 51 Potential - time curves in saline pH 6.5

its protective oxide film so quickly in saline yet after about 20 hours the rest potential attained was more noble than that produced with distilled water. T318, on the other hand, remained consistently at more basic potentials in saline than in distilled water. The behaviour of S316 in saline was similar to that observed in distilled water, but the final range of potential observed was between +50mV and -75mV: that is, a larger range of potential oscillation in saline pH 6.5 than in distilled water, surprisingly representing longer periods of film growth in saline before breakdown. A particularly long period of growth in saline is clearly shown for S316 in Fig. 51 between 2 hours and 1 week. The same period of time in distilled water contained four inflexions of growth and breakdown.

Fig. 52 shows the saline pH 1.5/material rest potential variation with time. Mild steel surprisingly here showed an initial move to a more noble potential before taking-up its final more negative potential. General corrosion was observed, however, from the start. T130 and T318 both showed good film growth characteristics. T130 had a final potential in saline pH 1.5 which was more noble than that with distilled water or at normal saline. T318 had a similar potential/time characteristic to that obtained in distilled water and much improved over that found in normal saline. S316 with saline pH 1.5, as shown in Fig. 52, remained at much

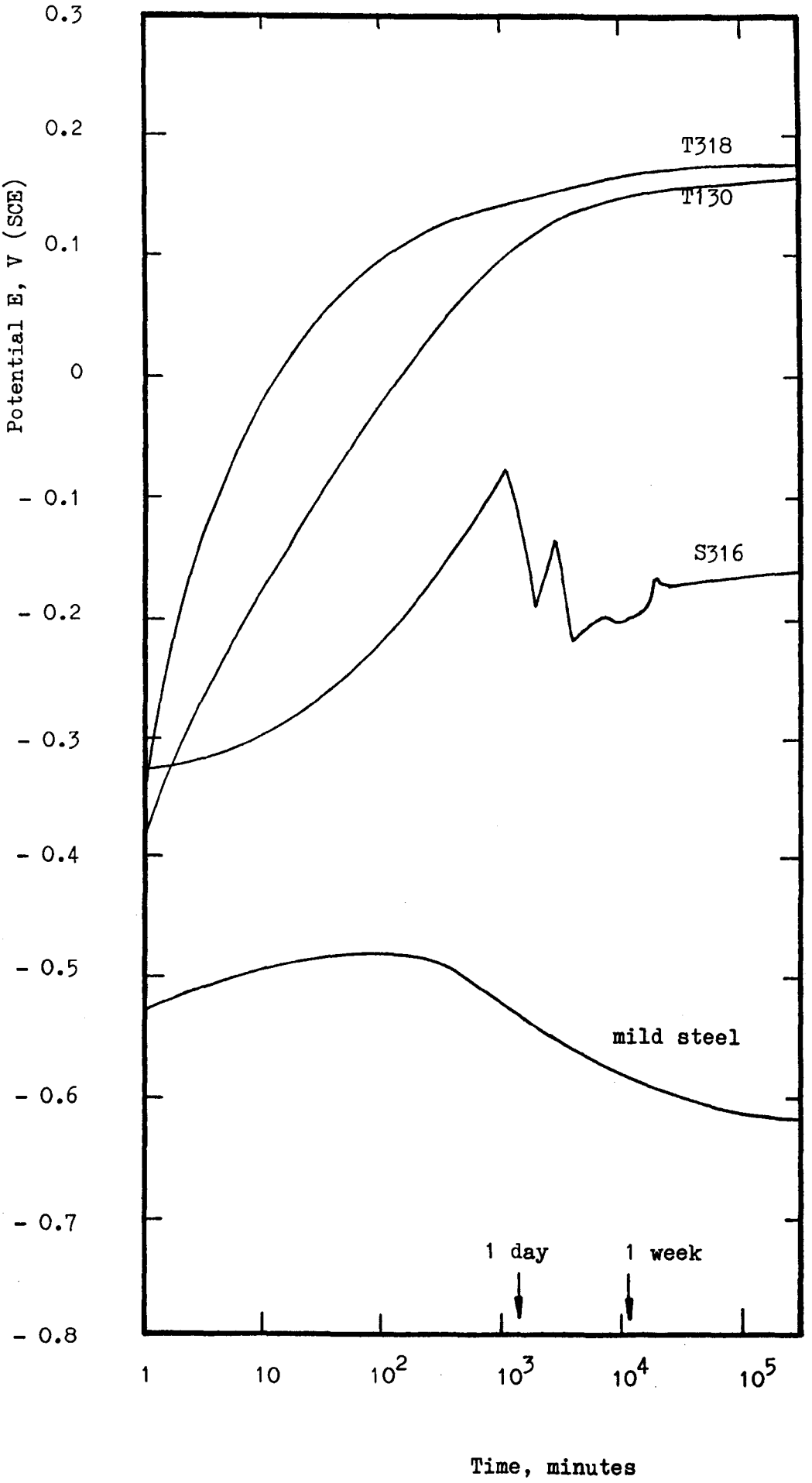

Figure 52 Potential - time curves in saline pH 1.5

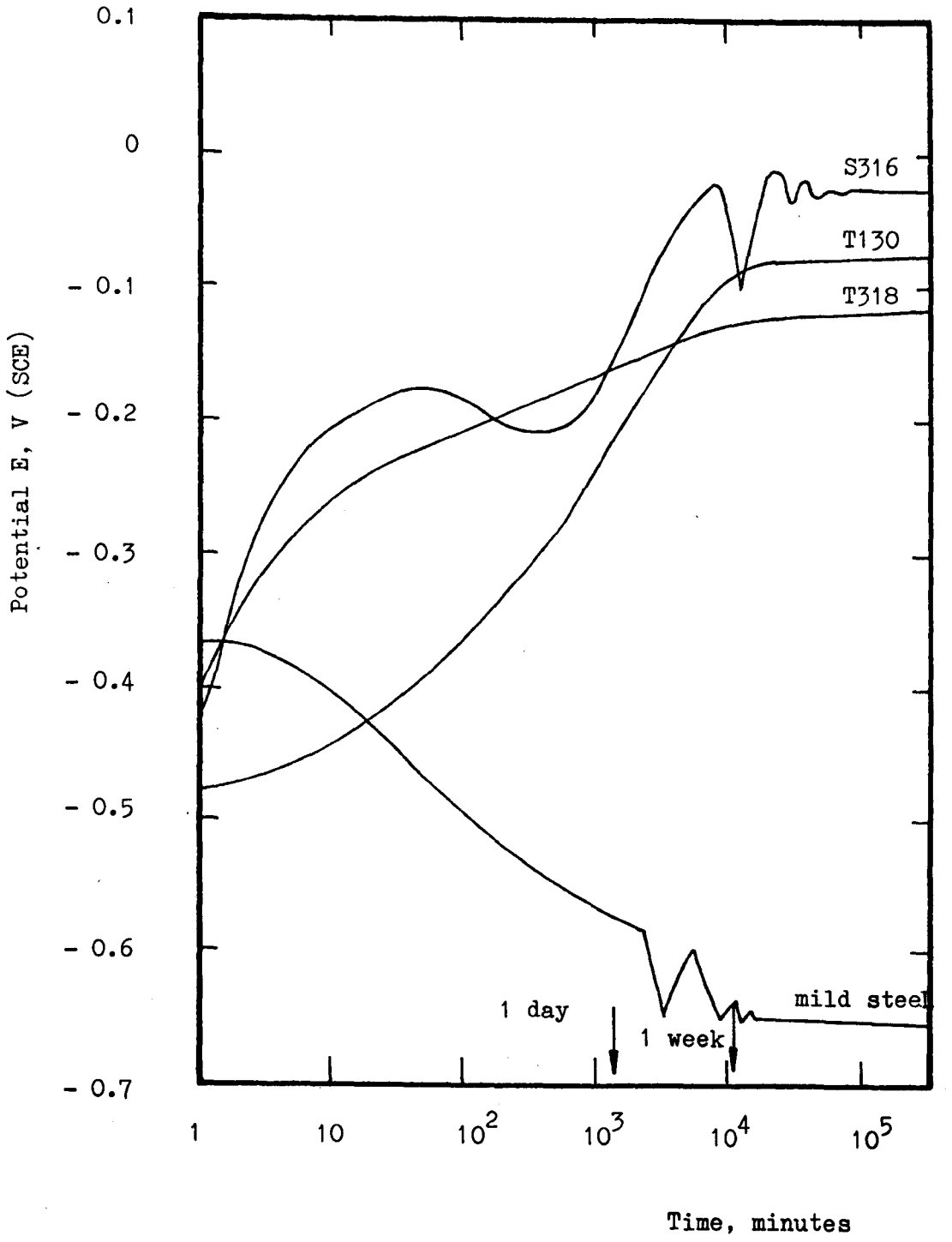

Figure 53 Potential - time curves in saline pH 11.5

less noble potentials than those generally found in distilled water and normal saline solutions. However, the most striking difference in behaviour here was the slow, exponential type growth as well as the final settling of potential, without oscillation, to approximately -170mV. General corrosion was clearly visisble after 5 days coinciding with a levelling-off in the potential curve.

Potential-time curves in saline pH 11.5 are shown for each material in Fig. 53. Mild steel again showed a general move to less noble potentials with time. However, some more sudden falls in potential, followed by sudden rises, were observed. Since this pH is on the border of that predicted by Pourbaix (Fig. R15, page 73, Section 2.6.5.) for passivation by $Fe(OH)_3$ and $Fe(OH)_2$ it is possible that the steps here represented a change in the type of film formed. General corrosion was observed after about two weeks of this weakly-passive behaviour. T130 in this solution was far less noble than in any other solution but nevertheless exhibited good resistance after an exponential potential rise and sudden levelling-off after about 1 week. T318 in this solution was almost identical with the performance in normal saline, both performances being less noble than those in distilled water or in saline pH 1.5. S316 was again interesting in pH 11.5. It was noticeable that the film growth/breakdown inflexions were much less sudden in this solution, being more like the

result in distilled water than the resultant sharp peaks obtained for saline pH 1.5 and 6.5 solutions. The final settling-down value for potential at -25mV for S316 here was the average of the range exhibited in distilled water. The behaviour of S316 in saline pH 11.5 was more strongly-passive than for the other solutions.

For purposes of comparison, and as a basis for later discussion regarding the effect of stress, these stress-free rest potential ranges observed with time were superimposed on the relevant potential - pH equilibrium diagrams reviewed in Section 2.6.5. Fig. R15 (page 73) and in Section 2.8.2. Figs R32 to R34 (pages 145-146). On Fig. R15, 1→2 represents that change in potential with time, from potential "1" to potential "2", for mild steel in each saline solution. 3→4 represents the S316 result which was also shown on Figs R32 to R33; fluctuations in potential are indicated by a wavy-line. 5→6 represents the maximum range recorded for T130 and/or T318. Distilled water results are included in the pH 6.5 range for saline: the maximum range observed was indicated on each diagram. The same relevant potential ranges were also superimposed on Figs. 34 to 49 for later discussion.

4.6. Corrosion Fatigue Potential-Cycles Data

Figs 54 to 57 show the results obtained from a recording of the open circuit potential of each material/environment

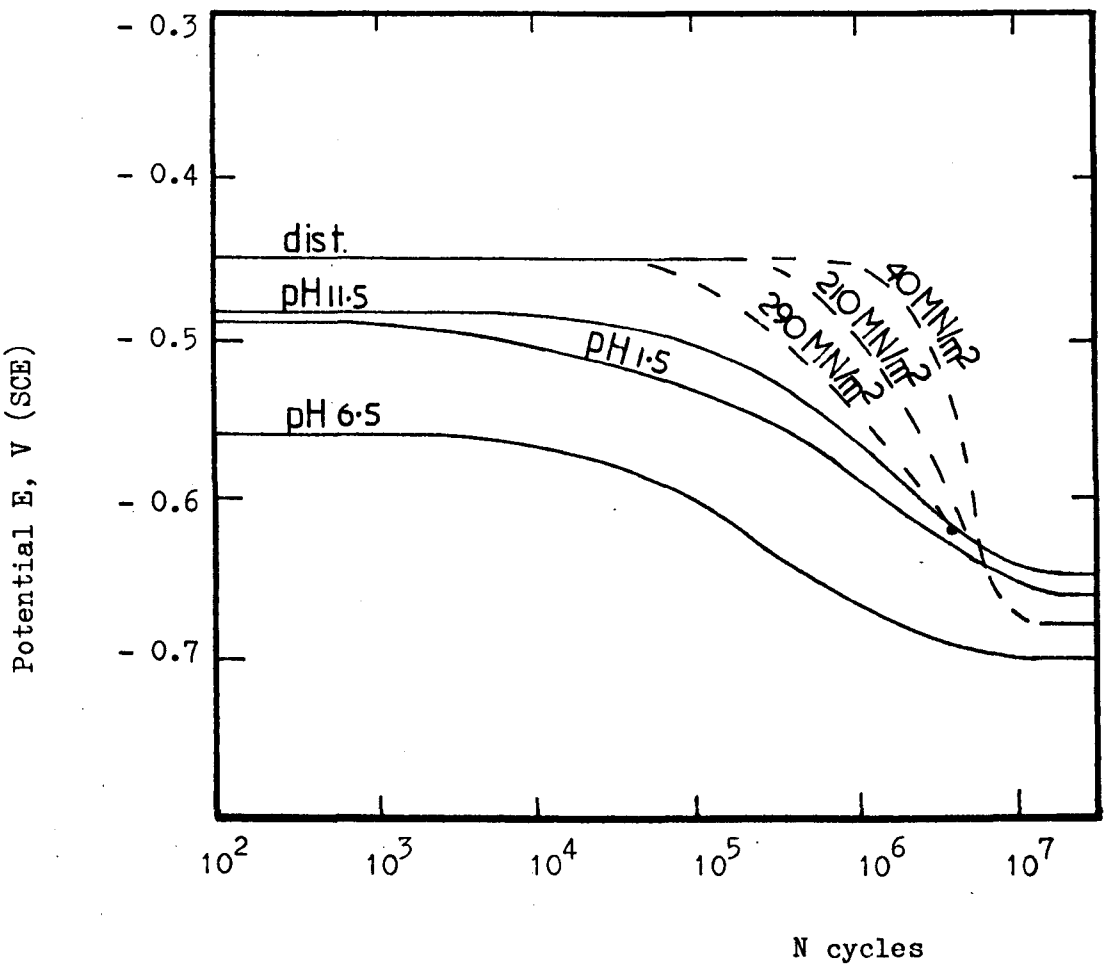

Figure 54 Corrosion fatigue potential - cycles trace for mild steel, in various electrolytes, followed at all stress amplitudes until fracture except for the indicated variation with stress for distilled water.

combination with cycling under fatigue loading at 1.7 Hz (1.028×10^6 cycles = 1 week).

The corrosion fatigue potential-cycle trace for mild steel is shown in Fig. 54. The trace obtained in distilled water was sensitive to stress amplitude, as indicated by the three dashed-line curves shown. Higher stress amplitudes resulted in the earlier fall in potential. The starting potential was not affected by stress amplitude. The final potential attained was similarly uninfluenced by stress amplitude except where fracture occurred before 10^7 cycles. Potential-cycle results for mild steel in the saline solutions were completely uninfluenced by the stress amplitude.

Hydrogen, evolved during the corrosion fatigue of mild steel resulted in bubbles of a black sooty deposit of carbon being distributed all around the specimens in saline pH 1.5. Corrosion in pH 11.5 however, was visible only at the areas of local stress concentration throughout the fatigue. Black magnetite whiskers on top of Fe_2O_3 were adherent to those areas where cracks initiated. Fatigue in saline pH 6.5 resulted in normal rusting all over the steel but originating initially in the most highly stressed regions.

Fig. 55 presents a typical result for S316. Since this material produced potentials in each solution which were sensitive to stress amplitude, for clarity, two magnitudes of stress amplitude are shown here only. The curves at 350 MN/m^2 to

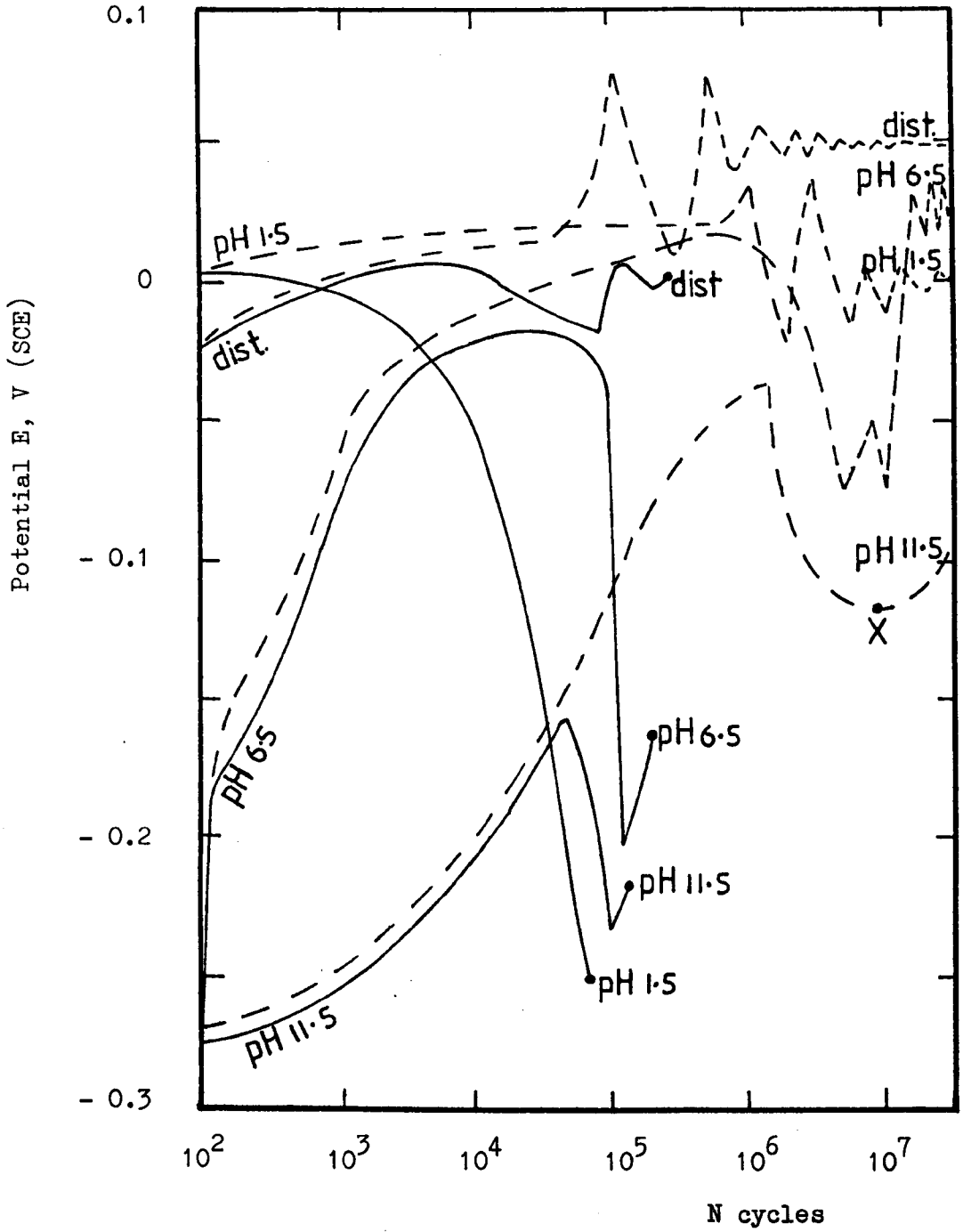

Figure 55 Corrosion fatigue potential - cycles traces for S316, in various electrolytes at approximately 350 MN/m^2 stress amplitude to fracture ——●
Fatigue limit traces also shown — — — — —
for comparison

fracture are compared with the curves produced at the fatigue limit, shown by dashed-lines, for each solution. That is, a plot which resulted in fracture is compared with a successfully corrosion fatigue resistant result. The difference between any two different stress amplitudes tested in this work was generally shown by a similar difference in potential-cycle trace obtained. Generally at fracture the final potential was less noble than that at the fatigue limit: this was particularly noticeable in saline solutions. However, in the case of saline pH 6.5 almost any potential plot could be obtained with different specimens within the range -390MV (not shown here) and +50mV. The result shown in Fig. 55 at the fatigue limit for saline pH 6.5 is one where the potential fluctuated in the more noble range towards +50mV. Oxide film breakdown, as indicated by a fall in potential, was followed in each case except for saline pH 1.5 by a short period of potential rise before fracture. The shape of the saline pH 1.5 curve was quite unlike the other passive-behaviour results, and was consistent with the general corrosion observed in this solution. A weakly passive behaviour was exhibited in pH 1.5 at the fatigue limit of only 35 MN/m^2 ($^1/_{10}$th the stress amplitude of the other result shown.) Considerable fluctuations in potential were recorded generally for S316 at the fatigue limit stress amplitudes. It seems, however, that the potential for these tests never fell to that minimum potential from which film repair was not possible.

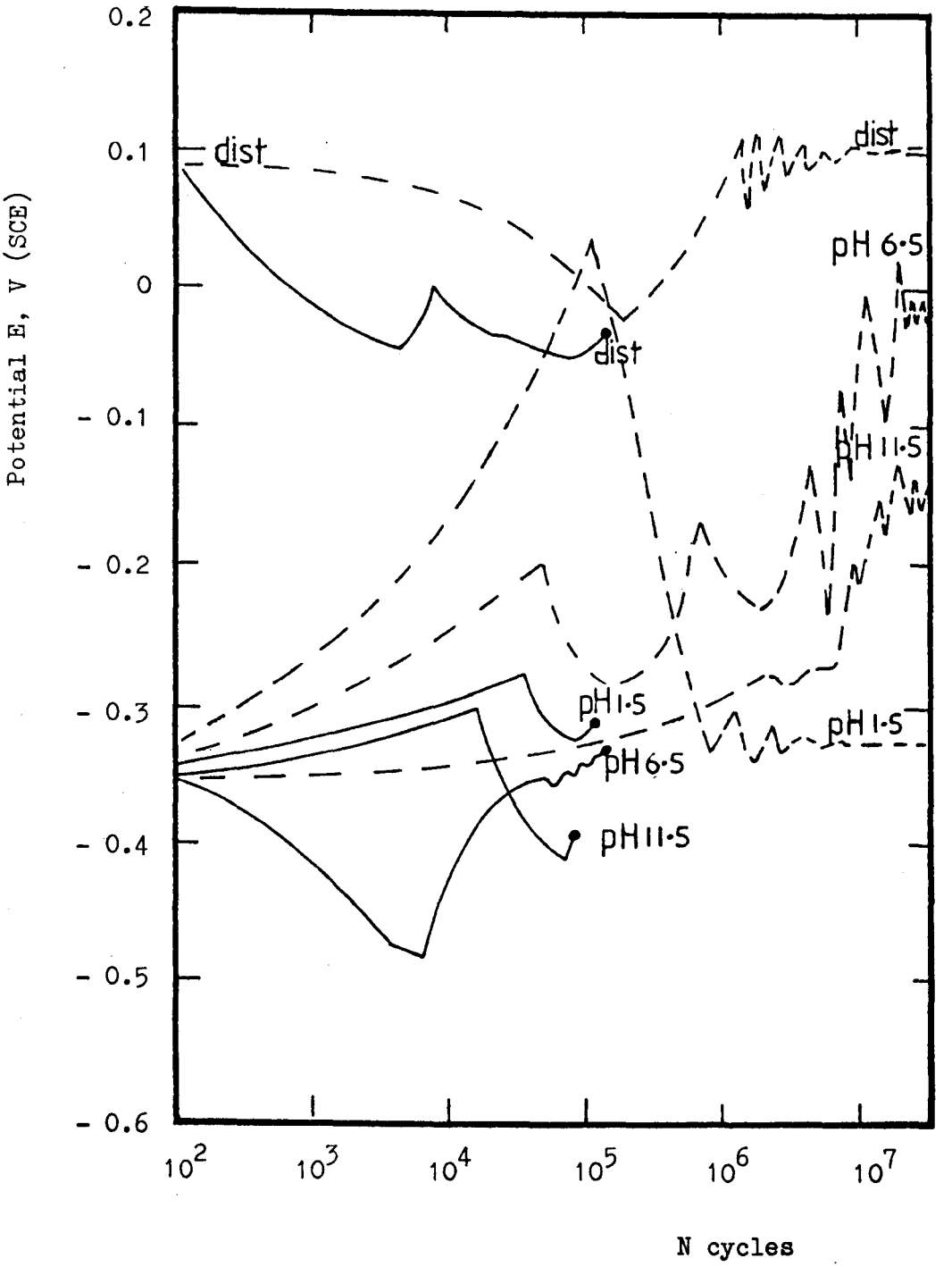

Figure 56 Corrosion fatigue potential - cycles traces for T130, in various electrolytes at approximately 360 MN/m^2 stress amplitude to fracture ——●
Fatigue limit traces also shown — — — — for comparison

Some idea of the magnitude of this minimum potential in each solution should be given by the lower limit of oscillation of the dashed-line fatigue limit curves, e.g. the potential corresponding to X for pH 11.5 curve in Fig. 55. The failed specimens had seemingly reached a less noble potential from which they could not recover. Initiation of cracks was observed in each case during the final upturn in potential and attempt at film repair.

Fig. 56 shows the corrosion fatigue potential-cycles trace for T130 in each solution tested at a stress amplitude of 360 MN/m^2, and also at individual solution fatigue limit stress amplitudes. With the exception of saline pH 1.5, the failed specimens all had potentials which were finally less noble than those reached at the fatigue limit. These results are similar to those obtained for stainless steel. The pH 1.5 saline final potential was always approximately the same, however, irrespective of stress amplitude. The difference in this solution between failed and fatigue limit specimens was characterised by the very large early rise and fall in potential obtained on surviving specimens: this peak was reduced with increasing stress amplitude.

The potential-cycles trace for T318 during fatigue in each solution tested is shown in Fig. 57. Similar potential changes to values far less noble at failure than at the fatigue limit were found here to those observed for S316 and T130.

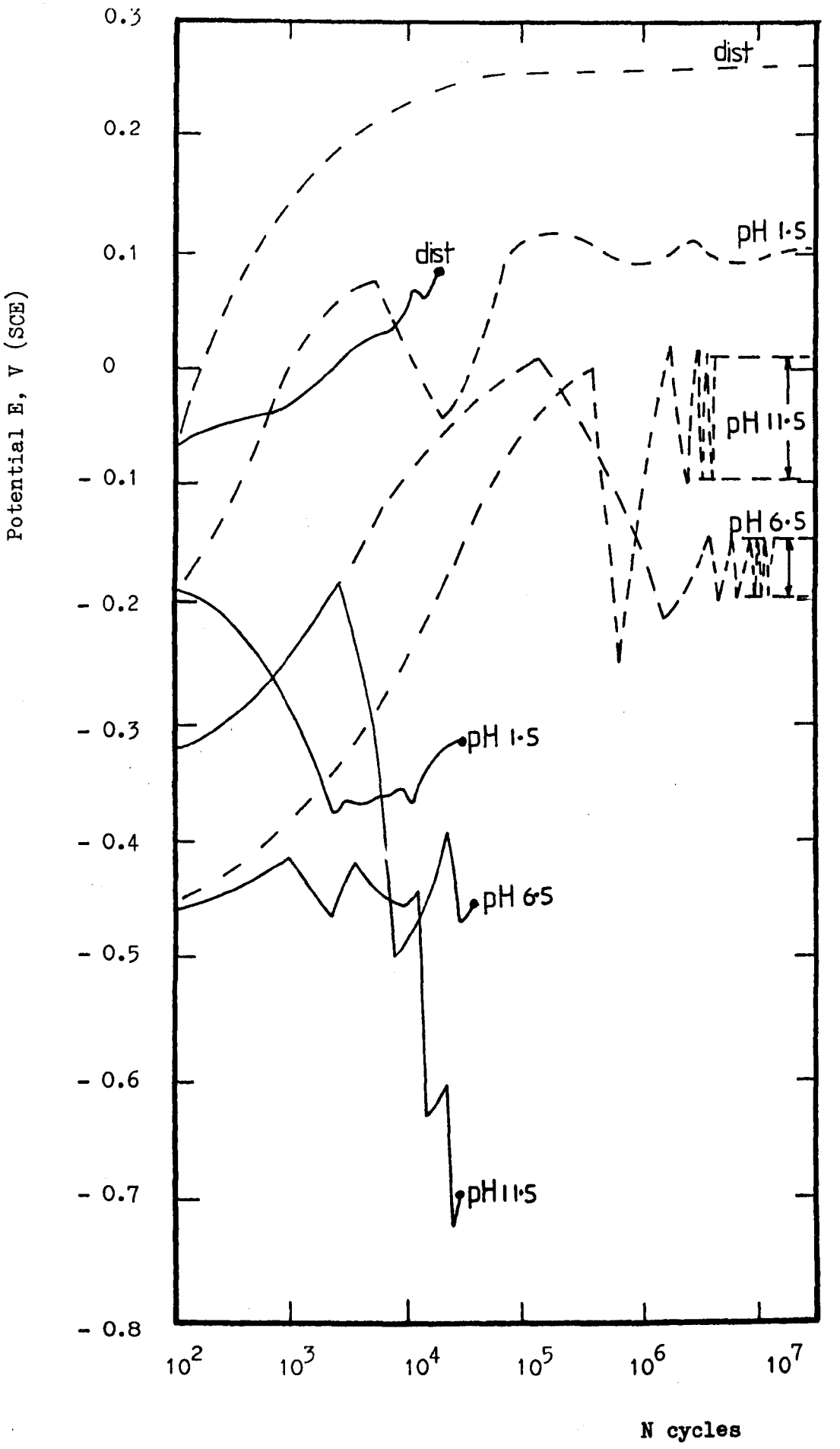

Figure 57 Corrosion fatigue potential - cycles traces for T318, in various electrolytes at approximately 800 MN/m^2 stress amplitude to fracture ——●

Fatigue limit traces also shown — — — — for comparison

It was noted that in each case of passive behaviour, saline pH 11.5 specimens reached a far less noble potential before fracture than those in normal saline. This was the same order of potential found when comparing fatigue limit lower oscillation values, marked X in Figs. 55 to 57, for a possible minimum 'critical' potential criterion of film repair.

Potential ranges observed with time for these dynamic tests, at one typical stress amplitude, were also superimposed on on Fig. R15 (page 73), R32 to R34 (pages 145 to 146) and Figs. 34 to 49 (pages 224 to 245) where the static ranges previously recorded were extended or significantly different. For distilled water immersion of mild steel, Fig. 34 (page 224), no difference was found between the change in stress-free rest potential with time and the dynamic stress values of potential: starting approximately at the unpolarized stirring potential E'_o, the rest potential drifted down to the unpolarized static case E_o with time. Mild steel in saline pH 6.5 however, showed a much greater change in rest potential for the stress-free case 1→2 than for the dynamic stress 1'→2', as shown in Fig. 35. It was considered noteworthy that, as in the case of distilled water, the dynamic stress rest potential was originally coincident with the unpolarized stirring potential. This same result was also true of saline pH 1.5 and pH 11.5, Figs. 36 and 37 (pages 226 and 227) respectively. The downward drift observed in all cases for rest potential with mild steel was characteristic of

the poor corrosion resistance in all the solutions tested, and the final rest potentials showed generally less difference between static and dynamic tests than that between the initial potential readings.

S316 in all solutions, Figs. 38 to 41 (pages 230 to 233) produced dynamic rest potential changes, 3'→4', which were smaller than those produced in the static case, 3→4 . The upward direction of potential change was indicative of the better corrosion resistance here. However, in each case the position of 'dynamic case' breakdown potential E_b (as defined in Fig. R11 Section 2.6.4.), although not sharply defined here, was only slightly more noble than the rest potential range recorded. This result for S316 confirmed the likelihood of film breakdown: the oscillations, marked Σ on the diagrams represent the breakdown and repair ranges observed.

T130 rest potentials were very much less than any breakdown potential. Although steps in the trace of potential were found no breakdown potential was recorded in the range investigated. In O_2 free saline solutions this has been recorded by other research [311] in the region of 9V. Since the oxygen reduction potential (0.82V SHE at pH 7) is so far below this breakdown potential, there is no possibility of corrosion in the transpassive region or in aereated media. The theoretical prediction of the impossibility of film breakdown for T130 was confirmed here in all the solutions tested: no potential

oscillations with time were observed for stress-free specimens (Figs. 50 to 53, pages 248 to 252). However, film breakdown was clearly indicated for titanium in the presence of dynamic stress at the fatigue limit, with the exception of T318 in distilled water (Figs. 56 and 57). Figs. 42 to 49 (pages 236 to 245) show also the dynamic range of rest potentials obtained marked 5'→6'.

4.7. Potentiostatically Controlled Corrosion Fatigue

Potentiostatically controlled corrosion fatigue tests were not planned in this work as part of the main research programme, although other research with implant alloys has incorporated such studies [325,335]. The large amount of scatter obtained for S316 in the saline pH 6.5 solution required further investigation, and for this reason a limited number of tests on S316 were conducted in this solution under potentiostatic control.

It had been earlier noted that the unexpectedly long life specimens, at any given stress amplitude level, showed an open circuit potential range during fatigue which was more noble than that recorded for specimens with shorter life. On average it was noted that the long life specimens had spent most of the time at open circuit potentials in the region of +50mV (SCE), while short life specimens consistently showed potentials during fatigue in the region of -390mV. For this reason it

was decided to control the potential at these two different values so that the natural fluctuations were eliminated.

Fig. 58 illustrates the results obtained at two stress amplitude levels 401 MN/m^2 and 270 MN/m^2, that is above and just below the mean fatigue limit in saline pH 6.5 of 300 MN/m^2. Many more such experiments were carried out at different stress amplitudes, omitted here for clarity in Fig. 58, and the same differences in behaviour were always observed between the two potentials. Specimens at the same stress amplitude had a longer life when controlled potentiostatically at -390mV. This was thought surprisingly, at the time it was observed, because this was the exact opposite order of performance to that under unpolarized corrosion fatigue conditions. The differences in the life are not very noticeable on Fig. 58 owing to the log scale. The increase in the number of cycles endured at the less noble potential over that observed for the more noble potential was 123% at 401MN/m^2 (the highest stress amplitude tested). This was bettered at the lower stress amplitudes, becoming an increase of 216% at 270 MN/m^2. However, it was noted that for these potentiostatically controlled experiments fracture occurred at both potentials for a stress amplitude of 270 MN/m^2. The natural corrosion fatigue tests generally produced a higher fatigue limit (300 MN/m^2) as well as slightly longer lives at any level of stress. It seems that the natural fluctuations in potential are related to film breakdown and

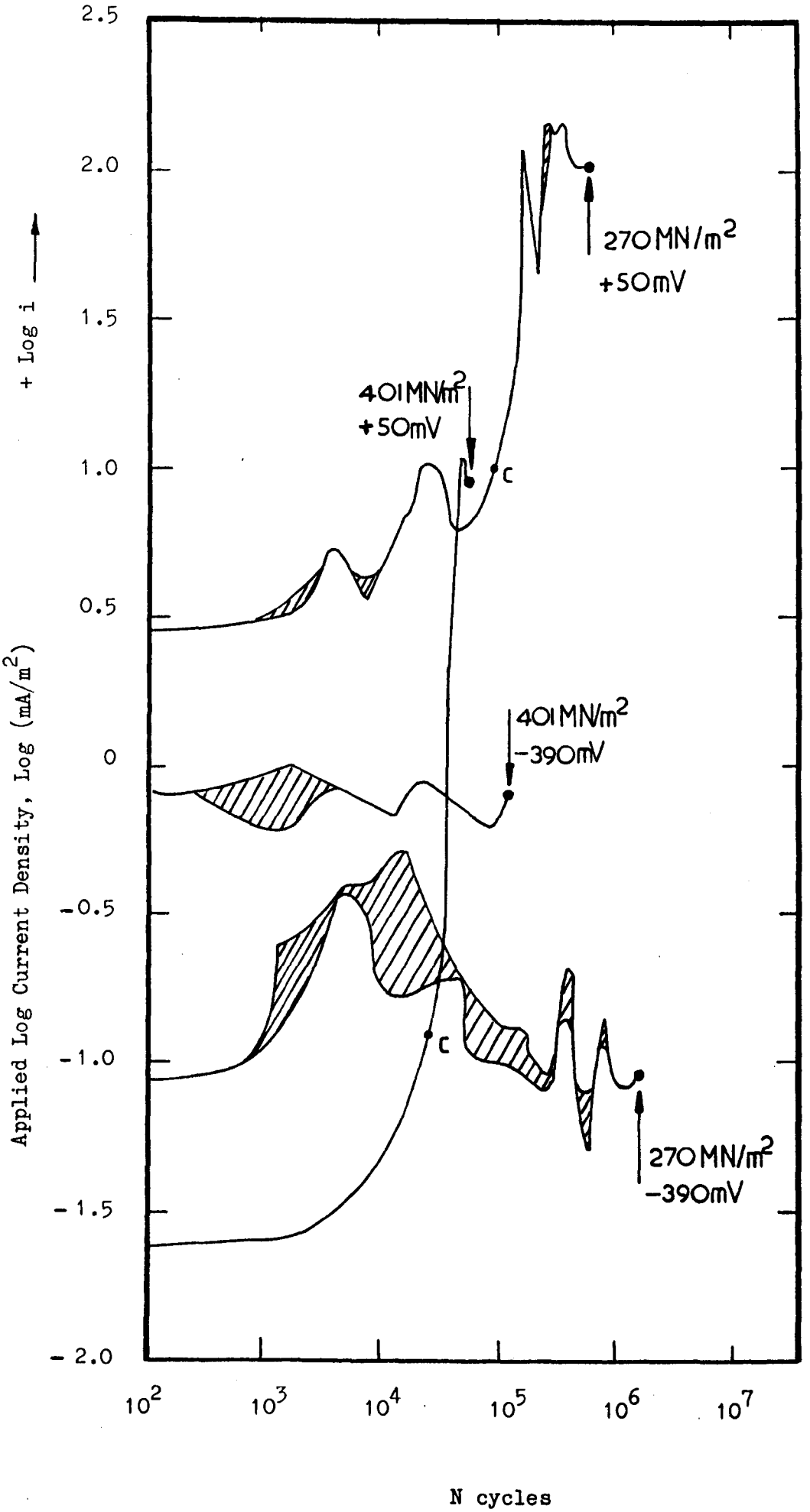

Figure 58 Potentiostatic controlled fatigue of S316 in saline pH 6.5: current density fluctuations for + 50 mV and - 390 mV potential at two stress amplitudes

repair so that the process under controlled potential is not so effective. At +50mV the current density applied for control of potential showed a general change to more positive values accompanied by general corrosion, visible at point 'c' (in Fig. 58) on the specimens. At -390mV there was no such clearly defined change, but rather more oscillations (shown shaded in Fig. 58) in current density, especially at lower stress amplitudes: once again longer life for S316 was commensurate with less stability of an electrochemical variable.

Some specimens which had been tested under potentiostatic control at the -390mV level were allowed to become free of control during fatigue. The open circuit potential immediately oscillated wildly as rust formed in the highly stressed regions with pitting. A black film was then formed all over the material when potential control was reintroduced. No pitting was produced under controlled potential at -390 mV but, as soon as control was lost, pitting occurred locally at film breakdown. This loss and reintroduction of potentiostatic control was also tried at +50mV. The result at this potential was similar but the pitting produced was far less severe. Pits were far more widely spread and much shallower than those found at -390 mV.

4.8. Examination of cracks and fracture surfaces

4.8.1. TEM and SEM studies

Transmission Electron Microscopy (TEM), using carbon shadowed plastic coated replica techniques, was used to investigate the fracture surface derived from each material/environment combination tested. Scanning Electron Microscopy (SEM) was also employed and the results used as a check on the findings of TEM studies on the same test specimens.

TEM studies using 80kV and magnifications in the range 1000 to 32000 were used. SEM studies were carried out at magnifications in the range 500 to 10000. Some 300 to 400 microphotographs were taken during the course of these studies. Positions on the fracture surface were examined ranging from 'near initiation', through intermediate areas, to areas of final rupture. In order to more effectively compare SEM and TEM results, microphotographs were generally standardized at magnifications of 1000 and 10000. It was found advantageous to examine the relatively larger surface features such as the larger etch pits, ductile dimples, and the larger striations with SEM (owing to the large depth of focus), since TEM often did not show these structures (because of the flat replicated surface - depth impression given only by the shadowing). The advantage in also using TEM was that the finer details, including any striations below 1μm, were clearly seen. Such surface topography detail was often lost when SEM examinations

were made.

It was considered useful to present here a series of microphotographs, all representing fracture surface areas in the vicinity of crack initiation (and at least in the region of the start of stage II type crack growth) and each one respectively typical of several similarly observed specimen fractures in its specific material/environment situation. Reversed stress levels S just above the appropriate S / N endurance graph knee were taken for comparison. It is worth noting that, although such a comparison between specimens implies that some will have endured longer test lives than others (approx. 6×10^4 cycles for example, in the case of T318 and 1.2×10^4 cycles for mild steel), the total crack propagation times at these stress levels (as discussed in Section 2.7.3) are not so dissimilar. The environmental exposure time of these fracture surfaces, removed from the test machine immediately after failure, is therefore similar. In all cases presented here, the direction of crack propagation is vertical from the top of the microphotograph.

Fatigue of mild steel in air at $\pm$ 330 MN/m^2 is shown at a magnification of 1000 using TEM for Fig. M1 (a), and using SEM for Fig. M1 (b). Both SEM and TEM showed the typically ductile fracture surface. Striations, of approximately 2.5 μm spacing were only visible, using SEM, in Fig. M1 (b). Fatigue of S316 in air also at $\pm$ 330 MN/m^2 and shown at 1000

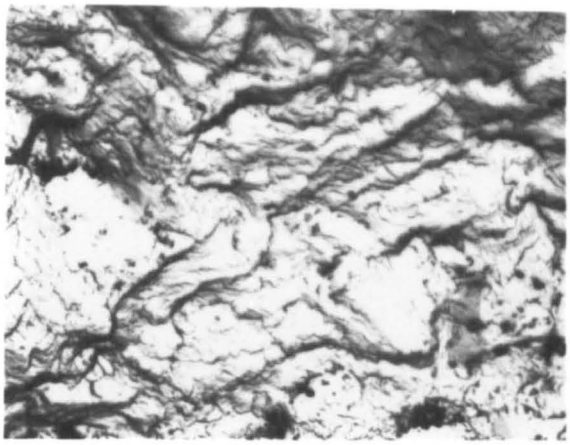

FIGURE M1(a)

Fatigue of Mild Steel in air.
$\pm$ 330 MN/m^2
T.E.M. x 1k

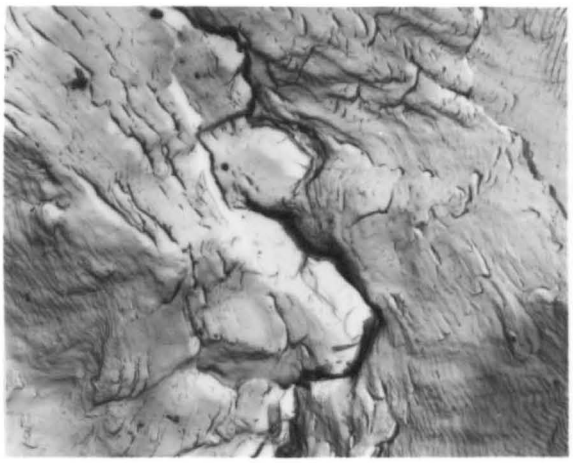

FIGURE M2(a)

Fatigue of S316 in air.
$\pm$ 330 MN/m^2
T.E.M. x 1k

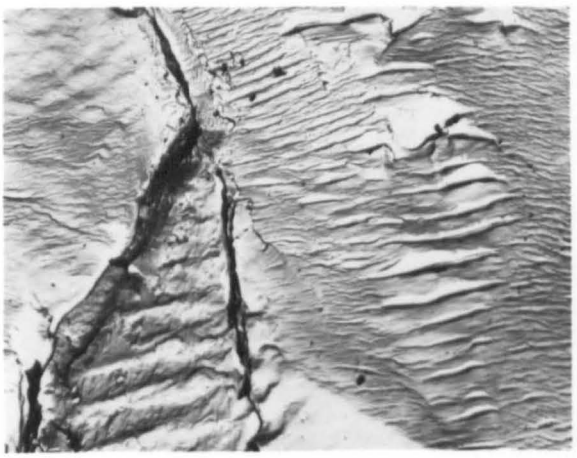

FIGURE M3(a)

Fatigue of T130 in air.
$\pm$ 480 MN/m^2
T.E.M. x 1k

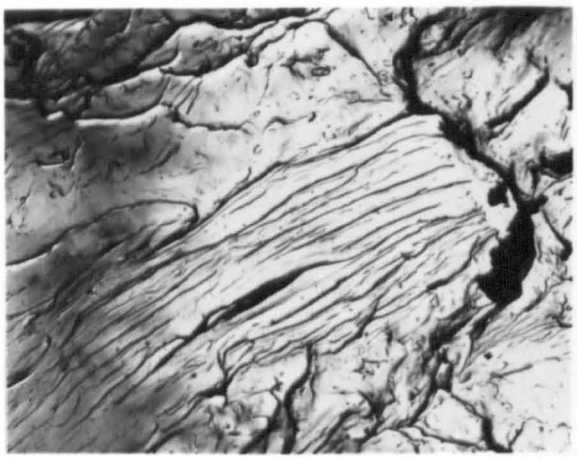

FIGURE M4(a)

Fatigue of T318 in air.
$\pm$ 560 MN/m^2
T.E.M. x 1k

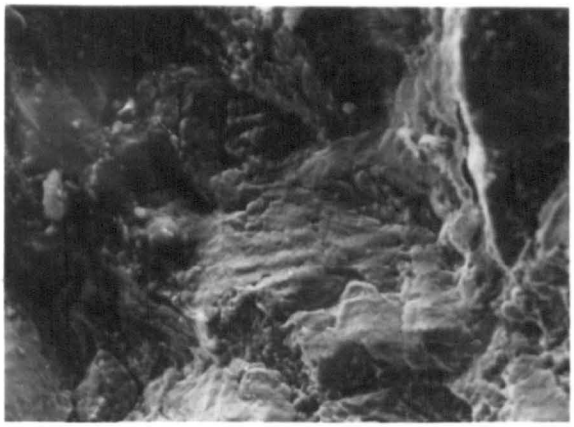

FIGURE M1(b)

Fatigue of mild steel in air
$\pm$ 330 MN/m^2
S.E.M. x 1k

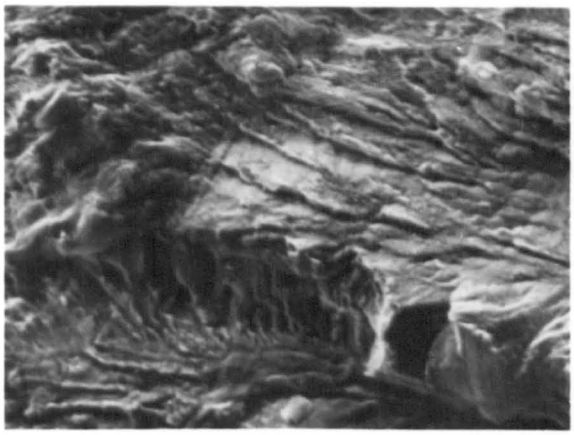

FIGURE M2(b)

Fatigue of S316 in air.
$\pm$ 330 MN/m^2
S.E.M. x 1k

FIGURE M3(b)

Fatigue of T130 in air
$\pm$ 480 MN/m^2
S.E.M. x 750

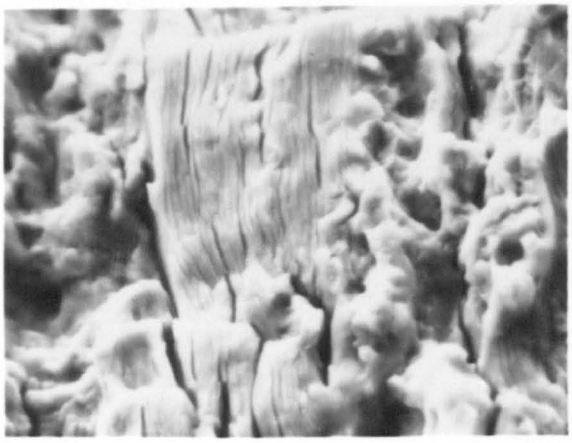

FIGURE M4(b)

Fatigue of T318 in air
$\pm$ 560 MN/m^2
S.E.M. x 1k

magnification in Figs. M2 (a) and M2 (b) is presented here for comparison with the mild steel. The fracure surface of the S316 was more brittle than that of the mild steel: Fig. M2 (b) using SEM, showed the mixed ductile/brittle transgranular cleavage step failure, while TEM observations showed ductile type striations of approximately 1.0μm spacing in Fig. M2 (a). Observation of several fracture surface areas showed that there was a trend for the final fracture regions to exhibit relatively greater ductility. Fig. M3 (a) and M3 (b) respectively show the TEM and SEM fracture details for T130 in air at $\pm$ 480 MN/m^2. River patterns, platelets, and tyre markings were commonly found, with superimposed 45^o shear ripples and striations, using TEM. Ductile striations and a ductile type fracture were clearly seen using SEM. Large angles were found, in both TEM and SEM, between adjacent groups of striations. These striations were found to be grain orientated rather than stress direction orientated. The spacing of striations found varied from approx. 1.3μm to 3.3μm according to orientation. Fig. M4 (a) and M4 (b) respectively show TEM and SEM results for T318 in air at $\pm$ 560 MN/m^2. Some ductility was indicated by the dimpling features found using SEM. However, families of micro-cracks running parallel to the macro-crack propagation direction with an approx. spacing of 0.6μm were common, as shown in Fig. M4 (b). The fracture surface of this alloy was mostly of a brittle nature. Grain orientated brittle striations, having

a spacing of approximately 1.4 μm over large flat areas, were found only on TEM examination.

The environmental effect of distilled water on each of the materials tested is shown by the fracture surfaces Figs. M5 (a) and M5 (b) to M8 (a) and M8 (b). Mild steel, shown in Fig. M5 (a) using TEM showed corrosion products on a brittle fracture surface. Quasi-cleavage facets were clearly seen, quite different from the fracture surface obtained in air as shown by Fig. M1 (a). SEM examination revealed slightly more ductility than was apparent from TEM. Conical etch pits were also visible in the SEM examination of Fig. M5 (b). A mixed ductile/brittle fracture surface was generally seen in distilled water and both SEM and TEM showed some intergranular fracture. Distilled water also produced, as seen in Fig. M6 (a), a more brittle fracture in S316 than that obtained for air. A mixed ductile/brittle surface containing pockets of striations, spaced approximately 1.0 μm was seen using TEM. Direction changes of 120° were commonly observed for striations in both TEM and SEM studies. Fig. M6 (b) shows a view by SEM. The corrosion fatigue of T130 at $\pm$ 480 MN/m^2 in distilled water is shown by Figs. M7 (a) and M7 (b). Striations of 1.0 μm to 1.2 μm spacing on local cleavage facets were found in TEM studies as shown in Fig. M7 (a). Study by SEM revealed clearly, as shown in Fig. M7 (b), the cleavage step type fracture in distilled water which contrasts

FIGURE M5(a)

Fatigue of Mild Steel
in distilled water
$\pm$ 330 MN/m^2
T.E.M. x 1k

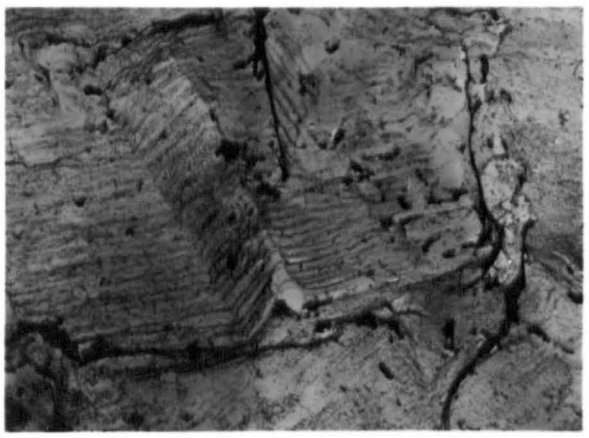

FIGURE M6(a)

Fatigue of S316
in distilled water
$\pm$ 330 MN/m^2
T.E.M. x 1k

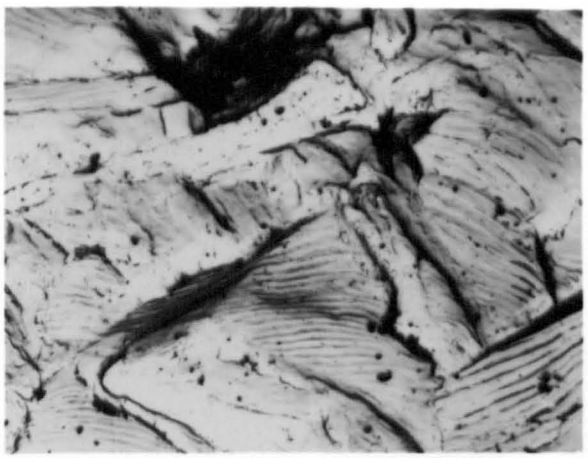

FIGURE M7(a)

Fatigue of T130
in distilled water
$\pm$ 480 MN/m^2
T.E.M. x 1k

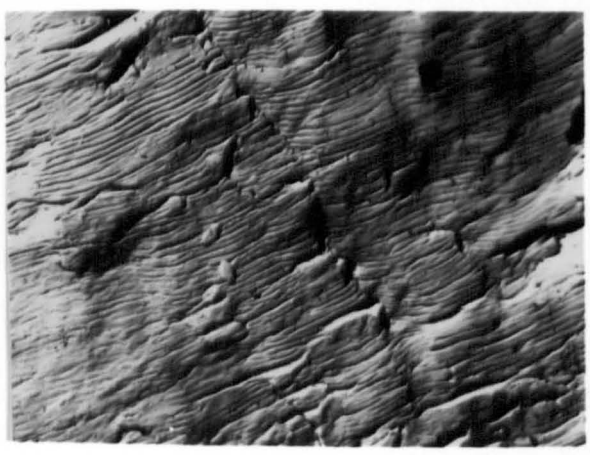

FIGURE M8(a)

Fatigue of T318
in distilled water
$\pm$ 560 MN/m^2
T.E.M. x 1k

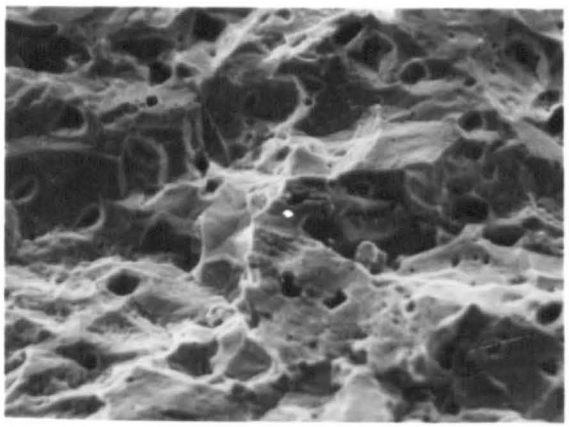

FIGURE M5(b)

Fatigue of Mild steel
in distilled water
$\pm$ 330 MN/m^2
S.E.M. x 1k

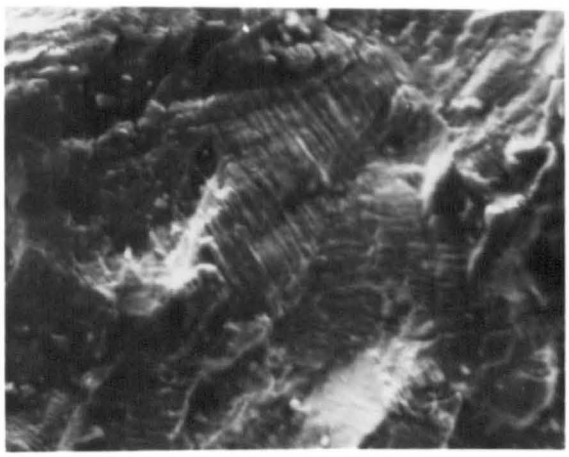

FIGURE M6(b)

Fatigue of S316
in distilled water
$\pm$ 330 MN/m^2
S.E.M. x 1k

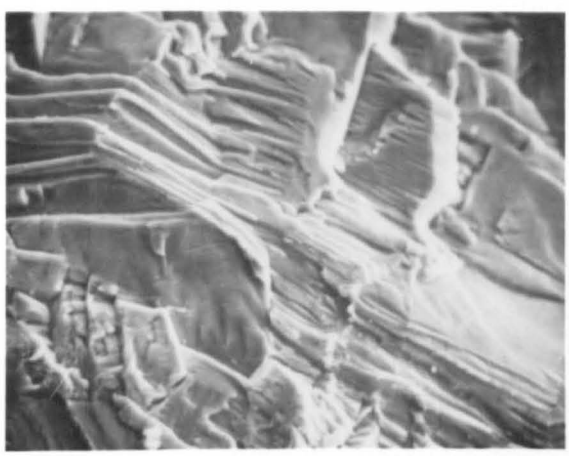

FIGURE M7(b)

Fatigue of T130
in distilled water
$\pm$ 480 MN/m^2
S.E.M. x 530

FIGURE M8(b)

Fatigue of T318
in distilled water
$\pm$ 560 MN/m^2
S.E.M. x 1k

strongly with the more ductile failure of T130 in air, shown in Fig. M3 (b). Figs. M8 (a) and M8 (b) show the typical TEM and SEM result respectively of viewing the surface of T318 after fracture at $\pm$ 560 MN/m^2 in distilled water. In this case very little difference could be found in the fracture surface from that in air, shown in Figs. M4 (a) and M4 (b). Striations were again only seen using TEM examination, Fig. M8 (a), and these were spaced at 0.6μm, somewhat smaller than those observed in air.

The environmental effect of saline pH 6.5 on each material is shown by Figs. M9 (a) and M9 (b) to M12 (a) and M12 (b). Mild steel, shown in Fig. M9 (a) by TEM, showed transgranular cleavage, less corrosion products, and relatively more ductility than for distilled water. It clearly presented a mixed ductile /brittle mode of failure which was confirmed, in Fig. M9 (b), by both SEM and TEM. Comparing the SEM results, in Figs. M5 (b) and M9 (b) it is clear that distilled water at pH 6.5 produced a more brittle type of fracture in mild steel than was produced by the saline at pH 6.5.

Fig. 10 (a), TEM and Fig. 10 (b), SEM, show similar fracture surfaces on S316 in saline pH 6.5 to those obtained in distilled water: striation spacings from 0.9μm to 1.4μm were noted. A TEM study of T130 in saline pH 6.5, Fig. M11 (a), showed striations of 1.0μm to 1.2μm spacing, on local brittle facets, in a mixed ductile/brittle/cleavage fracture surface.

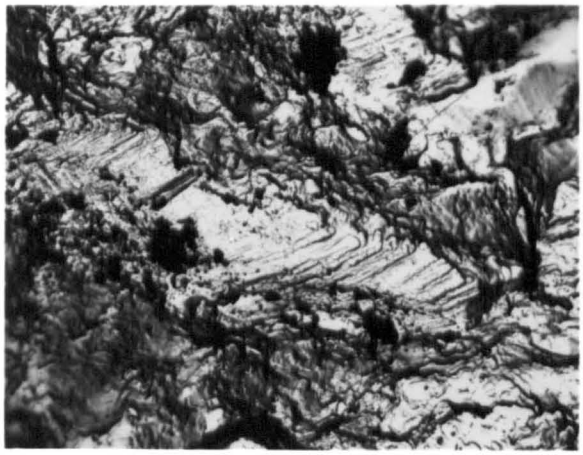

FIGURE M9(a)

Fatigue of Mild steel in saline pH 6.5

$\pm$ 330 MN/m^2

T.E.M. x 1k

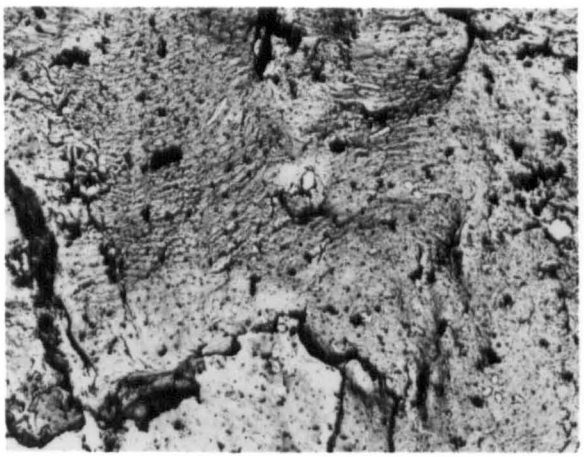

FIGURE M10(a)

Fatigue of S316 in saline pH 6.5

$\pm$ 330 MN/m^2

T.E.M. x 1k

FIGURE M11(a)

Fatigue of T130 in saline pH 6.5

$\pm$ 480 MN/m^2

T.E.M. x 1k

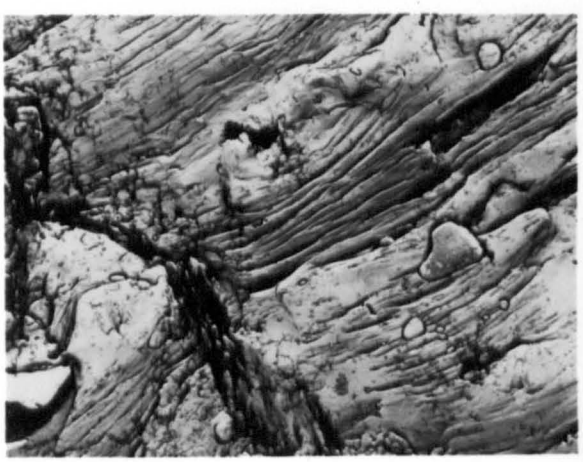

FIGURE M12(a)

Fatigue of T318 in saline pH 6.5

$\pm$ 560 MN/m^2

T.E.M. x 1k

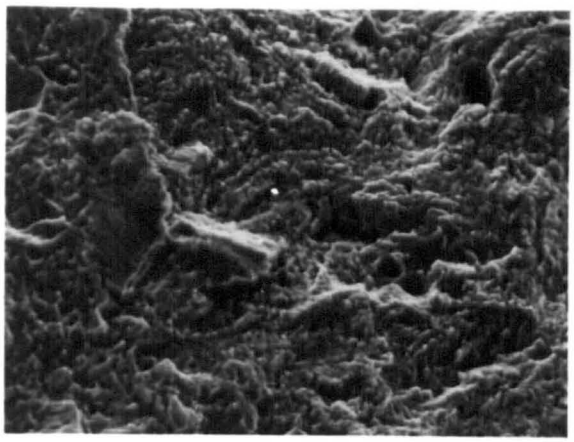

FIGURE M9(b)

Fatigue of Mild steel in saline pH 6.5

$\pm$ 330 MN/m^2

S.E.M. x 1k

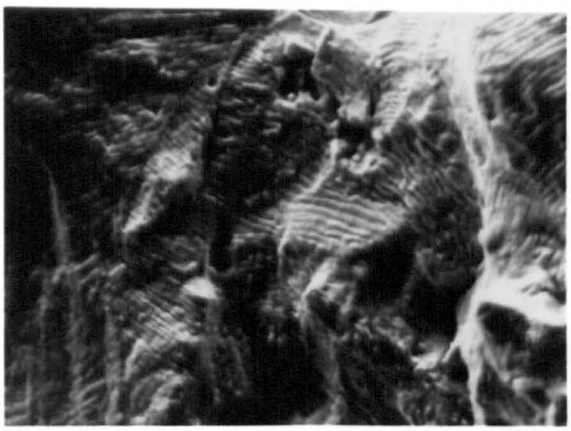

FIGURE M10(b)

Fatigue of S316 in saline pH 6.5

$\pm$ 330 MN/m^2

S.E.M. x 1k

FIGURE M11(b)

Fatigue of T130 in saline pH 6.5

$\pm$ 480 MN/m^2

S.E.M. x 700

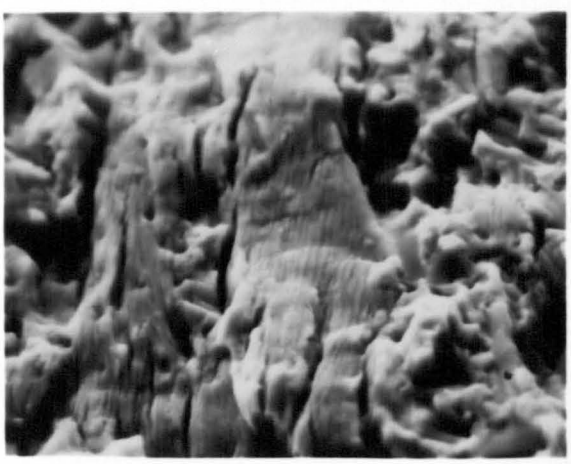

FIGURE M12(b)

Fatigue of T318 in saline pH 6.5

$\pm$ 560 MN/m^2

S.E.M. x 1k

As shown in Fig. M11 (b), SEM studies also confirmed this result. Results as viewed by SEM and TEM for T318 are shown respectively in Fig. M12 (a) and M12 (b). It was found that in saline pH 6.5, as in distilled water, that the fracture surface was not dissimilar from that obtained in air. Striation spacings, seen only with TEM, were, however, half that found in air.

Fracture surfaces fatigued in saline pH 1.5 for each material are shown in Figs. M13 (a) and M13 (b) to M16 (a) and M16 (b). The large quantities of corrosion product, shown as black areas in Fig. M13 (a) and M13 (b), produced in saline pH 1.5 largely masked the gross attack on the mild steel. Large etch pits, more clearly seen with SEM and shown in Fig. M13 (b), were also a feature, and these were found linking across the crack-front. S316 in saline pH 1.5 produced a fracture surface which, when viewed by TEM as shown in Fig. M14 (a), revealed a transgranular brittle structured fracture with small etch pits and elongated "dendrite" or "feather" morphology. This result from TEM study is similar to that frequently found in stress corrosion cracking tests with S316. This structure was however not seen clearly by SEM studies which showed, in Fig. M14 (b), some ductility and the presence of striations of approximately 1.1μm to 1.5μm spacing. Striations here were not found with TEM studies. Saline pH 1.5 produced fracture surfaces on T130, shown in Figs. M15 (a) and

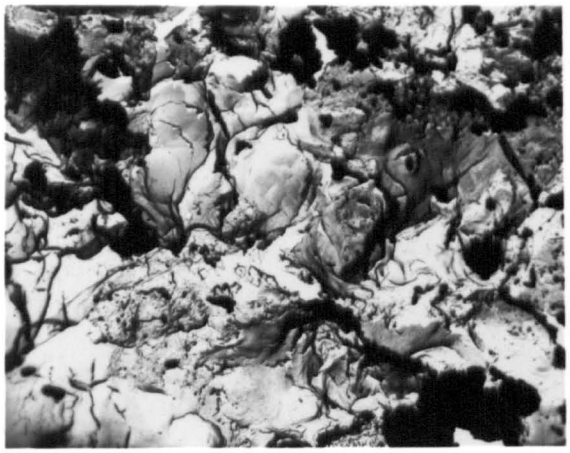

FIGURE M13(a)

Fatigue of Mild steel
in saline pH 1.5
$\pm$ 330 MN/m^2
T.E.M. x 1k

FIGURE M14(a)

Fatigue of S316
in saline pH 1.5
$\pm$ 330 MN/m^2
T.E.M. x 1k

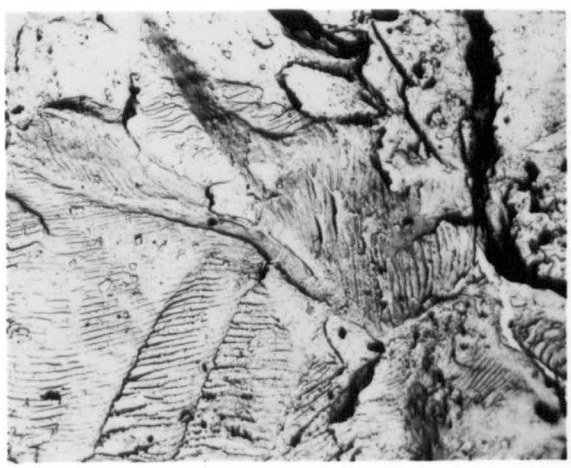

FIGURE M15(a)

Fatigue of T130 in
saline pH 1.5
$\pm$ 480 MN/m^2
T.E.M. x 1k

FIGURE M16(a)

Fatigue of T318
in saline pH 1.5
$\pm$ 560 MN/m^2
T.E.M. x 1k

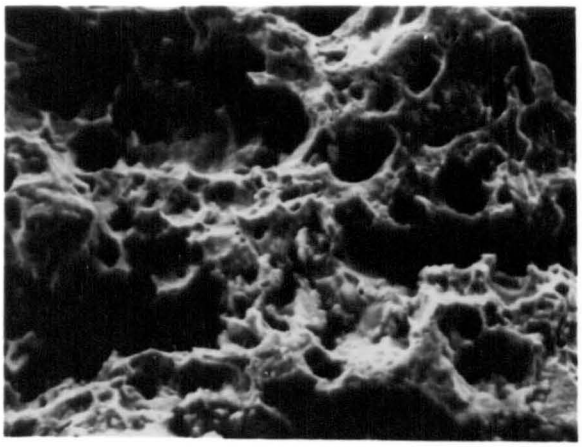

FIGURE M13(b)

Fatigue of Mild steel
in saline pH 1.5
$\pm$ 330 MN/m^2
S.E.M. x 1k

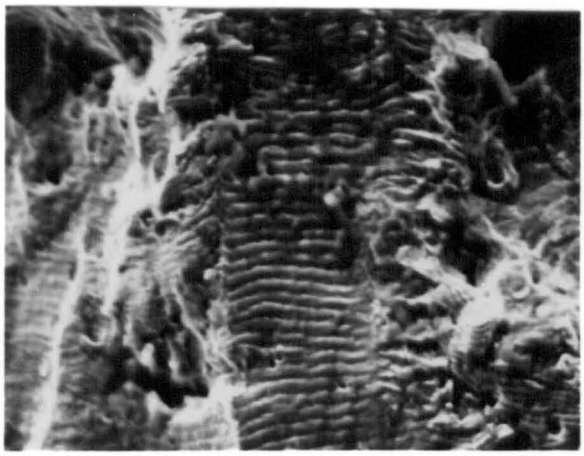

FIGURE M14(b)

Fatigue of S316 in
saline pH 1.5
$\pm$ 330 MN/m^2
S.E.M. x 1k

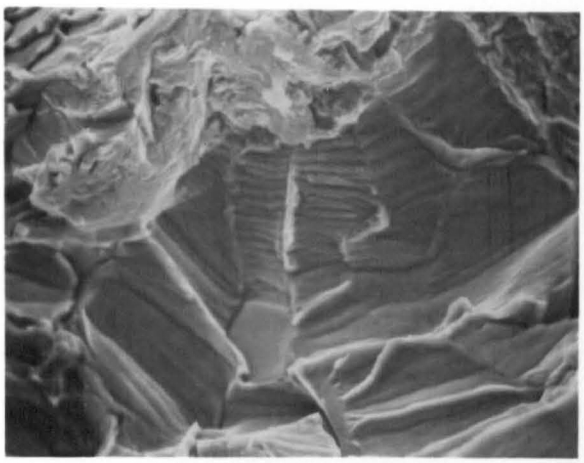

FIGURE M15(b)

Fatigue of T130
in saline pH 1.5
$\pm$ 480 MN/m^2
S.E.M. x 530

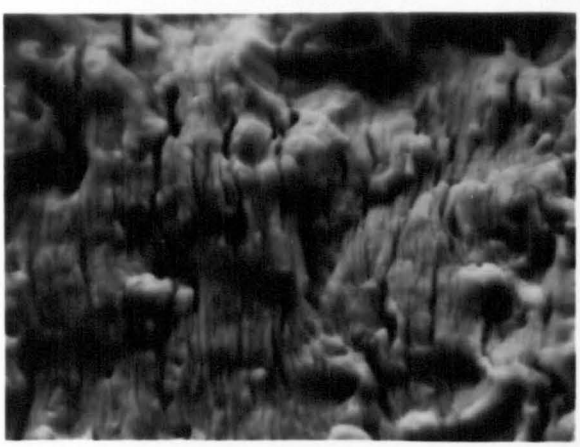

FIGURE M16(b)

Fatigue of T318 in
saline pH 1.5
$\pm$ 560 MN/m^2
S.E.M. x 1k

M15 (b), which were similar to those obtained for saline pH 6.5 Figs. M11(a) and M11 (b). Striations were found here varying from approximately 1.0μm to 1.4μm spacing. A 90^{o} striation direction change was also commonly found, shown in Fig. M 15 (a). T318 fracture surfaces were not very different here to those observed for air. Fig. M16 (a) shows the generally brittle surface revealed by TEM, and Fig. M16 (b) shows the SEM view which is not unlike Fig. M4 (b) for air. Striations were found by TEM to have a spacing of approximately 1.0μm.

The environmental effect on the fracture surface in saline pH 11.5 for each material is shown by comparing Figs. M17 (a) and M17 (b) to M20 (a) and M20 (b) with the respective surfaces in air. The mild steel fracture surface is shown in Fig. M17 (a) as viewed by TEM. Striations were found for this environment with mild steel, having a spacing of approximately 0.7μm, which was somewhat smaller than that found in air, the only other case where striations were found. Such fine striations were not seen using SEM, Fig. M17 (b), when very large ductile dimples were seen to be present on the fracture surface which had been lost during replication for TEM. Examination of S316 fractures in saline pH 11.5, shown in Figs. M18 (a) TEM and M18 (b) SEM, indicated similar features to those seen for distilled water and saline pH 6.5: striation spacing was approximately 1.0μm. T130 fractures with the saline pH 11.5 also gave similar results, shown in Figs. M19 (a) and M19 (b),

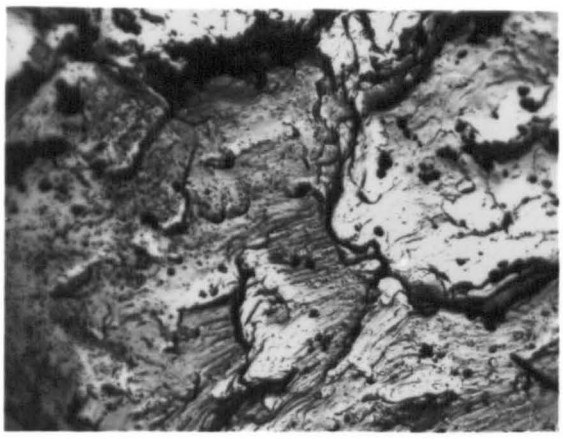

FIGURE M17(a)

Fatigue of mild steel in saline pH 11.5

$\pm$ 330 MN/m^2

T.E.M. x 1k

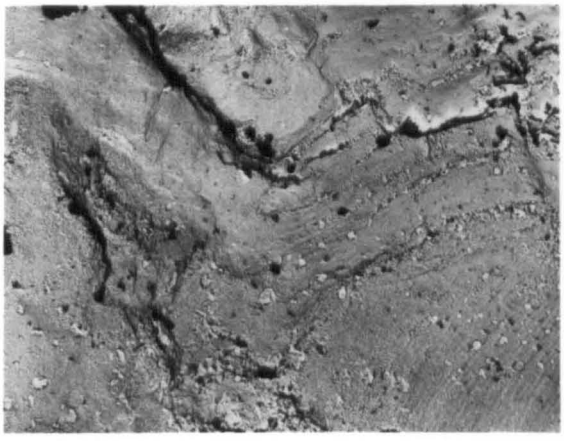

FIGURE M18(a)

Fatigue of S316 in saline pH 11.5

$\pm$ 330 MN/m^2

T.E.M. x 1k

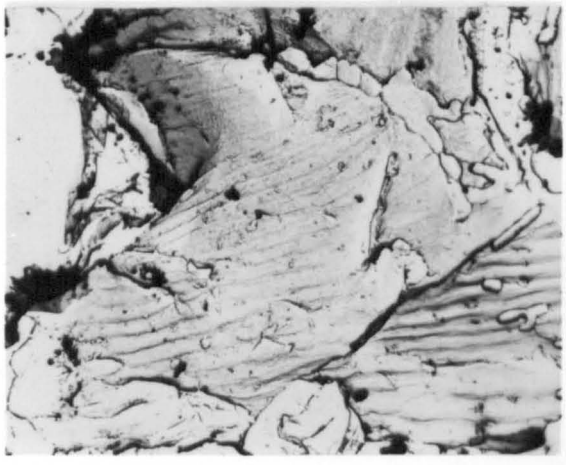

FIGURE M19(a)

Fatigue of T130 in saline pH 11.5

$\pm$ 480 MN/m^2

T.E.M. x 1k

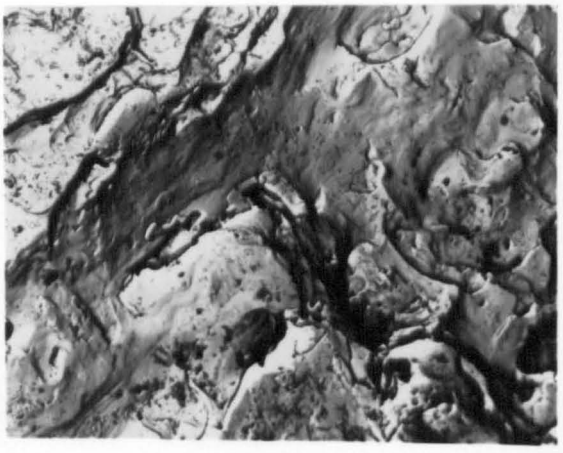

FIGURE M20 (a)

Fatigue of T318 in saline pH 11.5

$\pm$ 560 MN/m^2

T.E.M. x 1k

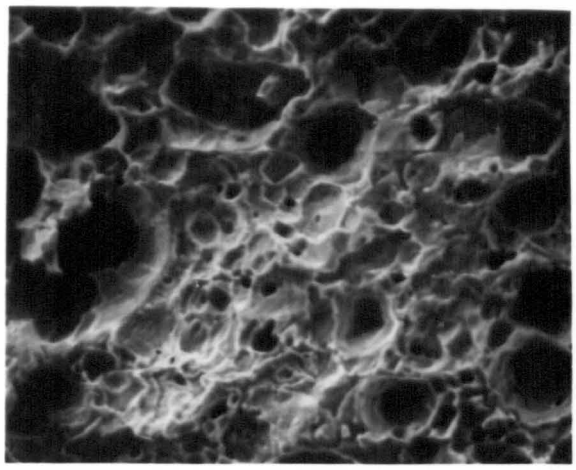

FIGURE M17(b)

Fatigue of mild steel
in saline pH 11.5
$\pm$ 330 MN/m^2
S.E.M. x 1k

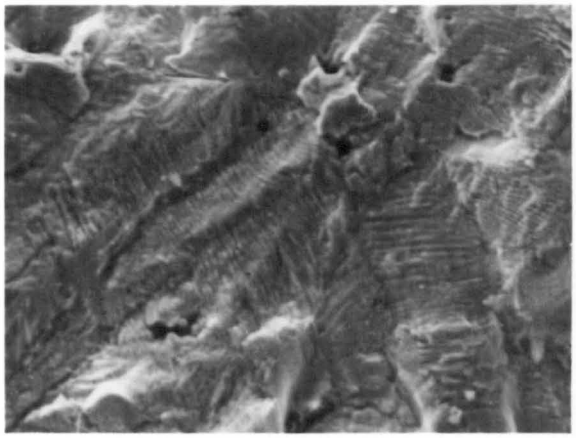

FIGURE M18(b)

Fatigue of S316 in
saline pH 11.5
$\pm$ 330 MN/m^2
S.E.M. x 1k

FIGURE M19(b)

Fatigue of T130
in saline pH 11.5
$\pm$ 480 MN/m^2
S.E.M. x 530

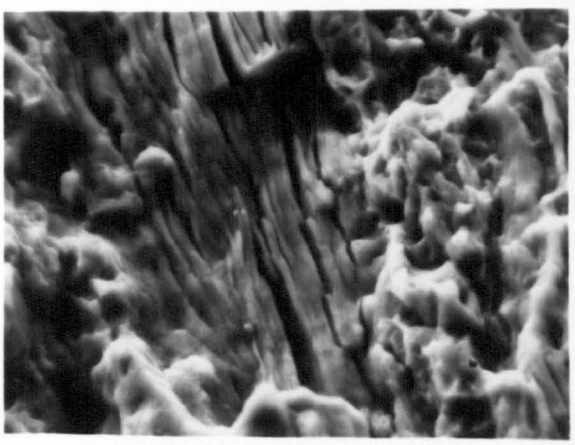

FIGURE M20(b)

Fatigue of T318
in saline pH 11.5
$\pm$ 560 MN/m^2
S.E.M. x 1k

to those seen for saline pH 6.5 and pH 1.5. Striation spacings at approximately 2.0 μm were however much larger, as seen using TEM in Fig. M19 (a). The proportion of cleavage was also larger for pH 11.5 saline tests than for the other environments. The environmental effect of saline pH 11.5 on the fatigue of T318 was shown, in Figs. M20 (a) and M20 (b), to be not unlike that of air in respect of fracture-surface damage features. Very little difference in the appearance of the fracture surface was found for T318 in any of the solutions tested. However, for saline pH 11.5 no striations were seen at any position over the entire fracture surface. Families of micro-cracks, running parallel to the fracture propagation direction, were revealed by SEM as shown in Fig. 20 (b). This was a feature of all T318 fracture surfaces which distinguished them from those of other materials viewed by SEM. Figs. M4 (b), M8 (b), and M16 (b) for the other environments showed the micro-crack spacing to be of the same order of magnitude as the striations observed only by TEM. Micro-cracks having lengths into the surface proportional to their spacing were always observed. A spacing of 2 μm was found for saline pH 11.5 which, as shown in Fig. M20 (b), is significantly larger than that found in other environments. This environment thus failed to produce the striation-marked fracture surface on T318, seen with all the others tested, and produced instead families of micro-cracks having approximately twice the depth

and spacing observed in other environments. Table 9 shows the striation spacing (in μm) noted for each material/ environment combination.

Environment → / Material ↓	AIR	Distilled Water pH 6.5	Saline		
			pH 6.5	pH 1.5	pH 11.5
Mild Steel	2.5	none	none	none	0.7
S316	1.0	1.0	0.9-1.4	1.0-1.5	1.0
T130	1.3-3.3	1.0-1.2	1.0-1.2	1.0-1.4	2.0
T318	1.4	0.6	0.7	1.0	none

Table 9 Striation spacings observed in μm

Where single figures appear in the table, the recorded range of spacing was less than 0.1 μm. The results appear to fall into two distinct groups: those whose ranges started at values near 1.0 μm and those near 2.0 μm or marked "none". The results for the first group yield a mean striation spacing of 0.97 μm with a standard deviation of 0.21 μm. T130 in air was found to have a very wide range of striation spacing but it was thought correct to incluce this in the first group, because the upper limit of the range was not significant. The striations

were clearly shown in Fig. M3 (b) to be grain direction orientated, and the higher spacing distances are the result of cosine error. The lower limits of each of the ranges found are, for this reason, more significant. Mild steel in air at 2.5μm spacing and T130 in saline pH 11.5 at 2.0μm spacing, together with T318 in saline pH 11.5 and mild steel in all environments except saline pH 11.5, were perhaps indicative of a different mechanism for crack growth.

Figs. M21 (a), M21 (b), M22 (a) and M22 (b) show the various fracture surfaces of S316 in saline pH 6.5 obtained with reference to the high S/N data scatter obtained, as reported in Section 3.3.1. and 3.3.7. A "low result", that is one exhibiting a corrosion fatigue life below the mean value expected for a given stress amplitude, was found to have a fracture surface as illustrated in Fig. M21 (a) and M21 (b). The respective SEM and TEM views for a specimen exhibiting a longer than expected, or "high result", are shown in Figs. M22 (a) and M22 (b). These four photo micrographs showing 1000 mignification with SEM and 10000 with TEM were typical of the very many specimens examined at the extreme high and low endurances of the scatter-band. The views shown earlier in this section, Figs. M10 (a) and M10 (b) represented the fracture surface of a specimen having an average life predicted by the S/N curve. All these micrographs represent fracture surfaces in the region just above the fatigue limit. The small

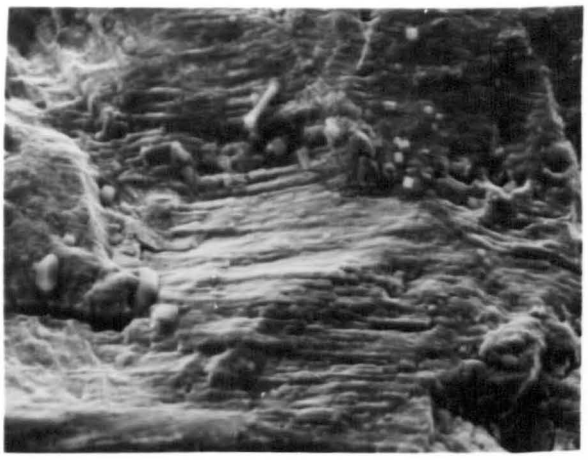

FIGURE M21(a)

Fatigue of S316
in saline pH 6.5
$\pm$ 350 MN/m^2
"Low result" 265 000 c
S.E.M. x 1k

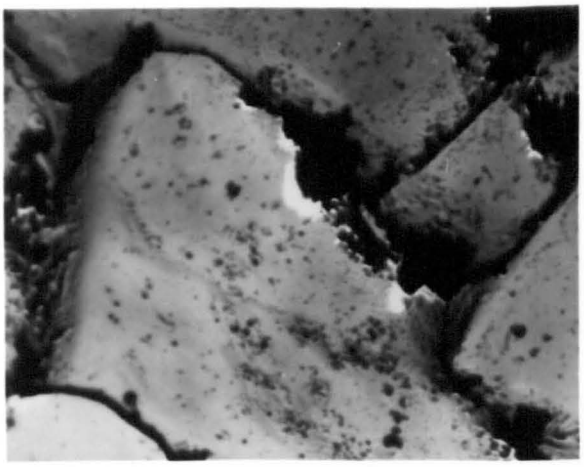

FIGURE M21(b)

Fatigue of S316 in
saline pH 6.5
$\pm$ 350 MN/m^2
"Low result"265 000 c
T.E.M. x 10k

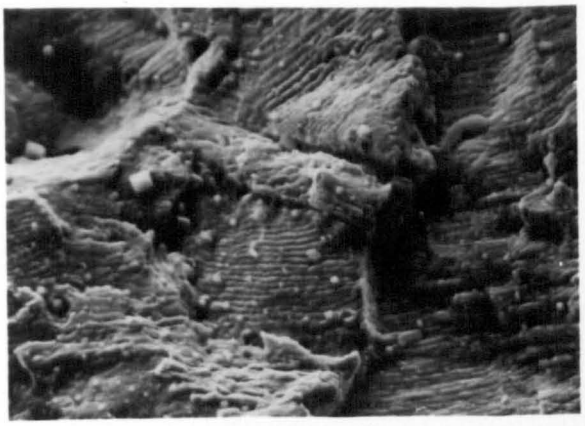

FIGURE M22(a)

Fatigue of S316 in
saline pH 6.5
$\pm$ 375 MN/m^2
"High result" 595 000 c
S.E.M. x 1k

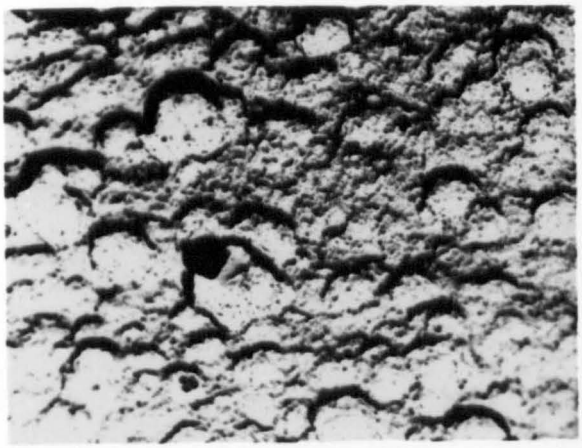

FIGURE M22(b)

Fatigue of S316 in
saline pH 6.5
$\pm$ 375 MN/m^2
"High result" 595 000 c
T.E.M. x 10k

differences in stress amplitude between each one was not thought significant when compared with the very great differences in the fracture surface observed.

"Low results" when viewed by SEM, Fig. M21(a) showed striations over a broader crack front than those shown in Fig. M10 (b) for an "average result". The striation spacing was however identical. TEM views of "low result" specimens, shown in Fig. M21 (b) were quite different from the normal view shown in Fig. M10 (a). Boundary granular attack with pitting was clearly evident.

"High results" when viewed by SEM, Fig. M22 (a) showed cleavage steps, as well as striations of the same spacing as low and average result fractures. The "high result" fractures, like the "average result" specimens, showed many changes of striation direction with grain orientation, unlike the broad -front "low result". TEM views of "high result" fractures showed a surface covered with corrosion products and nodular dimples characteristic of general attack as shown in Fig. M22 (b). This view was quite unlike the grain boundary pitting attack found for "low result" specimens.

The normal result, Fig. M10 (a) TEM and M10 (b) SEM produced views of fracture surface mid-way between the extremes shown here for "high result" and "low result" specimens. Since the striation spacing was approximately 1μm for all cases, it was considered that the differences in life between

specimens was that of time to initiate and develop stage I cracks only.

4.8.2. Optical Metallography

All cracks observed in the various material/environment combinations under fatigue were found to be transgranular, propagating from the top surface downward as shown in Figs. M23 to M27. The environmental effect was most clearly seen for mild steel: Fig M23, in air, does not have the width or secondary dissolution features present in distilled water, shown in Fig. M24. Some influence of environment could also be seen in the series of micrographs Figs. M25 to M27, where an increasingly aggressive solution widened the crack. No influence of environment on crack appearance could be found for titanium. A view of the top surface of a mild steel specimen, shown in Fig. M28, shows the spread of cracks from the edge of a drilled hole across the width of the specimen. Fig. M29 shows the same view at a larger magnification for T130. Fracture surfaces of such specimens with holes were not found to show any features which were different from those of plain specimens.

Generally, families of parallel cracks were initiated on the surface of mild steel in all solutions as well as in air extending approximately 5 mm either side of the crack resulting in fracture. Similar families of cracks were seen for S316 in air and in distilled water, but one crack resulting in fracture

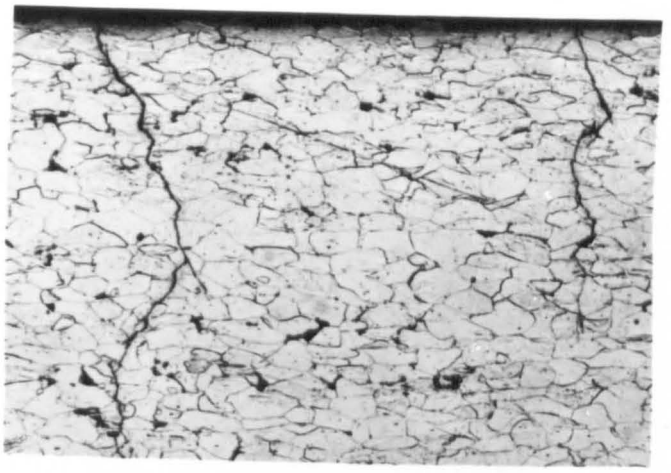

FIGURE M23

Fatigue of mild steel in air $\pm$ 310 MN/m^2 after 1.18 Mcy. Optical mag. x 100, showing transgranular propagation of cracks from the top surface.

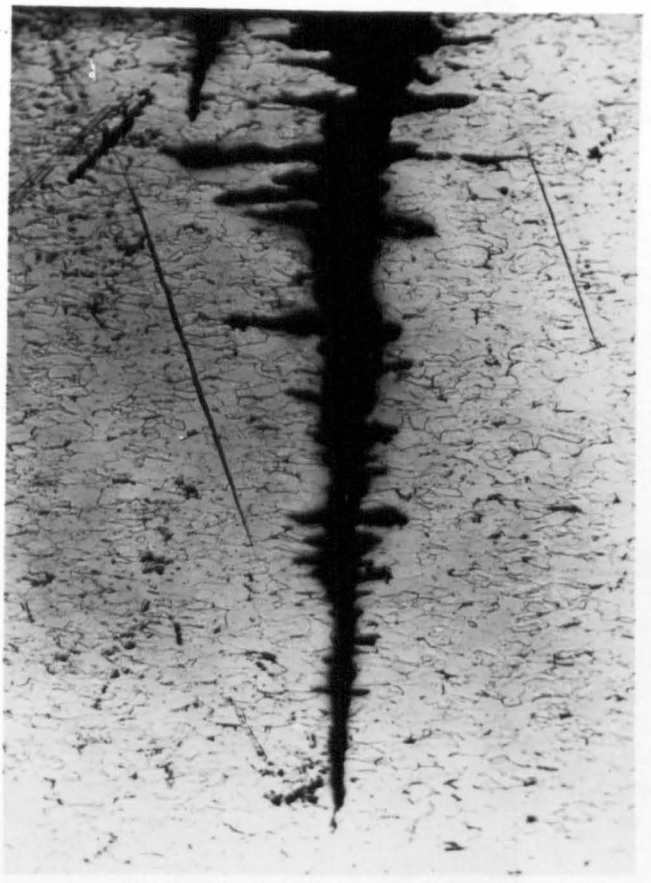

FIGURE M24

Fatigue of mild steel in distilled water $\pm$ 301 MN/m^2 after 0.9 Mcy. Optical mag. x 100, showing transgranular crack propagation and secondary disssolution of steel in the direction of applied strain.

FIGURE M25

Fatigue of S316 in air $\pm$ 465 MN/m^2.

Optical mag. x 190, showing transgranular crack.

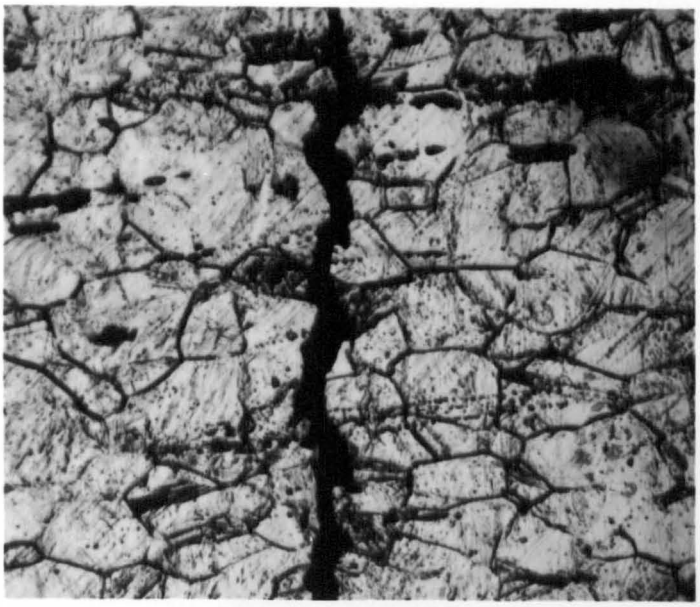

FIGURE M26

Fatigue of S316 in saline pH 6.5

455 MN/m^2. Optical mag. x 190, showing transgranular crack typically wider than those in air.

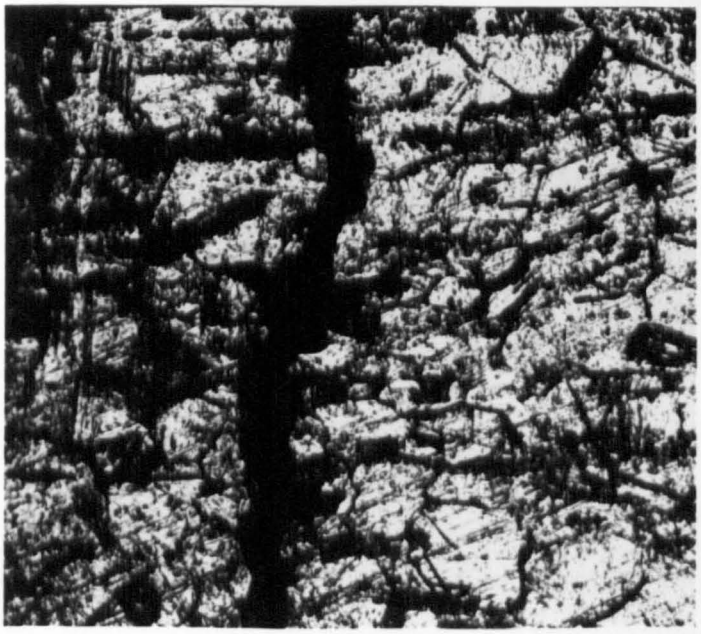

FIGURE M27

Fatigue of S316 in saline pH 1.5
450 MN/m^2. Optical mag. x 190. showing transgranular crack typically wider than in other environments.

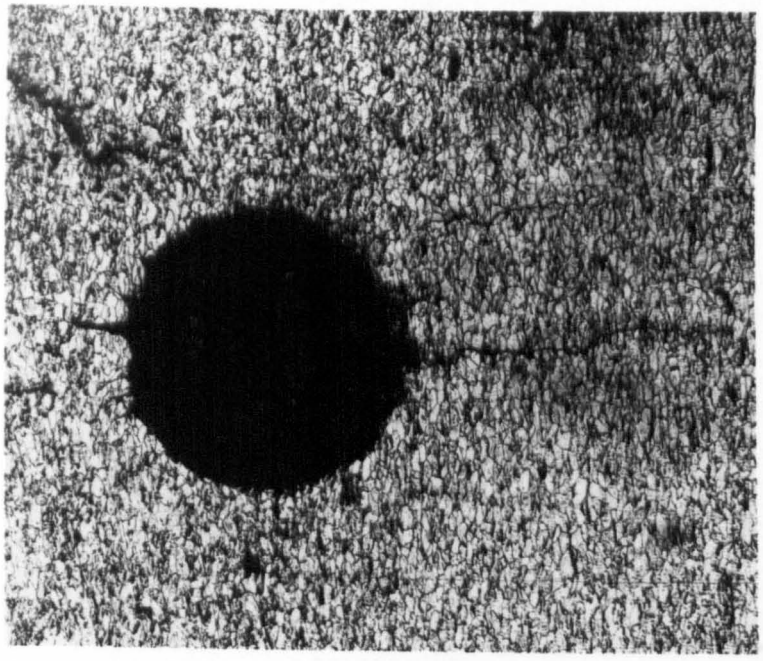

FIGURE M28

Fatigue of mild steel in distilled water $\pm$ 270 MN/m^2 at 0.74 Mcy. Optical x 70, showing top surface multi-crack growth from edge of hole perpendicular to applied strain direction.

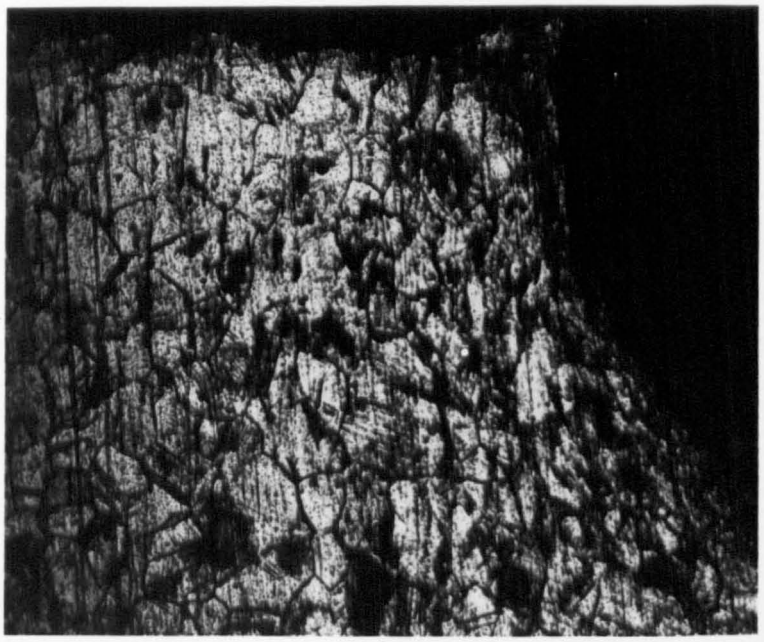

FIGURE M29

Fatigue oi T130 in distilled water $\pm$ 530 MN/m^2. Optical x 190, showing transgranular fracture from a single crack propagating from edge of hole.

was observed only in saline solutions. T130 and T318 did not show more than the one crack originating on their surface. Crack propagation times associated with these results varied from a few seconds at high stress amplitudes to 4.4 minutes at high cycle tests for the longest time to fracture after visual crack initiation. The proportion of the test time spent during stage II crack propagation was thus estimated at $<0.005\%$ for any experiment.

5. GENERAL DISCUSSION AND CONCLUSIONS

5.1. Discussion of Results

5.1.1. The influence of the chloride ion

This variable, discussed in Section 2.6.2., was identified in its effect here by noting the differences in the behaviour of each material fatigued in saline pH 6.5 compared with that seen in distilled water.

Table 2 (page 206) together with the S/N curves in Figs. 14 and 15 (page 188) showed that for mild steel the chloride ion was responsible for a 39% increase in Endurance Limit at 2×10^7 cycles with plain specimens. A further remarkable improvement in the presence of chloride ions was found for specimens having drilled holes: an increase of over 700% in endurance being noted for 2 mm diameter hole specimens in saline pH6.5. Leaving a discussion on the influence of drilled holes until Section 5.1.4, it remains to be seen why there is such a significant increase in high cycle fatigue performance, in the presence of chloride ions, with plain specimens of mild steel. Chloride ions were not found to be responsible for this improvement at all stress amplitudes. The opposite effect was also observed. A complication in assessment was the two discontinuities obtained in distilled water for mild steel (Fig. 14), similar to some curves produced by Luther & Williams[228] in air, which were extended and confirmed from previous work[108].

The chloride ion was thus seen, by comparison between Fig. 14 and Fig. 15, to be responsible for a reduced fatigue performance at stress amplitudes above 120 MN/m^2. The magnitude of the reduction varies with stress amplitude, because of discontinuities in the "rate of damage" relationships, but was in general agreement with work reported earlier [116-118] in Section 2.6.2. The lower discontinuity has been found to disappear at higher frequencies [228] in previous work, and if this would indeed happen here, for distilled water with mild steel, the improvement found for saline solutions might not then occur. The present method of loading specimens was, however, unsuitable for high frequency experiments so that this supposition remains unconfirmed. The estimated corrosion current densities obtained from linear polarization studies, given in Table 8, (page 221) showed similar results for mild steel with and without chloride ions. The corrosion potential, shown in Figs. 50, 51 and 54 (pages 248 to 255) was less noble in saline pH 6.5 at all times so that these variables could not account for the changing effect of chloride ions with stress amplitude. The polarization curves, shown in Figs. 34 and 35, however, showed an interesting difference in behaviour due to stirring. Mild steel in distilled water became considerably more noble in potential when stirred. The potential shift was five times that found for mild steel in saline pH 6.5. The introduction of chloride ions effectively depolarized the system both anodically and cathodically.

At moderate to high stress amplitudes the depolarizing effect with fatigue and concomitant stirring action was found to be greater in saline pH 6.5 than in distilled water. This finding was consistent with the reduced endurance for mild steel in saline at higher stresses. At low stress amplitudes both systems were less effectively depolarized. However, the corrosion potential with fatigue in saline pH 6.5 was far less noble and nearer the cathodic protective value [123] of -0.734 V (SCE) than that in distilled water (Section 2.6.5. Fig. R15). The change-over in the influence of the chloride ion with stress amplitude is thus seen, from this data, to be the result of a balance between depolarization and the shift in corrosion potential. This balance was found to be tilted in favour of a more protective potential with time in the solution containing chloride ions compared with distilled water. The improved corrosion fatigue performance at high cycle-low stress amplitude for mild steel in saline pH 6.5 found here was therefore not inconsistent with the electrochemical observations.

The results for plain specimens of S316, from Table 2 (page 206) and Figs. 18 and 19 (page 193) show that the chloride ion was responsible for a reduced fatigue limit; yet some of the widely scattered data for S316 in saline pH 6.5 suggested an improvement in performance. The scatter in the low amplitude region is such that the influence of the chloride ion is not clear from the S/N curves except at high stresses where

longer life definitely results from the addition of chloride ions. Observation of similar data, from Table 2 with Figs. 22 and 23 (page 197) and Figs. 26 and 27 (page 202) for T130 and T318 showed that the influence of chloride ions on these materials is insignificant at stress amplitudes near the fatigue limit. Again, however, it was noted that at the higher stresses the addition of chloride ions was beneficial.

The corrosion current density (Table 8) for S316 is increased by a factor of over 3 as the result of chloride ions in solution. The increase for T130 was slightly more than this while that for T318 was a little less at approximately 2.4. These significant relative differences had, however, no influence on the establishment of a fatigue limit in distilled water and saline pH 6.5. It is also difficult to see this difference as being responsible for the general improvement in fatigue resistance in saline over that in distilled water at high stresses. Anodic and cathodic polarization curves, Figs. 38 and 39, 42 and 43, 46 and 47, (pages 230 to 243) respectively showed that the effect of chloride ions was always to lower the unpolarized potential. An increase in the passive current density was produced with S316 but the opposite effect was found for T130 and T318. High stress amplitude corrosion fatigue potential traces (Figs. 55, 56 and 57) showed that less noble potentials were always produced in each system than those found near the fatigue limit; this is in agreement with previous

research [33]. However, each trace in saline pH 6.5 showed a considerable initial rise in potential, followed by a fall at film breakdown or dissolution and a further rise with film repair, which was barely noticeable in distilled water. These differences between behaviour in saline and distilled water were greatly magnified at the higher amplitudes of stress. Many times in this research it was found that a longer fatigue life was accompanied by less stable electrochemical behaviour. The mechanism of passive film growth, followed by a dissolution which removes cracks as they initiate, was considered to operate at high stress amplitudes more effectively when chloride ions are present: hence the improved corrosion fatigue performance in this situation.

Fracture surfaces examined generally did not show any clear evidence of the influence of chloride ions for T130 or T318. Surfaces formed in distilled water being very similar to those in saline. Mild steel, however (Fig. M5 (a) and M9 (a), Section 4.8.1.) showed improved ductility in saline pH 6.5 and the quasi-cleavage facets, found by TEM, in distilled water fractures, were absent. The results for S316 in saline pH 6.5 were noted for the scatter which had been remarkably absent in this research for all the other results. Photomicrographs (shown in Fig. M21 (a) to M22 (b)) were obtained showing quite different fracture surfaces for specimens having endurances at the extreme limits of the scattered results. "Low result"

specimens exhibited boundary granular attack with pitting in saline pH 6.5 when viewed by TEM. "High result" specimens showed instead a fracture surface covered with general corrosion products and nodular dimples. Normal, mid-scatter, result specimens produced fracture surfaces which were mid-way between these two extremes and which were very similar to the results in distilled water. The effect of the chloride ion here was critical and responsible for the scatter in the saline pH 6.5 results. Potentiostatically controlled tests produced results which helped to determine the difference in the nature of these fractures. Under controlled potentials of +50mV life was substantially shorter than at controlled potentials of -390 mV (SCE): the exact opposite order of performance found under "free" corrosion fatigue conditions. Without control "high result" specimens were observed to spend most of the test time at rest potentials near +50 mV, while the "low result" specimens were at -390 mV. Other experiments where potentiostatic control, at these two potentials, was interrupted for a short period showed that it was "loss of control" which accounted for the difference in performance. Potentiostatically controlled specimens at both potentials were not subjected to pitting. At the time of interruption of control, however, specimens at -390 mV were seen to suffer rapid pitting accompanied by the formation of a black film when control of potential was regained. Specimens at +50 mV in the same experiments had a far less

localized attack on interruption of control and had then longer lives than those at -390mV. This work went some way to simulating the conditions found under "free" corrosion fatigue, and enabled the scatter to be explained in terms of a critical combination of chloride ions and potential.

At +50mV a general passive film dissolution process on S316 was enhanced by chloride ions and localized breakdown of the film retarded. At -390mV passive behaviour under fatigue was less pronounced with chloride ions, leading to earlier film breakdown and pitting. Any average open-circuit potential between -390mV and +50mV was found possible for S316 in saline pH 6.5, producing a corresponding scatter of endurance data.

Because of the geometrical restrictions imposed by specimen dimensions in this work, it was not possible to study extended crack growth data. Examination of the striation spacings on fracture surfaces, however, indicated similar growth rates in distilled water to those in saline for all the materials tested; Table 9 (page 286). This finding is contrary to the results often found from crack growth studies, as discussed in Section 2.6.2.

5.1.2. The influence of low pH

Section 2.6.5. discussed the influence of pH as a controlled variable generally: here the results at pH 1.5

for saline solutions is discussed for each material. Table 2 (page 206) shows that the fatigue limit or endurance at pH 1.5 was always less than that at pH 6.5. Figs. 15 and 16, 19 and 20, 23 and 24, 27 and 28, (pages 188 to 203), all show that this reduction in performance exists at all stress amplitudes.

Mild steel at pH 1.5, not unexpectedly according to the potential - pH diagram (Fig. R15, page 73 Section 2.6.5.), showed H_2 evolution. Bearing in mind the limitations in application of Pourbaix diagrams for systems in equilibrium to corrosion fatigue processes, and modifications owing to the presence of chloride ions, it is neverthleess useful to discuss potential shifts with respect to such data. The initial corrosion fatigue potential moved with time towards a less noble, more protective, potential (marked 1' → 2'). Table 8 shows that the corrosion rate was increased by a factor of approximately 18 in the pH 1.5 solution over that at pH 6.5. The corresponding general corrosion was initially very rapid. Polarization curves (Fig.35 and 36) showed a more noble unpolarized potential at pH 1.5 than that found at pH 6.5; the effect of stirring was also greatly reduced. This finding was supported by similar results for corrosion fatigue potentials with cycling, Fig. 54 (page 255). The fracture surfaces (Figs. M13 (a) and M13 (b) for pH 1.5) showed large quantities of corrosion products around large etch-pits linking

across the crack front characteristic of the grossly enhanced rate of general corrosion at low pH.

Results for S316 in pH 1.5, Fig. 20 (page 194), showed that this steel performed in a similar manner to mild steel, developing a fatigue limit only at extremely low stress amplitudes: the reduction in performance at pH 1.5, from that at pH 6.5, at 88% was approximately double the reduction found for mild steel. Table 8 (page 221) shows that the current density at the lower pH was twice that found in normal solutions but far from camparable with the gross change found for mild steel. Polarization curves, Fig. 39 and 40 (pages 231 and 232), showed that in pH 1.5 a relatively more noble open-circuit potential was established, with dynamic conditions, and current density was reduced compared with that at pH 6.5. Corrosion rate was seemingly therefore not the cause of the poor fatigue performance of S316 at pH 1.5. Potential-time curves, Figs. 51 and 52, (pages 249 and 250) show that a less noble potential was found in pH 1.5 saline. Corrosion fatigue potential traces Fig. 55 were also found to result in failure in pH 1.5 at less noble potentials: they also failed to show the initial rise in potential, with subsequent fluctuations, so typical of S316 in saline pH 6.5. From these observations it would appear that in pH 1.5 saline the corrosion fatigue potential (marked 3'≃4' in Fig. 40 on page 232) as well as the static potential (marked 3→4) are within the "more

active" region compared with the more certainly passive behaviour (Fig. 39) found for pH 6.5. The effect of low pH here was to reduce the initial surface film formation and prevent subsequent repair of the weak film on breakdown. The longer life at pH 6.5 was predictable from the relative instability of the electrochemical parameters found indicative of passive film formation. The difference in behaviour was also predictable from the Potential - pH diagram (Fig. R15 page 73). At pH 1.5 the small potential shift with time (marked as 4') under fatigue remains in the zone of corrosion. At pH 6.5 similar data shows the diretion of potential shift with oscillations (marked Σ) into the passive region. The potential - pH diagram for the Cr/H_2O system (Fig. R32, page 145) however is usually thought more relevant to the behaviour of these stainless steels. A prediction from this diagram at the measured potentials (marked $3' \simeq 4'$), showed the dissolution to $Cr(OH)_2^+$ at pH 6.5 becoming dissolution of Cr to Cr^{+++} at pH 1.5. The process at low pH due to the alloyed Cr in the steel does not then result in the formation of a protective passive film. The diagram for the Ni/H_2O system, discussed in Section 2.8.2. Fig. R33 (page 145), showed that dissolution of Ni to Ni^{++} occurred at both low and neutral pH. It was interesting to note, however, that the oscillation of potential observed at pH 6.5 coincided with the line of theoretical corrosion of Ni which has not been found in practice. The

measured range of potential oscillation at pH 6.5 also crossed the active-passive domain for the Fe/H_2O system. Film formation at the more noble limit of the range and metal dissolution at the other limit is thus predicted from both the Fe/H_2O and the Ni/H_2O systems at pH 6.5. At pH 1.5 no such behaviour was observed.

The fracture surface of S316, fatigued in pH 1.5 saline, when viewed by TEM showed (Fig. M14 (a)) quite different features to those observed at pH 6.5. Small etch pits and an elongated "feather" morphology, similar to that frequently found in stress corrosion cracking tests for S316, was revealed. Striation spacing, however, was similar on fractures in both neutral and low pH saline, and it therefore seems that the reduced performance of S316 at low pH was due to a faster crack nucleation.

As discussed in Section 2.6.5. stainless steel in neutral solutions [159] can have local crevices where pH≃1. When pH<4 the fatigue performance has been recently found to be dramatically reduced[160]. The results of this research, at comparatively low frequency, confirm this for S316 in bending. The critical current density required for passivation has been found to increase with decreasing pH [160] a result which is also confirmed here (Figs. 39,40 and 41) for S316. The depassivating pH is thought to be a critical factor [161] for stainless steels so that fatigue strength decreases [142] with low pH can be explained in

terms of the electrochemical parameters observed and discussed in this research.

The result for titanium T130 at pH 1.5, resulting in a 25% reduced fatigue limit compared with that found for pH 6.5 saline, was quite understandable in view of the relative domains shown in the potential - pH diagram, Fig. R34 (page 146). Potential movements with time (marked 5→6) and corrosion fatigue potentials (marked 5'→6') at pH 1.5 were entirely within the corrosion domain. Similar data at pH 6.5 was clearly within the passive zone. An estimated concentration of approximately 10^{-4} at pH 1.5 for Ti^{+++} soluble ions, possibly becoming TiO^{++} later in the process, was predicted as the process for dissolution at pH 1.5, rather than the $TiO_2.H_2O$ passivating film at pH 6.5. Table 8, however, shows that the corrosion rate was nearly halved in pH 1.5 compared with pH 6.5. Corrosion potential-time data (Fig. 51 and 52) was similar at both pH values and this data, together with the initial steep rise in potential found under corrosion fatigue (Fig. 56), suggested that in fact some degree of passivity was present at pH 1.5. From electrochemical parameters it would appear that a passive film was initially rapidly built-up but, once ruptured, could not be effectively repaired in the pH 1.5 saline in competition with the process of metal dissolution. Fractographic studies did not show any clearly defined difference between the fracture surfaces

produced in pH 1.5 and pH 6.5. The reduced performance with fatigue in pH 1.5 was therefore thought to be the result purely of the initiation mechanism differences described.

The performance of T318 with fatigue in pH 1.5 compared with pH 6.5 was reduced by only 9% at the fatigue limit, a much improved result compared with T130. Table 8 shows a reduction in corrosion rate at pH 1.5 for T318. However, the reduction in this case is significantly more than that found for "pure" titanium. A factor of nearly 8 reduces the T318 value of i_{corr} to only approximately one third of that found for T130. Polarization diagrams (Figs. 47 and 48), together with potential-time results (Figs 51 and 52) showed that relatively more noble potentials were attained in the pH 1.5 saline. This result was further supported, as shown in Fig. 57, by corrosion fatigue potential traces with cycling. Once more it was noted that electrochemical parameter instability (marked ≷ with dynamic results 5'→6' superimposed on Fig. 47) accompanied improved endurance: such oscillations were absent at pH 1.5. Photomicrographs also showed very little difference between fractures at pH 1.5 and pH 6.5. Both systems exhibited passivity under corrosion fatigue so that pH changes from 6.5 to 1.5 had very little effect on fatigue performance for T318.

5.1.3. The influence of high pH

Table 2 (page 206) shows that pH 11.5 saline solutions

reduced to nearly the same extent the fatigue performance of mild steel, compared to neutral solutions, as did solutions of low pH. This was a rather unexpected result in view of previous work at slightly higher pH where a certain passivity was shown together with the establishment of a fatigue limit near that for air [123,162] (Section 2.6.5.). The prediction from the potential-pH diagram, as shown in Fig. R15 (page 73) with the measured potential movement (marked 1→2), is for passive behaviour with a possible $Fe(OH)_3$ film initially formed on the steel surface possibly becoming $Fe(OH)_2$ with time. The final position on the diagram was, however, noted to be in the vicinity of the high pH corrosion zone. At high stress amplitudes the performance in pH 11.5 was very similar to that in saline pH 6.5, much improved over results at pH 1.5. It was at low stress amplitudes in this research where performance at pH 11.5 was so disappointing for mild steel. The estimated corrosion rate at pH 11.5 was slightly lower than that at pH 6.5, and certainly of a different order from that found at pH 1.5 (Table 8). Polarization curves (Figs. 35 and 37) showed clearly that mild steel in saline at pH 11.5 had an unpolarized potential considerably more noble than that measured in pH 6.5 saline. A slightly more noble potential in pH 11.5 saline was in fact produced than the unpolarized value found in distilled water (Fig. 34). The main difference here between the behaviour of mild steel at pH 11.5 and other solutions, however, was that

the unpolarized potential moved in a less noble direction under conditions of stirring. This effect was in the reverse direction to that found for any other material/ environment system. The behaviour in this case, although unlike that for mild steel in the other solutions, was certainly not characteristically passive.

Potential-time curves (Fig. 53) in saline pH 11.5 for mild steel showed some minor fluctuations in their otherwise gradual change to less noble potentials. Some attempt at film formation was thus indicated, but the overall change to less noble potentials was such that passive behaviour was not promoted here. The final potential at long endurance, as shown in Fig. 54 (page 255) indicated, in fact, the least protection for general corrosion at pH 11.5. Fracture surfaces for mild steel in saline pH 11.5, as shown in Figs. M17 (a) and M17 (b) (pages 283 and 284), showed finely spaced striations, the only system in which these were found except for fatigue in air.

The evidence thus shows that, during this research, mild steel in saline pH 11.5 suffered early general corrosion resulting in eventual crack initiation. A tendency towards passivity was evident but not effective except possibly during the very short time of crack propagation.

Results for S316 show that fatigue performance in saline pH 11.5 is slightly improved at low stress amplitudes, with considerably less scatter, over those obtained in neutral saline

(Table 2, Figs. 19 and 21): the performance at higher stress amplitudes, however, was less satisfactory than at pH 6.5. Observation of the fracture surfaces for S316 did not reveal any significantly different features for specimens fatigued in saline pH 11.5 from those seen at pH 6.5 or distilled water. Potential-pH diagrams (Figs. R15, R32 and R33) with the observed potential ranges (marked 3→4) showed passivity for the stainless steel with Cr dissolution to CrO_4^{--} . The domains were more clearly defined at pH 11.5 so that the more stable passivity was predictable. The corrosion current density at pH 11.5 was reduced, from that measured in neutral saline, by a factor of 15. Polarization curves (Figs. 39 and 41) showed that a distinct critical current density was absent in pH 11.5 saline and that the passive range to breakdown potential was considerably extended compared with pH 6.5 results. The large range of potential oscillation found for pH 6.5 corresponded with the natural critical current density and breakdown potential positions found by anodic polarization experiments. The almost complete absence of such oscillations of potential for pH 11.5 corresponds with the improved range of passivity found. At high stress amplitudes, however, the dynamic line (Fig. 41) for anodic polarization shows that the breakdown potential occurs at much less noble potentials so that conditions for passivity within the measured potential range were far less stable at high stresses. The estimated

corrosion rate was also clearly considerably increased by stirring and the application of fatigue load. The influence of stress amplitude on breakdown potential was further confirmed by the corrosion fatigue potential-cycles trace (Fig. 55) at pH 11.5. Fatigue limit specimens showed a breakdown of passive film in the region of -0.03 V (SCE) whereas -0.16 V, for example was recorded at $\pm$ 350 MN/m^2. High stress amplitudes are thus seen clearly here to result in earlier breakdown of the passive film in pH 11.5 than for fatigue in saline pH 6.5. These observations account completely for the differences in behaviour under low and high amplitude stress between high and neutral pH saline solutions.

Table 2 showed that the fatigue limit in pH 11.5 was not substantially different to that found for neutral solutions for T130 and T318. In the case of T130, however, the endurance of specimens at stress amplitudes above the limit was substantially reduced at pH 11.5: a similar result to that found with S316. The estimated corrosion rate for both titanium materials was also comparable with S316 in saline pH 11.5, being substantially reduced from their respective values in neutral saline (Table 8). Polarization diagrams for T130 showed the same difference between pH 6.5 and pH 11.5 (Figs. 43 and 45) as that found for S316. The neutral saline behaviour, despite its two-step anodic polarization characteristic, was unaffected by stress. The saline pH 11.5 anodic polarization, however, was considerably

changed in character by stirring and dynamic load. The breakdown potential was depressed in a similar manner to that found for S316. Similar curves for T318 (Figs. 47 and 49) showed that there was no influence of stress on the polarization of this material in either saline pH 11.5 or pH 6.5. These findings are consistent with the result that corrosion fatigue performance was similar at all stress amplitudes for T318 in high and neutral pH saline. They are also consistent with the result that, while the fatigue limit is similar for high and neutral pH saline, the high stress amplitude performance of T130 at pH 11.5 was considerably reduced compared with that at pH 6.5. The reason for this result for T130 is also consistent with the result for S316 discussed above. In addition, it was noted that potential-time curves (Figs. 51 and 53) for T318 were almost identical for pH 6.5 and pH 11.5, while for T130 the potential progress towards more noble values at pH 11.5 was much slower than that attained in pH 6.5. The potential range superimposed on the potential-pH diagram (Fig. R34, Section 2.8.2.) predicted passive behaviour at pH 11.5 although this was close to the corrosion zone at pH$\geq$12. Passive behaviour was in fact observed during corrosion fatigue for titanium T130 and T318, However, the protection offered by the passive film at high stress amplitudes for T130 is less effective than that in neutral pH saline solutions. In this respect T130 is similar in its behaviour to S316.

5.1.4. The influence of drilled holes

Corrosion fatigue limits or endurances, for the various material/environment systems tested, are shown in Table 2 (page 206). The results obtained for plain specimens have been discussed in the preceding sections. The results for specimens with drilled holes were frequently found to reveal an interesting difference in behaviour from that of plain specimens.

All results for stress amplitude were calculated on the basis of average stress in bending across the net material width at a hole. Identical S/N curves for plain specimens and specimens with a hole would therefore indicate that any stress concentration or the effect of localized strain at the edges of the hole, was of no consequence. Differences in fatigue performance, at the same stress amplitude, between the various environments should describe the environmental contribution in fatigue in the presence of a drilled hole.

Mild steel in air results, Fig. 10 (page 184), showed that drilled holes are effective in reducing the S/N curve downwards, so that the notch reduction factor N (equation 39, page207) given in Table 3 (page 209) for 2 mm diameter holes, was 0.49 at the limit. The value of N was somewhat higher at high stress amplitudes showing that the presence of a hole was less damaging in this region (i.e. N = 1 indicates no effect on equivalent cross-sections). Data for the smaller hole

(Fig. 10) showed that, in this material, a 1 mm hole was less damaging throughout the stress amplitude range than the larger diameter hole with equivalent material cross-section. A clear stress concentration effect of holes was therefore established for mild steel, in accord with previous research [108], during reverse bending fatigue. Distilled water immersion showed that results for the specimens with small diameter holes were again less damaging than those with the larger holes. The environmental effect found for plain specimens which resulted in the double "knee" S/N curve, Fig. 14 (page 188) was completely modified to give a single rate curve in the presence of a hole. The corrosion reduction factor C (equation 40), varied considerably with stress amplitude, but the value of I showed less variation. An increasing deviation of I from -1 generally at the lower stress amplitudes was observed.

Immersion in saline solutions (Figs. 15 to 17) produced a double rate curve for specimens with holes, similar to that found for the corresponding plain specimen S/N curve. The same overall mechanism would therefore seem to apply here for both types of specimen at all stress levels. The total effect of introducing a hole in mild steel on the corrosion fatigue endurance, shown in Table 1, was extremely damaging in respect of high cycle performance. The multiple regression model, equation 44 (page 214), developed to predict

the interaction I, to within 0.078 standard deviation for all mild steel/environment combinations showed that N and C produced opposite contributions to I. The notch reduction factor N was contributing towards a more negative interaction I, while the corrosion reduction factor C contributed towards a more positive value for I. For this reason it is not possible to say here that any particular value of I represents zero interaction. It is a limitation of the model used here that, while the total effect may be predicted with equations 41 and 44, it is not immediately obvious from the value of I whether the effect is greater or smaller than the effect of each factor considered separately.

Referring now to the S316 results for drilled holes (Fig. 11 and Table 2) in air, it was found that the presence of such notches had very little effect indeed! This material was found to be highly tol erant of such notches when subjected to fatigue in air. Table 4 shows that the values of N found were near unity for high stress amplitudes and, at 0.887 for the fatigue limit value, approximately double the value obtained for mild steel. In distilled water (Fig. 18), the improvement over the performance in air found near the fatigue limit for plain specimens was not produced for specimens with holes. Holes of 1 mm and 2 mm diameter produced the same results near the fatigue limit in distilled water as in air. Whatever mechanism was responsible for the increased fatigue

limit in distilled water, it was obviously rendered inoperative by the presence of a hole. Data in saline pH 6.5 showed more precise results for specimens with holes than for the plain specimens discussed previously. The same fatigue limit (Table 2 and Fig. 19) was obtained for both sizes of hole and similar performances were produced in saline pH 6.5 to those in distilled water and air. Tests at pH 11.5 (Fig. 21 and Table 2) showed identical results for specimens with or without holes above the fatigue limit, and also very little change in fatigue limit because of the introduction of a hole. These results for S316 suggested that while the presence of a hole did not significantly reduce the air fatigue performance, calculated on net cross-section, it did cause the earlier breakdown of the protective passive film. Film breakdown at the edge of a hole, where the strain was maximum, was deferred at pH 11.5 by the more protective film formed in this solution, together wihh the improved stability discussed in the previous Section. At pH 1.5 the drastic reduction of endurance life discussed previously for plain specimens was also found for specimens with holes. Except for some deviation at intermediate stress amplitudes the results obtained for specimens with holes were identical to those for plain specimens (Figs. 20, Table 2). This result confirmed the high tolerance of S316 to the presence of drilled holes in all the tested environments. Table 4 (page 210) showing the range of values for C and I obtained, was found to separate

the results of saline pH 1.5 quite clearly from those of the other environments. Fatigue limit corrosion factors $C \simeq 1$ were obtained for passivable behaviour and approximately one tenth of this value for C was produced at pH 1.5 saline. In spite of this clearly different result for pH 1.5, the interaction factors I obtained were not so different. Saline pH 1.5 results for S316 were well described by the model represented by equation (44) which was also applied to mild steel in all environments. The behaviour of S316 in saline pH 1.5 was thus grouped together with mild steel for corrosion fatigue under non-passive conditions. S316 in all other environments, however, produced results which could only be satisfied together in the model by quite a different interaction relationship, equation (43) (page 214). This relationship was found to predict passive corrosion fatigue behaviour, and the essential difference in this relationship was one of factor sign. Both N and C were found in this case to contribute to a more negative interaction factor I. For passive behaviour it was then possible to recognise values for $I < -1$, from the results in Table 4, where synergistic behaviour caused a reduction in fatigue life greater than the sum of notch and corrosion effects considered separately. On the other hand S316 in saline pH 11.5 with $I > -1$ at the fatigue limit, exhibited synergistic behaviour with reduction in fatigue life less than that of the notch and corrosion effects separately. This result

where $I > -1$ for passive behaviour corresponded with the result shown in Table 2 for pH 11.5 saline.

The equation (43) relationship form for the model was found to be applicable to T130 and T318 in all environments as well as to S316 for distilled water, saline pH 6.5 and pH 11.5. $I > -1$ was again found for T130 in distilled water and saline pH 11.5 where combined effects of notching and corrosion were actually less than the sum of the separate reductions in corrosion fatigue performance. (Tables 2 and 5) The opposite resultant behaviour was noted in every other case, where $I < -1$. The model which was fitted to all the results, irrespective of the value of I, was thus found to be generally applicable to any of the passivable metal/environment situations in this research with titanium and stainless steel. Table 2 and Fig. 12 show that for T130 in air the effect of a 2 mm diameter hole was considerable at high stress amplitudes. The 1 mm hole was less damaging for the same net cross-section. At stress amplitudes near the fatigue limit the damaging effect of the smaller hole was greater. Table 5 (page 211) shows the variation of notch factor N with endurance for 2 mm diameter holes. These results for T130 are contrary to all other results found in this research. Values of N for T130 were found to increase with increasing endurance life so that the notch effect for this material was seen to be more

damaging at high stress amplitudes than at low amplitudes of stress. For all other materials the reverse result was established. The results for 1 mm holes showed less high to low amplitude variation of notch sensitivity, so that the size of the notch was an important feature in these results.

S/N curves for T130 in distilled water (Fig. 22) and in saline pH 6.5 (Fig. 23) also showed interesting differences in the order of damage for the large and small diameter holes. The cross-over in the curves for air was not found under immersed conditions. Distilled water fatigue limits for T130 for 1 mm and 2 mm diameter holes were not significantly different from those established respectively for each size in air. Saline pH 6.5 results showed that 1 mm diameter holes were slightly less damaging to the fatigue limit in this case than for distilled water. The mildly improved situation for 1 mm holes in saline, was however, surprisingly turned into a considerable reduction in performance in saline for the 2 mm diameter holes. Compared with the performance in distilled water, the decrease in fatigue limit for the specimens with the larger hole was quite drastic. Why was it found here that saline caused increased notch sensitivity for the larger holes while at the same time causing reduced notch sensitivity for the smaller holes at low stress amplitudes? The smaller hole was clearly more damaging in distilled water, yet in saline it was actually the larger hole which was more damaging at all

stress amplitudes. Can the mechanism involved for saline corrosion fatigue be similar to that for air at high stress amplitude, where a similar order of hole size damage effect was noted (Figs. 12 ane 23)? And, by similar results, can the mechanism involved for distilled water corrosion fatigue be that operating in air for low stress amplitudes (Figs. 12 and 22)? The results a least indicate differences in mechanism for interaction between geometric size variables, stress and environment. From a stress concentration analysis, K_f = 1.52 for the 1 mm diameter hole and 1.45 for the 2 mm diameter hole [108,242,341-342]. The smaller hole was therefore slightly more damaging in theory than the larger one. As discussed in Section 2.4.3, however, environmental interactions have been known to change the order of such values. Here it would seem that the reversal of the damaging order for holes in T130 with saline pH 6.5 is not simply an environmental effect since a similar result was obtained at high stress amplitudes in air as well as for mild steel generally.

The results for T130 specimens with holes in saline pH 1.5 (Fig. 24) were quite distinctly different to those obtained in saline pH 11.5 (Fig. 25). The much lower fatigue limit for plain specimens in pH 1.5 was further reduced substantially when holes were introduced, so that the limit was not established below 10^6 cycles. By contrast the fatigue limit of T130 in saline pH 11.5 was reduced insignificantly further by the

presence of a hole. The high stress amplitude results, however, showed that the presence of a hole was more damaging at pH 11.5: the fatigue limit was established earlier than 10^5 cycles. T130 was thus seen to be notch sensitive in saline pH 1.5 at low stress amplitudes but not so sensitive at higher stresses. In pH 11.5 saline the reverse order of notch sensitivity with stress amplitude was found to that for pH 1.5. Comparison of these results with those for T130 in air (Fig. 12) shows that high stress amplitude results in air are very similar to pH 11.5 saline results, while fatigue limits in air and distilled water are not significantly different from pH 11.5 saline with 2 mm diameter holes. The results for pH 1.5 are quite different from those in air with holes in T130, and represent unacceptably poor performance at low stress amplitudes.

T318 was much more sensitive to the presence of drilled holes in air (Fig. 13) than T130 at the fatigue limit. Much of the advantage therefore, in using this high fatigue strength material, was lost when holes were present: a 45% improvement for T318 over T130 with plain specimens in air fatigue, was reduced to one of only 15% here for specimens with a drilled hole. Table 2 and Fig. 26 shows that when fatigued in distilled water this notch sensitivity is further enhanced. The fatigue limit for plain specimens, as discussed earlier, was actually increased over that obtained in air. Owing to the presence

of a hole, however, the corrosion fatigue limit was dramatically reduced: a 53% reduction in fatigue limit as the result of the hole in T318 with distilled water, compared with a reduction of only 30% in air because of a hole. The reductions of fatigue limit in saline solutions (Figs. 27 - 29, and Table 2) were also similar to that found for distilled water for specimens with a hole. Neutral saline solutions were less damaging than other solutions, but generally the presence of saline had little effect on the performance of specimens with a hole. Table 6 (page 212) illustrates that the corrosion factor C had little effect for any solution tested: i.e. it was near unity at the fatigue limit. The value of the notch factor N was clearly the dominant feature here respeonsible for the reduced fatigue limit. Above the fatigue limit the S/N curve for both plain and holed specimens was unremarkable in shape for air fatigue. For all immersed solution environments, however, the curve obtained was nearly vertical, illustrating that endurance was almost independent of stress amplitude. A mechanism, different to that operating for T318 in air, and largely independent of stress amplitude, chloride ion, and pH would seem to operate. The presence of a hole in T318 here drastically reduced the threshold for crack initiation with this common mechanism. No similar result was found with a hole for other materials.

5.1.5. Mechanisms

A variety of theories and mechanisms which have been advanced to explain the behaviour of corrosion fatigue was discussed in Section 2.7. The S/N curves obtained in the results here together with the interaction analysis has enabled the passive behaviour to be clearly separated from the non-passive corrosion fatigue irrespective of material. In Section 2.7.1. a classification, for passive behaviour, based upon the existence or otherwise of a corrosion fatigue limit was observed to be in general use: "true corrosion-fatigue" being referred in the literature to the case where no limit was observed. It seems likely, however, that some fatigue limit will always exist if only testing of materials is conducted at sufficiently low stress amplitudes. In the case of mild steel this was found here to be $<3 MN/m^2$ for saline pH 1.5 and such a limit, if it exists, is hardly of practical use. In the case of S316 in pH 1.5, however, a fatigue limit was established at 35 MN/m^2. This limit was clearly established as the level of stress amplitude below which corrosion fatigue failure was not possible in saline pH 1.5 for S316. For all practical purposes this limit was unacceptably low and normal passive behaviour for this material was not observed. Was this therefore an example of "true corrosion fatigue" even though a fatigue limit was established? The behaviour of S316 during fatigue in saline pH 1.5 was not described by the traditional

definitions, unless "true corrosion fatigue" results are considered above some limit of fatigue too low to be of practical importance. Such a limit probably exists in all cases but has remained undetermined in most research because of frequency and time constraints.

Truly passive behaviour during corrosion fatigue in all solutions tested was confirmed for all medical implant alloys except in the case of S316 in saline pH 1.5, using the same multiple regression model for interaction, equation (43). The behaviour of mild steel in all environments tested and that of S316 in pH 1.5 saline was described using another variation of the model, equation (44). This separation in the model between passive and non-passive corrosion fatigue by the sign of the corrosion factor constant was considered significant and useful. A negative constant was characteristic of passive behaviour and a positive one characteristic of fatigue in the active condition.

Landgraf's classification of fatigue behaviour [40], discussed in Section 2.7.2. puts this present research clearly into the low stress amplitude-high cycle fatigue category. This classification of strong, tough, and ductile metals into progressively steeper slopes for strain controlled endurance curves was, however, not found generally applicable to the results. Reference to Table 1 (page 177), shows that T318 was the strongest and least ductile material tested, yet it produced the steepest S/N curve slope above the fatigue limit in air. T130, by comparison, was more ductile and not so strong, yet it

exhibited less than half the S/N curve slope found for T318. These were strain controlled tests in air and the reverse order of slope should have been found according to this classification of mechanical properties. The results in corrosion fatigue for all the other solutions tested showed a similarly contrary order of magnitude for slope. A general classification of the results here according to mechanical properties was therefore not appropriate in terms of Landraf's analysis.

The comparatively short time observed for crack propagation, being $<0.005\%$ in any experiment, was consistent with the striation spacing found on the fracture surfaces. Assuming one striation per cycle progressing across the entire depth of the 3.18 mm specimen (a most improbable happening) at 1 μm spacing, this represents 3.18×10^3 cycles for propagation as an absolute maximum. At the maximum observed time of 0.005% endurance this corresponds to a total endurance life of approximately 6.4×10^7 cycles. Since this is outside the range for these experiments it is evidently the case that crack initiation exceeded 99.995% of the total life for this research. Mechanisms responsible for corrosion fatigue fracture here were primarily those of crack initiation.

Several mechanisms were discussed in Section 2.7.4. and the experimental evidence which has been found to support some of these is considered here. The critical corrosion rate

below which a fatigue limit may be established has been advanced as an important factor for corrosion fatigue [149,123] (Section 2.6.4.) For steels it has been suggested that a critical current density of at least $2\mu A/cm^2$ was necessary to nucleate a crack. Since this current density is equivalent to only 1×10^{-4} atomic layers per stress cycle, it cannot be responsible for crack nucleation on its own. It must represent an overall rate when local rates are very much higher. The overall rates recorded in this research are shown in Table 8. For mild steel, except for pH 1.5 saline where the current density was far in excess of the "critical" value, the rates were approximately half that suggested to nucleate a crack, yet no fatigue limit was produced in any solution. A much lower critical current density than $1\mu A/cm^2$ was indicated therefore, if overall rates are a significant indication of the existence of a fatigue limit. Local dissolution rates, which are difficult to measure, are important but it seems that the effects of total dissolution behaviour might be extremely small for active corrosion during fatigue. The results for S316 in saline pH 1.5, as discussed in Section 3.4.4, showed certain similarities with the behaviour of mild steel. The corrosion current density was a tenth of the critical value and a fatigue limit was indeed produced, albeit a very low one. Local rates in this solution were probably very similar to the overall rate and therefore also below the critical value. However, for the other

solutions with mild steel, local rates were probably far in excess of the overall rate and therefore well above the critical value. Again, in pH 1.5 saline the high corrosion current density, recorded as an overall rate, was probably similar to the local values. The idea of a critical corrosion rate as a factor in the mechanism of active corrosion fatigue is not incompatible with these results.

Pitting, as discussed in Section 2.7.4, cannot be regarded as a general mechanism for fatigue crack initiation. It is probably more the result, and not the cause, of corrosion fatigue cracking. S316 in saline pH 6.5 producing the large scatter of results, discussed in Section 3.4.1, was an example here of pitting on the surface of some specimens during fatigue. Photomicrographs clearly showed this pitting (Fig. M21 (b)) on the fracture surface also. The passive layer was destroyed by chloride ions at the grain boundaries for these specimens. Cracks initiated in this situation at pits simply because they were, by geometry and corrosion history, the more anodic sites. Preferential dissolution of emergent slip steps here, in the same way as from the surface of an unpitted material, being the likely mechanism for fatigue.

The absorption of a liquid on the metal surface, causing a reduction of surface energy [245], has been advanced as a mechanism of fatigue in distilled water for mild steel. The difference in the air and immersed solution results could owe

something to this mechanism in the very early stages of fatigue cycling for all materials. It has, however, many limitations as an overall mechanism, as discussed in Section 2.7.4. The results for stainless steel and T318 in distilled water showed that the fatigue limit was higher than in air, a fact which is not compatible with a reduction in surface energy It is also unlikely that the higher fatigue limit was the result of a cooling effect in aqueous solutions at the relatively low frequency of cycling used here. An oxide removal mechanism [246], however, could account for a vertical displacement of the S/N curve in either direction relative to air. The reduction in fatigue limit in aqueous solutions is the likely result of increased rates of oxide growth and removal so that it is less effective in protecting the underlying metal from selective attack. An increase in fatigue limit over that found in air could result, however, from a high rate of uniform anodic dissolution[236] so that cracks are removed as they form in the oxide. A different result could also be obtained at different stress amplitudes with the uniform anodic dissolution mechanism. At higher amplitudes of stress for materials other than titanium, fatigue strength could be reduced by oxide interaction at PSB's. At lower stress amplitudes, oxide removal is more likely to remove the cracks as they nucleate in the oxide and produce a fatigue limit sooner. The cross-over in S/N data frequently observed, relative to performance in air, could be explained in terms of such a mechanism. S316 in distilled water and pH 11.5 saline, with T318 in all solutions except

pH 1.5 saline, were examples of such a cross-over phenomenon in this research. It would appear that this mechanism represents a strengthening component within the overall weakening mechanism of "true corrosion fatigue", however ill defined!

A critical passive current density has been advanced as a cause of failure during fatigue in the passive state provided the pH is low enough[142]. Steels have been noted to be more sensitive to fatigue failure in the passive state the higher the current density required for repassivation. Reference to Figs. 38, 39 and 41 with Table 2, as indicated below, shows that for S316 this relationship between endurance limit and relative passive current density is confirmed.

Distilled water	330 MN/m^2	0.20 $\mu A/cm^2$
saline pH 11.5	320 MN/m^2	0.32 $\mu A/cm^2$
saline pH 6.5	300 MN/m^2	0.56 $\mu A/cm^2$

A mechanism whereby, following rupture of the passive layer by a slip step, the local area is repassivated as metal is dissolved is most attractive here. Both from mechanical and electrochemical considerations, this weak passive-filmed-notched area would be activated repeatedly so that a crack is nucleated. Cracks would, by this mechanism, be nucleated faster with higher local dissolution of metal the higher the current density for repassivation. Such a mechanism fits the results obtained for S316 and accounts for the appearance of the relatively few cracks observed compared with active state corrosion fatigue. It also accounts for the grain

boundary localized attack found on some stainless steel specimens and the eventual generation of pits.

Hydrogen embrittlement by adsorption at cathodic areas is not a general mechanism for low stress amplitudes[252]. However, as discussed in Section 2.7.4 (page 103), pseudo-elastic materials[198, 200] (page 91), such as T318, have been found to initiate cracks as the result of internal stress intensification in the high cycle range. This is an alternative mechanism of mechanically generating cracks rather than the PSB formation responsible in "plastic" material. Initiation of cracks in T318 type material has been observed at the interface between the hcp α-grains and the bcc β-grains without detectable slip[201]. A hydride layer which is a hard and brittle phase is thought to form on the surface of these titanium alloys during cathodic charging which should serve as loci for crack initiation. The presence of a hydride on commercially pure titanium, however, has been found not to impair its ductility[253, 256]. The initiation of cracks generally in titanium is thus thought to owe something to a H_2 embrittlement process[254]. As discussed in Section 2.7.5, crack growth of titanium alloys in NaCl solutions is also thought to be the result of H_2 embrittlement[282]. The evidence of the present research, whereby near vertical S/N curves were obtained for T318 above the fatigue limit, strongly suggests a mechanism different from that operating for the other materials. The data for T318 were clearly quite different in many ways from those of commercially pure titanium T130. The results in air for T318 show that the S/N curve has a slope just over twice

that of T130, Figs. 12 and 13 with equations (7) and (8) (page 218). In distilled water the slope for T318 was ten times as large while the slope for T130 increased only slightly, Figs. 22 and 26 with equations (24) and (35) (pages 229-233). The very substantial difference in the behaviour of T318 from that of T130 when fatigued in aqueous solutions, which was not so apparent for fatigue in air, suggests that H_2 embrittlement could be responsible. Such a mechanism could explain why, above the fatigue limit, the fatigue life was relatively independent of the stress amplitude. Crack initiation was seen to be a primarly time dependent process. Fracture resulted after a certain number of cycles, $<10^5$, regardless of stress amplitude, salinity and pH (Figs. 26 to 29). A minimum amplitude of stess, corresponding to the fatigue limit, was apparently necessary for the mechanism of embrittlement and crack initiation. Further increasing amplitudes of stress, thereafter had very little influence on the acceleration of the process.

Apart from explaining the results obtained for T318 with plain specimens, a mechanism of H_2 embrittlement could also explain the very large sensitivity to notching found for this material. The brittle hydride layer would be more easily ruptured by stress concentration at the edge of a hole. As discussed in Section 2.8.1, smooth specimens of titanium implant alloys have similar fatigue limits in aqueous environments to those in air[296-299]. This finding was confirmed in this research generally, except for the low pH saline

(Table 2). Specimens having a 2 mm diameter hole in this research with T318, however, showed that the fatigue limit was significantly lower than that in air. Other research with steel specimens, as discussed in Section 2.7.2 (page 80), having transverse holes showed that PSB's appeared earlier than for plain specimens near the edge of holes owing to stress concentration[24]. With cold working resulting from drilling of the holes, crystallites adjacent to the edge of holes were strengthened so that slip started some 70 μm from the edge. No other difference was noted between plain specimens of steel and those with holes. Stress concentration for "plastic" materials seems responsible for both lowering the fatigue limit and reducing the endurance life of specimens generally: i.e. S/N curve is moved downward and to the left. For the so called pseudo-elastic materials such as T318, however, stress concentration will be responsible for reducing the fatigue limit only: i.e. S/N curve is moved downward only. Since a PSB mechanism is not found for these materials, endurance life is not reduced so dramatically by stress concentrations at higher stress amplitudes. The results obtained for T318 with 2mm diameter holes (Figs. 26 to 29) clearly support a mechanism of H_2 embrittlement for initiation at the edge of the hole, owing to increased probability of hydride film rupture with stress concentration. The minimum stress amplitude required for the embrittlement mechanism, the fatigue limit, is thus considerably reduced by the presence of the hole. The effect of a hole in T318 was therefore much greater than in any other material tested in reducing the corrosion fatigue limit.

5.2 Conclusions

The corrosion fatigue performance of some surgical implant alloys, in reversed bending at a typical frequency for human limb movement, has been investigated. A rather different performance picture was presented here than that to be concluded from some earlier work at much higher test frequencies and with push-pull or rotating bending load arrangements[62, 318-322]. In this respect the importance of more realistic test conditions has been emphasized.

In addition to presenting results in body saline under more realistic loading, the performance of the materials in an extended range of the normal body environment has been determined. Performance with high pH, encountered perhaps in sterilization and cleaning processes, and with low pH for post operative shock and crevice conditions in service, has been examined. The drilling of holes in surgical implant alloys when fitting is not uncommon, and the effect of this on subsequent corrosion fatigue life has been found to vary considerably from one material to another.

Comparison with the results for mild steel in the same range of environments, and for implant materials in air and distilled water, has widened the scope of this investigation. Metal/environment combinations resulting in either active-state corrosion fatigue or passive-filmed fatigue were thereby more easily studied and separated. A variety of electrochemical measurements and electron fractography studies, together with

an analysis of S/N data, provided evidence to support various mechanisms for the nucleation of a crack. This research produced results which were compatible with 99.995% of the total fatigue life spent in crack initiation.

The behaviour of mild steel in all the environments tested, and that of S316 in pH 1.5 saline, was described using a single model, equation 44 (page 214), for interaction between stress concentration and corrosion during fatigue. A different model, having the opposite corrosion factor sign, equation (43), was found to represent all other metal/environment combinations tested here. The two models represented active-state corrosion fatigue for S316 in pH 1.5 saline and for mild steel generally while passive-state corrosion fatigue was represented in all other cases. The idea of a critical corrosion rate as a factor of the mechanism for active-state corrosion fatigue was not incompatible with the results obtained. A similar requirement for a critical passive current density was compatible with the results for S316, in all environments except pH 1.5 saline. An oxide removal mechanism was considered as a possible explanation of "higher-than-air" fatigue limits and "cross-over" between aqueous and air S/N curves. Such a mechanism could have accounted for the S316 in distilled water, and saline pH 11.5, results. It could also have been a mitigating factor in the overall mechanism for T318 which was considered to be primarily that of hydrogen embrittlement. T130 showed that, contrary to all other results, notch effects were greater at higher stress amplitudes than

near the plain specimen fatigue limit. This difference between T130 and T318, together with a lower strength and greater ductility for T130, seems likely to account for the sensitivity to stress amplitude above the fatigue limit for T130 which was not found with T318. The early fracture of a brittle hydride layer on the surface of T318 by stress concentration at the edge of a hole, was considered to be a probable explanation for the drastic reduction in fatigue limit for this material in the presence of a hole.

The influence of the chloride ion on the fatigue performance of each material was investigated. For mild steel a remarkable improvement in high cycle fatigue performance was found in saline pH 6.5 compared with that in distilled water. The opposite effect was produced at higher stress amplitudes and this behaviour was related to a change in electrochemical variables with stress. Chloride ions were found to reduce the fatigue limit of S316 slightly and to have an insignificant effect on T130 and T318. At higher stress amplitudes, however, the addition of chloride ions was found to be beneficial for the passive-state material/environments, unlike the effect produced with active-state corrosion fatigue. A wide scatter band of results was obtained for S316 in saline pH 6.5 and attributed to instability of passive film breakdown. This instability was manifest in open-circuit, potentials oscillating in the region -390mV to +50mV (SCE). Local breakdown of the passive film with pitting and shorter life was produced at -390mV. A more general passive film dissolution process appears to have been enhanced by chloride

ions at +50mV, so that localized breakdown was delayed.

The influence of low pH on S316 was dramatic. Passive behaviour at pH 6.5 and pH 11.5 in saline, as well as in distilled water, was not observed at pH 1.5. Active-state corrosion fatigue behaviour was produced instead during the acceptably useful stress amplitude range. A fatigue limit, of academic interest only, was determined at only 35 MN/m^2, compared with 300 MN/m^2 at pH 6.5 in saline. T130 was also substantially reduced in fatigue limit by saline at pH 1.5, but no significant influence of pH on the performance of T318 was found. The drilling of holes in specimens was compared on a net cross-section basis for each material. Mild steel generally showed a stress concentration effect, moving the S/N curve downward, but it was found that no such effect was produced for S316. Thus stainless steel was shown to be very little affected by the presence of a hole. By contrast the fatigue limit of T318 was approximately halved as a result of a hole in distilled water and in saline solutions. The reduction in fatigue limit for air with T318 was 30% and it is clear that this material is very notch sensitive. The behaviour of T130 was less dramatic with respect to reduction in performance in the presence of holes. Some interesting differences in order of reduction was found for holes of different size. Further research is required to fully evaluate the effect of this geometric variable generally. However, it was shown that 1 mm diameter holes are more damaging than 2 mm diameter holes for T130 in distilled water and in air: the reverse result was shown in saline pH 6.5. The dramatic reduction in the performance of T318 can be judged by the

results for distilled water and saline pH 11.5 with 2 mm diameter holes: T130 has been found to have a higher fatigue limit than T318 in these solutions.

The evidence produced during this research shows that the use of S316 for surgical implants cannot be recommended where conditions of low pH are known to exist. It is generally believed that low pH saline solutions have to be resisted during corrosion fatigue in service, especially if crevice situations arise. The fact that current orthopaedic practice has not yet revealed widespread failures, attributed to the corrosion fatigue of stainless steel, may indicate that prolonged acid conditions are infrequent.

Since T130 plain specimens were found to have a lower endurance limit in all environments tested than T318, the latter material would normally be preferred. The advantage of using the higher strength alloy T318, also with excellent corrosion resistance, was clearly seen to be lost, however, when a hole was drilled through the material. Research into alternative ways of producing holes in practice, or of subsequently strengthening the surrounding material, would be very valuable for T318. Reservations have been noted regarding the possible further damage by fretting corrosion with alloys such as T318. Further research is required to fully evaluate this possibility with various implant designs. The results of the present work show clearly that designs requiring the drilling of holes in T318 during fitting should be avoided. In such cases the endurance of implants manufactured from T318 is

likely to be only slightly improved over that produced using commercially pure titanium implants. When plain smooth-surfaced surgical implant designs can be used, T318 will have a corrosion fatigue performance far exceeding that of any of the other materials tested.

5.3 Suggestions for Further Work

1) A further investigation into the corrosion fatigue resistance of S316 over a range of pH between 1.5 and 6.5 would be interesting. Does the drastic reduction of endurance and fatigue limit occur at one critical value of pH or is there, for example, a linear relationship between pH and endurance?

2) It would be useful to conduct a two-stage environment test for S316, possibly more typical of service conditions after the fitting of implants. Corrosion fatigue initially in saline pH 1.5 would be followed by a gradual change of environment to pH 6.5.

3) Fretting-corrosion fatigue experiments with T318, using the test facility described in this work, with implant fixing screws and plates would be valuable. Such a series of experiments could further investigate possible way of strengthening the material surrounding a hole and generally improve implant design.

6. REFERENCES

1. W Fairbairn — Phil Trans R Soc 154, 311 (1864)

2. A Wöhler — Engineering 11,199-441 (1871)

3. J Bauschinger — Mitt Mech-Tech Lab Munch 13,1 (1886)

4. H Gerber — Z Bayer Ark Ing-Vereins 6, 101 (1874)

5. J Goodman — "Mechanics Applied to Engineering", Longmans, Green & Co. London (1899)

6. J A Ewing & J C W Humphrey — Phil Trans R Soc A200, 241 (1903)

8. H J Gough — Proc Am Soc Test Mat 33, 3 (1933)

9. H J Gough — "The Fatigue of Metals", Scott, Greenwood & Son, London (1924)

10. H F Moore & J B Kommers — "The Fatigue of Metals", McGraw Hill Pub.Co., New York (1927)

11. R H Parsons — "History of the Instn Mech E 1874 to 1947" Inst Mech E (1947)

12. C E Inglis — Trans Instn Nav Archit 55,219 (1913)

13. H Neuber — "Theory of Notch Stresses", J Edwards, Ann Arbor, Michigan (1946)

14. A A Griffith — Phil Trans R Soc 221A, 163-198 (1920)

15. G I Taylor — Proc R Soc A145, 362-404 (1934)

16. H J Gough & W A Wood — Proc R Soc A154, 510 (1936)

17. C S Barrett — Trans Am Soc Met 25 115 (1937)

18. F Wever, H Moller & M Hempel — Archiv Eisenhutten-wessen 11,315 (1937-38)

Contd .....

19. P J E Forsyth — Nature 171, 172 (1953)

20. P J E Forsyth & C A Stubbington — J Inst Met 85, 339 (1957)

21. P J E Forsyth & C A Stubbington — Nature 175, 767 (1955)

22. N Thompson & N J Wadsworth — Adv Phys 7, 72 (1958)

23. N Thompson, N J Wadsworth & N Louat — Phil Mag 1, 113 (1956)

24. M Hempel — Internat Conf Fatigue Metals: Instn Mech E (London), 543-544 (1957)

25. G C Smith — Proc R Soc 242A, 189-97 (1957)

26 A H Cottrell & D Hull — Proc R Soc 242A , 211 (1957)

27 W A Wood & R L Segall — Bull Inst Met 3, 160 (1957)

28. D Hull — J Inst Met 86, 425 (1957)

29 B P Haig — J Inst Met 18, 55 (1917)

30. D J McAdam — J Proc Am Soc Test Mat 26, (11) 224 (1926)

31. H J Gough & D G Sopwith — J Iron & Steel Inst 93, 97 (1932) & 127, 301 (1933) Also J Inst Met 49, 93-112 (1932) & 72,415-421 (1946)

32. U R Evans — "Metallic Corrosion, Passivity & Protection", Arnold 1946

33. U R Evans & M T Simnad — Proc R Soc 188, 372 (1946) Also J Iron & Steel Inst 156, 531 (1947)

34. M T Simnad — J Electrochem Soc 97, 31c-44 (1950)

35. A J Gould & U R Evans — J Iron & Steel Inst 24, 325 (1939)

Contd.....

36. N P Inglis & G F Lake — Trans Faraday Soc 27, 803 (1931)

37. A J Gould — J Iron & Steel Inst 161, 11 (1949)

38. P J E Forsyth — Proc Crack Prop Symp College of Aeronautics, Cranfield, 1961 76-94 (1962)

39. P J E Forsyth & D A Ryder — Metall 63, 117 (1961)

40. R W Landgraf — In High Fatigue Resistance in Metals & Alloys, ASTM STP 467 (1970)

41. W J Plumbridge & D A Ryder — Metall Rev 14, 119 (1969)

42. J C Grosskreutz — Corrosion Fatigue: NACE - 2, 201 Univ Connecticut (1971)

43. ASTM Designation — E 399-70T "Plane-strain Fracture Toughness of Metallic Materials"

44. E T Wessel, W G Clarke, W K Wilson — "Engineering Methods for the Design and Selection of Materials against Fracture" Rep Westinghouse Research Lab Pittsburgh, Penn (1966)

45. P Paris, W E Anderson & E Gomez — Trans ASME J Basic Eng 83, (1961)

46. P Paris & F Erdogan — Trans ASME J Basic Eng 85, 528 (1963)

47. L P Pook — J Strain Anal 10, 4 & 9 (1975)

48. P E Irving & L N McCartney — Fatigue 1977 - Conf Univ Cambridge, Met Soc, 43-53 (1977)

49. A J McEvily & R P Wei — Ref 42, 381

50. H W Liu — Proc 10th Sagamore Army Mat Res Conf New York 127 (1964)

51. E K Priddle — Cent Elect Gen Board Berkely Nuc Lab RD/B/N 2390/XE073 (1972)

52. N E Frost, L P Pook & K Denton — Eng Fract Mech 3, 109-126 (1971)

Contd.....

53. R O Ritchie — Metall Trans A Berkeley Lab Rep 5498 (1976)

54. R A Schmidt & P C Paris — ASTM STP 536, 79 (1973)

55. B M Wundt — ASTM STP 490 (1970)

56. T H Topper, R M Wetzel & J Marrow — J Mat Sci 4, 200-209 (1969)

57. ASTM Designation — ASTM STP 595 "Fatigue-crack growth under spectrum loads" (1976)

58. J D Atkinson & T C Lindley — Conf "The Influence of Environment on Fatigue", Inst Mech E, 65-74 (1977)

59. H J Gough — J Inst Met 49, 17 (1932)

60. L A James — ASTM STP 218, 229 (1975)

61. C J E Smith & A N Hughes — AWRE Rep 44/83/189 Aldermaston, Berks (1977)

62. B A Jordan — AWRE Rep GRO/44/83/140, also private communication AWRE Aldermaston, Berks (1973)

63. R G Luther & T R G Williams — Met Sci 10, 367 (1976)

64. P J E Forsythe — "Strain Enhanced Corrosion Failure of Metals", Conf Lanchester Polytechnic (1976)

65. D A Ryder & S P Lynch — Ref 58, 21-36

66. C Laird & G C Smith — Phil Mag 7, 847 (1962)

67. R M N Pelloux — Eng Fract Mech 1, 697 (1970)

68. C E Richards & T C Lindley — Eng Fract Mech 4, 951 (1972)

69. H Kitagawa, H Nishitani & J Matsumoto — Proc 3rd Int Congr Fract V 444/A Munich (1973)

70. J L Robinson & C J Beevers — Metall Trans 5, 391 (1974)

Contd.....

71. P E Irving & C J Beevers — Ibid

72. J Masounave & J P Bailon — Met Sci 10, 165 (1976)

73. R O Ritchie — Metall Trans A Lawrence Berkeley Lab Rep 5496 (1976)

74. R J Cooke, P E Irving, G S Booth & C J Beevers — Eng Fract Mech 7, 69 (1975)

75. M Klesnil, M Holzman, P Lukaš & P Ryš — J Iron & Steel Inst 203, 47 (1965)

76. R C Boettner, C Laird & McEvily — Trans AIME 233, 379 (1965)

77. M Gell, G R Leverant & C H Wells — ASTM STP 467, 113-153 (1970)

78. R E Peterson — "Methods of Correlating Data from Fatigue Tests of Stress Concentration Specimens", Mechs of Solids, Macmillan (1939)

79. R O Ritchie — Ref 48, 61-74

80. I R Kramer — Trans ASM 62, 521 (1969)

81. C E Feltner & C Laird — Acta Met 15, 1633 (1967)

82. D S Kemsley & M S Patterson — Acta Met 8, 453 (1960)

83. D H Avery & W A Backofen — Acta Met 11, 653 (1963)

84. O Helgeland — J Inst Met 93, 570 (1965)

85. C T Mackenzie & P P Benham — Proc Instn Mech E 180, 709 (1965)

86 G Oates & D V Wilson — Acta Met 12, 21 (1964)

87 M Klesnil & P Lukas — J Iron & Steel Inst 205, 746 (1967)

88. C E Feltner & P Beardmore — ASTM STP 467, 77-112 (1970)

Contd.....

89. C E Feltner & C Laird — Trans Met Soc AIME 245, 1372 (1969)

90. A Fero, P Mazzetti & G Montalenti — Phil Mag 12, 86 (1965)

91. P G Partridge — Acta Met 13, 517-525 (1965)

92. I R Kramer & A Kumar — Ref 42, 146

93. N Polakowski & A Palchoudhuri — Proc ASTM ASTEA 54, 701-716

94. R Ham & T Broom — Phil Mag 7, 95-103 (1962)

95. L F Coffin & J H Read — Ref 24, 415-424

96. C E Feltner & C Laird — Acta Met 15, 1621-1653 (1967)

97. G A Miller, D H Avery & W A Backofen — Trans Met Soc AIME 236, 1667-1673 (1966)

98. R C Boettner & A J McEvily Jr — Acta Met 13,937-946 (1965)

99. A J McEvily Jr & R C Boettner — Acta Met 11,725-743 (1963)

100. M F Ashby — "Oxide Dispersion Strengthening", Gordon & Breach New York, 143-212 (1968)

101. C Laird & C E Feltner — Trans Met Soc AIME 239, 1074-1083 (1967)

102. E T Gill & R Goodacre — J Iron & Steel Inst 130, 293 (1934) also 132, 143, (1935)

103. B Cina — J Iron & Steel Inst 190, 144-157 (1958)

104. A J McEvily, R C Boettner & A P Bond — J Inst Met 93, 481-482 (1965)

105. C Williams & R A F Hammond — Trans Inst Metal Finishing 34, 317-349 (1957)

106. W H J Vernon F Wormwell & T J Nurse — J Iron & Steel Inst 150, 81 (1944)

Contd.....

107. A T Steer, J K Wilson & O Wright — Aircraft Production 15, 177-242 (1953)

108. R A Whitaker & C J L Booker — Br Corros J 8, 246-251 (1973)

109. P J E Forsyth — "The Physical Basis of Metal Fatigue" Blackie & Sons, London & Glasgow (1969)

110. J Feeney, J C McMillan & R P Wei — Met Trans 1, 1741 (1970)

111. R P Wei & J D Landes — Mat Res & Stands 9, 25 (1969)

112. M Achter — "Fatigue crack propagation", ASTM STP 415 (1967)

113. L P Pook — Ref 48, 75-82

114. N E Frost, K.J. Marsh & L P Pook — "Metal Fatigue" Clarendon Press, Oxford (1974)

115. L P Pook & N E Frost — Int J Fract 9, 53-61 (1973)

116. D J McAdam — J Proc Am Soc Test Mat 28,117 (1928) also 31, 259 (1931)

117. A J Gould — Engineering 136, 453 (1933) also 141, 495 (1936)

118. I Cornet & S Golan — Corrosion 15, 262 (1959)

119. L P Pook — ASTM STP 513 , 106-124 (1972)

120. H H Uhlig — Corrosion Handbook (1948)

121. A M Binnie — Engineering 128, 190 (1929)

122. G D Lehmann — Engineering 122, 807 (1926)

123 D J Duquette & H Uhlig — Trans Am Soc Met 61, 449 (1968)

124. P Mehdizadeh, R L McGlasson & J E Landes — Corrosion 22, 325 (1966)

Contd.....

125. A J McEvily — Ref 48, 1 - 9

126. H Grafen — Metalloberflache 19, 40-46 (1965)

127. N D Greene & G Judd — Corrosion 21, 15-18 (1965)

128. V M Novakovski & A N Sorokina — Corros Sci 6, 227-233 (1966)

129. J R Ambrose & J Kruger — J Electrochem Soc 121, 599-604 (1974)

130. T W Crooker & E A Lange — ASTM STP 432 251-267 (1968)

131. D B Dawson & R M Pelloux — Metal Trans 5, 723-731 (1974)

132. R G Luther & T R G Williams — Metal Sci 10, 367-372 (1976)

133. L L Shreir — "Corrosion Vol 1" 2.16 Newnes London (1976)

134. R B Waterhouse — Fatigue of Metals Refresher Course Instn Metallurgists 105-131 (1955)

135. P H Frith — Ibid 132-148

136. D J Duquette & H H Uhlig — Trans ASM 62, 839 (1969)

137. L A Gilkman & L A Luprun — Metalloved Obrabotka Metalov No 6, 10 (1955)

138. B F Brown — Ref 42, 25-29

139. L P Pook & A F Greenan — NEL Report No 571 Glasgow (1974)

140. O Vosikovsky — J Eng Mat Tech Paper No 75 Trans ASME 298-303 (1975)

141. "The Reproducibility of Potentiostatic & Potentiodynamic Anodic Polarization Measurements" — ASTM G-1/X MTRSA 9, No 9 25-26 (1969)

Contd.....

142. H Spahn — Ref 42, 40-57

143. Ya M Kolotyrkin — Corrosion 19, 261 (1963)

144. T P Hoar & D C Mears — Proc R Soc 294, 486 (1966)

145. A J Gould — Ref 24, 341-347

146. AC Fraker, A W Ruff & M P Yeager — Metall Div National Bureau of Stands Washington D C 20234, 2447-2457 (1970)

147. H H Uhlig — Ref 42, 270-278

148. G E Journeaux J W Martin & D E J Talbot — Internat Conf "Mechanisms of Environment Sensitive Cracking of Materials" Univ Surrey, 322 eds P R Swann, E P Ford & A R C Westwood, Met Soc (1977)

149. K Endo & K Komai — Ref 42, 437-450

150. M Pourbaix — "Atlas of Electrochemical Equilibria in Aqueous Solutions": Pergammon (1966)

151. J H Payer & R W Staehle — Ref 42, 211-269

152. M Pourbaix — "The Theory of stress corrosion cracking in Alloys" Ed J C Scully, NATO, Brussels, 17 (1971)

153. J A Smith,M H Peterson & B F Brown — Corrosion 26, 539 (1970)

154. R N Parkins — J Strain Anal 10, 251-257 (1975)

155. B F Brown, C T Fujii & E P Dahlberg — J Electrochem Soc 116, 218-219 (1969)

156. E J Radd,L H Crowder & L H Wolfe — Corrosion 16, 121-124 (1960)

157. M Stern — J Electrochem Soc 102, 609-616 (1955)

158 P Stretton — Conf Instn Corr Tech, Disc 2 (1970)

Contd.....

159. C A Zapffe — Met Prog 68, 95-98 (1965)

160. V Rollins, B Arnold & E Lardner — Brit Corros J 5, 33 (1970)

161. J L Crolet & J M D Defranou — Corros Sci 13, 575-585 (1973)

162. H Spahn — Metalloberflache 16, 197-369 (1962)

163. R E Peterson — Mat Res & Stands 3, 122-139 (1965)

164. J Morrow & T A Johnson — Mat Res & Stands 5, 30-32 (1965)

165. W A Wood — ASTM STP 237, 110-119 (1958)

166. C E Feltner & J Morrow — Trans ASME J Basic Eng 83, 15-22 (1961)

167. F Wever, M Hempel & A Schrader — Arch Eisenhuttenw 26, 739 (1955)

168. O Helgeland — J Inst Met JIMEA 93, 570-575 (1965)

169. W N Roberts — "PSB in Copper" Rep PM-M-68-19 Bureau of Mines, Ottawa, Canada (1968)

170. C E Feltner — Phil Mag 12, 1229-1248 (1965)

171. C Laird — Mat Sci & Eng 25, 187-191 (1976)

172. P Lukas, M Kesnil & J Krejci — Phys Status Solidi 27, 545 (1968)

173. D F Watt — Czech J Phys 19, Sect B, 337 (1969)

174. D H Avery, G A Miller & W A Backofen — Acta Metall 9, 892 (1961)

175. D F Watt, J D Embury & R K Ham — Phil Mag 17, 199 (1968)

176 M L Ebner — Trans AIME 215, 510 (1959)

Contd.....

177. D H Avery & W A Backofen — "Fract of Solids" 339-382 eds D C Drucker & J J Gilman, John Wiley, New York (1963)

178. J C Grosskreutz — Phys Status Solidi 47,359-396 (1971)

179. C Laird & D J Duquette — Ref 42, 88-117

180. P Lukas & M Klesnil — Ref 42, 118-132

181 E E Laufer & W N Roberts — Phil Mag 10, 883 (1964) also 14, 65 (1966)

182. E E Laufer — Czech J Phys 19 Sect B, 333-334 (1969)

183. D Kuhlmann-Wilsdorf & H D Nine — J Appl Phys 38, 1683 (1967)

184. H J Gough & H L Cox — Proc R Soc A123, 143 (1929) & A127 431-453 (1930)

185. N Thompson & N J Wadsworth — Brit J Appl Phys Suppl 6,51 (1957)

186. C J Beevers & M D Halliday — Czech J Phys 19, Sect B, 343-346 (1969)

187. C H Wells — Acta Met 17, 443-449 (1969)

188. F A McClintock — Ref 177, 65-102

189. A S Argon — Ref 42, 176 - 182

190. A S Argon & J A Godrick — Czech J Phys 19, Sect B, 341 (1969)

191. N F Mott — "Dislocation & Mechanical Properties of Crystals", 458-478 Eds J C Fisher etal John Wiley, New York (1957)

192. P G Partridge — Czech J Phys 19 Sect B, 323 (1969)

193. P Neumann — Ibid, 349

194. W A Wood, S Cousland & K R Sargent — Acta Met 11, 643 (1963)

Contd..... .....

195. W D Dover & W J D Jones — Brit J App Phys 18, 1257 (1967)

196. J G Antonopoulas, L M Brown & A T Winter — Phil Mag 34, 549 (1976)

197. L M Brown — Ref 48, 11-15

198. A M Fredenthal — Eng Fract Mech 6,775-793 (1974)

199. W A Wood — Eng Fract Mech 8, 69-80 (1976)

200. R K Steele & A J McEvily — Eng Fract Mech 8, 31-37 (1976)

201. D K Benson, J C Grosskreutz & G C Shaw — Met Trans 3, 1239-1248 (1973)

202. W J Plumbridge D A Ryder — Met Rev 14, 119-142 (1969)

203. R A T Dawson, W J Elder, G J Hill & A T Price — "Thermal & High-Strain Fatigue" Inst Met London 239 (1967)

204. C Laird — ASTM STP 415, 139 (1967)

205. B Tomkins — Phil Mag 18, 1041 (1968)

206. W R Tyson & L C R Alfred — Ref 42, 281-288

207. J C Grosskreutz & G G Shaw — ASTM STP 226 (1967)

208. M A Wilkins & G C Smith — Acta Met 18, 1035 (1970)

209. C Q Bowles & D Broek — Internat J Fract Mech 5, 350 (1969)

210. S Karashima H Oikawa & P Ogura — Japan Inst Met 9, 205 (1968)

211. M Klesnil & P Lukas — "Fracture 1969" Ed P L Pratt, Chapman & Hall Ltd London, 725 (1969)

212. R J H Wanhill — Proc 2nd Int Conf Mech Behaviour of Materials, Cleveland Ohio (ASM), 558 (1976)

Contd.....

213. S P Lynch — Met Sci 9,401-410, (1975)

214. D A Meyn — NLR Mem Rep 1707 (1966)

215. C Q Bowles & D Broek — Int J Fract Mech 8, 75 (1972)

216. C E Richards — Acta Met 19, 583 (1971)

217 R C Bates, W G Clark & D M Moon — ASTM STP 453 192-214 (1969)

218. J C McMillan & R W Hertzberg — ASTM STP 436, 68 (1968)

219. B Tomkins — Ref 42, 303-311

220. B Tomkins — Phil Mag 23, 687 (1971)

221. K Erhardt & N J Grant — Fracture, Chapman & Hall Ltd 702-711 (1969)

222. B Tomkins & W D Biggs — J Mater Sci 4, 544 (1969)

223. P Lukas, M Klesnil, & R Fielder — "Plastic Zone around the Propagating Fatigue Crack" Czech Acad Sci Brno, (1969)

224. M Gell & G R Leverant — Acta Met 16, 553 (1968)

225. H D Williams & G C Smith — Phil Mag 13, 835 (1966)

226. R K Ham & M L Wayman — Trans AIME 239 721 (1967)

227. C A Stubbington & P J Forsyth — Metall 74, 15 (1966)

228. R G Luther & T R G Williams — Ref 48, 29-36

229. F E Fujita — Ref 177, 657

230. K Laute — Oberfalchentech 10, 281 (1933)

Contd.....

231. A B Ryabchankov — Zhur Fiz Chim 26, 542 (1952)

232. T J Smith & R W Staehle — Corrosion 23, 117 (1967)

233. E N DaC Andrade — "Properties of Metallic Surfaces" Symp Inst Met (1953)

234. U R Evans — "The Corrosion & Oxidation of Metals",681 Edward Arnold Ltd, London (1960)

235. R M N Pelloux, R E Stoltz & J A Moskovitz — Mat Sci Eng 25, 193 (1976)

236. R N Parkins & B S Greenwell — Ref 48, 84-105

237. L A G Likman & L A Suprun — Trudy Vsesoyuz Soveshchaniya Po Bor'be Smorskoi Korroziei Metal, Baku, 102 (1956)

238. D Whitwham & U R Evans — J Iron & Steel Inst 165, 76 (1950)

239. F Lihl — Metall 4, 130 (1950)

240. S Vedenkin & V Sinyavskii — Bar'by S Karrozei Azerb Inst Nefti 1 Khin 30 (1962)

241. D J McAdam Jr & G W Geil — Proc ASTM 41, 696, (1928)

242. E Reissner — Trans ASME 67, A69 (1945)

243. P A Rebinder — Z Physik 72, 191 (1931) also Nature 159, 866 (1947)

244. V I Liktman, E D Shohuklin & P A Rebinder — Physicochem Mech of Met 12-109 Acad of Sci USSR (Israel Prog Sci Trans) Jerusalem(1964)

245. G V Karpenko — Doklady Akademii USSR 5,827-830, 77, 827 & 79 287 (1951) also 87, (5) 797 (1952)

246. G V Karpenko — "Korriziya Metal" 1 Metody Bar'by S Neyu (Moscow) Sbarnik 52 (1955)

Contd.....

247. T Pyle, V Rollins & D Howard — Ref 42, 312-318

248. C Patel, T Pyle & V Rollins — Met Sci June 185-195 (1977) also Ref 148, 366 & 390

249. C A Zapffe & M E Haslem — Trans Am Soc Met 39, 214 (1947)

250. J T Brown & M W Baldwin — J Met (N Y) 6, 298 (1954)

251. A R Traiana J G Marlet & H H Johnson — J Iron & Steel Inst 189, 37 (1958)

252. G V Karpenko — Deyaki Pitannya Fiz Khim Mekhum Metal Akad Nauk Ukr RSR, Inst Machinoznavstra Ta Avlomatiki 47 (1958)

253. R Holder — Ref 148, 359

254. C D Beechem — Met Trans 3, 437 (1972)

255. F H Beck — NASACR 134796 Rep Ohio State Univ Res Found (1975)

256. R J Smith & D A Otterson — NASA Tech Note TND-6515 (1975)

257. P E Irving & C J Beevers — Mat Sci 7, 23, (1972)

258. R M Latanision & R W Staehle — Acta Met 17, 307 (1969)

259. I M Austen & E F Walker — Ref 58, 1 - 10

260. N J Wadsworth & J Hutchings — Phil Mag 3, 1154 (1958)

261. W G Clark — Proc Conf ASM SP 2, 148 Seven Springs, Penn. (1973)

262. D A Ryder, M Martin & M Abdulla — Ref 48, 62-73

263. R J Taunt & W Charnock — Ref 58, 43-51

264. D A Meyn — Trans ASM 61, 42 (1968)

Contd.....

265. R M N Pelloux — Trans ASM 62, 281 (1969)

266. J Schijve — ASTM STP 415 (1967)

267. J Schijve — Instn Mech E Proc 191, 14-77 (1977)

268. R B Waterhouse — "Fretting Corrosion" Pergammon M Sc & Tech 10, 233 & 56-59 (1972)

269. R B Waterhouse — Proc Conf ARGARD No 161 NATO (Munchen) 1, 8 (1974)

270. R G Weber & A J McEvily — "Fracture 1969" Proc 2nd Int Conf on Fracture Chapman & Hall Brighton (1969)

271. R M N Pelloux — Ibid

272. C A Stubbington P J E Forsyth — J Inst Metals 90, 348 (1961)

273. C A Stubbington — R A E Rep CPM-4 (1963)

274. T Misawa — Corros Sci 13, 659 (1973)

275. A R Traiano — Trans ASM 52, 54 (1960)

276. J P Gallagher — J Mat 6, 941-965 (1971)

277. J J Gilman — Phil Mag 23, 801-812 (1972)

278. D P Williams H G Nelson — Met Trans 1, 63-68 (1970)

279. J M Krafft & J H Mulherin — ASM Trans 62, 64-81 (1969)

280. H Okada, K Yukawa & H Tamura — Corrosion 30, 253-255 (1974)

281. B E Wilde — Corrosion 27,326 (1971)

282. H Doker & D Munz — Ref 58, 123-130

283. V J Colangelo — Handbook on Corrosion Testing & Evaluation ed W H Ailor Wiley 217-229 (1971)

Contd.....

284. D C Ludwigson — Met Eng Quart 5, 1-6 (1956)

285. Armco Research Lab — Armco Steel Corp Rep M982 (1968)

286. S Weisman — "The Skeletal Structure of Metal Implant", Biomech & Human Factors Symp ASME (1967)

287. J Brettle — AWRE Rep Aldermaston GRO/44/83/13 (1968)

288. J M Zarek, A S Smith & A E F Wilkinson — Nature Misc items p900 (1964)

289. T W Farthing — Instn Mech E Proc 191, 9/77 (1977)

290. G M Down — Down Bros Mayer & Phelps Ltd Church Path, Mitcham, Surrey (1971)

291. G H Hille — J Mat 1, 373 (1966)

292. O E Beder & G Eade — Surgery 39, 470-473 (1956)

293. P G Laing A B Ferguson & E S Hodges — J Biomed Mat Res 1, 135 (1967)

294. Imperial Metals Industries Ltd — Pub. 4Ed/Mk23/13/467 (1967)

295. J H Hicks — Chemy Ind No 28 1240 (1964)

296 J B Cotton & B P Downing — Trans Inst Marine Eng 69,311 (1957)

297. G T Harris,B C Child & A C Dalton — J Inst Metals 88,112 (1959)

298. M Levy, D B Dawson, G N Sklover & D W Seitz — Titanium Science & Tech 4,2459 Plenum Press New York (1973)

299. R J H Wanhill — Nat Aerospace Lab Rep TR71012U NLR Amsterdam (1970)

300. D Schlain — "Corr Prop of Ti & Alloys" Bur Mines Bull 610, US Dept of the Interior (1964)

Contd.....

301. J D Jackson & W K Boyd — DMIC Mem 218 Battelle Mem Inst Columbus, Ohio (1966)

302. R W Staehle, A J Forty & D van Rooyen — Proc Internat Conf "Fundamental Aspects of Stress Corrosion Cracking" Houston Texas ,591-700 (1969)

303. J T Scales, G D Winter & H T Shirley — Brit Med J Aug, 478-482 (1961)

304. J T Scales — J Bone & Joint Surgery, 38B, 754-761 (1956)

305. J Brettle & A N Hughes — AWRE Rep Aldermaston GRO/44/83/12 Also: Injury , 2, 143 (1970)

306. C Fischer & H Zitter Werkstoffe and Korrosion, 14 753-758 (1963)

307. J O Galante, W Rostoker & J M Doyle — J Bone & Joint Surgery 57A, 230 (1975)

308. J Charnley — Brit Ortho Res Soc Meeting, Nuffield Orth Centre Oxford (1975)

309. B Weightman — "Advances in Artificial Hip & Knee Joint Technology" -Springer - Verlog,139 Berlin(1976)

310. N Rydell — "Studies on Anatomy and Function of Bone & Joints", Berlin-Heidelberg - New York: Springer-Verlog (1966)

311. The Fixation of Fractures using Plates — Conf Report Instn Mech E 26 (1972)

312. G Friedebold & R Kolbel — Ref 309, 3-23

313. R Thull & M Schaldach — Ref 309, 242-256

314. J H Hanks & R E Wallace — Proc Soc Exp Biol (Wash) 71, 196 (1949)

315. H Zitter — Ref 309, 230

316. B A Jordan*, A N Hughes & C J E Smith — "Some experiences of Corrosion Phenomena in Surgery" Paper at 6th Int Conf on Metal in Sydney (1975) (*AWRE Aldermaston)

Contd.....

317. A B Ferguson, Y Akahoshi, P Laing & E S Hodges — J Bone & Joint Surgery 44A, 317-336 (1962)

318. A N Hughes, B A Jordan & S Orman — AWRE Rep Aldermaston 44/83/140 (1973)

319. C J E Smith — AWRE Rep DHSS Project A129, Aldermaston AWRE/44/83/179 (1976)

320. C J E Smith & A N Hughes — AWRE Rep Aldermaston AWRE/44/83/189 (1977)

321. C J E Smith & A N Hughes — Brit Corros J 11, 12, (1976)

322. C J E Smith & A N Hughes — AWRE Rep Aldermaston AWRE/44/83/165 (1975)

323. M B Bapna, E P Lautenschlager, J E Moser & P R Meyer — J Biomed Mat Res 9, 611 (1975)

324. V J Colangelo — J Basic Eng 581 (1969)

325. K R Wheeler & L A James — J Biomed Mat Res 5, 267 (1971)

326. L J Bartlo — ASTM STP 459, 144 (1969)

327. J J Lucas & P P Konieczny — Met Trans 2, 911 (1971)

328. J J Lucas — Titanium Sci & Tech 3, 208 (1973)

329. A W Bowen & C A Stubbington — 2nd Int Titanium Conf, Boston (1972)

Contd.....

330. J Braichhausen & K V Kann — Ref 328, 1785

331. R B Waterhouse & M K Dutta — Wear 25, 171 (1973)

332. R W Judy, T W Crooker, R E Morcy, E A Lange & R J Goode — Trans ASM, 59, 195 (1966)

333. C J E Smith & A N Hughes — AWRE Rep DHSS Project A129, Aldermaston AWRE/44/83/164 March (1975)

334. N D Green, C A Moebus & M H Baldwin — Corrosion 29, 234 (1973)

335. M R E Bloyce & E Jithoo — Private Communication - Middlesex Polytechnic

336. C Edeleanu — J Iron & Steel Inst 188, 122 (1958)

337. M Stern — Corrosion 14, 440 (1958)

338. M Stern & E D Weisert — Proc Am Soc Test Mat 59, (1959)

339. G M Bulman & A C C Tseung — Corros Sci 12, 415 (1972)

340. M P Sherwin, D E Taylor & R B Waterhouse — Corros Sci 11, 419 (1971)

341. J N Goodier — Phil Mag Serv 7, XXII 145 (1936)

342. R B Heywood — Designing by Photoelasticity, Chapman Hall Ltd (1952) also Engineering, Feb (1955)